AD-A109 621 CORNING GLASS WORKS NY F/G 20/6
SINGLE MODE OPTICAL WAVEGUIDE DESIGN STUDY.(U)
NOV 81 V A BHAGAVATULA, D B KECK, R A WESTWIG N00173-80-C-0563
UNCLASSIFIED NL

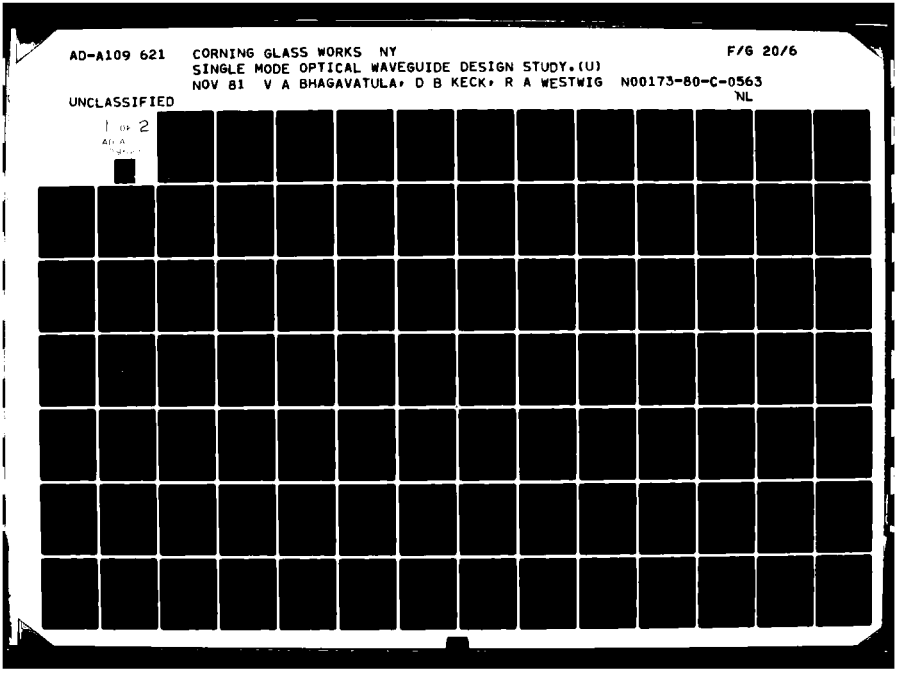

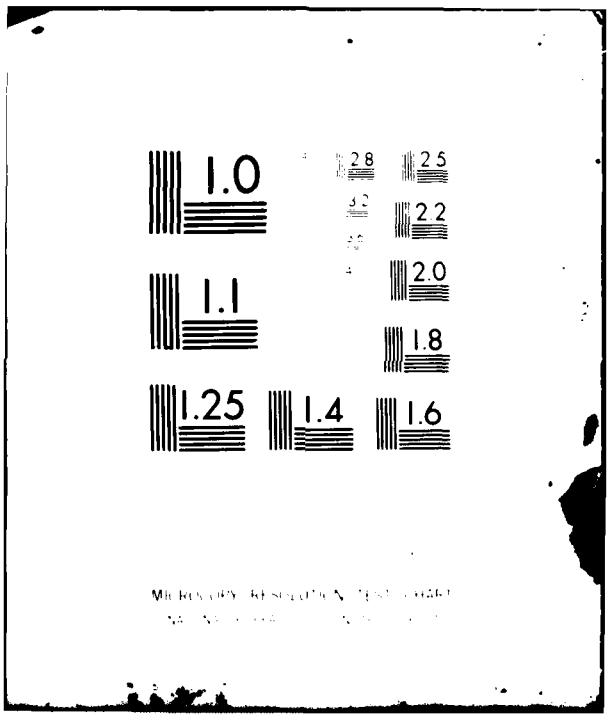
1.0
1.1
1.25
1.4
1.6
1.8
2.0
2.2
2.5
2.8

CORNING

LEVEL

(12)

AD A109621

Single Mode Optical Waveguide Design Study

FINAL REPORT

Naval Research Laboratory Contract No.
N00173-80-C-0563

November 23, 1981

Submitted to:

Dr. William K. Burns
Naval Research Laboratory
Code 6570
Washington, D.C. 20375

Authors:

Venkata A. Bhagavatula
Donald B. Keck
Ralph A. Westwig

Corning Glass Works
Research and Development Division
Sullivan Park
Corning, New York

Single Mode Optical Waveguide

Design Study

FINAL REPORT

Naval Research Laboratory Contract No.

N00173-80-C-0563

November 23, 1981

Submitted to:

Dr. William K. Burns
Naval Research Laboratory
Code 6570
Washington, D.C. 20375

Authors:

Venkata A. Bhagavatula
Donald B. Keck
Ralph A. Westwig

Corning Glass Works
Research and Development Division
Sullivan Park
Corning, New York

TABLE OF CONTENTS

TABLE OF CONTENTS (con't)

SINGLE MODE OPTICAL WAVEGUIDE DESIGN INVESTIGATION

1. Introduction

1.1 Purpose of Study

With the extremely low losses attained in optical waveguides over the past three years, it is expected that graded index multimode systems with long repeater spacing will be dispersion limited. In that case the only recourse is to use single mode waveguides. To fully utilize this potential, the single mode waveguide design has to be simultaneously optimized with respect to total loss and bandwidth of the system. Since the bandwidth of a single mode waveguide is considered sufficiently high for most telecommunication applications, the present work has concentrated on total waveguide loss as would be experienced in a real system. Many laboratories have fabricated low loss single mode waveguides[1,2,3,4] however, these have not been systematically optimized to minimize total system loss. The objective of this study is to experimentally determine the step index single mode fiber loss dependence, by all mechanisms likely to be experienced practically, upon the key fiber design parameters, core diameter (2a) and fractional index difference (Δ). Only with this systematic and comprehensive data base, will a rational choice of and/or criteria for choosing fiber design parameters optimized for a given application be obtained.

1.2 Technical Background

The basic mechanisms for attenuation in waveguides are well known, and have been extensively studied in multimode waveguides for several years. They are intrinsic absorption of the

base glass, impurity absorption, intrinsic scattering of the base glass, and losses due to externally induced perturbations such as micro- or macro-bending, and interconnection losses.

1.2.1 Absorption

Single mode waveguides have been fabricated using boron, fluorine, and phosphorus dopants in silica.[1,5,6] However, the simple binary system of germania doped silica has shown very low intrinsic absorption (0.2 dB/km at 1550 nm[4]) and hence is the system studied in this contract.

Impurity absorption in waveguides made today is virtually restricted to the hydroxyl radical. For long distance single mode waveguides the OH bands of particular interest are the first overtone occurring at approximately 1380 nm and the combination of this band with the fundamental ν_1 stretching vibration of the SiO_2 matrix which occurs at 1250 nm. From studies of the loss as a function of OH concentration which have been done,[7] it is required that the OH concentration be less than approximately 200 ppb in order to achieve the loss goals. This level was achieved in the processing used for the present work.

1.2.2 Scattering

Intrinsic glass scattering appears to be the dominant loss mechanism in the primary region of interest for single mode operation. This loss arises from two forms; density fluctuations frozen into the glass at the time of manufacture and concentration fluctuations arising from the use of multiple dopants in the waveguide. It is the latter loss which is of some concern for the proper design of single mode optical waveguides. It is

fairly well established[8,9] that as the Δ-value of the waveguide increases the scattering loss also increases,

$$\gamma_s = \frac{.45+1.16\Delta+0.43\ \Delta^2+0.06\ \Delta^3}{\lambda^4} \quad (1)$$

where Δ is expressed as a percentage difference in index.

1.2.3 Microbending Perturbation Loss

Many models for single mode perturbation losses exist. Peterman[10] shows the loss depends directly on a power of the mode spot size and propagation wavelength. Olshansky[11] has calculated the losses assuming a power law perturbation power spectrum and finds the loss to depend upon the characteristic V-parameter of the waveguide. A more recent analysis by Furuya and Suematsu[12] using a Gaussian power spectrum shows that Δ is the critical parameter and an experimental verification of the model is presented. The latter work indicates that to maintain microbending losses below 0.1 dB/km beyond a wavelength of 1.4 μm for the power spectrum presently observed in cabling, requires that $\Delta \gtrsim 0.004$. The microbending loss, $\gamma_{\mu\beta}$, from this model obeys the approximate relationship,

$$\gamma_{\mu\beta} \simeq X\ N\overline{(1/R)^2}\ \frac{\bar{W}^2}{\Delta} \exp\left[-187\left(\frac{\bar{W}n\Delta}{\lambda_c}\right)^2 e^{-4.36\ \lambda/\lambda_c}\right] (\mathrm{dB/km}), \quad (2)$$

where $\bar{W}$ is the width of the Gaussian power spectrum, N is the average number of perturbations per unit length, $\overline{(1/R)^2}$ is the mean square curvature of the bend, λ_c is the cutoff wavelength, n the

waveguide core index, Δ the fractional index difference, and λ the operating wavelength and X ~4 x 10^3 (see Section 5.1.1). The equation indicates that microbending losses in the single mode waveguide should increase dramatically as the wavelength is increased appearing very similar to a vibration band edge in the spectral transmission curve. For a given power spectrum associated with the cabling process this edge may be shifted to sufficiently long wavelengths by a proper choice of the guide parameters Δ and the cutoff wavelength λ_c. Changing the fractional index difference Δ from 0.004 to 0.005 moves the effect of this edge by approximately 100 nm to longer wavelength.

While experimental verification of Equation (2) was found for waveguides of two different Δ-values in jacketing and cabling tests,[13] the equation has not been systematically tested over a large range of fractional index differences and core diameters. Additionally, no laboratory test is known to exist which induces the Gaussian power spectrum on the fiber and hence simulates cabling. Such a laboratory test which predicts cable performance a priori would be extremely useful in the optimization of fiber design for various applications.

1.2.4 Macrobending Perturbation Loss

It is presently known that macrobending attenuation also shows an exponentially increasing loss as a function of decreasing bend radius and increasing wavelength. Marcatili and Miller[14] have posed a model for this loss in which radiation occurs as the wavefront exceeds the velocity of light as it traverses the bend. This model ha. been shown to be in qualitative agreement with experimental data.[15] It indicates that for the

characteristic guide parameter, $V \geq 1.5$, bend radii greater than ~10 cm will have very little effect on system loss. For the present work it will be assumed that this bend radius does not place a severe restriction on system deployment and it will be ignored.

1.2.5 Interconnection Losses

Since the attenuation rate of single mode waveguides is expected to be in the few tenths dB/km range, losses associated with the interconnection of single mode waveguide sections may represent a large fraction of total system loss. For this reason it is important that the sensitivity of these interconnection losses to the waveguide design parameters be quantified.

Using a Gaussian beam approximation to the field distribution for the HE_{11} mode, Gambling and co-workers[16,17] have modelled the interconnection loss dependence on core diameter and fractional index difference. Their companion experimental work, however, did not cover the full range of fiber parameters which may be necessary to properly optimize system performance.

1.2.6 Background Summary

The theoretical and experimental work cited above forms the base for the present work. The common thread in these previous studies is that either an isolated loss source and/or a limited range of fiber design variables were considered.

Considering the loss sources isolated from one another does not produce the optimum design. For example intrinsic scatter loss (Eqn. 1) is minimized by decreasing the fractional

index difference while the opposite is true for microbending loss (Eqn. 2). Further, the validity of the theories have not been tested over a wide range of fiber parameters hence extrapolation is to date open to question.

1.3 Summary of Accomplishments

In this study these previous deficiencies were overcome by a simultaneous investigation of all mechanisms having a significant impact on overall fiber system loss. Step index fibers were fabricated whose design parameters were varied over a sufficiently wide range of values to accommodate the majority of applications. The losses produced in these fibers by various mechanisms then were determined quantitatively and compared with the existing step index theory.

The following is a summary of the specific accomplishments and their interpretation with regard to the optimum design of a single mode telecommunication fiber.

- Twelve single mode waveguides were fabricated using both the "inside" and "outside" process.[18] The values of fiber parameters are given in Figure 1.
- A reproducible microbend measurement apparatus based on linear pin arrays was designed and constructed.[19]
- A reproducible apparatus for both lateral and angular offset loss measurements was designed and constructed.
- The twelve waveguides were measured for microbend and lateral-angular offset losses.

RANGE OF "STEP INDEX" SINGLE MODE DESIGN PARAMETERS INVESTIGATED.

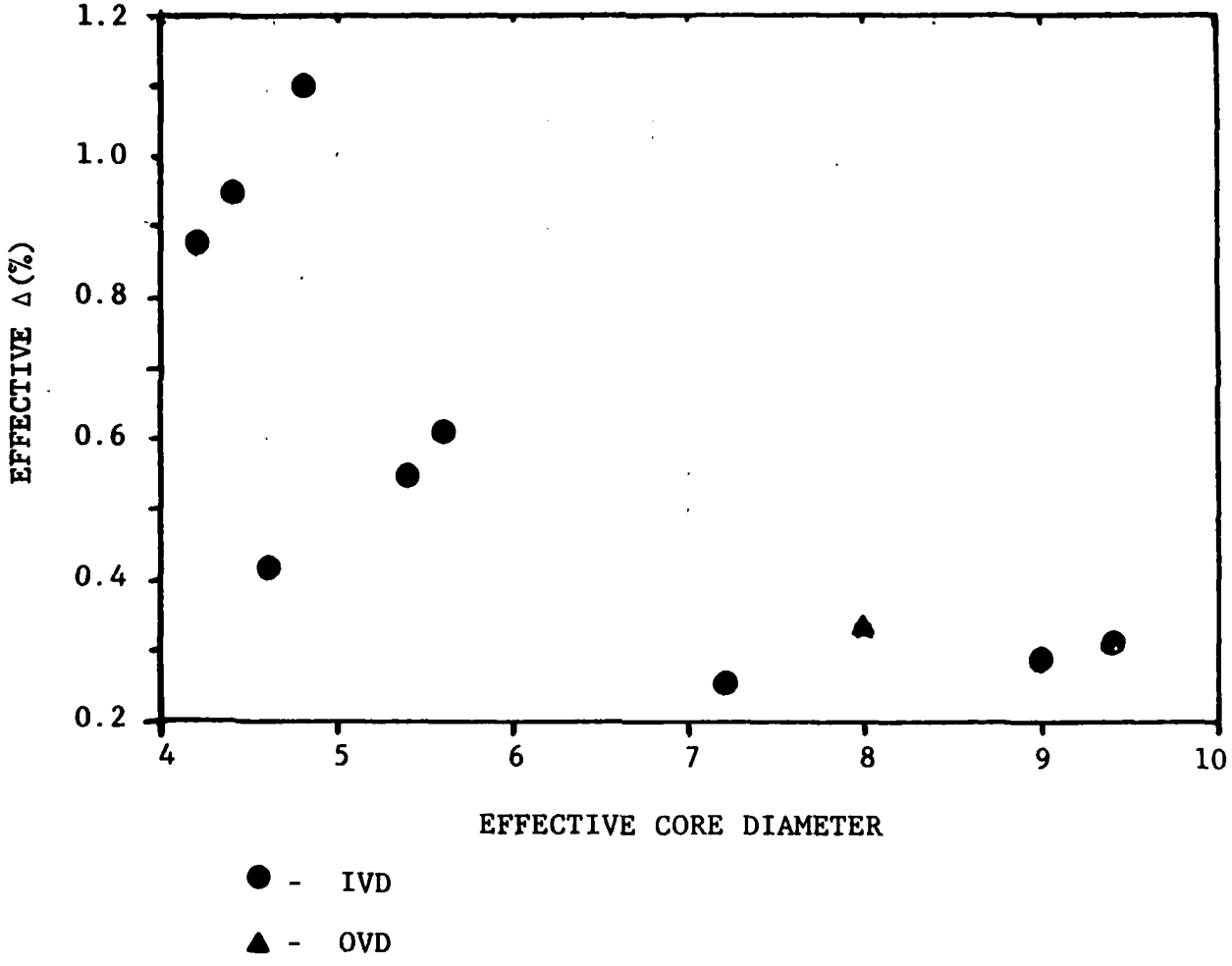

FIGURE 1

. Pin array microbending loss data fits the Gaussian power spectrum model extremely well over the entire range of design variables. This suggests the values, $\Delta > 0.003$ and $2a \leq 8.0$ μm to minimize cabling microbend loss. This provides the first good correlation between a laboratory test and actual cable results.

. Measured lateral offset loss follows the theoretical model to within 0.2 dB. Loss increases with decreasing core diameter and increasing Δ and suggests, $\Delta \leq 0.006$ and $2a \geq 4.8$ μm.

. Measured angular offset loss is ~50% less than theoretically predicted perhaps due to fiber end angle. Angular offset loss however is not found to be a significant effect in determining fiber design.

. Fabrication variability can strongly impact the design values chosen and this effect was quantized.

. Beyond the scope of the original proposal, the interconnection loss dependence upon wavelength was quantified. The data supports the theory.

. The lateral offset data quantifies the allowable fabrication tolerance on core concentricity.

Based on analysis of the present data for simultaneous minimization of all single mode loss sources, it is felt that the design range, $0.003 < \Delta < 0.006$ and 5.6 μm < core diameter < 8 μm, will encompass the majority of applications. The exact value within this range will depend critically upon the actual perturbation spectrum introduced by the cabling process as well

as fiber manufacturing variability of the key parameters. The present study allows extrapolation to the correct design as additional cabling data beocmes available. Additionally it was identified that the single mode fiber loss spectrum will provide a way of inferring the cable perturbation power spectrum.

As a final product of the study, 4 km of low-loss single mode fiber made by both the "inside" and "outside" vapor phase oxidation process[18] were fabricated. Two kilometers each of two design matrix points were prepared: 1) $\Delta \simeq 0.004$, $2a \simeq 8$ μm and 2) $\Delta \simeq 0.005$, $2a \simeq 6$ μm. Both fibers have a cutoff wavelength, $\lambda_c \simeq 1100$ nm as determined by short length transmittance. This should be appropriate for 1300 nm operation. The first of these is believed to be the lowest Δ-value acceptable given the present level of cable perturbation and fiber processing variations. With improvement in cabling and processing it is expected that the $\Delta = 0.003$ design range extreme will be optimum for telecommunication applications. The other design range extreme, is approximated by the second pair of fibers. These would be expected to be useful if cabling perturbations are more severe.

Since the cable power spectrum has been shown to have such a dramatic effect on loss and fiber design, the present work suggests that a future study to determine the power spectrum associated with different cable designs and cable processes is required. Single mode fibers of a few designs should provide a powerful tool for determining the cable power spectrum.

2. Measurement System

2.1 Apparatus and Procedure

2.1.1 Microbend Test

The microbend test was modified from the random "sandpaper test," as described in the contract proposal, to more reproducible linear pin arrays of different pin spacings.[19] A schematic diagram of the test is shown in Fig. 2. In this test a 2 m length of the single mode fiber is "woven" through the pin array perturber and the transmitted power is monitored in the wavelength range (700-1800) nm. The microbend loss induced by the pin array is evaluated by comparing the transmitted power in the perturbed fiber with a reference. The reference used in this experiment is the transmitted power in the unperturbed fiber. This experiment is performed using pin array perturbers with nominal pin spacings of 8 mm, 5 mm, 4 mm and 3 mm. The pin diameters are 0.65 mm and the number of pins is held constant at 30. The purpose of using these four different pin arrays is to apply perturbations which differ primarily in frequency, however, amplitude change also occurs. Details of the perturbation spectrum applied by the various pin arrays are given in Section 5.1.

2.1.2 Lateral and Angular Offset Test

Equipment to measure lateral and angular offset loss has been designed and fabricated. A schematic diagram of the test setup is shown in Figure 3. To obtain accurate and reproducible results it is essential to carefully align the fibers.

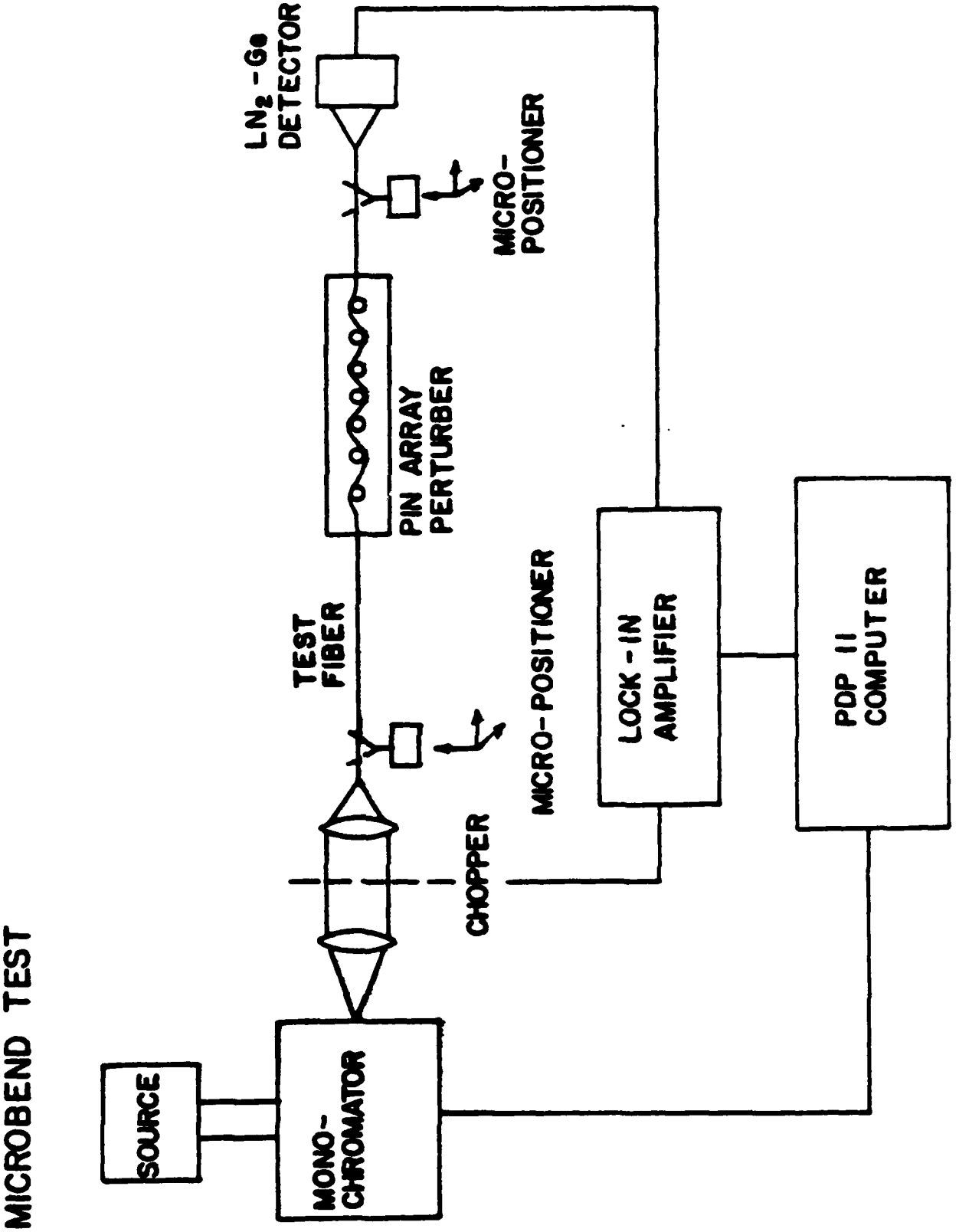
MICROBEND TEST
SOURCE
MONO-CHROMATOR
CHOPPER
MICRO-POSITIONER
TEST FIBER
PIN ARRAY PERTURBER
MICRO-POSITIONER
LN_2 - Ge DETECTOR
LOCK - IN AMPLIFIER
PDP 11 COMPUTER

FIGURE 2

OFFSET SENSITIVITY TEST

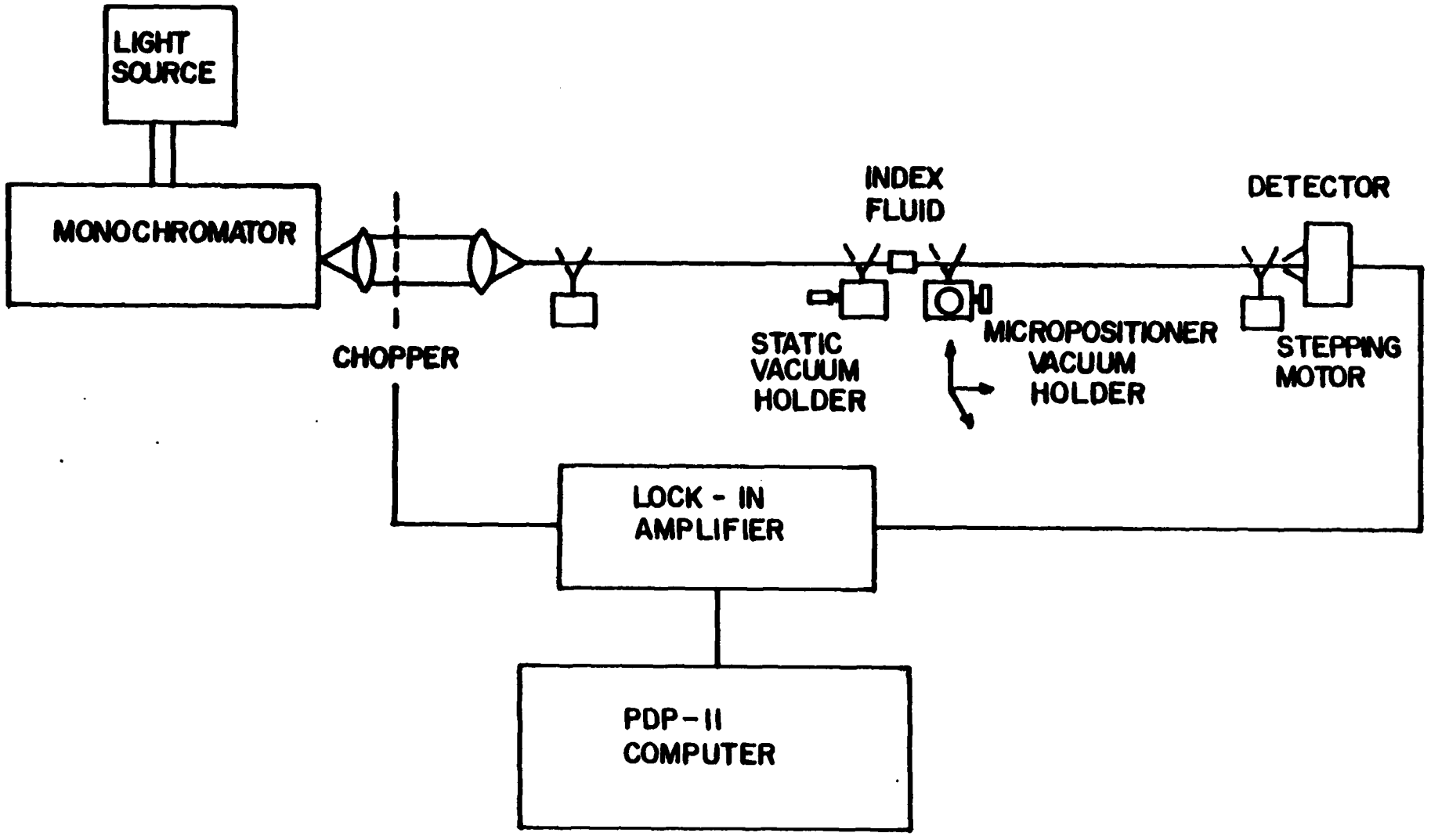

FIGURE 3

To achieve this, a system with various translational and rotational degrees of freedom has been fabricated. A schematic diagram indicating the various degrees of freedom and their tolerances is shown in Figure 4. Here LI, LII and LIII, represent the translational degrees of freedom and AI and AII are angular offsets around axes (I) and (II) respectively. The rotation of the receiver test fiber around its own axis "R" is "RI." For example, for lateral offset measurements, the data has been gathered along LI in steps of 0.1 μm. This is made possible by using a combination of computer controlled stepping motors, differential micrometer and 3-D micropositioner stages. Such an arrangement allowed the angular misalignment to be minimized during lateral offset measurement and vice versa. In the angular offset loss measurement, the fiber is indexed around axis (I) in 4.36 mrad (15 minute) increments. This is accomplished by means of a computer controlled rotary stepping stage.

To achieve detailed comparison of measurement data with splice loss models it was judged that complete lateral offset curves would be very useful. Thus the lateral offset loss data were taken over a range of $\pm$ 12.5 μm from the zero offset position in 0.1 μm increments. In addition the lateral offset measurements have been performed at various wavelengths that cover an extended range of V-values both in single mode and double mode regions of the waveguide. Such measurements have been performed on all of the fibers and the data is presented in Section 4.

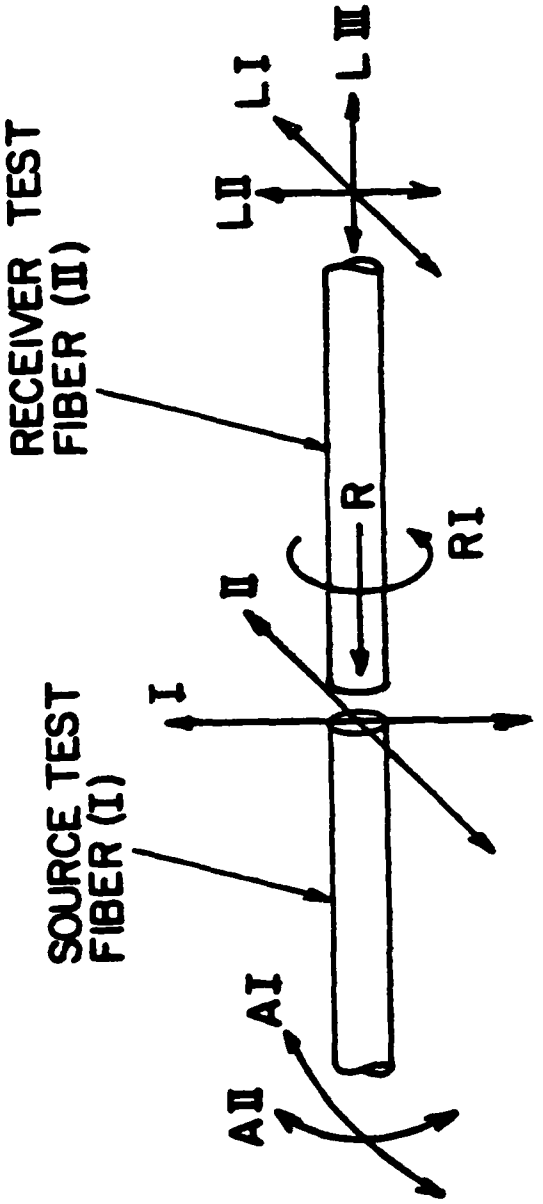

DEGREES OF FREEDOM IN OFFSET SENSITIVITY SYSTEM.

FIGURE 4

In the case of the angular offset loss measurements, data is taken over a ± 10 degree range from zero offset position in 4.36 mrad (15') increments. As in the case of lateral offset, the experiments have been performed at various wavelengths. To eliminate the effect of lateral offset during the angular offset measurements, it is essential to align the test fiber end I (Fig. 4) with the axis of rotation. Even a small misalignment in this respect leads to lateral offset loss contributions in the angular loss measurement. To eliminate this possibility, the fibers are tested for zero lateral offset after each angular offset increment. For accurate and reproducible results, the test procedure is automated and computer controlled.

In both the lateral and angular offset loss measurements a 4 m length of the test fiber is used for the source (input) section (Fig. 3). For the output section, a 1 m length of test fiber is used. In the present experiments, no index matching oil is used at the splice junction of the test fiber as it leads to "dragging" of the fibers during measurements.

2.1.3 Input Optics

The input optics associated with this study includes a 500 watt tungsten filament lamp and condenser lens, and a 3/4 meter grating monochromator (SPEX Model 1700). A pinhole at the monochromator output is imaged onto the core of a 25 meter length of graded index multimode fiber. (Core diameter: 60 μm; NA: 0.20). This input-relay-fiber transfers the input light from the master bench to a separate test bench constructed

for this study. The input light is coupled from the relay fiber to the single mode fiber under test via a butt joint, in air. Maximum coupling is achieved manually by adjustments of a 3 axis micropositioner.

2.1.4 Output Optics

The output of the single mode fiber under test is coupled to a graded multimode output-relay-fiber identical to the input-relay-fiber described in 2.1.3. Coupling is achieved in the same manner as described in 2.1.3. The output signal from the single mode fiber under test is relayed back to the master bench. A final relay is performed which transfers the output signal to the detector. The detector relay fiber is a short length of large core step index multimode fiber. Coupling is achieved as described earlier. The detector is a high sensitivity, low noise liquid nitrogen cooled germanium detector (North Coast Co., Model EO-817-L).

2.1.5 Electronic Instrumentation and Computer

The high degree of reproducibility achieved in the work performed for this contract was largely due to the employment of computer assisted experimentation techniques. Wavelength scanning, lateral and angular incremental positioning, and data taking are accomplished under computer control (Computer: DEC PDP-11/10; Interfacing: CAMAC Standard, Kinetic Systems Corp.). Electronic amplification is achieved by standard lock-in techniques (Amplifier: PAR Model 124A; Preamplifier: PAR

Model 116 Differential Preamp; Chopper: PAR Model 125A). The initial stage of low noise preamplification before the lock-in is preformed within the North Coast LN_2 cooled germanium detector assembly employing a FET first stage operating at 77 K.

Data handling, computation, and display are under computer control. Graphical display of final data is computer drawn on a X-Y recorder (HP Model 7045A).

3. Waveguide Specimens

Before a fiber is selected for design study, various measurements are done during and after fabrication to characterize the product.

Electron microprobe analysis is performed on the waveguide blank to determine the level of dopant in the core and the dopant radial profile. This measurement is performed to supply a verification of processing control and to assure that in the case of the IVD process, that there is minimum loss of dopant in the center of the core caused by "burnout." Optical micrographs are made of the blank cross section to assure that the core is concentric and non-elliptical.

The fiber attenuation is measured from 700 to 1600 nm by the standard cut-back technique and a determination of the cut-off wavelength, λ_c, is made by the transmission technique.

The refracted near field technique[20] is used to determine the refractive index profile of the fiber. From that measurement the two key parameters of core radius, a, and fractional index difference, Δ, are computed.[21,22] The equivalent step values, thus obtained, are designated $a_{(EQ.ST.)}$ and $\Delta_{(EQ.ST.)}$. From these the equivalent step value for the cutoff wavelength, $\lambda_{c(EQ.ST.)}$, is calculated. The difference between $\lambda_{c(EQ.ST.)}$ evaluated from the index profile and $\lambda_{c(TRANS)}$ obtained by transmitted power techniques on a 2 m length of fiber is in the range of 100-200 nm. The reasons for this difference are known[21,22] and the cutoff value $\lambda_{c(EQ.ST.)}$ is more appropriate for comparison of experimental data to models as

it represents the intrinsic guide parameters. In this study, the equivalent step values are used in the comparison of the experimental data with models.

A listing of the fibers evaluated in this study with the key parameters of $a_{(EQ.ST.)}$ and $\Delta_{(EQ.ST.)}$ is given in Table I. Also included are values of the cutoff wavelength determined by the refracted near field technique, $\lambda_{c(EQ.ST.)}$ and the transmitted power technique, $\lambda_{c(TRANS.)}$.

TABLE I

WAVEGUIDES STUDIED IN THIS CONTRACT

#	Fiber #	$a_{(EQ.ST.)}$ (μm)	$\Delta_{(EQ.ST.)}$	$\lambda_{c(EQ.ST.)}$ (nm)	$\lambda_{c(TRANS.)}$ (nm)
1	507205	3.6	0.0025	970	950
2	510802 (depressed clad)	4.5	0.0029	1305	1115
3	509503	4.7	0.0031	1410	1206
4	343105 (OVD)	4.0	0.0033	1240	1050
5	506902	2.3	0.0042	800	812
6	502905	2.7	0.0055	1100	1060
7	503103	2.8	0.006	1170	1140
8	503403	2.8	0.0062	1190	1210
9	509906	2.1	0.0077	990	930
10	506803	2.2	0.0095	1155	1180
11	508403	2.4	0.011	1355	1269
5A	434004 (depressed clad)	3.5	0.0042	1230	1020

4. Measurement Results

4.1 Microbend Test Data

The microbend test has been performed with various linear pin array perturbers as described in 2.1.1. Examples of the data are shown for one fiber in Figure 5. The excess attenuation due to the microbend perturbation is plotted as a function of wavelength in the range from 700-1800 nm. Depending on the cutoff wavelength of the waveguide, the LP_{11} mode loss may also be observed.

The complete set of experimental results for the microbend test is given in Appendix A.

4.2 Lateral Offset Loss Data

An example of the data collected for the lateral offset measurement is shown in Figures 6(a),(b). The raw data shown in Figure 6(b) indicates the power transmitted through the fiber for different lateral offset values. The peak of the curve indicates the zero offset position. From such raw data the excess loss (attenuation in dB) is evaluated as a function of lateral offset in microns (Figure 6(a)). The attenuation is estimated with respect to the peak value of the power. The complete set of lateral offset loss data is given in Appendix B. It should be noted that the measurements have been performed at various V-values for the majority of fibers tested.

During the course of a lateral offset measurement, the possibility exists for an inadvertant angular offset either

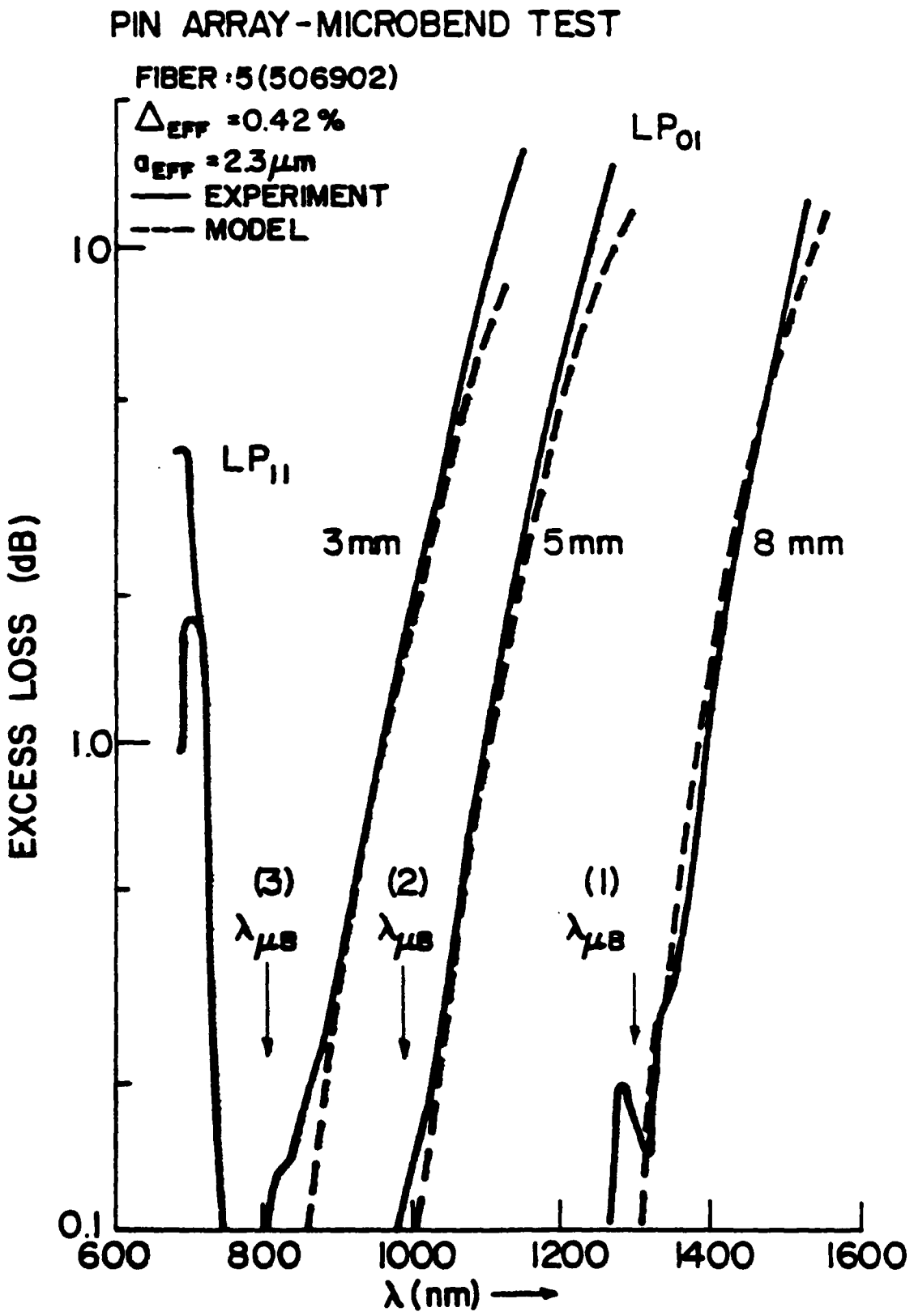
PIN ARRAY - MICROBEND TEST
FIBER : 5 (506902)
Δ_{EFF} = 0.42 %
a_{EFF} = 2.3 μm
EXPERIMENT
MODEL
LP_{01}
LP_{11}
3mm
5mm
8 mm
(3) $\lambda_{\mu B}$
(2) $\lambda_{\mu B}$
(1) $\lambda_{\mu B}$
EXCESS LOSS (dB)
10
1.0
0.1
600
800
1000
1200
1400
1600
λ (nm) ⟶

FIGURE 5

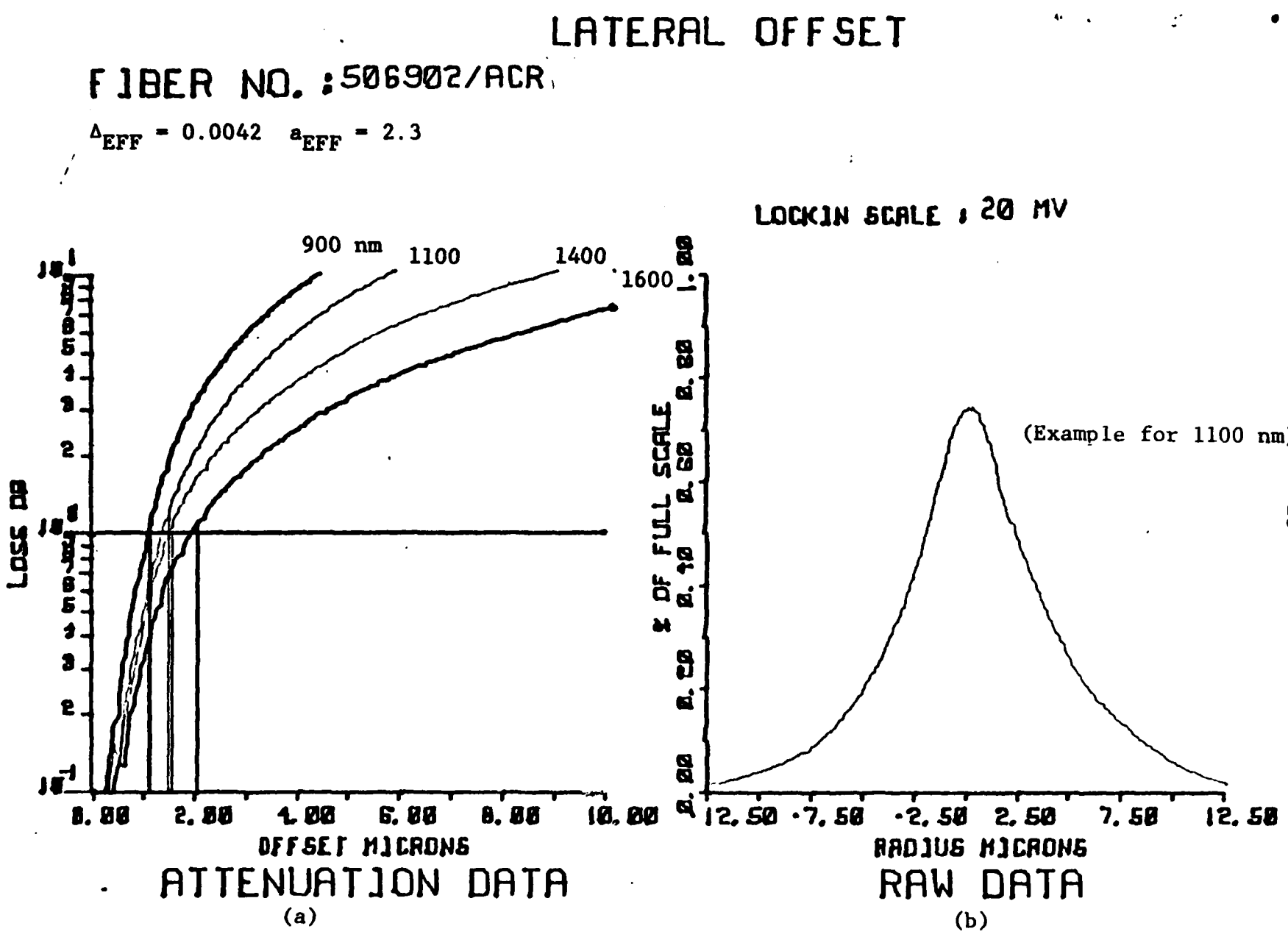

FIGURE 6
Example of lateral offset loss data.

due to fiber misalignment or the end angle being different from zero degrees. This was found to have a large, undesirable effect. With the addition of an angular misalignment, the resulting lateral offset loss curve is not symmetric. An example of this effect is presented in Figure 7 where the normalized power as a function of lateral offset is shown for various angular misalignments. As the angular misalignment direction is changed the asymmetry of the plot changes, correspondingly. In this study, much effort has been taken to minimize this type of problem.

4.3 Angular Offset Loss Data

The format used for collecting the angular offset loss data is similar to the one used for the lateral offset loss. An example of the angular offset loss data for one fiber at one wavelength is given in Figures 8(a),(b). The raw data is shown in Figure 8(b) along with a smoothed normalized plot of output power vs. angular offset.

The angular offset loss (dB) is calculated from the smoothed data and is presented in Figure 8(a).

Similar to the problem of unwanted angular misalignments compounding the lateral offset loss data we found that the inverse is also true. During the angular offset loss measurement great care had to be exercised to prevent unknown amounts of lateral offset. This is done by verifying that the lateral offset is zero after each angular offset increment. If this procedure is not followed, there could be a significant lateral offset contribution. The power vs. angular offset is narrower than it should be when lateral offset effects are not eliminated. The

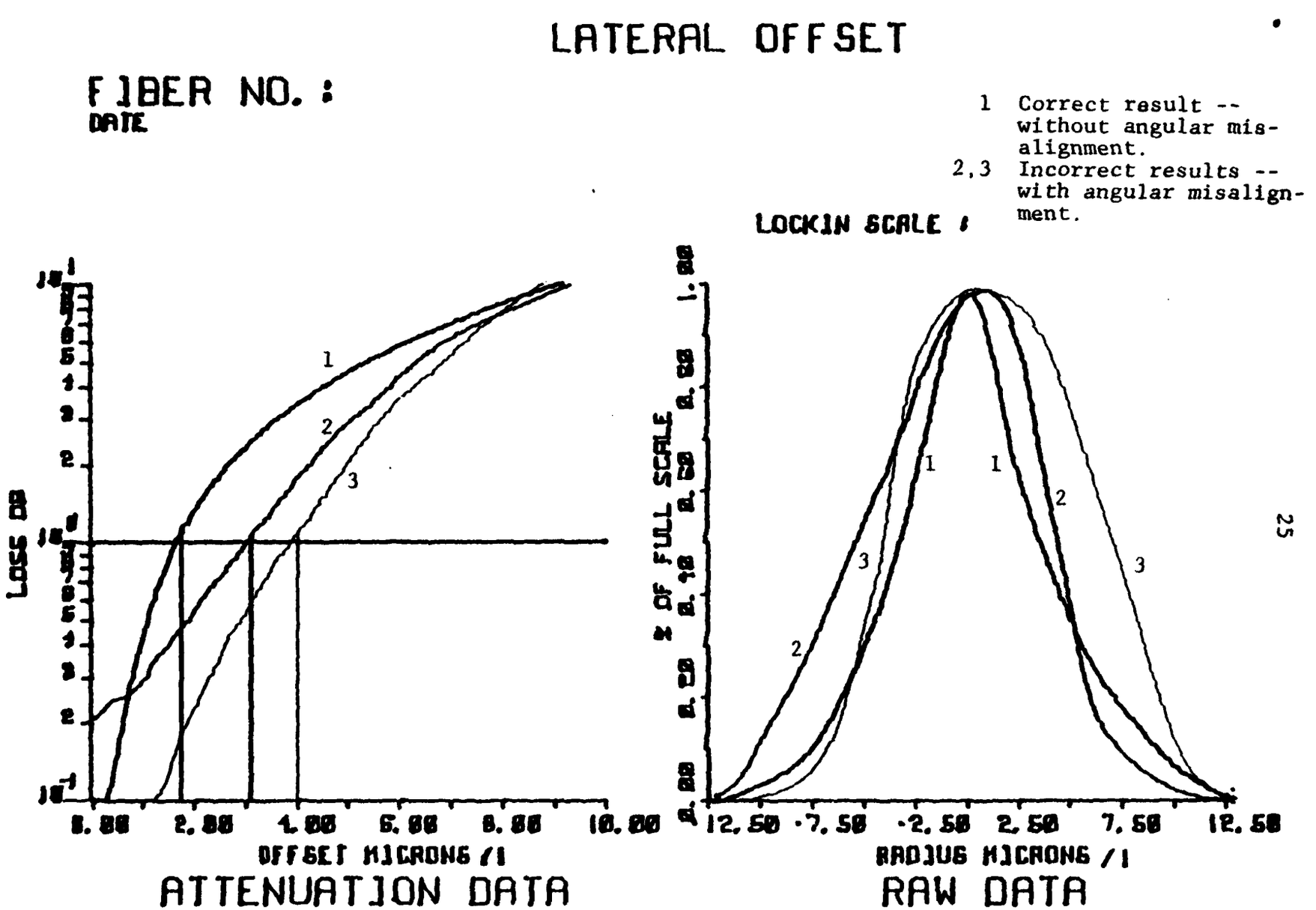

FIGURE 7

The effect of unwanted angular misalignment on the lateral offset loss measurement.

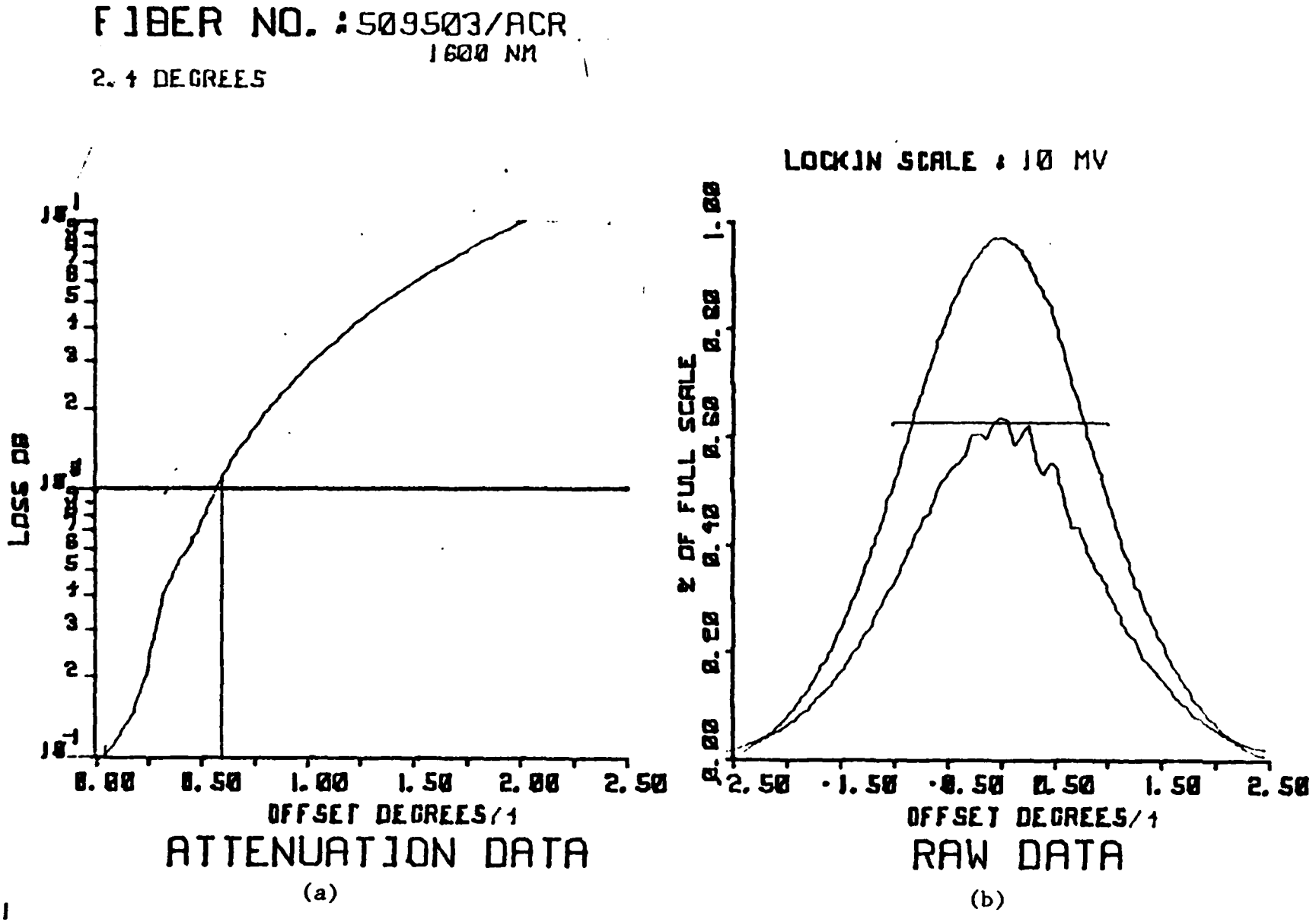

FIGURE 8

Example of angular offset loss data.

seriousness of this effect is shown in Figure 9.

Extensive angular offset data has been collected during this study and the complete set is included in Appendix C.

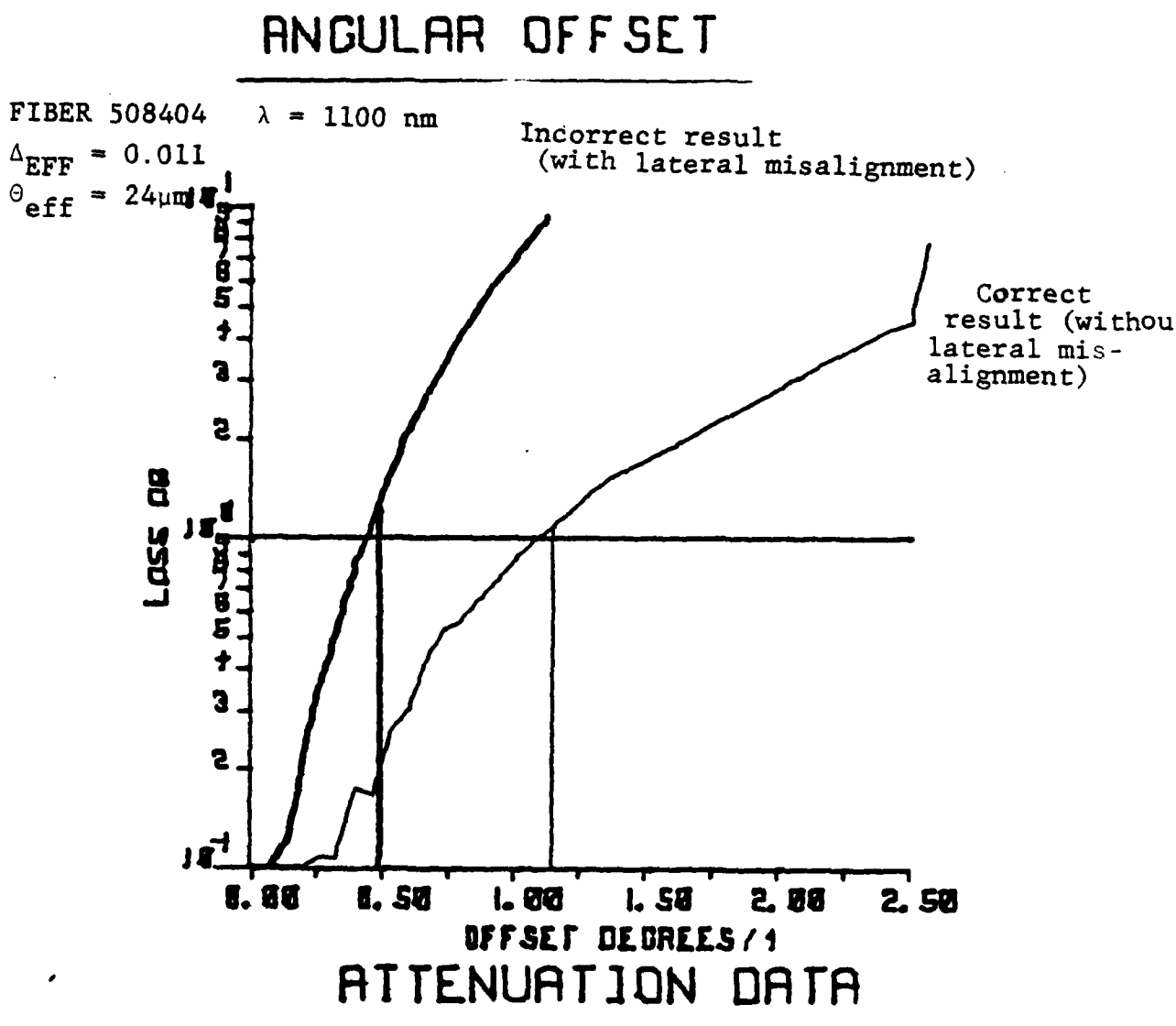

FIGURE 9

The effect of unwanted lateral misalignment on the angular offset loss measurement.

5. Analysis and Discussion

The experimental data obtained during this study is used to understand the parametric dependences of the microbend and splice losses. To obtain quantitative understanding of the loss mechanisms, a comparison of the experimental data to the models indicated in the technical proposal is done. Such analysis which helps in the identification of the key tradeoffs involved in optimizing the total system loss, is expected to be critical in the design of single mode optical communication systems.

5.1 Microbend Test

5.1.1 Model

Various microbend loss models have been developed for both multimode and single mode applications. The results depend to a great extent on the type of perturbation spectrum which is assumed. Various spectra including exponential and more general power law dependences have been considered. Some of the recent work by Furuya and Suematsu[12] indicates that the perturbation applied by the cabling process can be fitted by a Gaussian spectrum. For this reason, the experimental data obtained by the pin array test is compared to this model. In this model the microbend loss is given by,

$$\gamma_{\mu B} = xN\overline{(1/R)^2}\,\bar{W}^2\,(1/\Delta)\exp\left[-y\left(\frac{\bar{W}\,n_1}{\lambda_c}\right)^2\Delta^2\right] \quad \text{dB/km}, \qquad (3)$$

where N is the average number of bends per unit length, $\overline{(1/R)^2}$ is the mean square of the curvature of the fiber axis, $\bar{W}$ is the

correlation length, λ_c is the cutoff wavelength, n_1 is the index of the core, and Δ is the relative refractive index difference. The factors x and y depend on (λ/λ_c) and are given in Reference 12 in both graphical and tabular form. Approximate analytical forms for the factors are given below.

$$x \simeq 17485-20833\left(\frac{\lambda}{\lambda_c}\right)+7596\left(\frac{\lambda}{\lambda_c}\right)^2 \quad (4)$$

$$y \simeq 187\ e^{-4.36(\lambda/\lambda_c)} \quad (5)$$

5.1.2 Comparison of Model and Data

To facilitate the comparison of the experimental data to the Gaussian model, a computer program has been developed. An attempt is made to fit the microbend losses induced by the various pin array perturbers to the Gaussian model by varying the two parameters $\bar{W}$ and $N\left(\frac{\overline{I}}{R^2}\right)$.

An example of such a fit is shown in Figure 10. The fit between the experimental data and the microbend losses predicted by the Gaussian model was found to be very good over a wide range of attenuation values. Thus, the following important conclusions can be drawn.

- The perturbation applied by the linear pin array perturbers can be modeled quite accurately by a Gaussian spectrum.
- The parameters of the Gaussian spectrum applied by the pin arrays can be controlled by the pin spacing.

Since the random microbends introduced by the cabling process is believed to be Gaussian[12] we have found a strong indication that the linear pin array test can duplicate

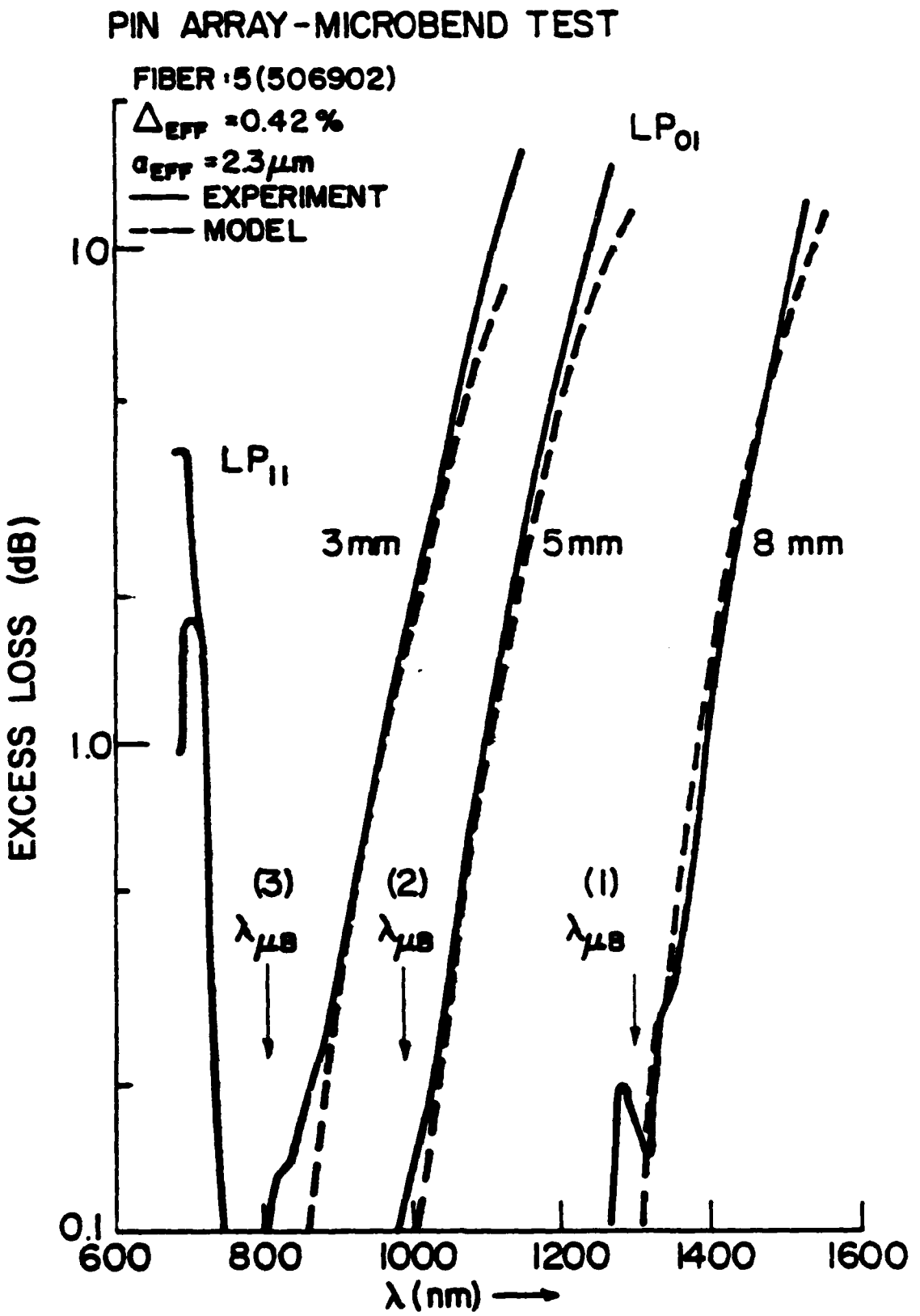

FIGURE 10
COMPARISON OF MICROBEND DATA AND GAUSSIAN PERTURBATION SPECTRUM MODEL.

the perturbation spectrum in a cabled fiber. Based on this result, the pin array perturber may be used not only for comparative evaluation of different designs, but also for a meaningful prediction of cabled fiber behavior.

From the above comparisons between the experimental data and Gaussian model the perturbation parameters for the various pin arrays have been obtained. The values are listed in Table II and indicate the average values. The variations in the perturbation values can be explained by an uncertainty in Δ and a, as measured by the refracted near field,and also by the profile variation from step values. The variation in Δ required to account for the variation in the perturbation parameters is less than 0.0005 which is within the experimental error.

TABLE II

PERTURBATION PARAMETERS FOR THE LINEAR PIN ARRAYS

Pin Spacing (mm)	$\bar{W}$ (μm)	$\overline{N(1/R^2)}$ $(\mu m)^{-3}$
8	800	1.9×10^{-20}
5	395	1.1×10^{-19}
4	320	1.4×10^{-19}
3	265	2.5×10^{-19}

The summary of microbend testing performed in this contract is shown in Figure 11. The notation, ($\lambda_{\mu B}$), denotes the wavelength at which the excess loss due to the linear pin array perturbation reaches the 0.1 dB level. In Figure 11 the Gaussian

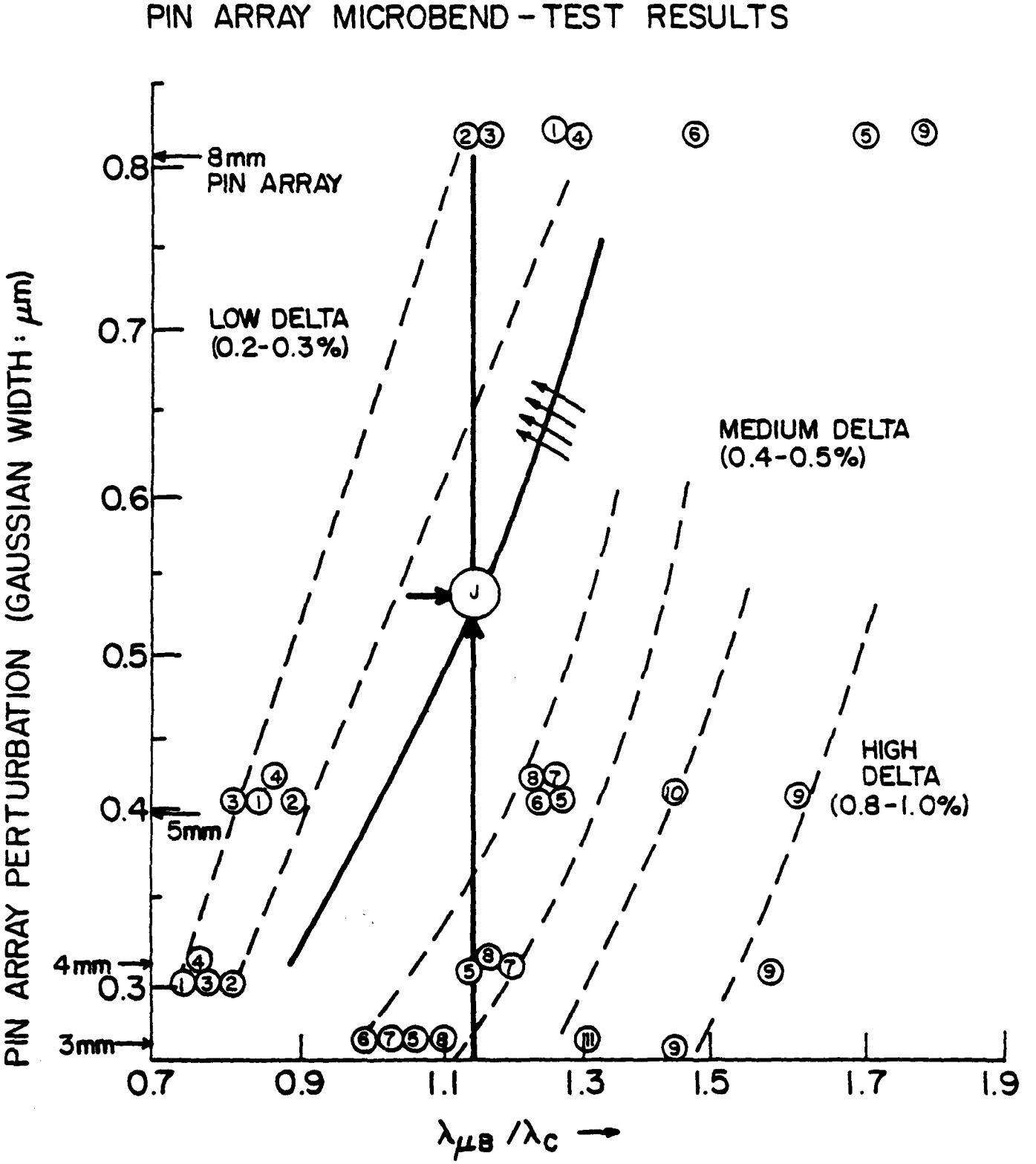

FIGURE 11
SUMMARY OF MICROBEND TESTING

perturbation width of the linear pin array is plotted against $\lambda_{\mu B}$ normalized to the cutoff wavelength. The numbers inside the data circles represent the fiber numbers listed in Table I. Based on the Δ values, the fibers can be catagorized into three broad groups of (1) low delta (0.002-0.003), 2) medium delta (0.004-0.006) and 3) high delta (0.008-0.01). The behavior within a group depends on the core radius. Results presented in the form of Figure 11 allows a comparative study to be made of various fiber designs from which a range of fiber parameters can be picked for an optimum design. To obtain a realistic design the expected value of cable perturbation is also shown (circle with letter "J").

This point is arrived at based on the observation that the cabled perturbation evaluated by Furuya et.al. leads to the microbend edges with $(\lambda_{\mu B}/\lambda_c) \sim (1.0\text{-}1.1)$ for fibers with $\Delta \lesssim .003$. The solid line drawn through the circle J , divides the "safe" designs from "unsafe" designs for this level of cabled perturbation. It should be pointed out that in arriving at the dividing line, a margin of safety of about 100 nm has been included. This allows for any variation that may be present in processing the fiber and cable.

Based on the above analysis, the optimum designs from a microbend point of view require index values $\Delta \gtrsim 0.003$ and core radii $a < 4.0$ μm. It should be pointed out that lower Δ values could be allowed for cable structures which are improved in design over the one cited in reference (12). As will be discussed later,

the lowest Δ design consistent with the microbend loss requirement, leads to the optimum design for 1300 nm operation.

5.2 Splice Loss Tests

5.2.1 Model

For comparison with experimental data, the model developed by Gambling and co-workers[16,17] has been used in this work. Considerable simplification was achieved in their work by assuming a Gaussian field distribution to replace the HE_{11} mode. To compare the model with results obtained over a wide range of V-values, the variation of normalized spot size w with V has been incorporated in this study.

The expressions for lateral and angular offset loss given in Reference 16 have been rewritten in the forms given below.

$$\text{Lateral offset loss:} \quad \gamma_{LAT} = \frac{2.17}{w^2} \left(\frac{\delta}{a}\right)^2 \text{ (dB)} \tag{6}$$

$$\text{Angular offset loss:} \quad \gamma_{ANG} = 1.09\, w^2 V^2 \left(\frac{\alpha}{\sqrt{\Delta}}\right)^2 \text{ (dB)} \tag{7}$$

where the normalized spot size is given by,

$$w = \frac{1}{\sqrt{2}} \left(0.65 + \frac{1.62}{V^{3/2}} + \frac{2.88}{V^6}\right) , \tag{8}$$

and, δ is the lateral offset, α is the angular offset, a is the core radius, and V is the normalized frequency. The parameters $\left(\frac{\delta}{a}\right)$ and $\left(\frac{\alpha}{\sqrt{\Delta}}\right)$, which appear explicitly in the equations for splice loss, will be used later to form a concise graphical summary of an analysis comparing the theoretical model with experimental data.

5.2.2 Comparison of Model and Data

5.2.2.1 Lateral Offset Loss

To facilitate the comparison of the model with data, a computer program has been developed which calculates the offset losses using the fiber parameters and the experimental conditions of the test. Thus a direct comparison is made of the model with data. An example of such a comparison is shown in Figure 12. The comparisons between data and experiment are made at three wavelengths for the lateral offset test. The comparison in this case indicates good agreement between the model and experimental data up to excess loss levels of 2-3 dB. Beyond this level, experimental splice loss does not fall off as rapidly as predicted by theory. Based on these observations, it can be concluded that:

- The Gaussian beam approximation is sufficiently accurate up to at least the 2.0 dB loss level.
- The departure between model and data beyond the 2 dB level may be either due to a non-Guassian field distribution in the wings, to higher order mode contributions, or, to reflections at the joint.

A summary of the lateral offset loss characteristics of the fibers tested and the comparison with the model is presented in Figures 13 and 14 where the parameter (δ/a) is plotted vs. (λ/λ_c) for excess losses of 1 dB and 0.25 dB, respectively. The numbers in the data circles represent the fiber numbers listed in Table I. The solid curve represents the average of the experimental data

FIBER: 509906/ACR

Δ_{EFF} = 0.0077 a_{EFF} = 2.1 μm

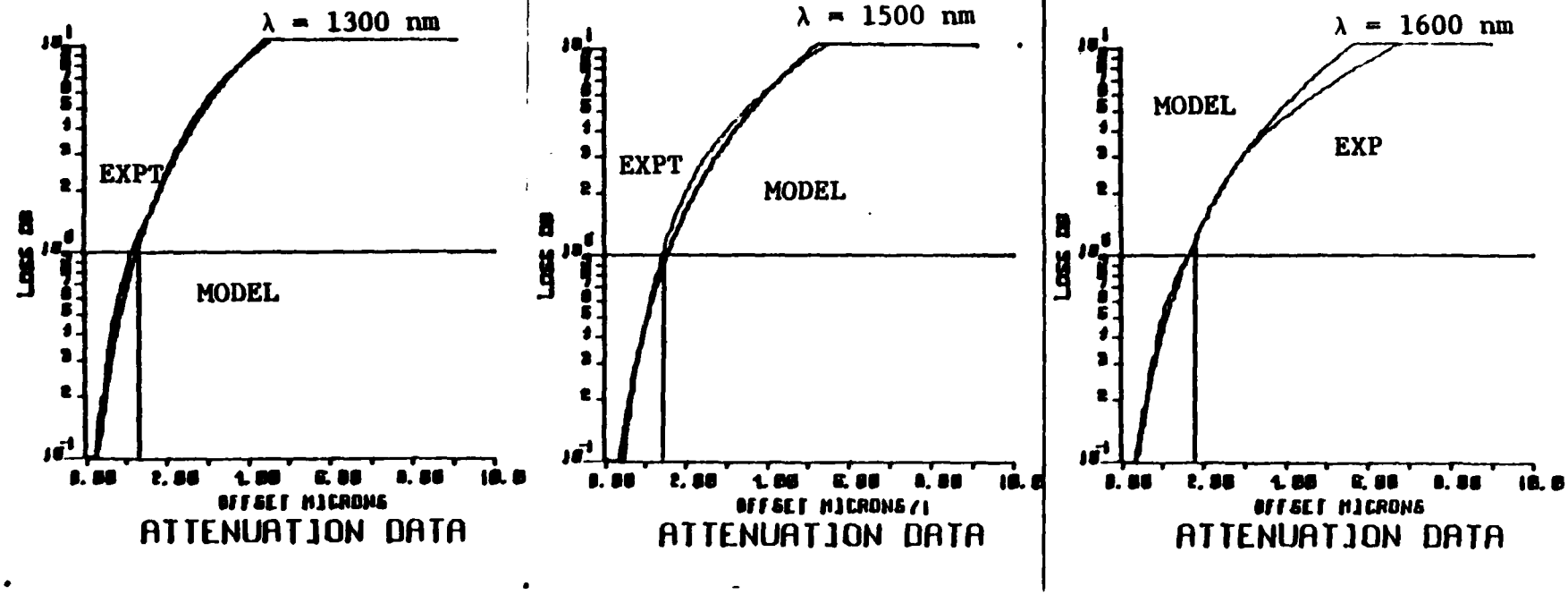

LATERAL OFFSET

COMPARISON OF MODEL AND EXPERIMENT

FIGURE 12

OFFSET SENSITIVITY: COMPARISON OF DATA AND MODEL

1.0 dB EXCESS LOSS

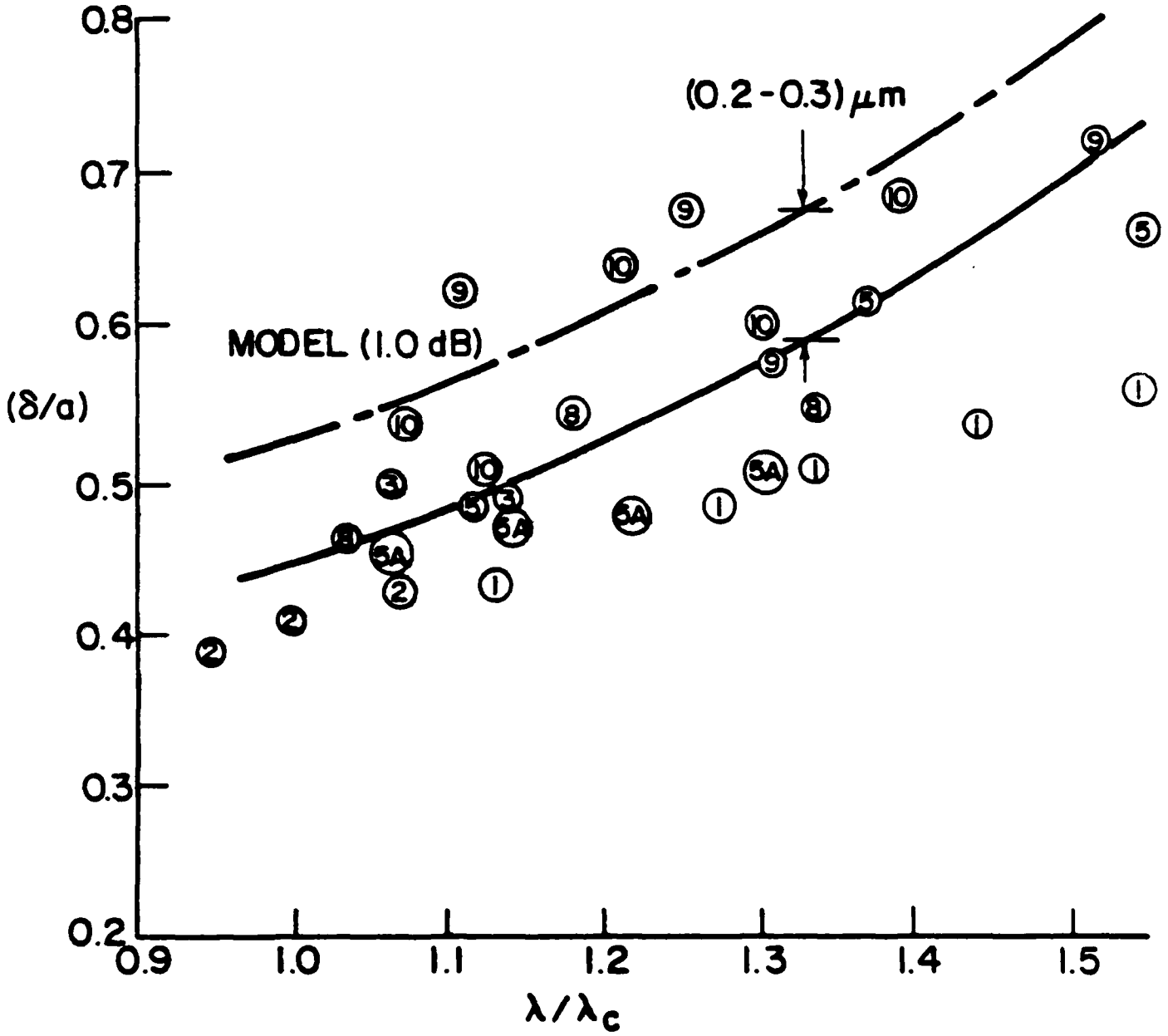

FIGURE 13

whereas the broken line represents the model. In Figure 13, representing 1 dB excess loss, the difference between the data and model is equivalent to an under estimation of the lateral offset by approximately 0.2-0.3 μm whereas in Figure 14, it corresponds to a difference of 0.15-0.25 μm. Such small differences lead to excess losses less than 0.15 dB and are thus within the experimental accuracy of the system. For example, the differences of the above magnitude can be introduced by scanning 0.1-0.2 μm below the core diameter.

Apart from this small shift, the variation of the parameter (δ/a) with (λ/λ_c) follows the trend predicted by the model. Based on this analysis, it can be concluded that the model and the data fit within the experimental accuracy over a wide range of Δ, a and wavelengths.

The representation given in Figures 13 and 14 allows the identification of design parameters necessary to keep the lateral offset loss below a certain value. For example, for lateral offset loss less than 0.25 dB and a waveguide operating at $\lambda/\lambda_c \simeq 1.15$ (i.e. 1310 nm operation for waveguide with $\lambda_c \sim 1150$ nm), the parameter (δ/a) has an experimental value of 0.215. This indicates that if a splice tolerance of 0.5 μm is possible, the core radius has to be greater than 0.5/0.215 i.e. $a \gtrsim 2.33$ μm. Similar estimates can be made for other possible splice loss tolerances.

The important conclusion of the analysis above is that for splice loss levels less than 0.25 dB, with practical splice misalignment of 0.5 μm, the optimum designs require core radii $a \gtrsim 2.4$ μm.

5.2.2.2 Angular Offset Loss

The analysis of angular offset loss is made in a fashion similar to the case of lateral offset loss. A summary of the data is given in Figure 15, where the parameters, $(\alpha/\sqrt{\Delta})$, is plotted as a function of (λ/λ_c) for the fibers analyzed. The solid line corresponds to the values predicted by the model. The dotted line corresponds to the line that represents the average of the data points. There appears to be a systematic offset between model and data of approximately 0.6 degrees. The scatter within the data is, on the average, 0.26 degrees, which corresponds to the offset step size used in the experiment.

The data indicates that the angular offset tolerance even for a fiber with $\Delta \sim 0.003$ is ~2 degrees for a 1 dB excess loss and approximately 1 degree for 0.25 dB excess loss. These tolerances are sufficiently large that angular offset loss is not expected to be a significant factor for the waveguide designs being considered for most applications.

ANGULAR OFFSET: COMPARISON OF MODEL AND DATA
(1 dB EXCESS LOSS)

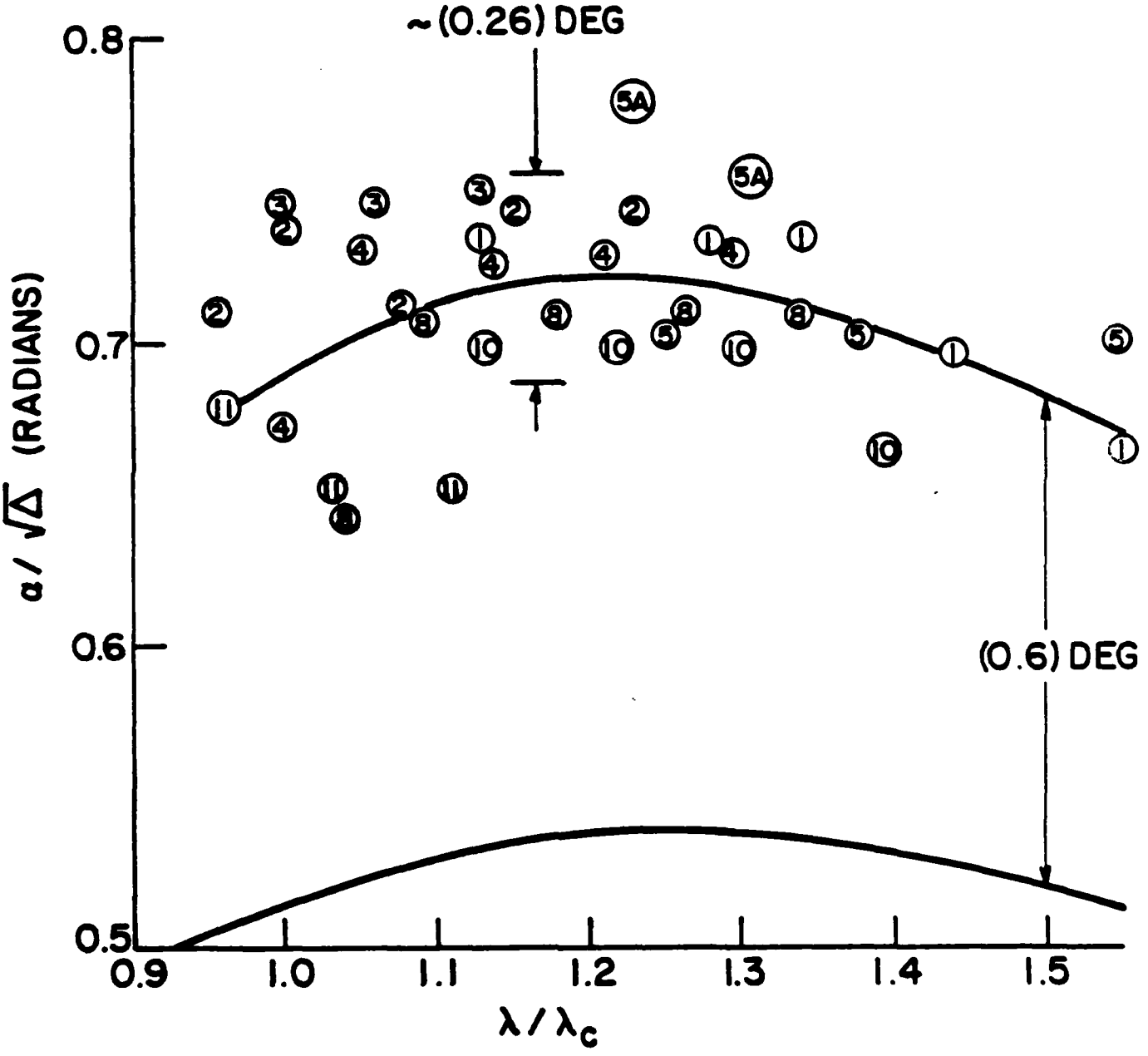

FIGURE 15

6. Deliverables

In addition to the final report presenting the experimental data and analysis, two 1.1 kilometer lengths of two differently designed single mode waveguides are provided to the sponsor. The two waveguide designs were chosen as a result of this study and are within the optimum design as described in Section 5. The values of core radii and fractional index differences that were picked are near two extremes within the defined region. The fiber identification numbers and the pertinent properties are given in Table III. Fiber numbers 3461-03 and -04 are 1.1 km lengths of OVD (outside vapor deposition) processed waveguide. They represent the low Δ, large radius extreme in the optimum design region. The index profile is the standard step-index type with some inevitable profile rounding caused by several phenomena, principally, high temperature diffusion of core dopant, which occur during the various fabrication steps.

Fiber numbers 4350-03 and -06 are 1.1 km lengths of IVD (inside vapor deposition) processed waveguide. They represent the high Δ, small radius extreme of the optimum design region. Additionally, the index profile for this design is chosen to be of the depressed cladding type. The reason for this choice is to allow a high Δ for increased protection against severe cases of cable induced microbending without suffering the penalty of an increase in fiber attenuation due to intrinsic scattering. A schematic of the profile for fiber numbers 4350-03 and -06 is shown in Figure 16.

TABLE III

Contract Deliverable Fibers

Length: 1.1 km each

	OVD Process		IVD Process	
Fiber No. / Parameter	346104	346103	435003	435006
a_{EFF}	4.0 μm	4.3 μm	3.2 μm	2.9 μm
Δ_{EFF}	0.0035	0.0035	0.0048	0.0055
$\lambda_c^{EQ\cdot ST}$	1299 nm	1385 nm	1206 nm	1182 nm
$\lambda_c^{Trans.}$	1130 nm	1140 nm	1048 nm	1018 nm
γ_{900}	1.8 dB/km	2.0 dB/km	2.49 dB/km	2.56 dB/km
γ_{1300}	0.44 dB/km	0.63 dB/km	0.66 dB/km	0.76 dB/km
γ_{1600}	0.31 dB/km	0.36 dB/km	0.32 dB/km	0.44 dB/km

DELIVERABLE FIBERS #4350-03, -06
DEPRESSED CLADDING DESIGN

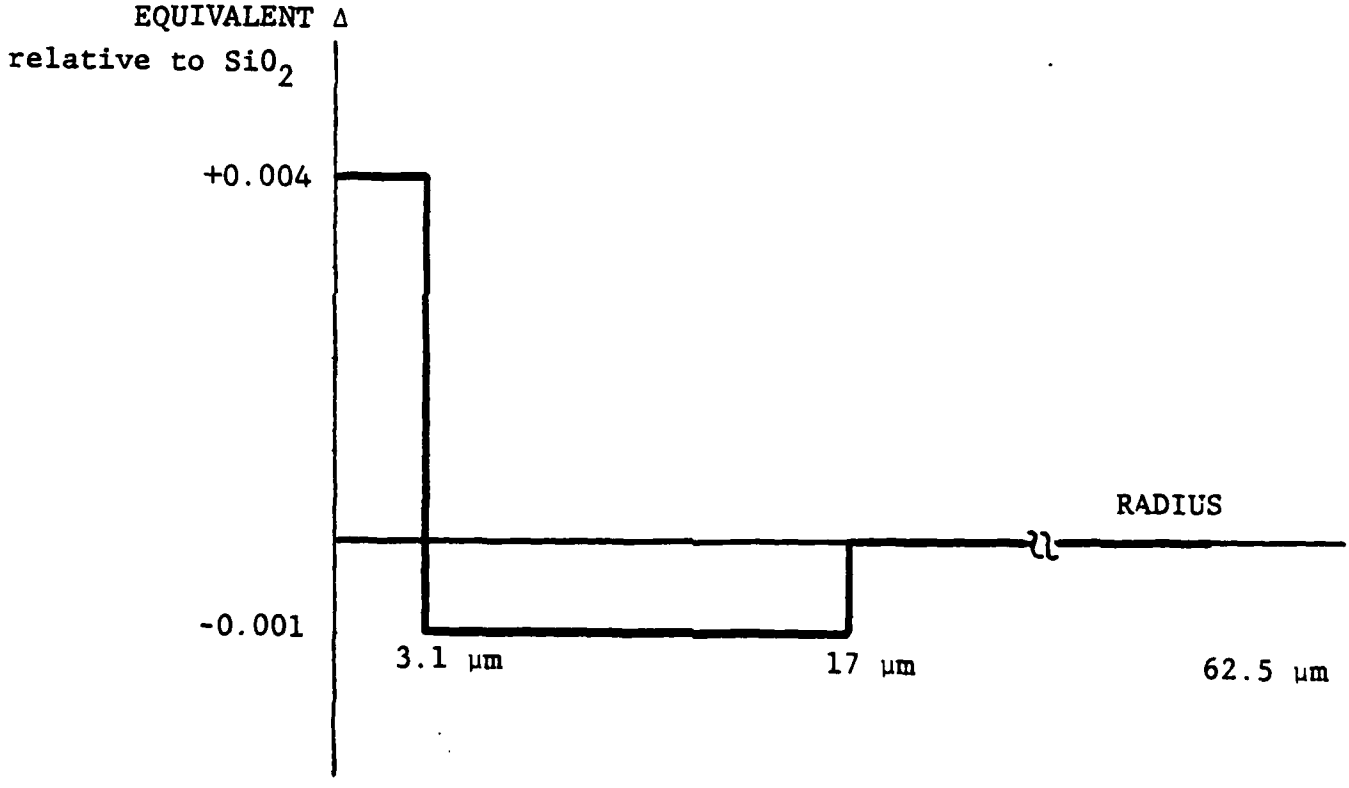

FIGURE 16

Fibers of both designs, chosen for the contract deliverables, have cut-off wavelengths ranging from 1018 to 1140 nm, as measured by the transmitted power technique on short lengths. This should be appropriate for 1300 nm single-mode operation. The fibers are acrylate coated for good strength protection and have been screen tested, on-line, at 25 KPSI (IVD) and 50 KPSI (OVD). The performance target, as listed in the original Technical Proposal, also called for $\gamma_{1550} < 0.8$ dB/km. It will be noted in Table that all four deliverable fibers are well below the target attenuation with values of 0.34 avg. (OVD) and 0.38 dB/km avg. (IVD).

7. Summary and Conclusions

This investigation is a broad based study of some of the practical factors affecting overall single-mode waveguide loss. The key objective is to determine the optimum range of design parameters which simultaneously minimizes splice, cabling, and intrinsic waveguide losses.

Step-index, single mode fibers were fabricated having a range of the key parameters (core diameter and fractional index difference) which is considered wide enough to accommodate the majority of applications. The losses produced by microbending and splicing were determined quantitatively and a comparison made with existing theories.

Resulting from this study an optimum design criteria is made. Fibers, of two designs, were fabricated, in long lengths, as deliverables to the sponsor.

The following is a summary of specific accomplishments and conclusions.

7.1 Test Fiber Fabrication

Eleven IVD ("inside" process) fibers and one OVD ("outside" process) fiber were fabricated on a best-effort-basis. The ranges of the key parameters that were achieved are

Core diameter: 4.2-9.4 μm
Fractional index difference: 0.0025-0.011

The fibers consist of a germania-silica binary core and a silica cladding. Outside diameter is nominally 125 μm and all fibers were coated with a protective acrylate compound.

Qualification measurements performed before accepting fibers into this program included standard attenuation measurements, with a determination of cutoff wavelength by the transmitted power technique; and, specialized composition and refractive index measurements. From the latter measurements, values were obtained for effective core diameter and effective fractional index difference.

7.2 Microbend Loss

7.2.1 Procedure

Apparatus was specifically designed and constructed for this program. Four linear pin arrays each of different pin spacings were used to measure the microbend loss of each fiber as a function of perturbation parameters and also as a function of wavelength in the range from 700 to 1800 nm.

7.2.2 Results

Linear pin array microbending loss data fits the Gaussian power spectrum model over the complete range of design parameters tested. A computer analysis of data has led to the following design criteria to minimize cabling microbend loss:

Fractional index difference: $\Delta > 0.003$
Core diameter : $2a \leq 8.0\ \mu m$

The measurements and analysis of microbend losses in this program have provided the first good correlation between a laboratory test on fibers and previously reported cabling results.

7.3 Splice Losses

7.3.1 Lateral Offset Loss

7.3.1.1 Procedure

Test apparatus was designed and built specifically for this program. A system with a number of degrees

of freedom was built to accurately and reproducibly measure the lateral offset loss of all fibers. Data were taken, under computer control, over the offset range of ± 12.5 μm from the zero offset position in 0.1 μm increments. In addition, measurements were made at a number of different wavelengths covering an extended range of V-values.

7.3.1.2 Results

A comparison was made of data with a simplified theoretical model based on the replacement of the HE_{11}-modes by an equivalent Gaussian field. The measured lateral offset loss follows the theoretical model to within 0.2 dB. The data comfirmed that loss increases with decreasing core diameter and increasing fractional index difference.

The analysis has led to the following design criteria to minimize lateral offset loss in splicing:

Fractional index difference: $\Delta \leq 0.006$
Core diameter : $2a \geq 4.8$ μm

7.3.2 Angular Offset Loss

7.3.2.1 Procedure

The test apparatus, described in 5.3.1.1, was also used for angular offset loss measurements. Data were taken over a ± 10 degree range from the zero offset position in 0.25 degree increments. Measurements were made at various wavelengths. To maximize accuracy and reproducibility the test procedure is automated under computer control.

7.3.2.2 Results

The analysis of angular offset loss is made similarly as in the case of lateral offset loss. The same theoretical model, based on an equivalent Gaussian field, was used to compare measurement with model.

The measured angular offset loss was found to be ~50% less than theoretically predicted. The cause may be fiber end angle effects. However, the offset loss due to an angular misalignment was not found to be significant. An example of this relatively high tolerance was shown for a $\Delta = 0.003$ fiber. Angular offsets necessary to produce 0.25 and 1.00 dB excess losses were measured at ~1 and ~2 degrees, respectively. These tolerances are sufficiently high that angular offset loss is not expected to be a significant factor for waveguide designs being considered in most applications.

7.4 Summary of Fiber Design Criteria

Based on the analysis of measurements performed in this contract the simultaneous minimization of all single mode loss sources, is achieved within the design range, $0.003 < \Delta < 0.006$ and 5.6 μm < core diameter < 8 μm. A more exacting definition of parameters within this range will depend critically upon the actual perturbation spectrum introduced by the cabling process as well as fiber manufacturing variability of the key parameters. The present study allows extrapolation to the correct design as additional cabling data becomes available. Additionally it was identified that the single mode fiber loss spectrum will provide a way of inferring the cable perturbation power spectrum.

7.5 Contract Deliverables

As a final product of the study, 4 km of low-loss single mode fiber made by both the "inside" and "outside" vapor phase oxidation processes were fabricated. Two kilometers each of two design matrix points were prepared: 1) $\Delta \simeq 0.004$, $2a \simeq 8.0$ μm and 2) $\Delta \simeq 0.005$, $2a \simeq 6$ μm. Both fibers have a cutoff wavelength, $\lambda_c \approx 1100$ nm as determined by short length transmittance. This should be appropriate for 1300 nm operation. The first of these is believed to be the lowest Δ-value acceptable given the present level of cable perturbation and fiber processing variations. With improvement in cabling and processing it is expected that the $\Delta = 0.003$ design range extreme will be optimum for telecommunication applications. The other design range extreme, is approximated by the second pair of fibers. These would be expected to be useful if cabling perturbations are more severe.

7.6 Future Study Recommendations

Since the cable power spectrum has been shown to have such a dramatic effect on loss and fiber design, the present work suggests that a future study is required to determine the power spectrum associated with different cable designs and cable processes. Single mode fibers of a few designs should provide a powerful tool for determining the cable power spectrum.

8. References

1. B. J. Ainslie, C. R. Day, P. W. Frame, K. J. Beales and G. R. Newns, Electron. Lett. 15, 411 (1979).
2. C. Lin, L. G. Cohen, W. G. French and H. M. Presby, J. Quantum Elec., EQ-16, 33 (1980).
3. R. Olshansky, Corning Glass Works, private communication (1979).
4. T. Miya, Y. Terunuma, T. Hosaka and T. Miyashita, Electron. Lett. 15, 106 (1979).
5. W. French and G. Tasker, Topical Meeting on Optical Fiber Transmission, Williamsburg, Va. (1975).
6. M. G. Blankenship, D. B. Keck, P. S. Levin, W. F. Love, R. Olshansky, A. Sarkar, P. C. Schultz, K. D. Sheth, R. W. Siegfried, Topical Meeting on Optical Fiber Communications, paper PD-3, Washington (1979).
7. D. B. Keck, P. C. Schultz, and R. D. Maurer, Appl. Phys. Lett. 22, 307 (1973).
8. R. Olshansky, Review of Modern Physics, 51, #2, 341 (1979).
9. H. Matsumura, T. Katsuyama and T. Suganuma, p. 49, Proceedings of the 6th European Conf. on Optical Communications, York, U. K. (1980).
10. K. Peterman, Electron. Lett. 12, 107 (1976).
11. R. Olshansky, Second European Conference on Optical Fiber Communication, Paris (1976).

12. K. Furuya and Y. Suematsu, Fifth European Conference on Optical Fiber Communication, Amsterdam (1979); and, Applied Optics 19, #9, 1493, May 1, 1980.

13. Y. Katsuyama, Y. Mitsunaga, S. Moduzuki, A. Kawana, K. Ishihara, H. Tsuchiya; IECE Technical Group Meeting, OQE 78-43, June 1978.

14. E. A. J. Marcatili and S. E. Miller, Bell Syst. Tech. J., 48, 2161 (1969).

15. F. P. Kapron, D. B. Keck and R. D. Maurer, Appl. Phys. Lett. 17, 423 (1970).

16. W. A. Gambling, H. Matsumura and C. M. Ragdale, Electron. Lett. 14, 491 (1978).

17. W. A. Gambling, H. Matsumura and A. G. Cowley, Electron. Lett. 14, 54 (1978).

18. P. C. Schultz, "Progress in Optical Waveguide Process and Materials," Appl. Optics 18, #21 (1979).

19. V. A. Bhagavatula, paper TUK5, Integrated Optics and Optical Communications Conf., San Francisco, CA (1981).

20. W. J. Stewart, Proc. of the Conference on Integrated Optics and Optical Communications (C2.2) 1977.

21. W. J. Stewart, Electron. Lett. 16, 380 (1980)

22. R. M. Hawk, private communication, Corning Glass Works.

9. Participants in this Investigation

The authors of this report wish to acknowledge the valuable efforts of the following people in the Research and Development Division at Corning Glass Works.

From the Optical Waveguide Development:

Paul E. Blaszyk

Arnab Sarkar

Donald J. Walter

From the Applied Physics Department:

Richard L. Anderson

Francis A. Annunziata

Robert M. Hawk

Joseph C. Sonner

From the Instrumental Analysis Research Department:

Stephen J. Tong

Robert F. Spaulding

APPENDIX A

Microbend Test Data

Excess loss as a function of wavelength comparison of experimental data (E) to Model (T).

MICROBEND TEST

FIBER NO.: 507205

PIN ARRAY = 4 MM

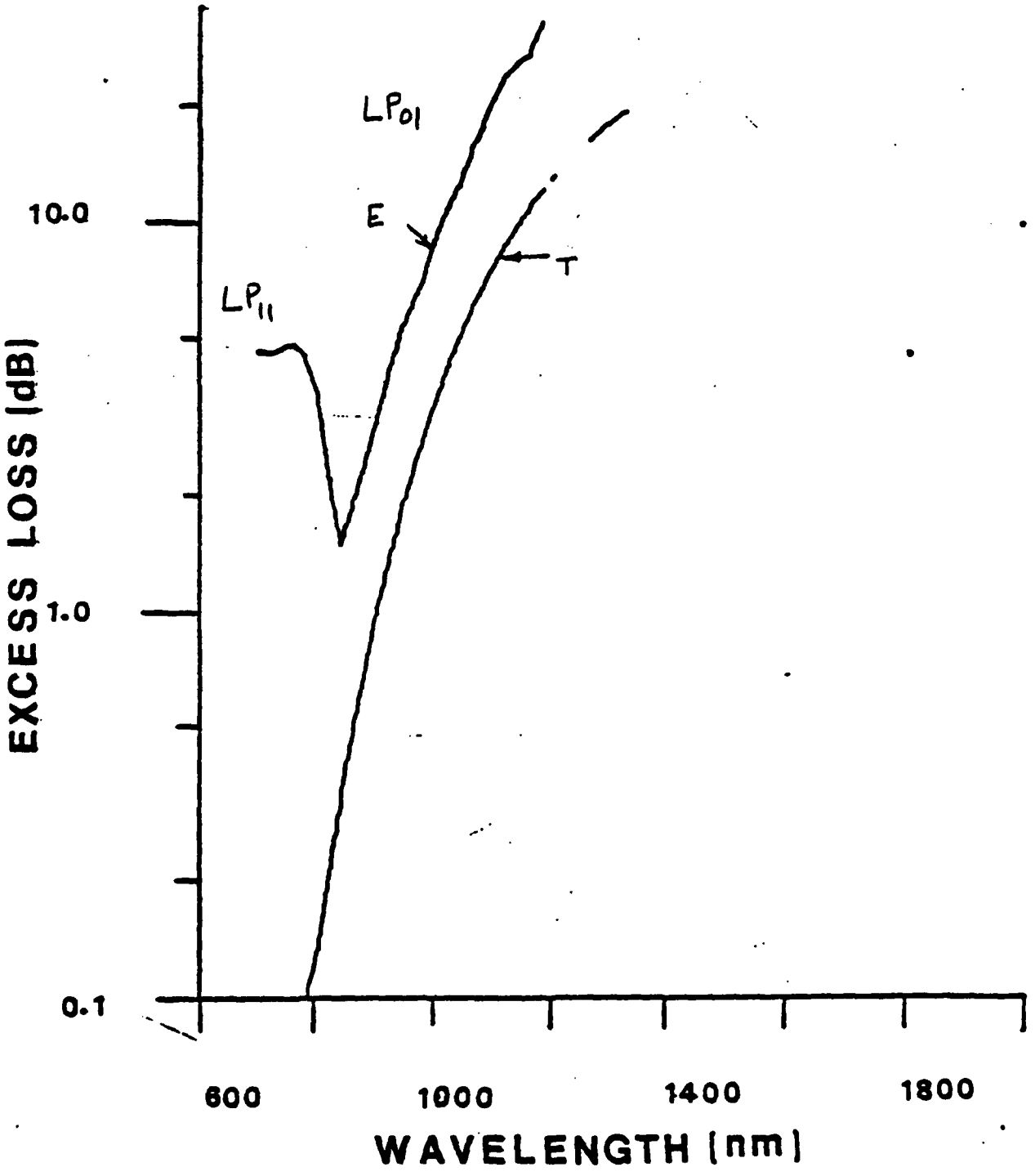

MICROBEND TEST

FIBER NO.: 507205

PIN ARRAY = 5 MM

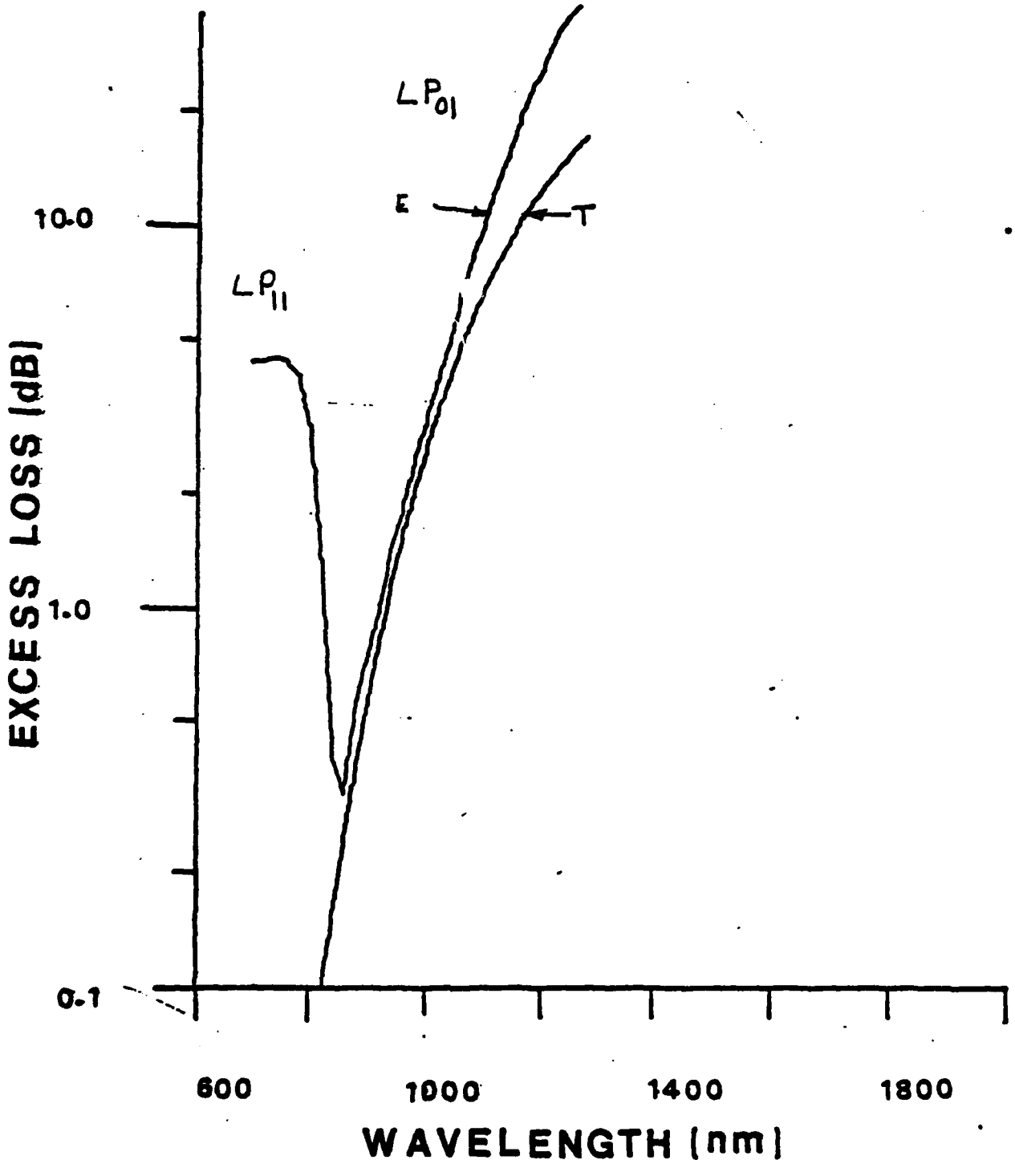

MICROBEND TEST

FIBER NO.: 507205

PIN ARRAY = 8 MM

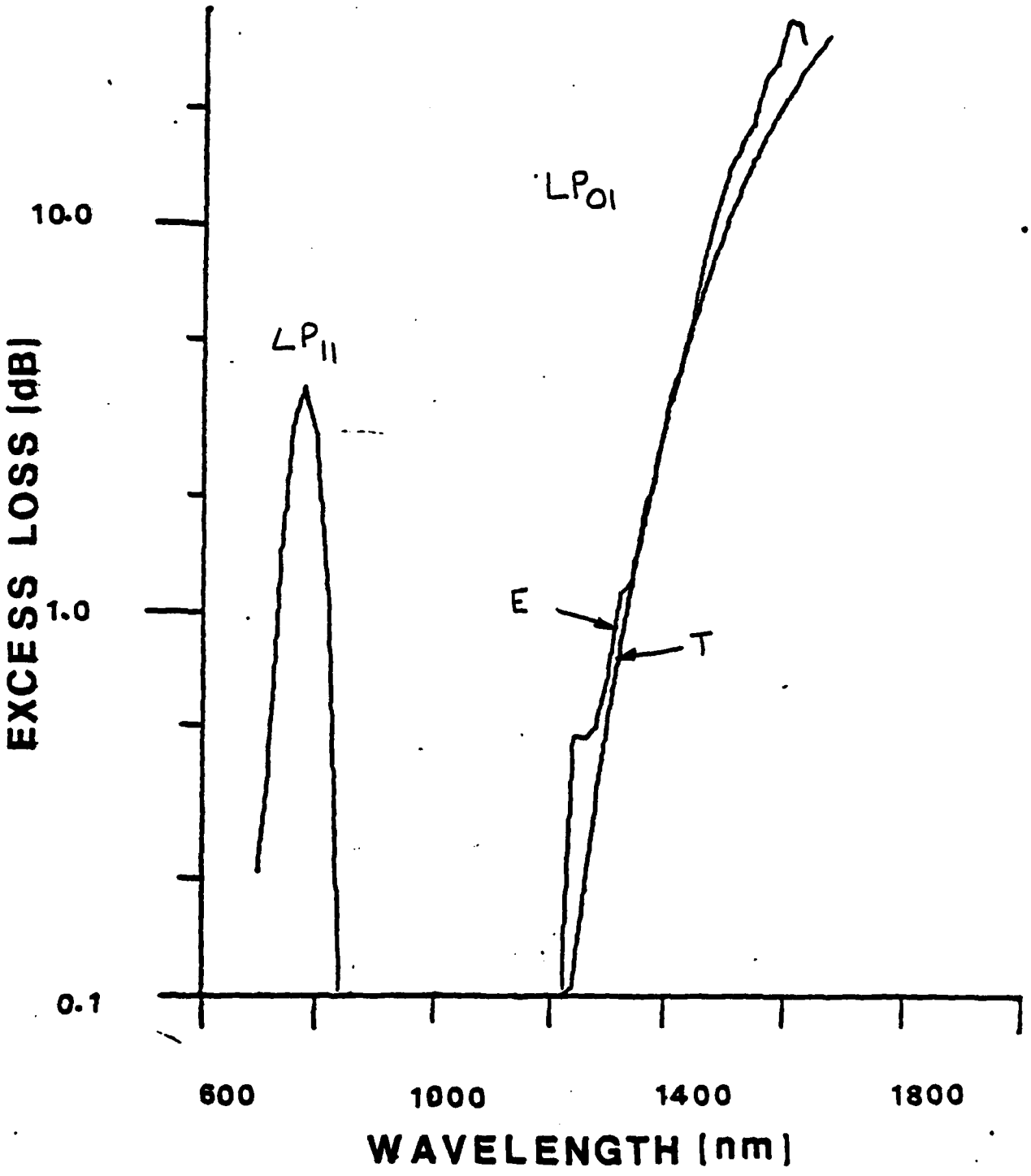

MICROBEND TEST

FIBER NO.: 5T0802

PIN ARRAY = 3 MM

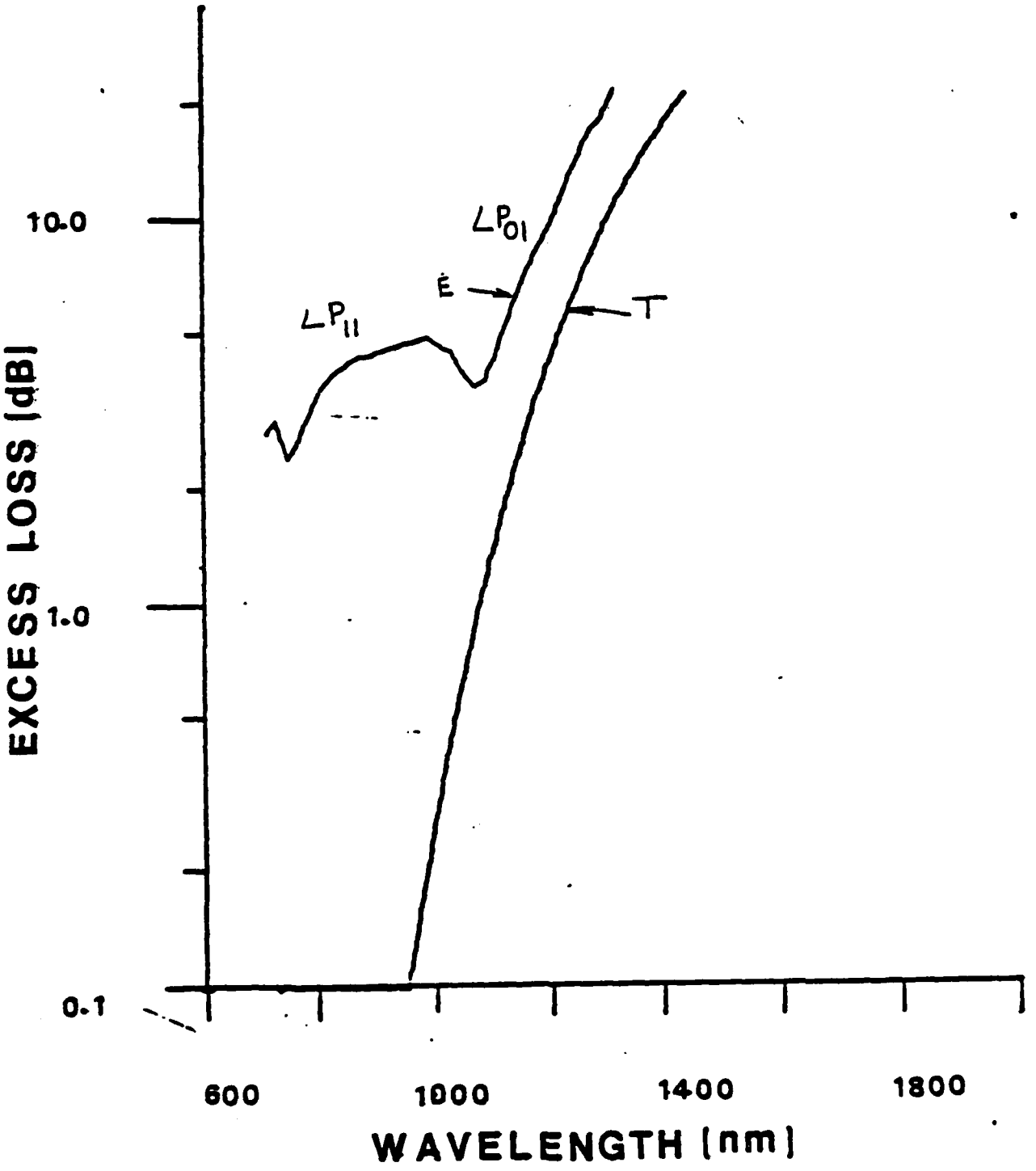

MICROBEND TEST

FIBER NO.: 510802

PIN ARRAY = 4 MM

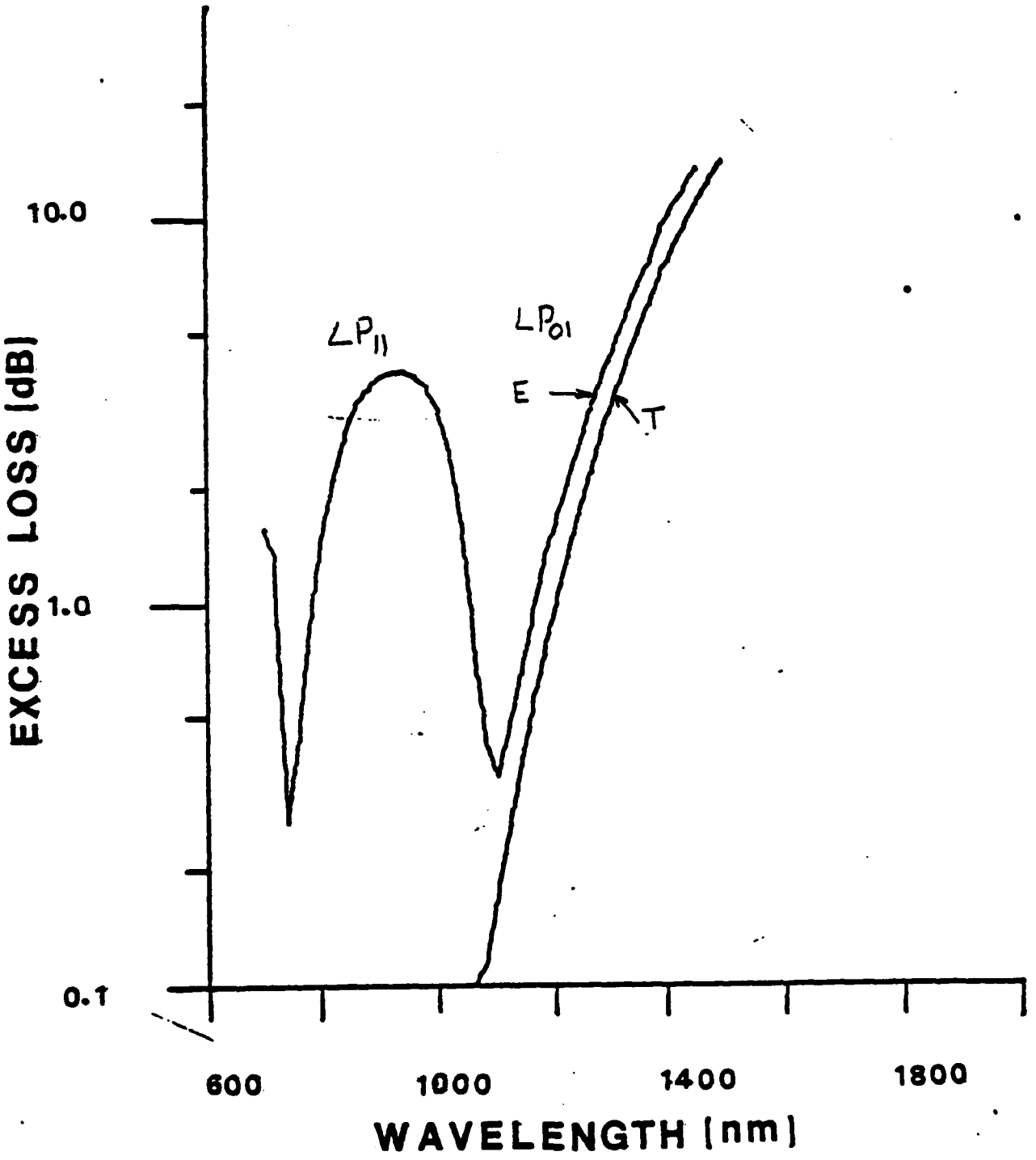

MICROBEND TEST

FIBER NO.: 510802

PIN ARRAY = 5 MM

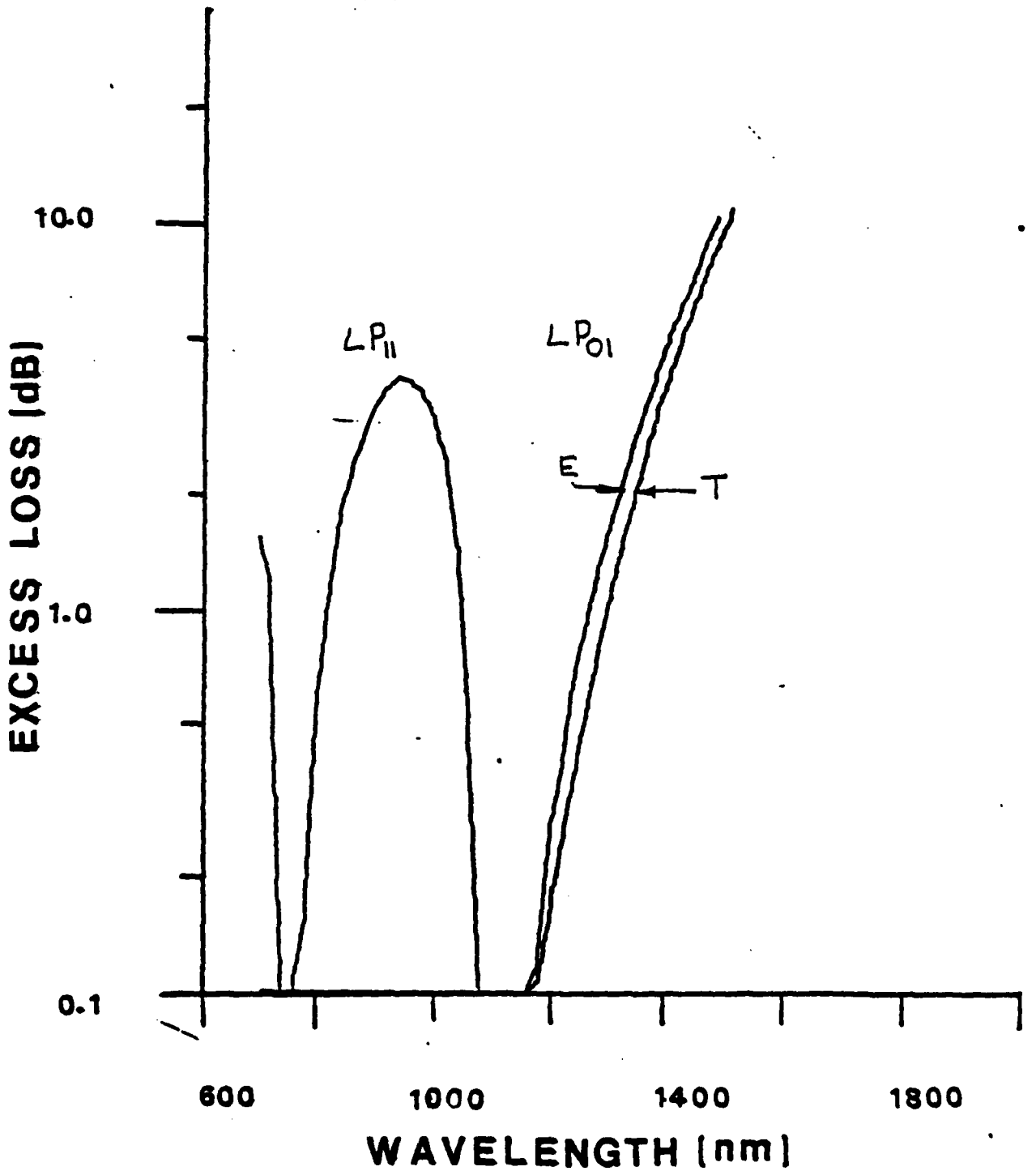

MICROBEND TEST

FIBER NO.: 510802

PIN ARRAY = 8 MM

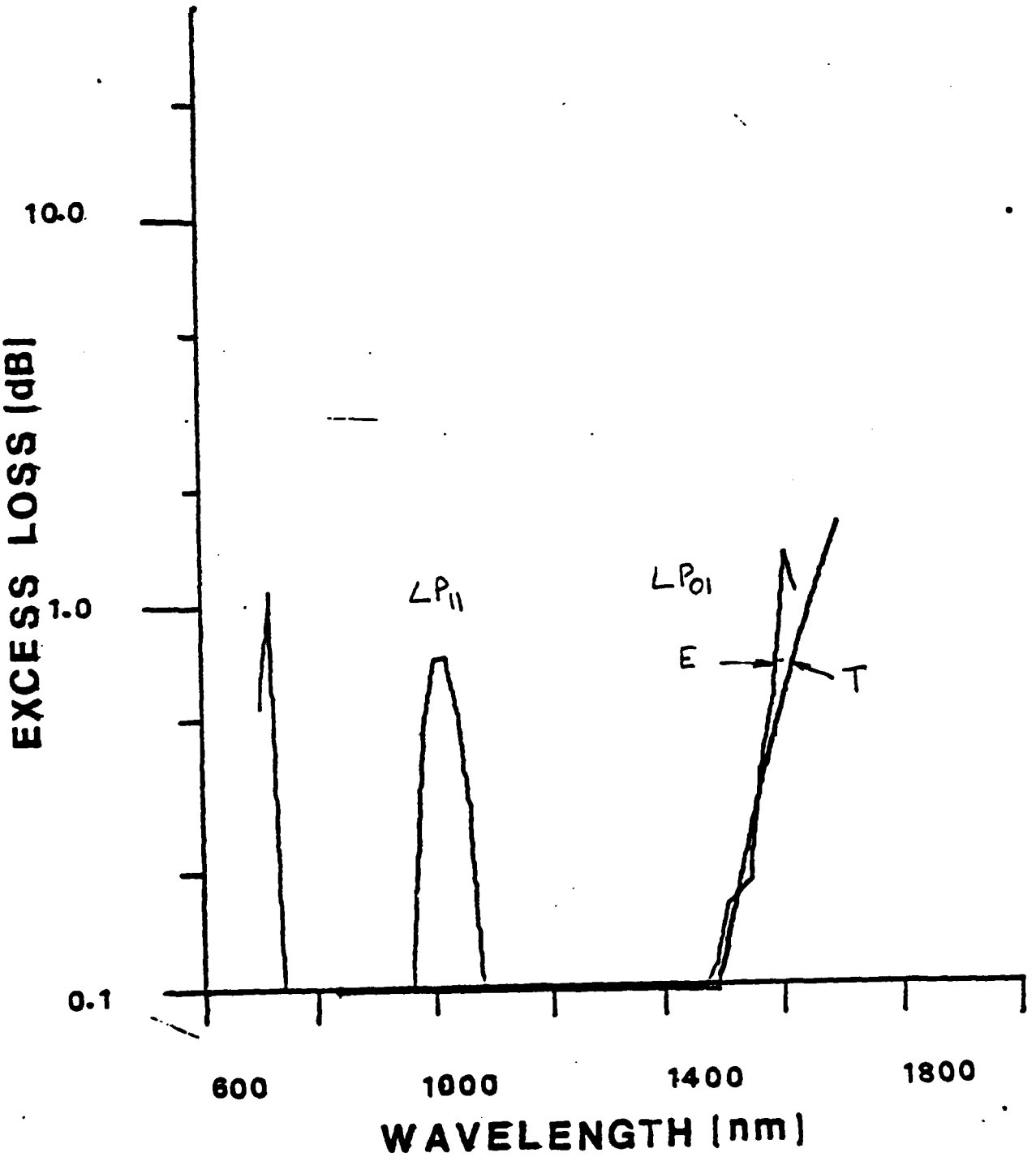

MICROBEND TEST

FIBER NO.: 509503

PIN ARRAY = 3 MM

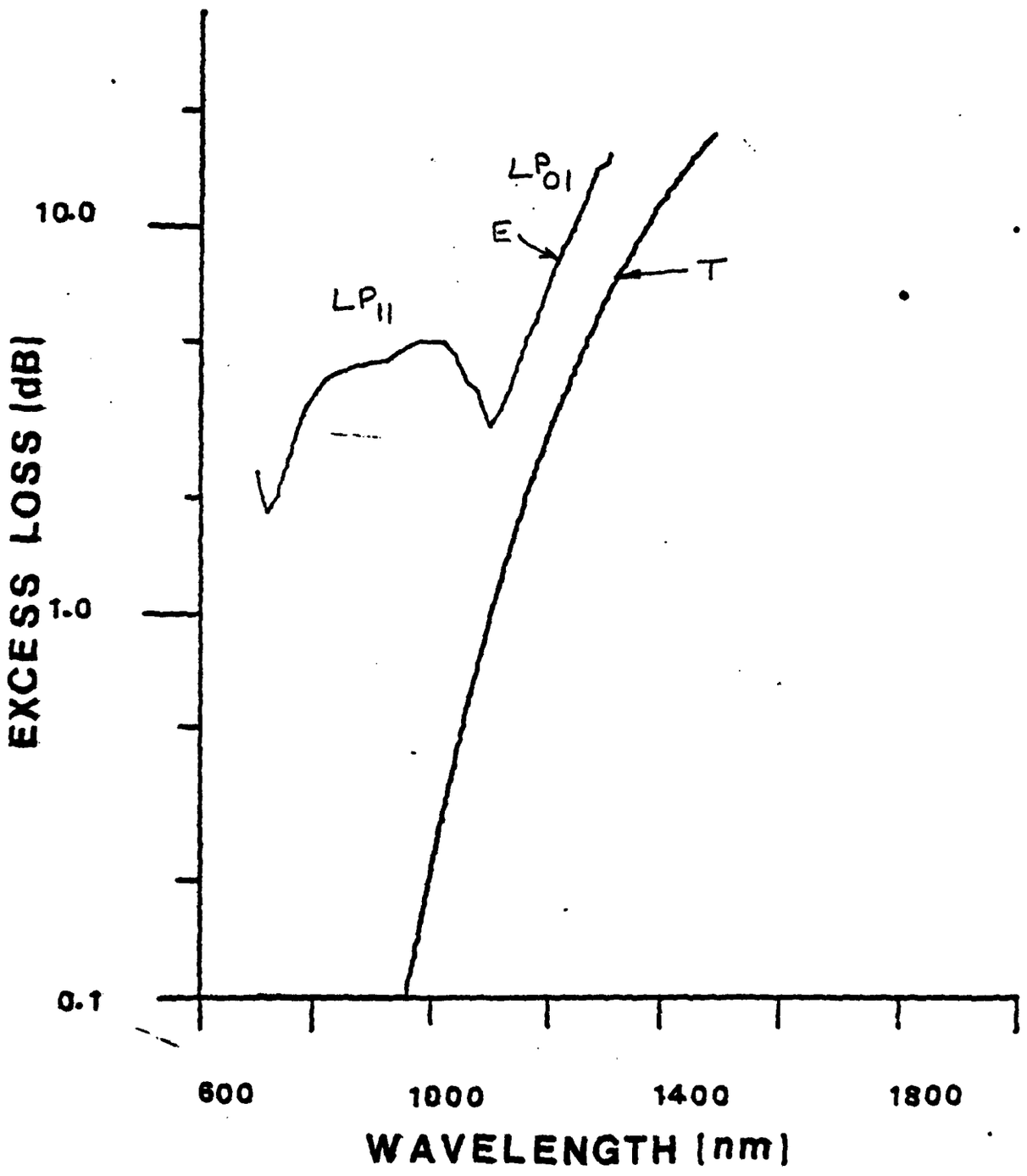

MICROBEND TEST

FIBER NO.: 509503

PIN ARRAY = 4 MM

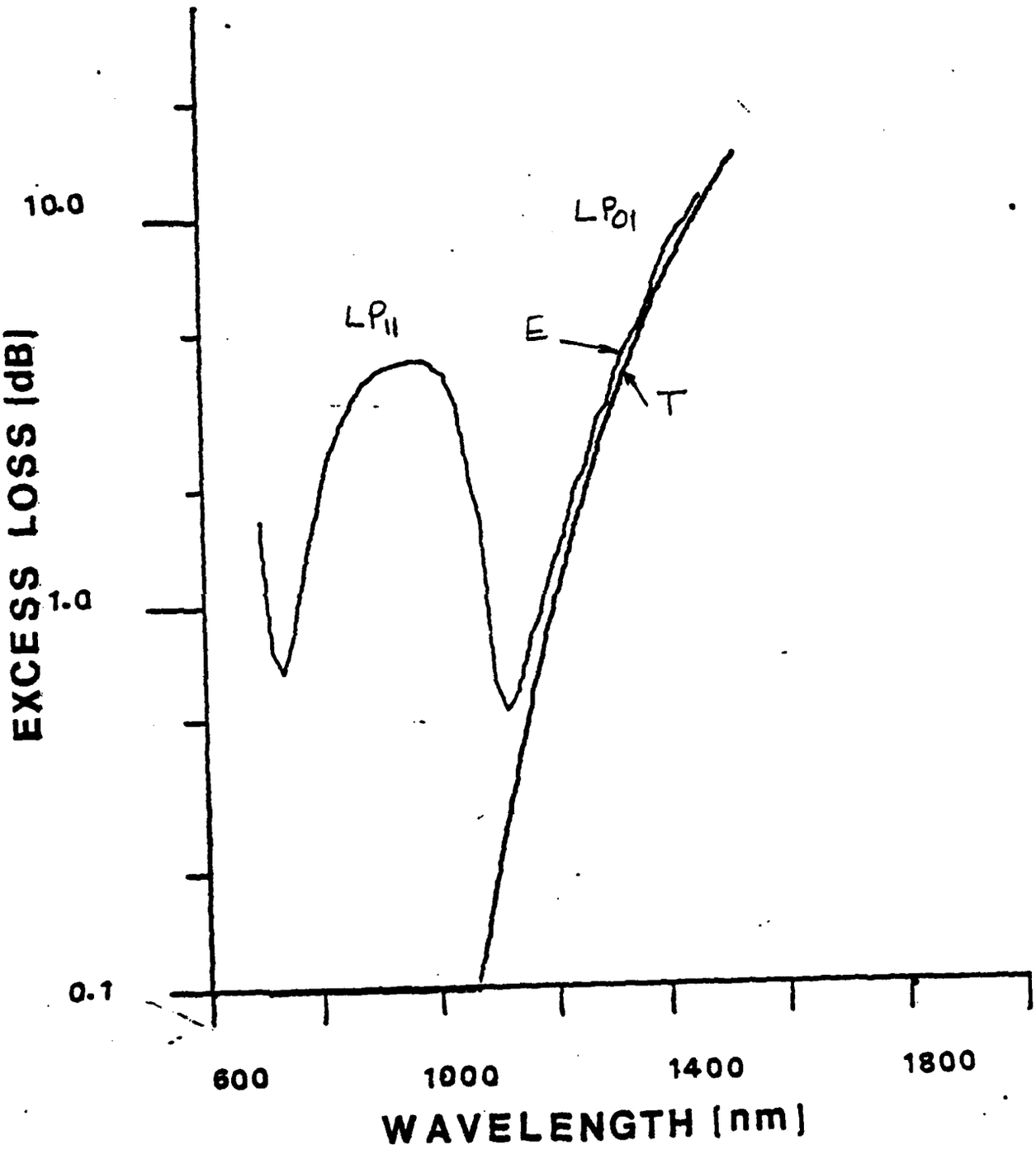

MICROBEND TEST

FIBER NO.: 509503

PIN ARRAY = 5 MM

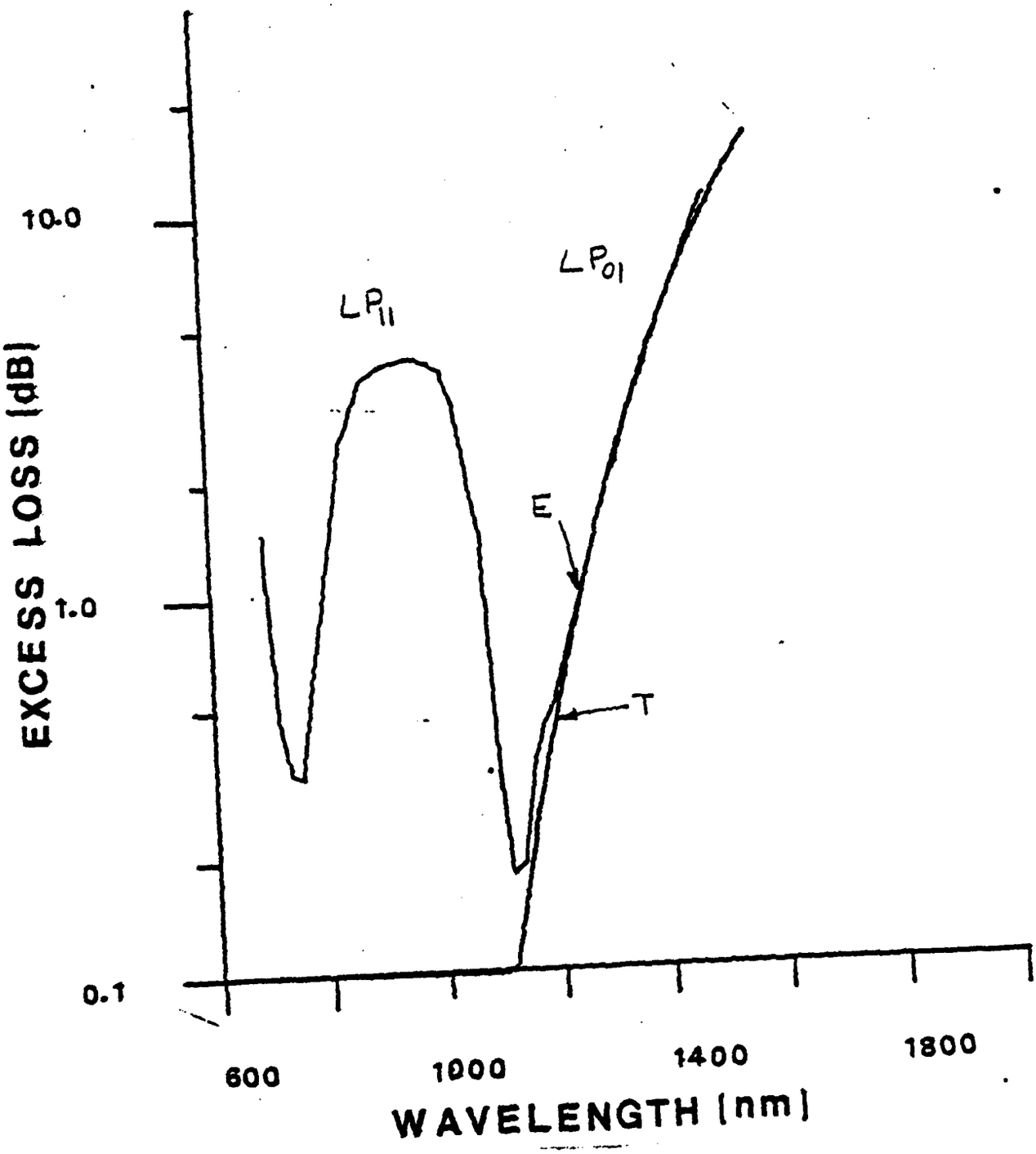

MICROBEND TEST

FIBER NO.: 509503

PIN ARRAY = $\frac{\infty}{8}$ MM

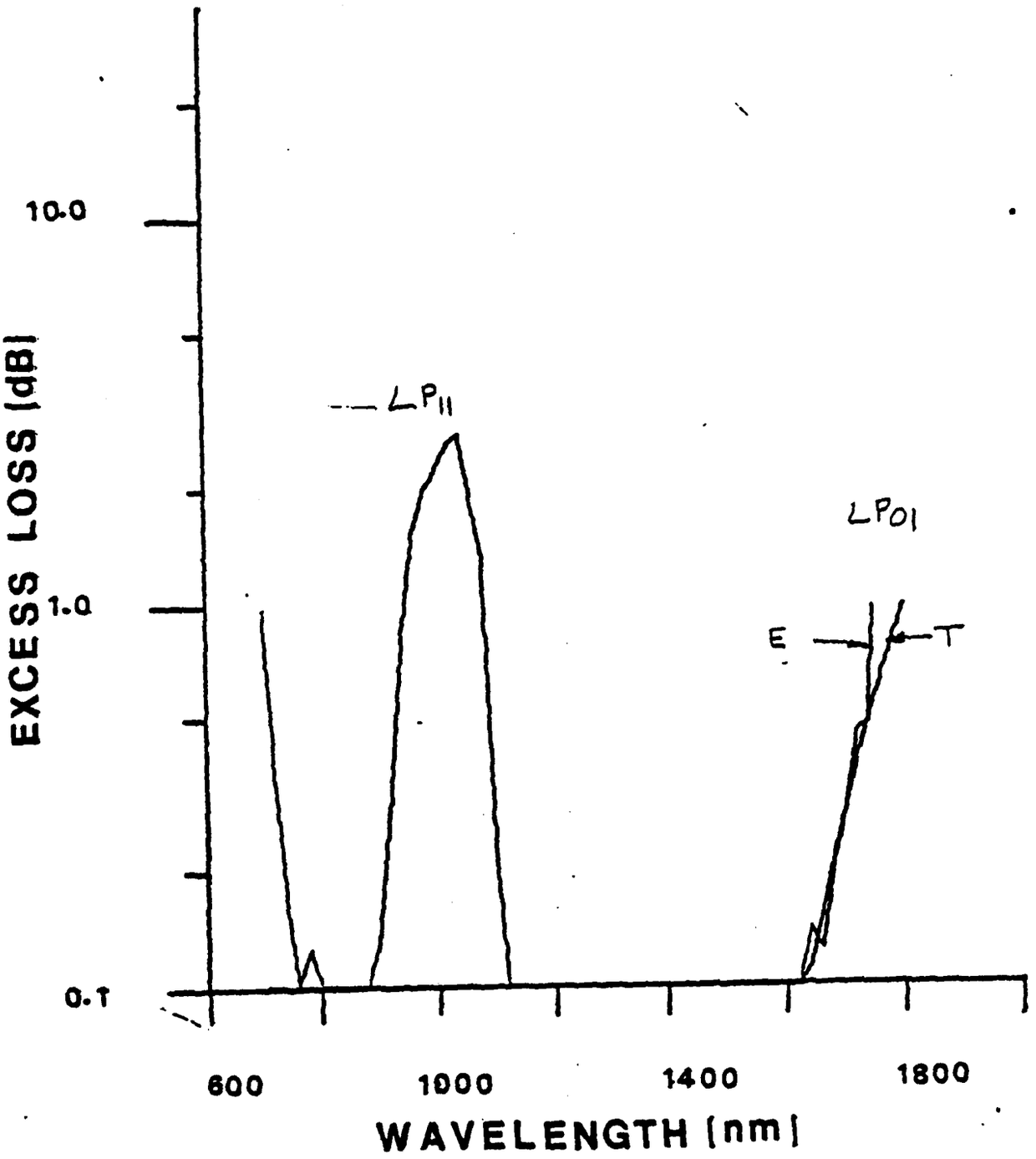

MICROBEND TEST

FIBER NO.: 343105

PIN ARRAY = 4 MM

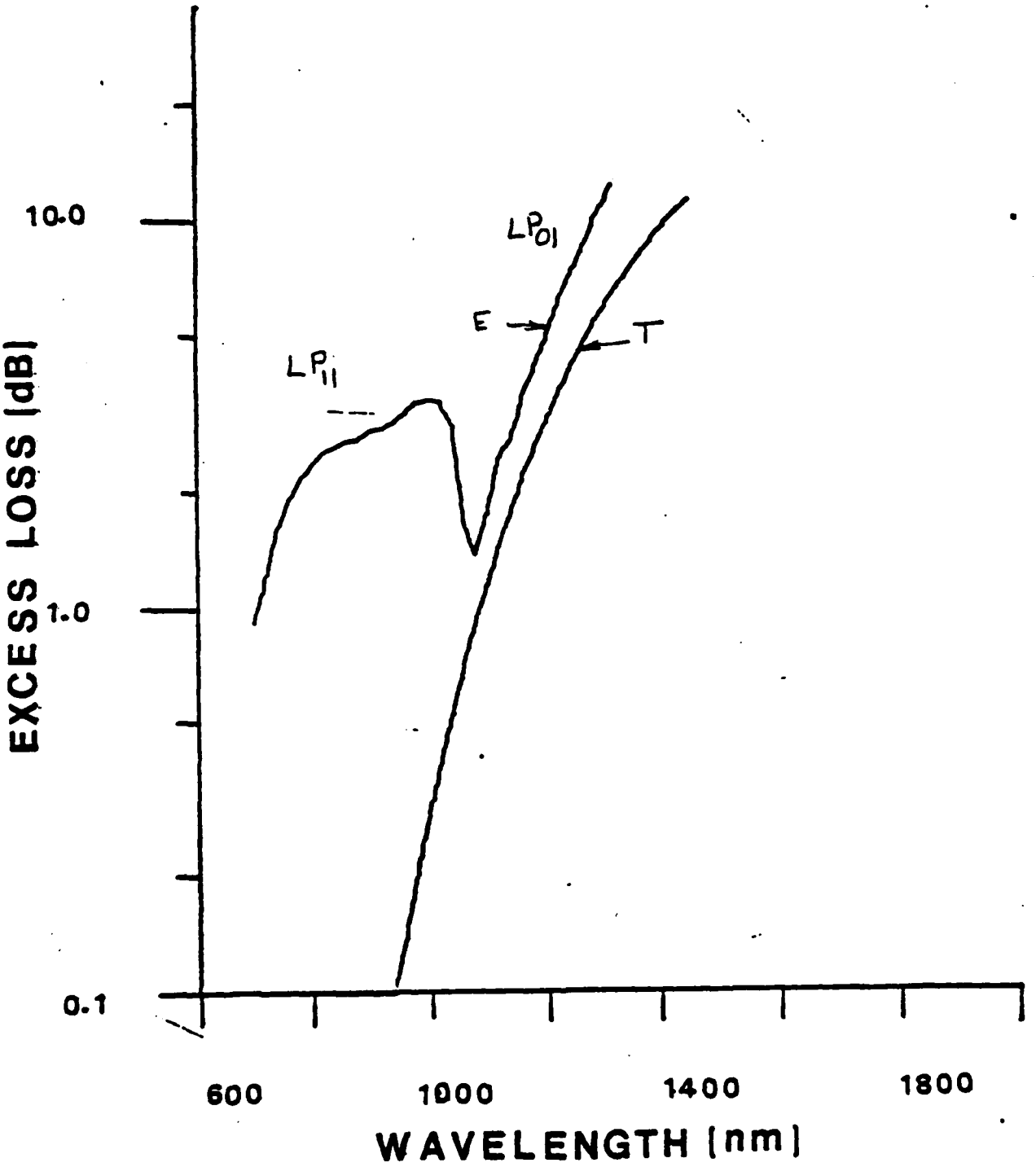

MICROBEND TEST

FIBER NO.: 343105

PIN ARRAY = 5 MM

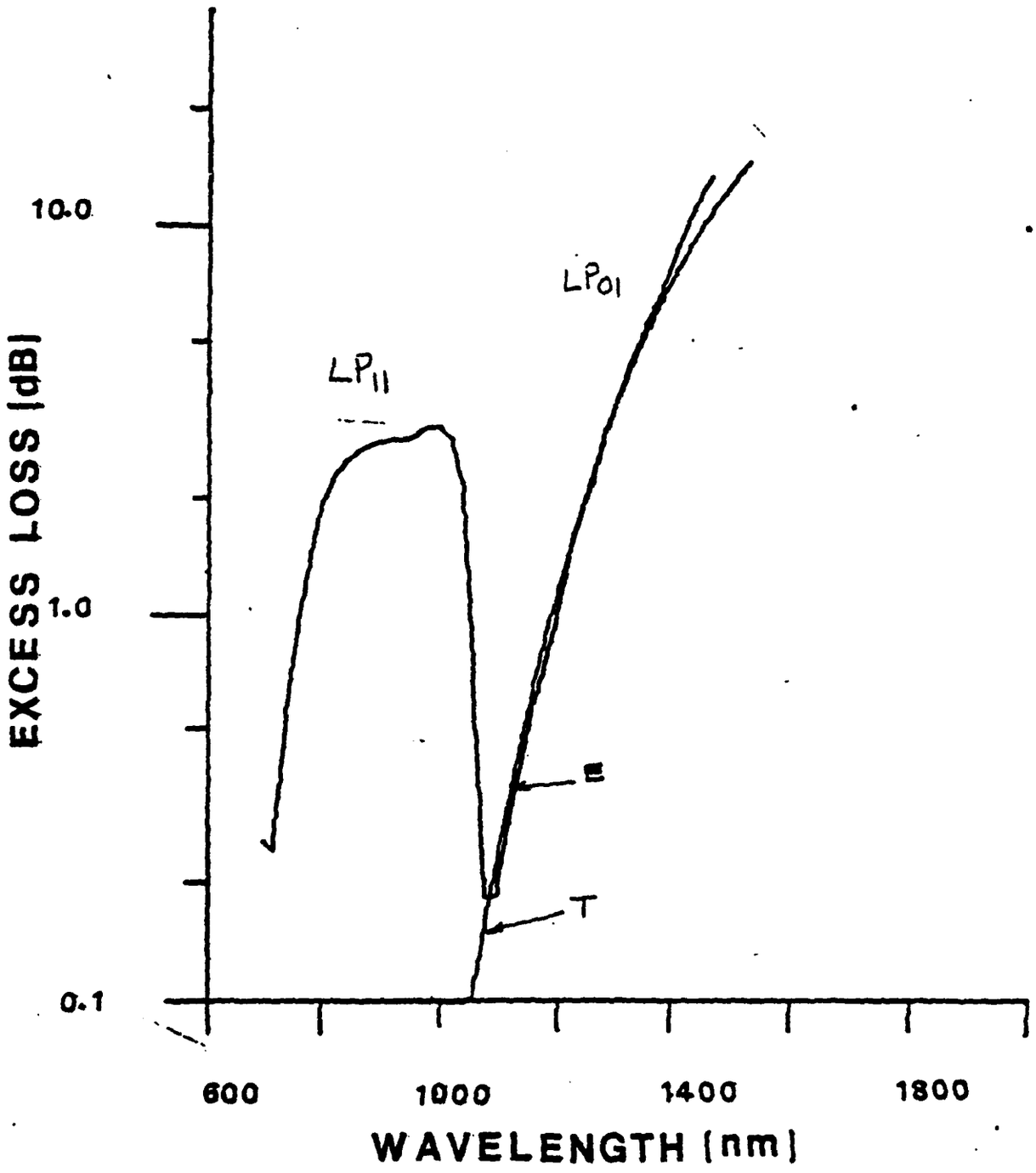

MICROBEND TEST

FIBER NO.: 343105

PIN ARRAY = 8 MM

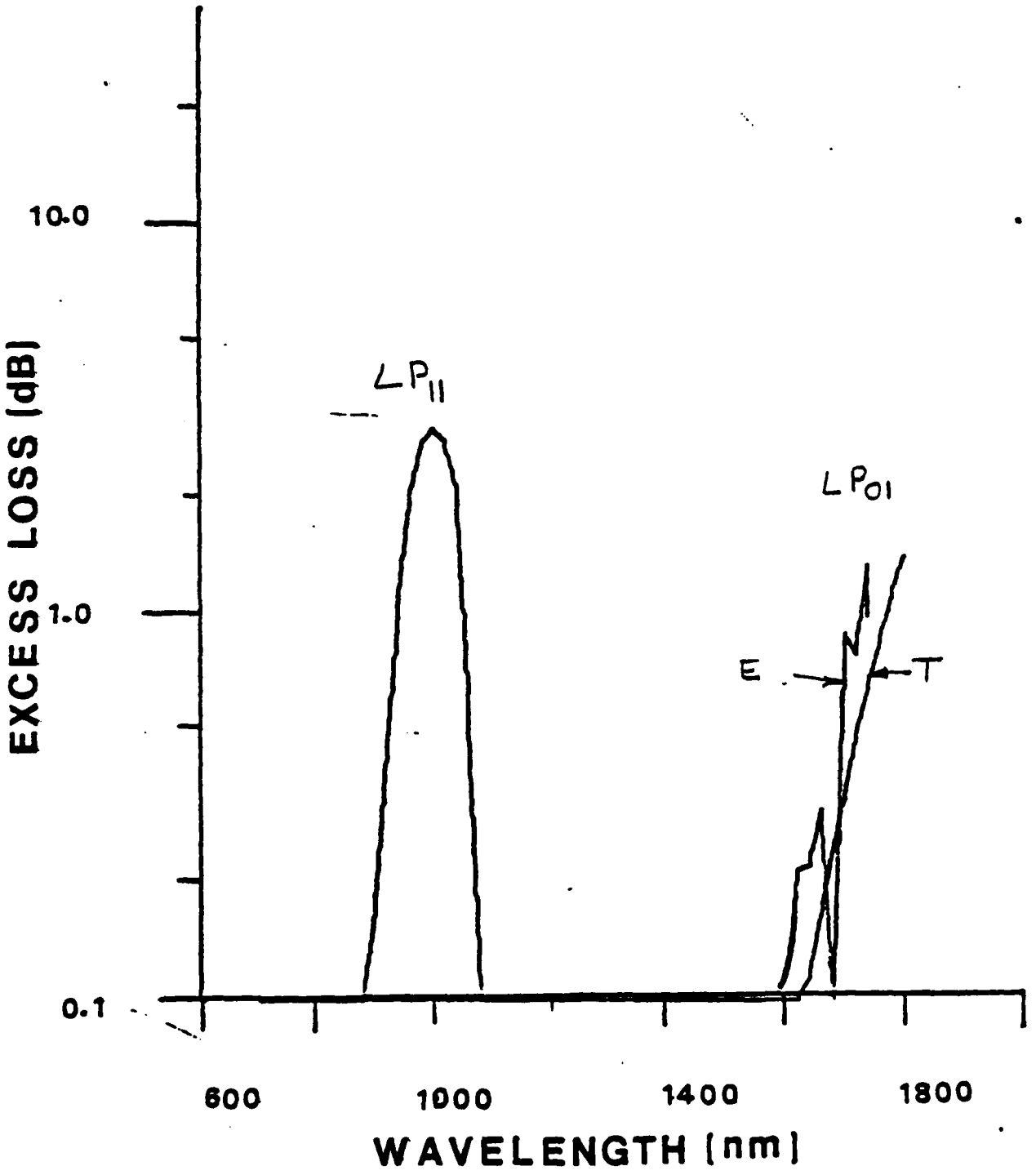

MICROBEND TEST

FIBER NO.: 506902

PIN ARRAY = 3 MM

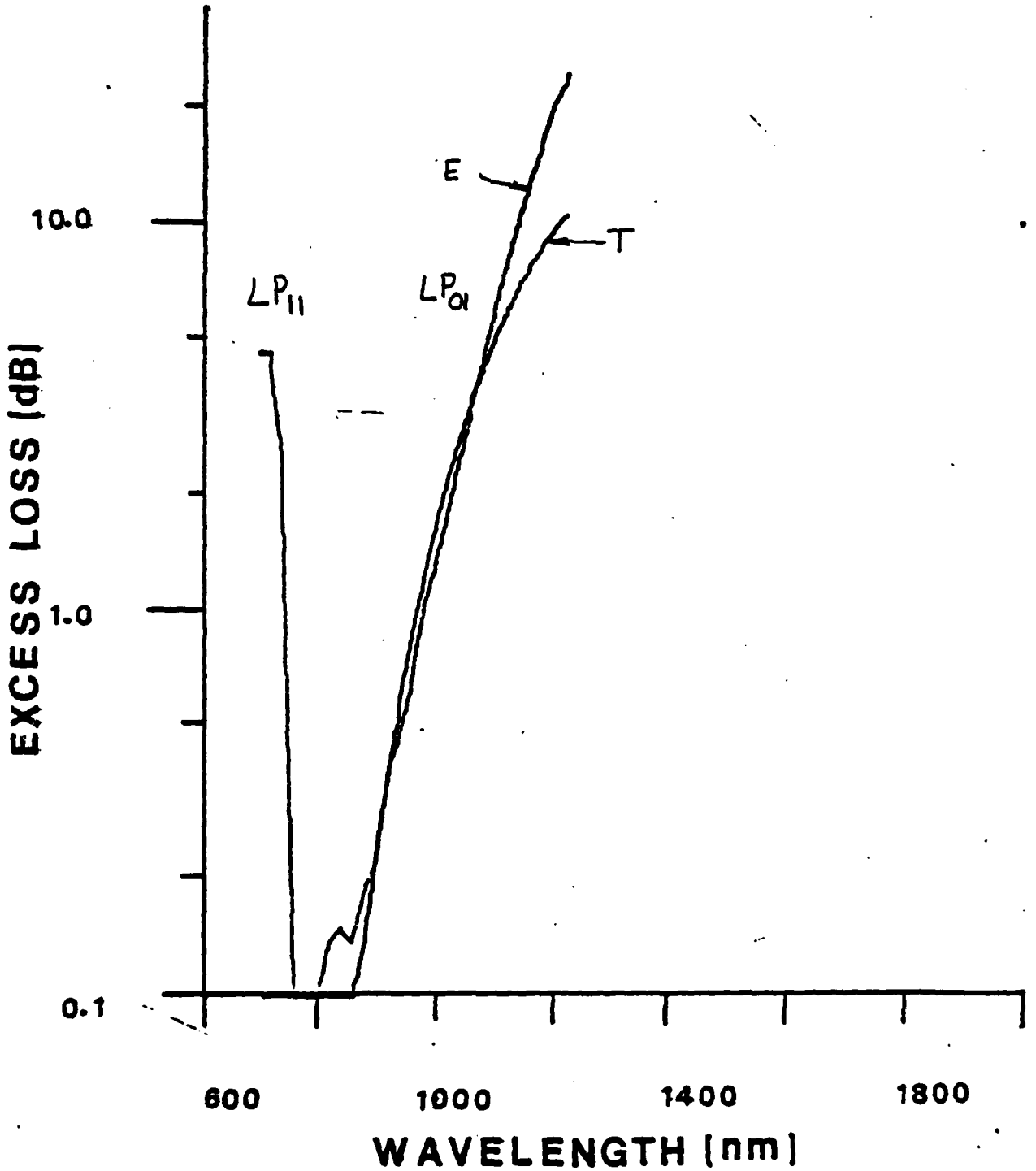

MICROBEND TEST

FIBER NO.: 506902

PIN ARRAY = 4 MM

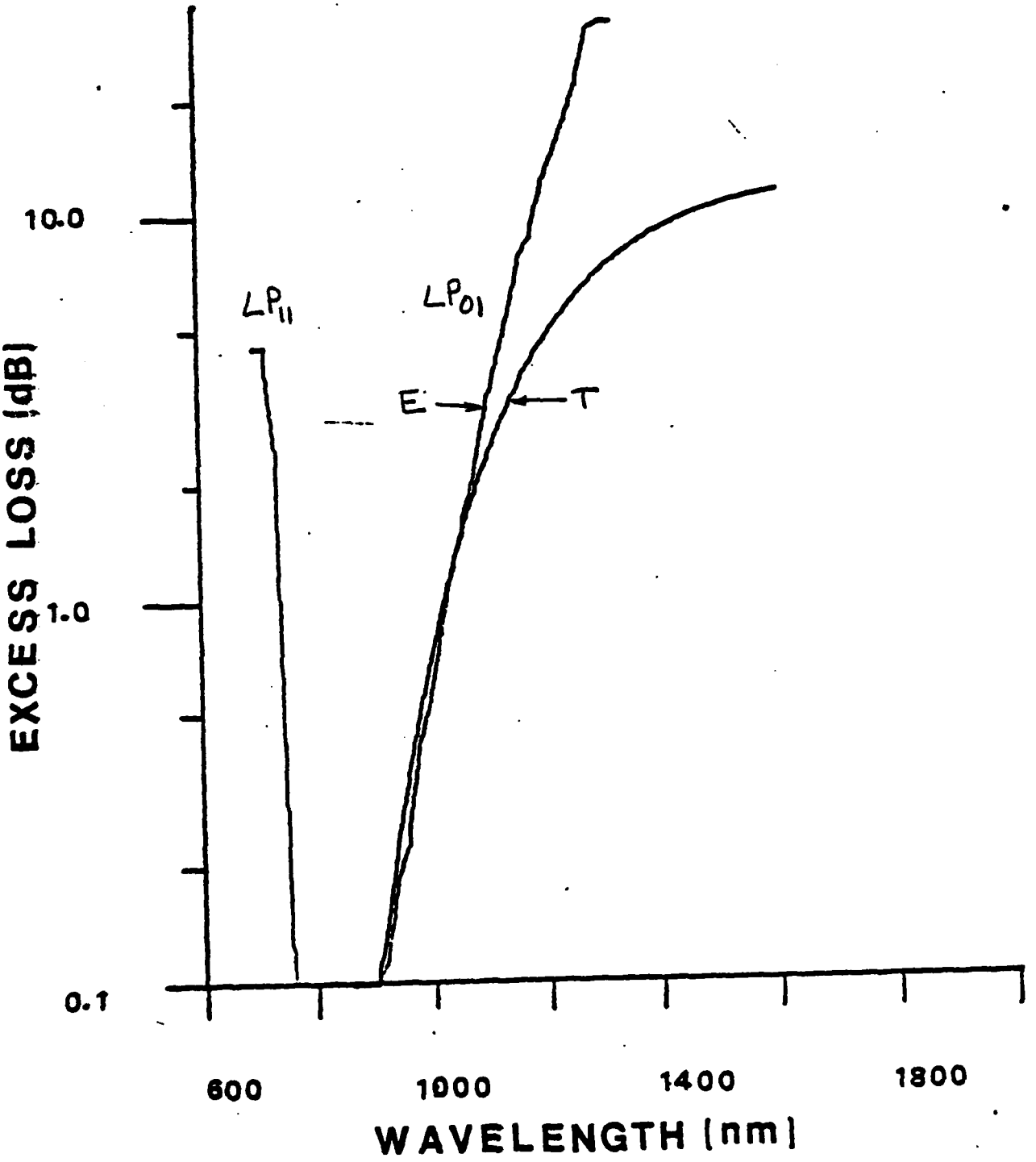

MICROBEND TEST

FIBER NO.: 506902

PIN ARRAY = 5 MM

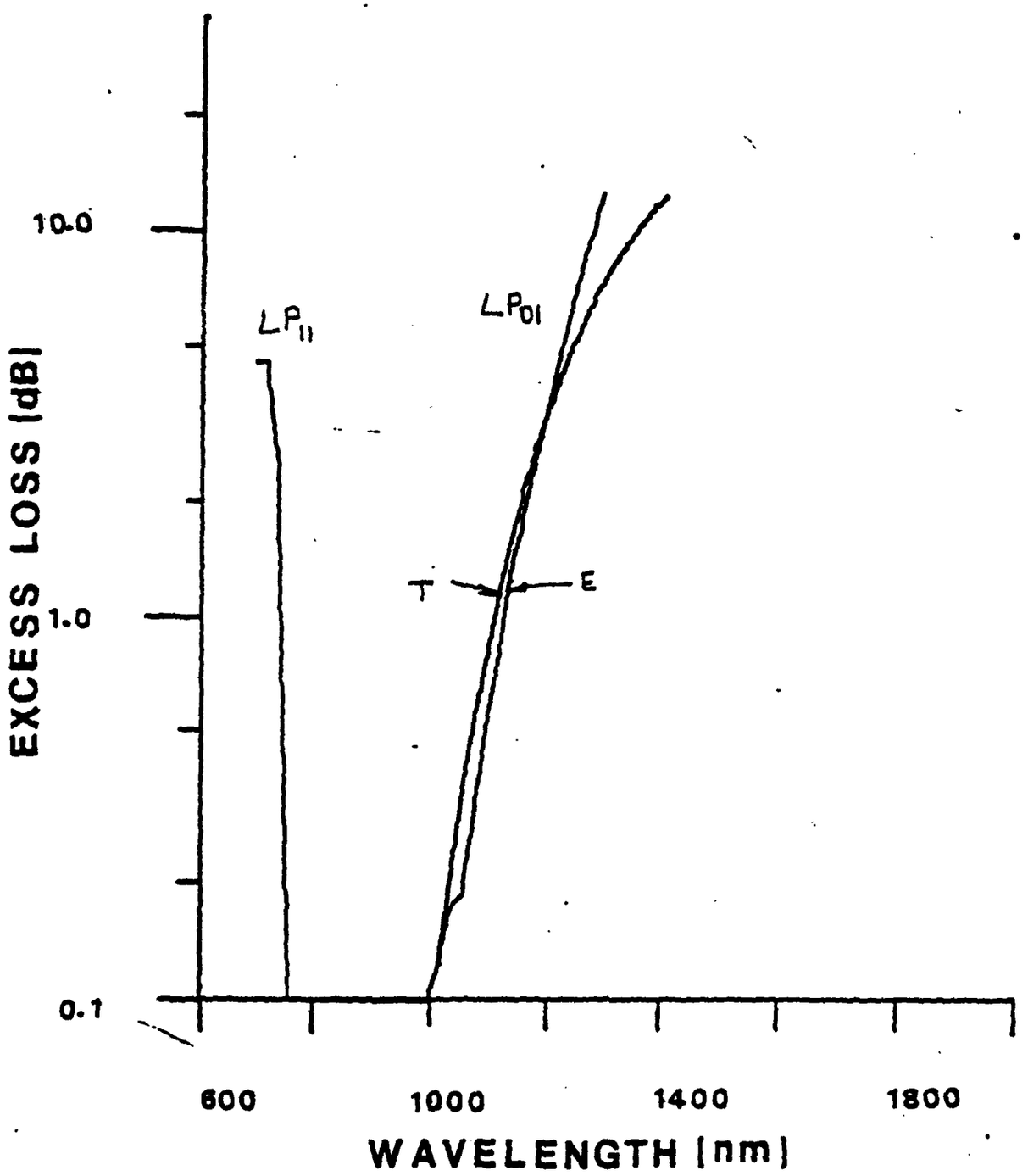

MICROBEND TEST

FIBER NO.: 506902

PIN ARRAY = 8 MM

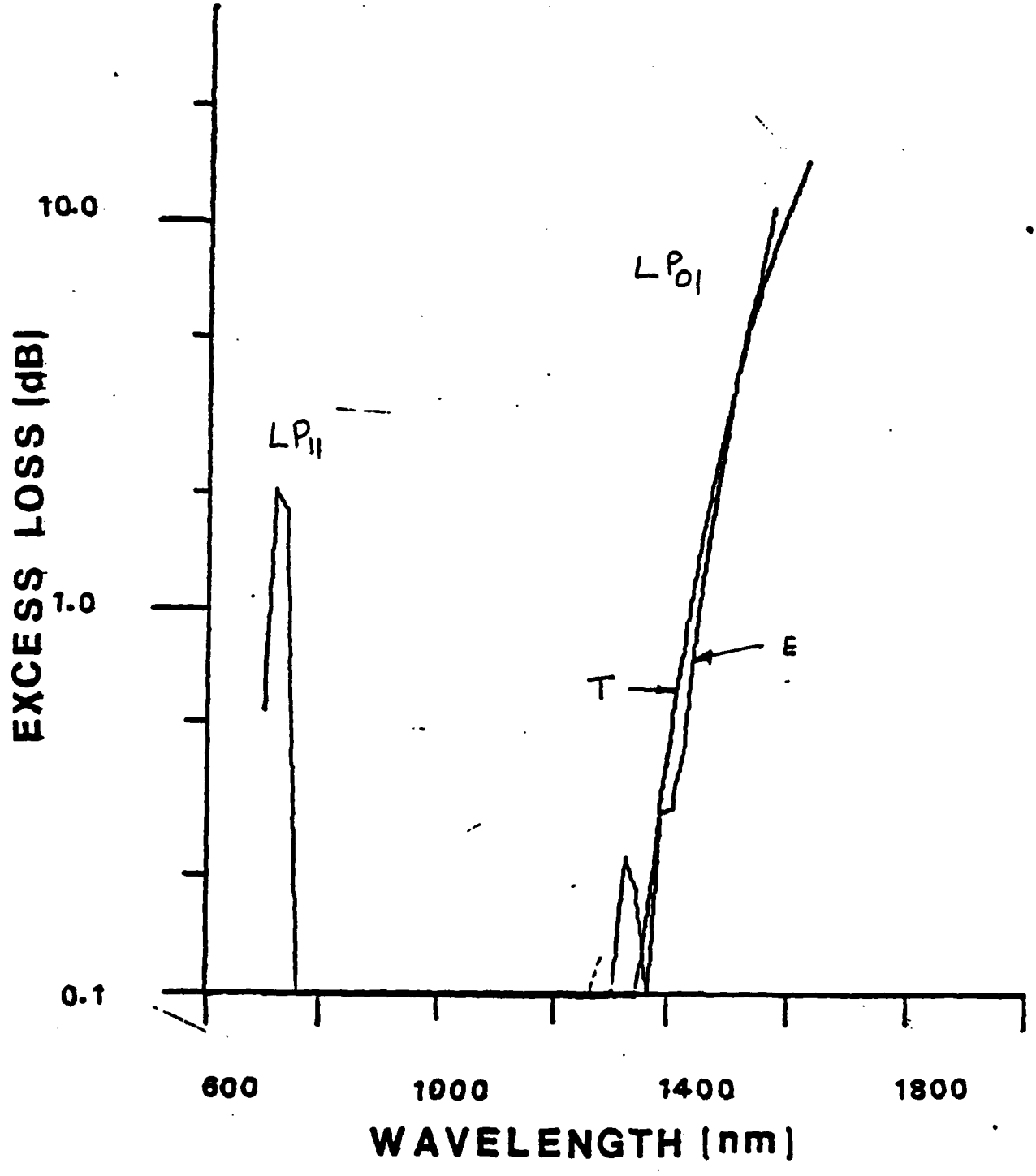

MICROBEND TEST

FIBER NO.: 503103

PIN ARRAY = 5 MM

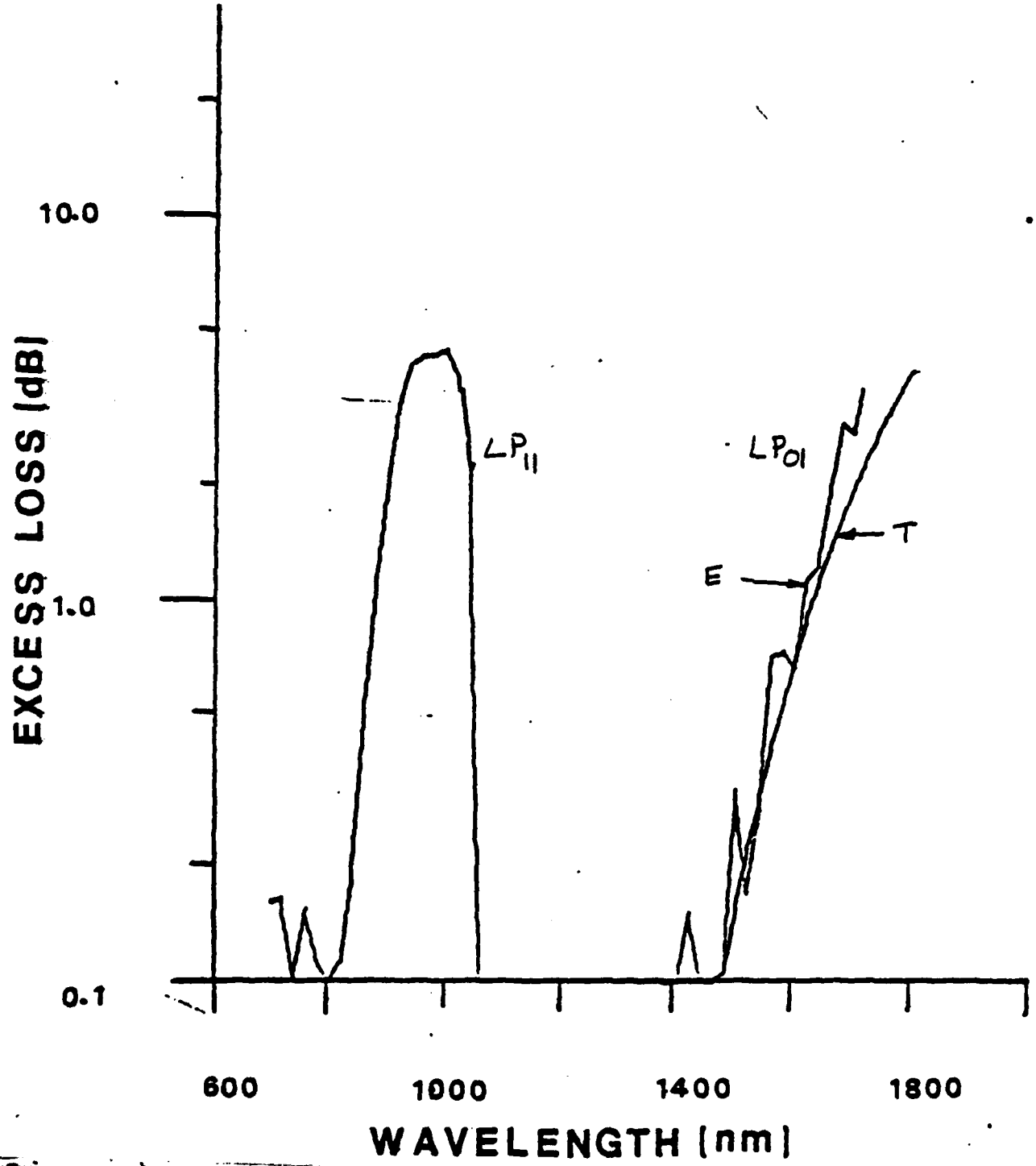

MICROBEND TEST

FIBER NO.: 503103

PIN ARRAY = 4 MM

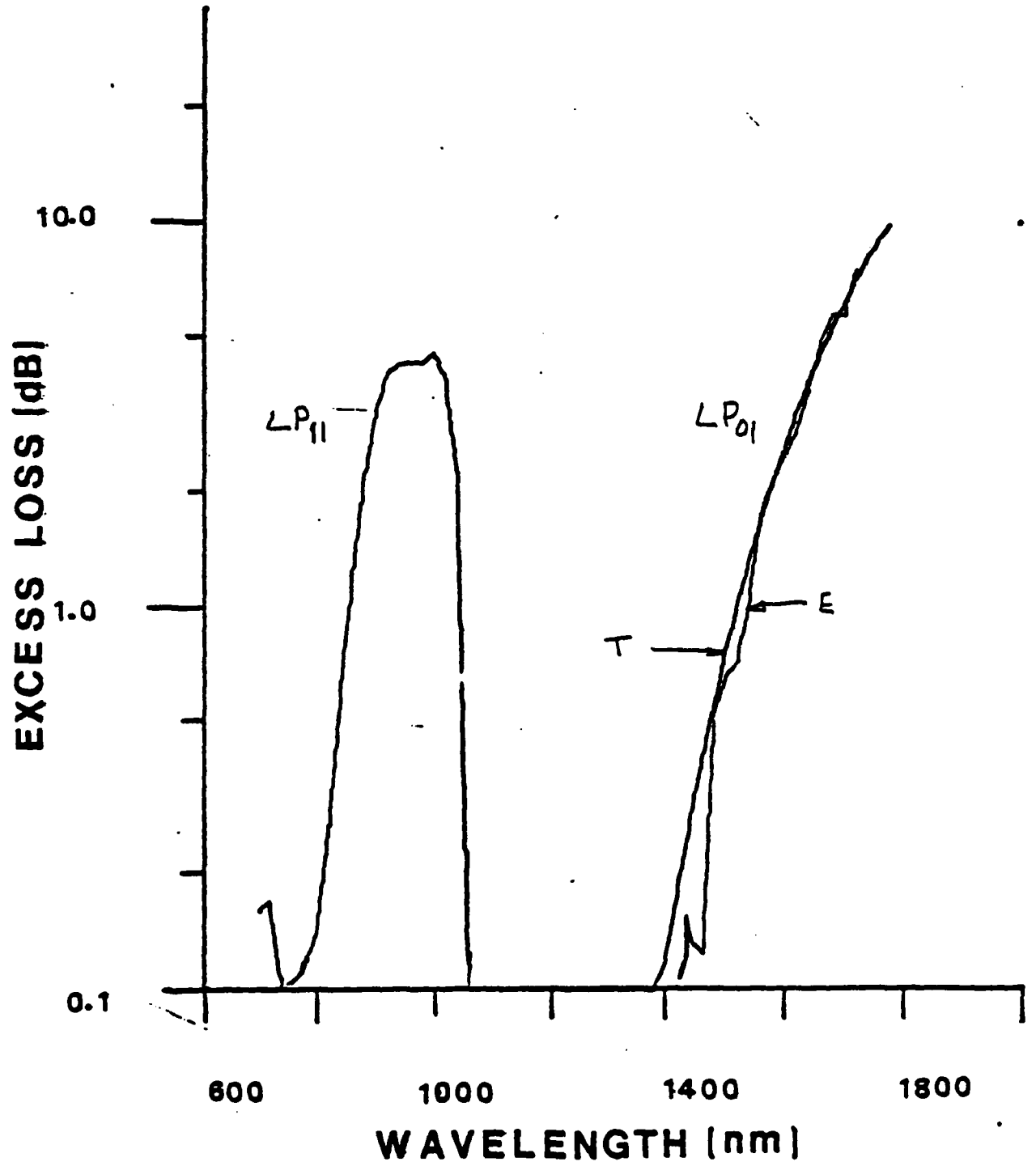

MICROBEND TEST

FIBER NO.: 502905

PIN ARRAY = 8 MM

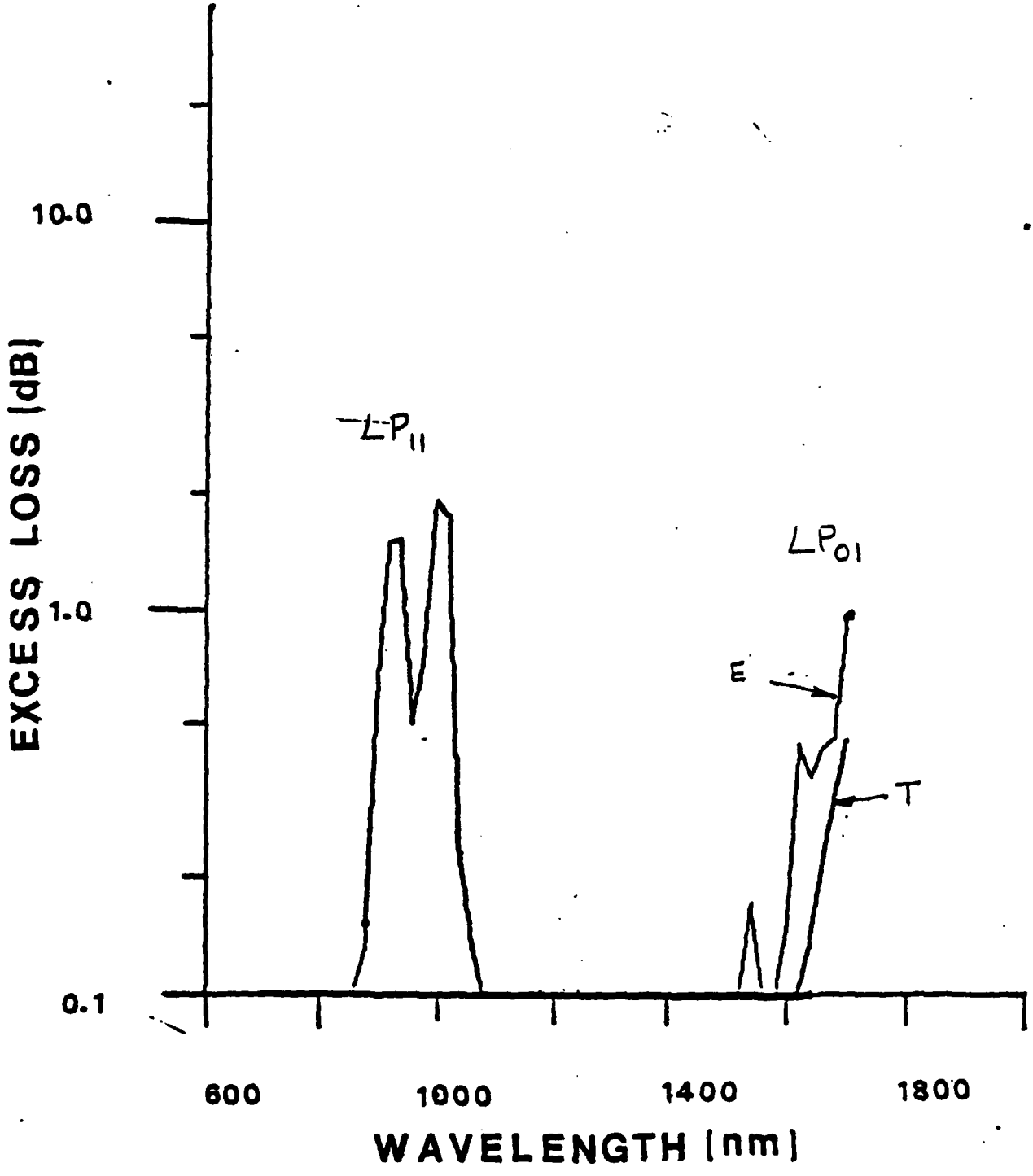

MICROBEND TEST

FIBER NO.: 502905

PIN ARRAY = 5 MM

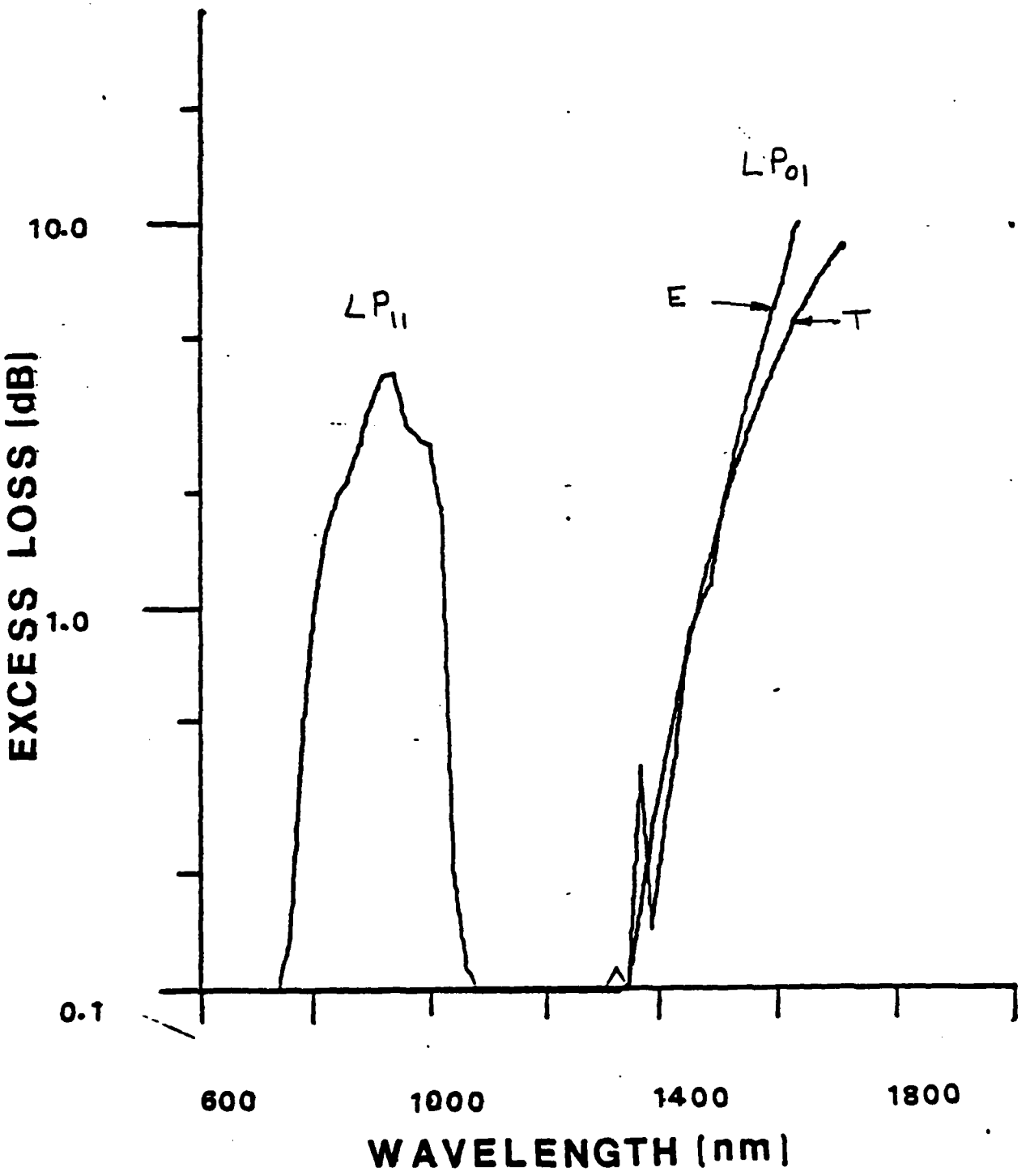

MICROBEND TEST

FIBER NO.: 502905

PIN ARRAY = 3 MM

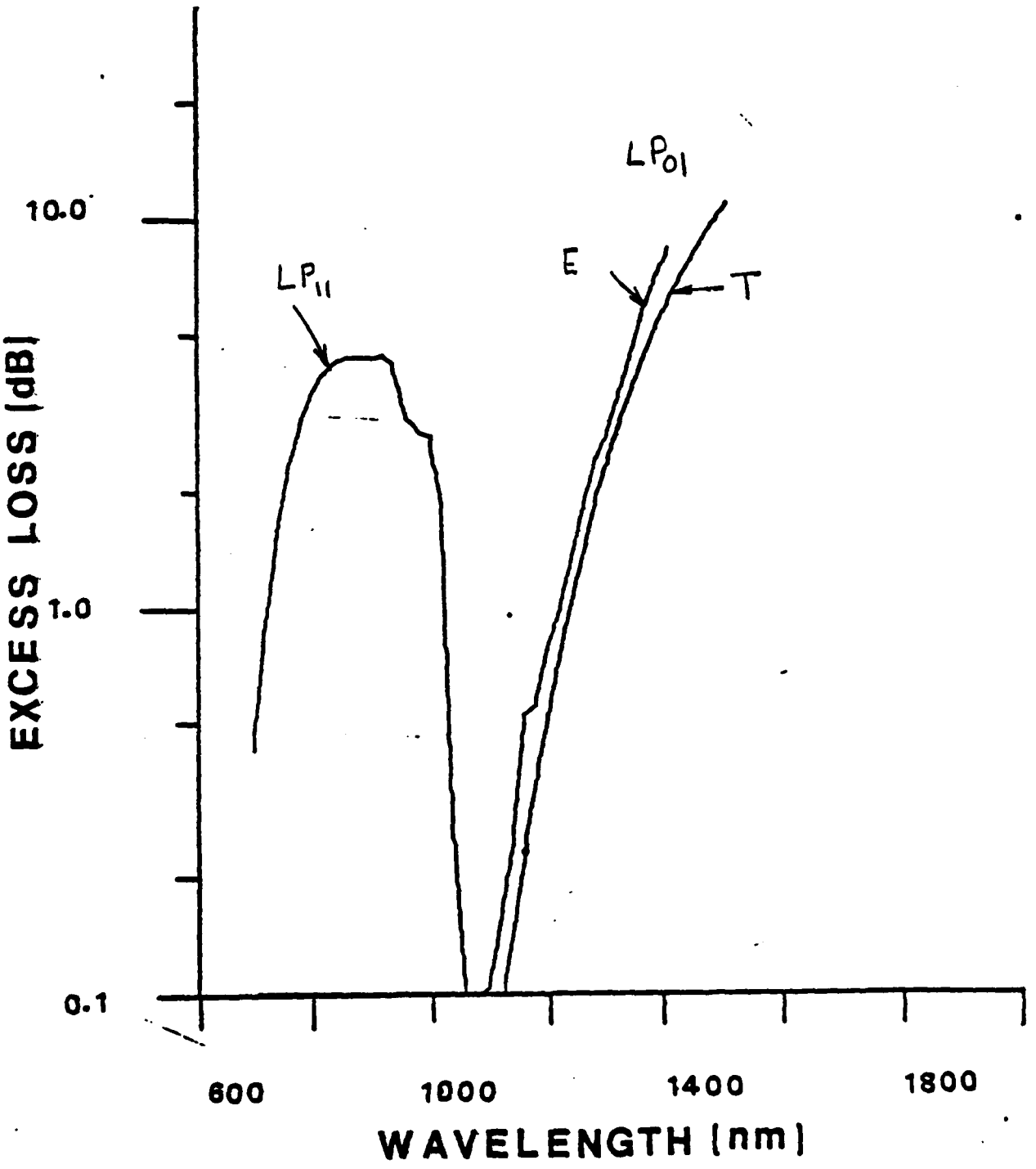

MICROBEND TEST

FIBER NO.: 503103

PIN ARRAY = 3 MM

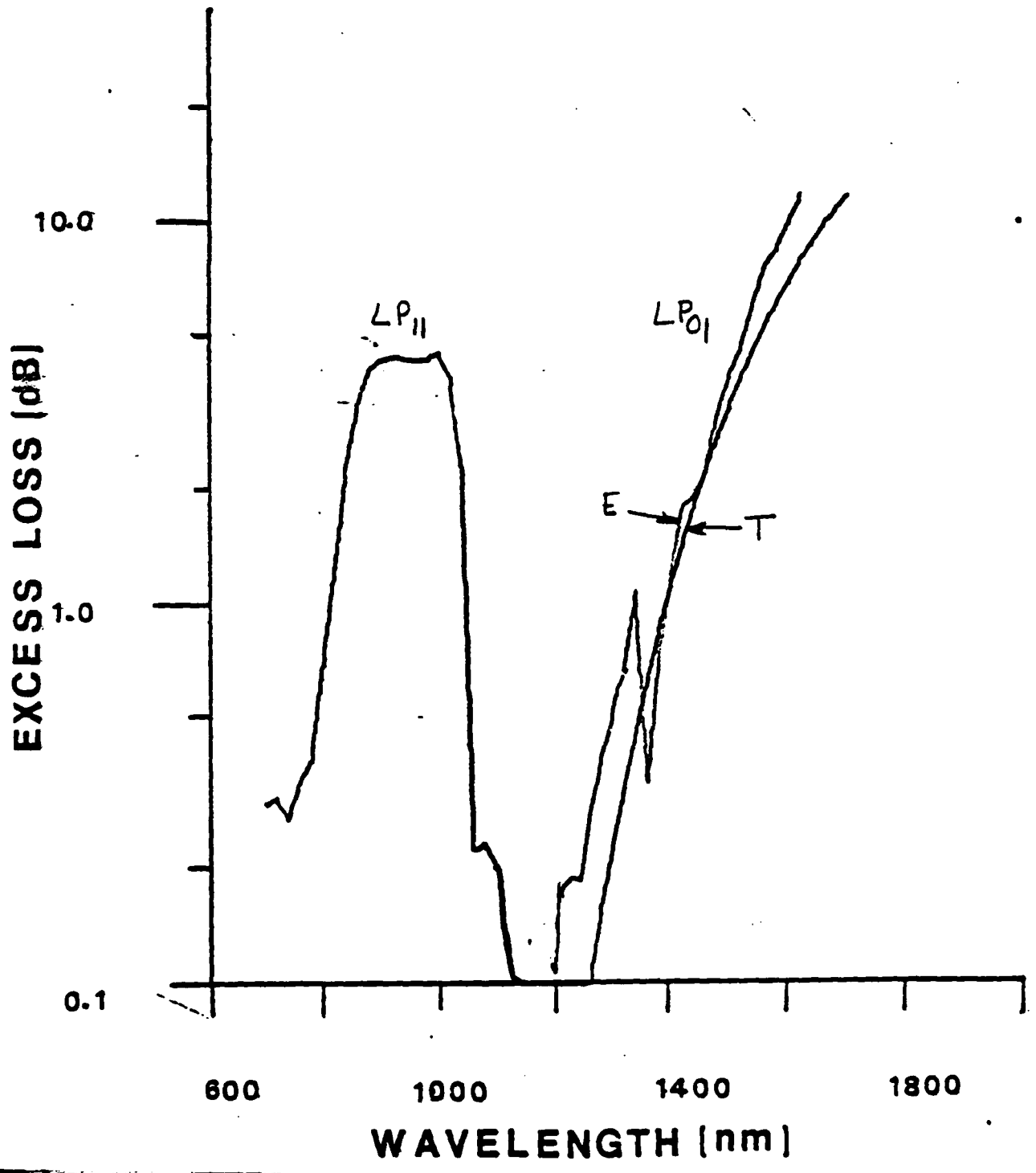

MICROBEND TEST

FIBER NO.: 503404

PIN ARRAY = 3 MM

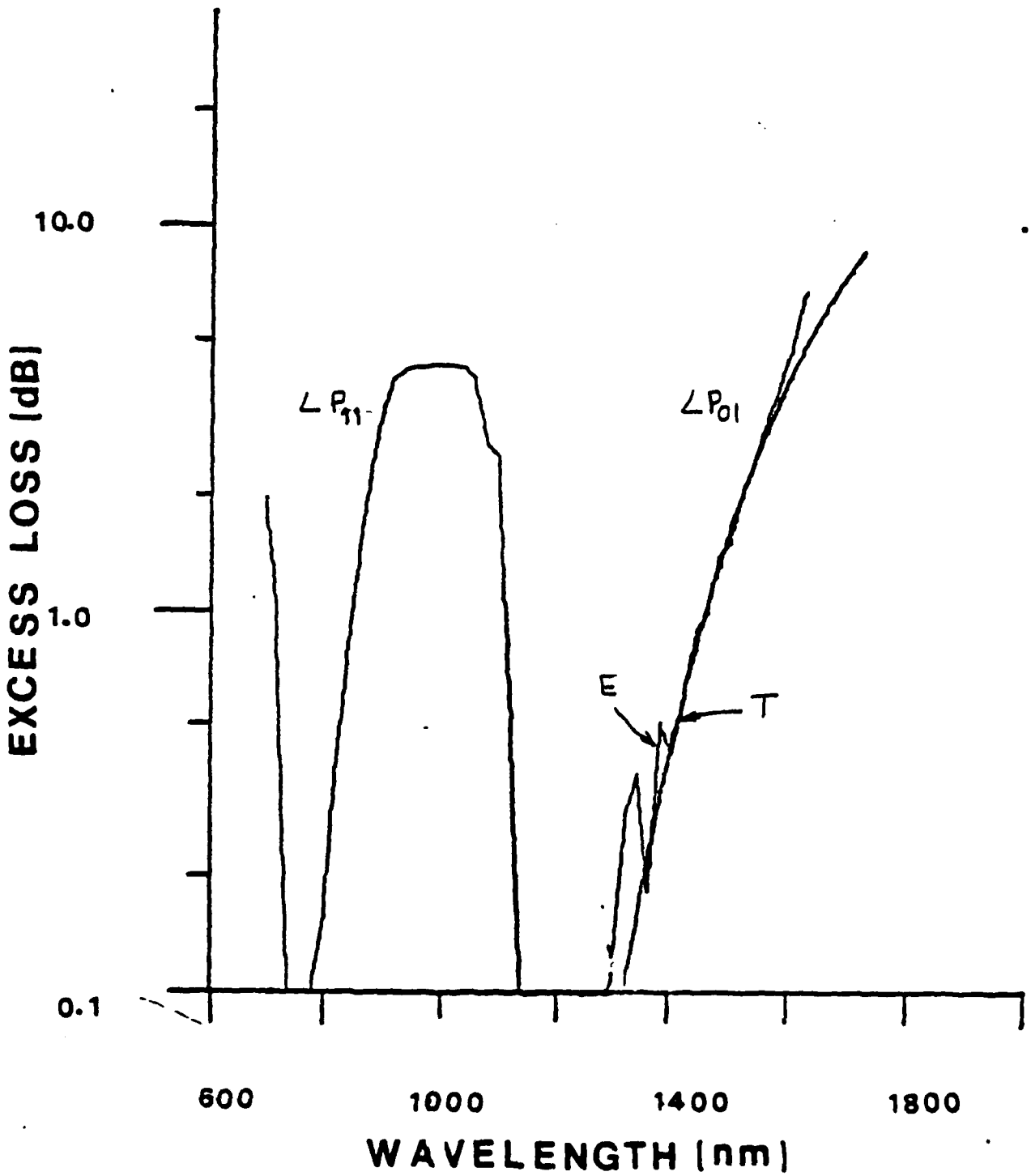

MICROBEND TEST

FIBER NO.: 503404

PIN ARRAY = 4 MM

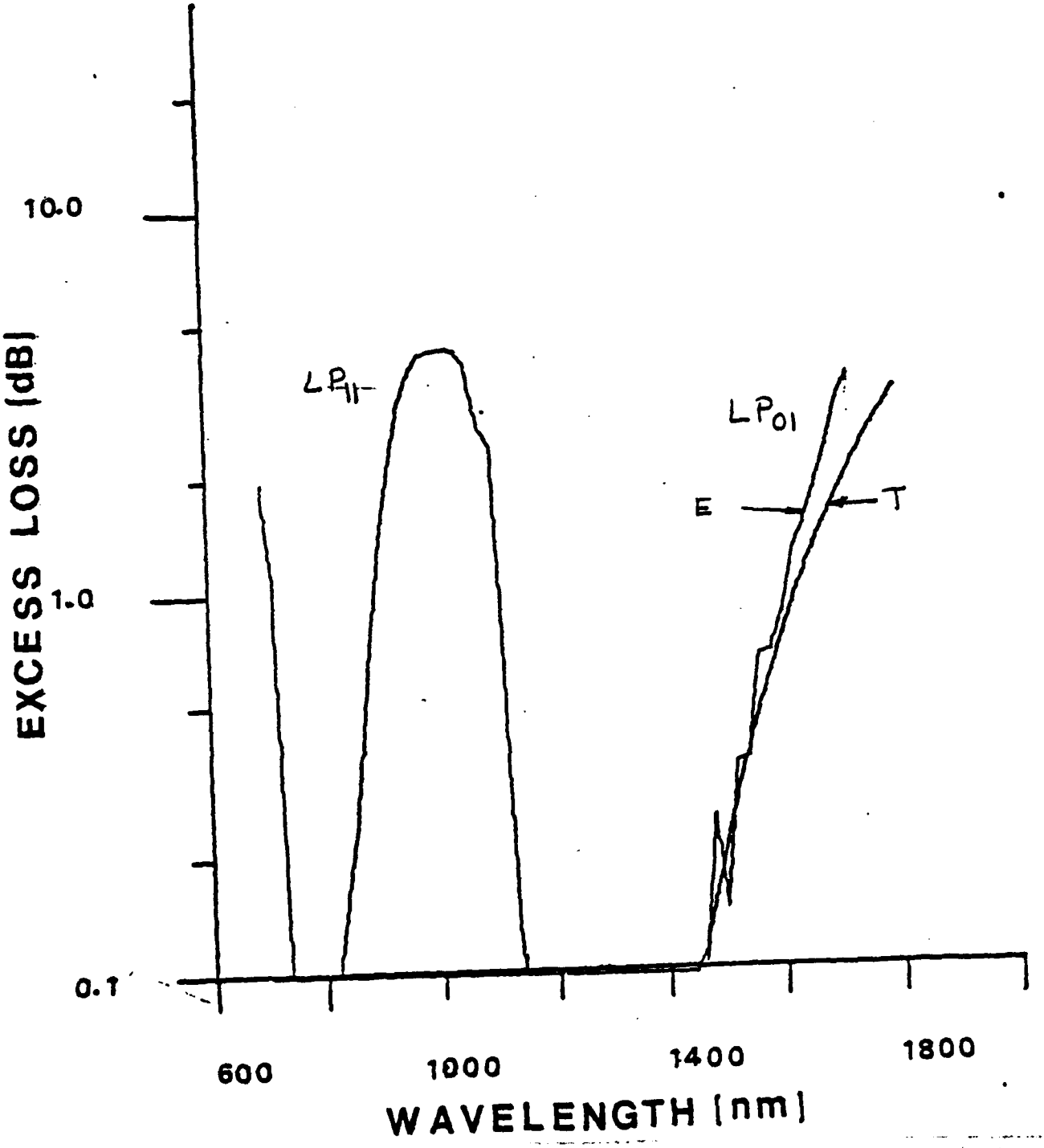

MICROBEND TEST

FIBER NO.: 503404

PIN ARRAY = 5 MM

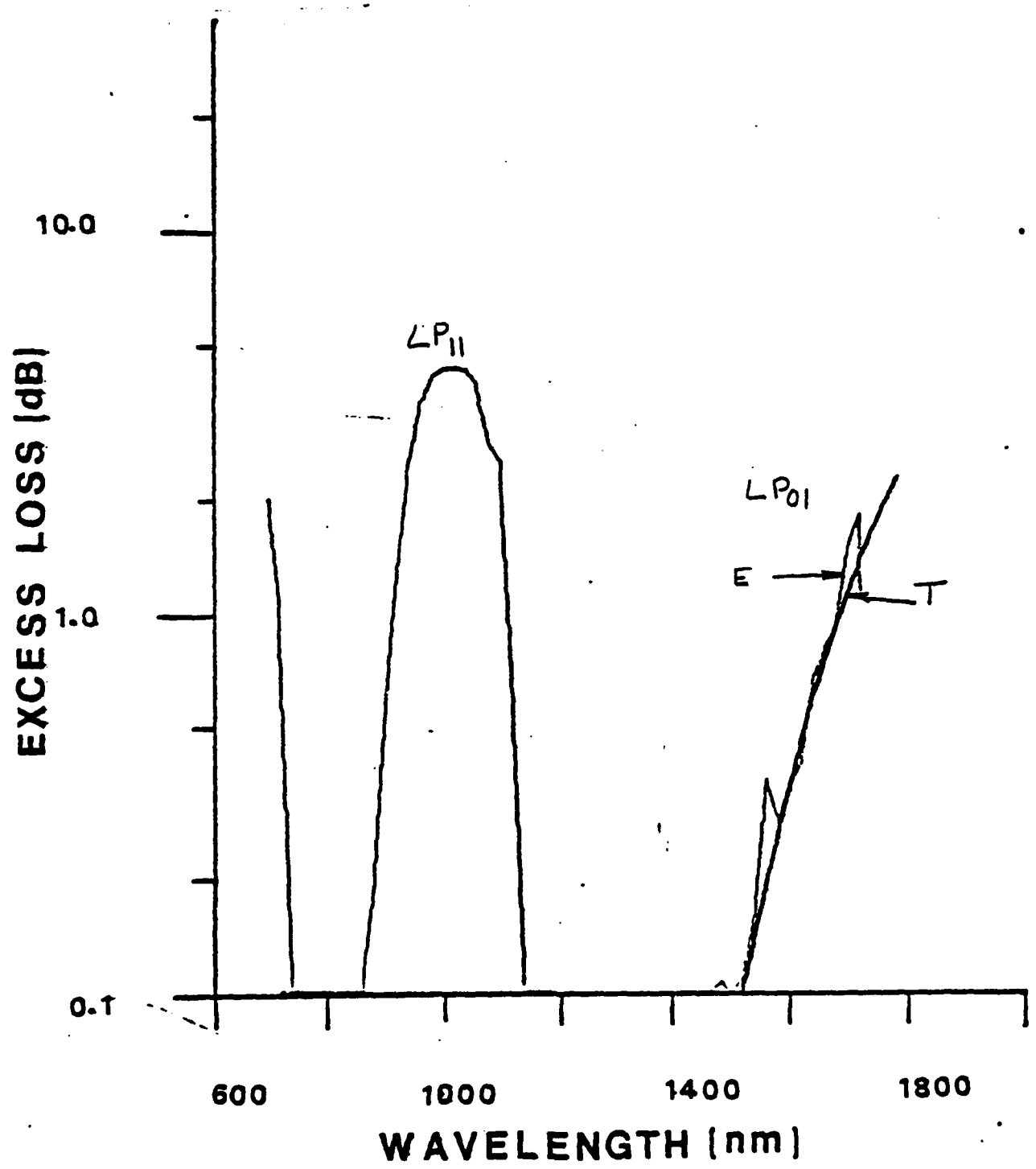

MICROBEND TEST

FIBER NO.: 509906

PIN ARRAY = 3 MM

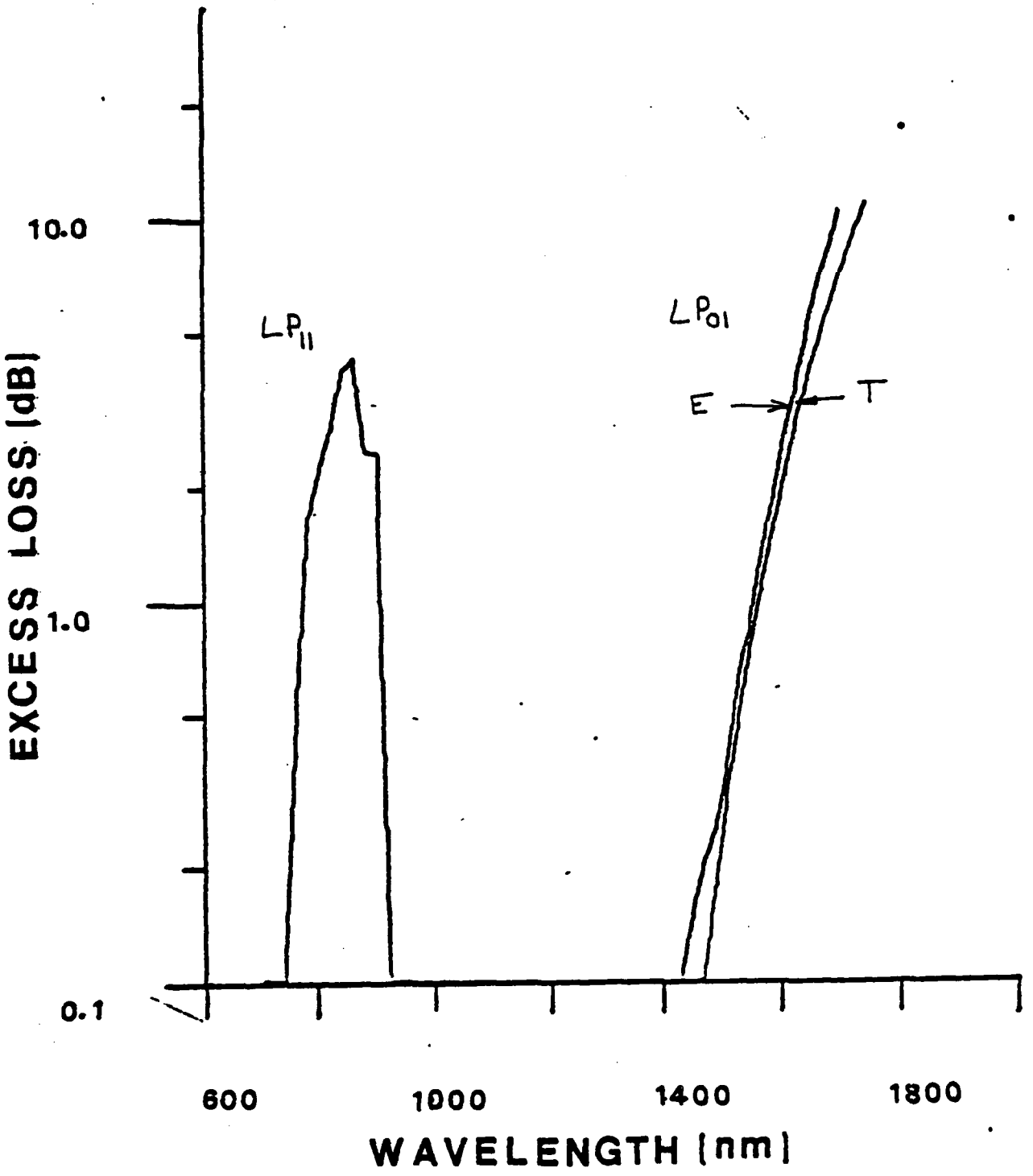

MICROBEND TEST

FIBER NO.: 509906

PIN ARRAY = 4 MM

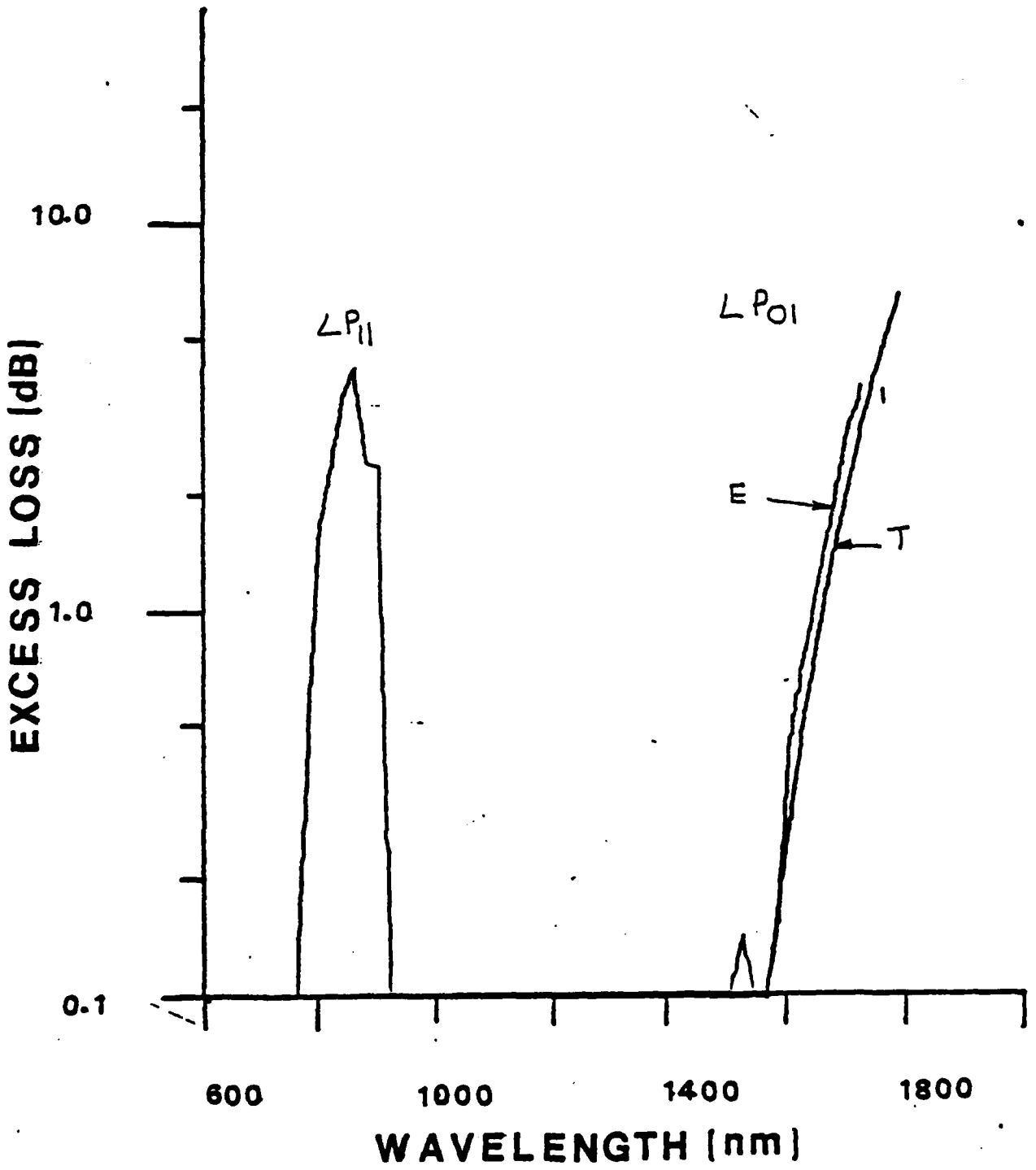

MICROBEND TEST

FIBER NO.: 509906

PIN ARRAY = 5 MM

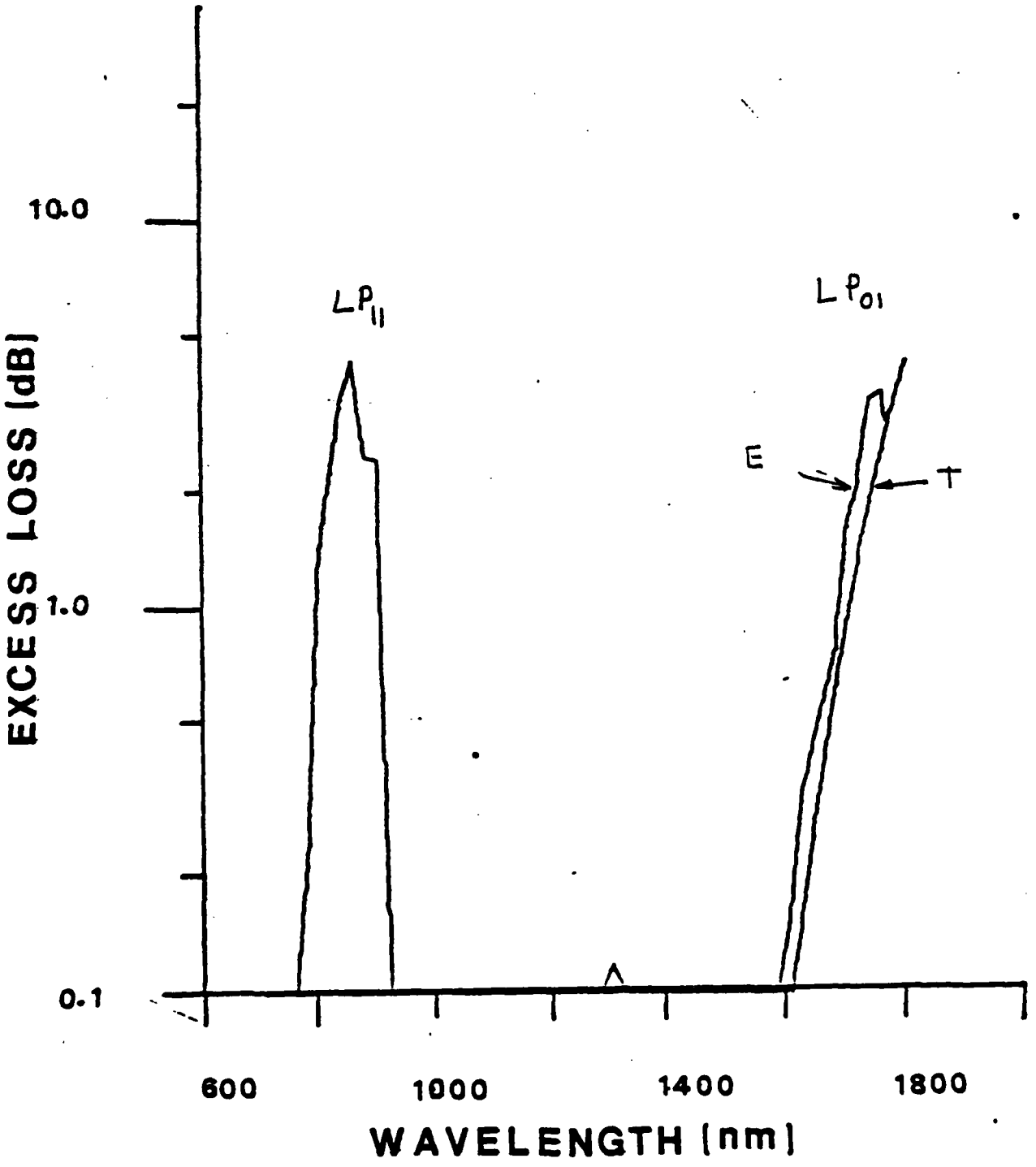

MICROBEND TEST

FIBER NO.: 509906

PIN ARRAY = 8 MM

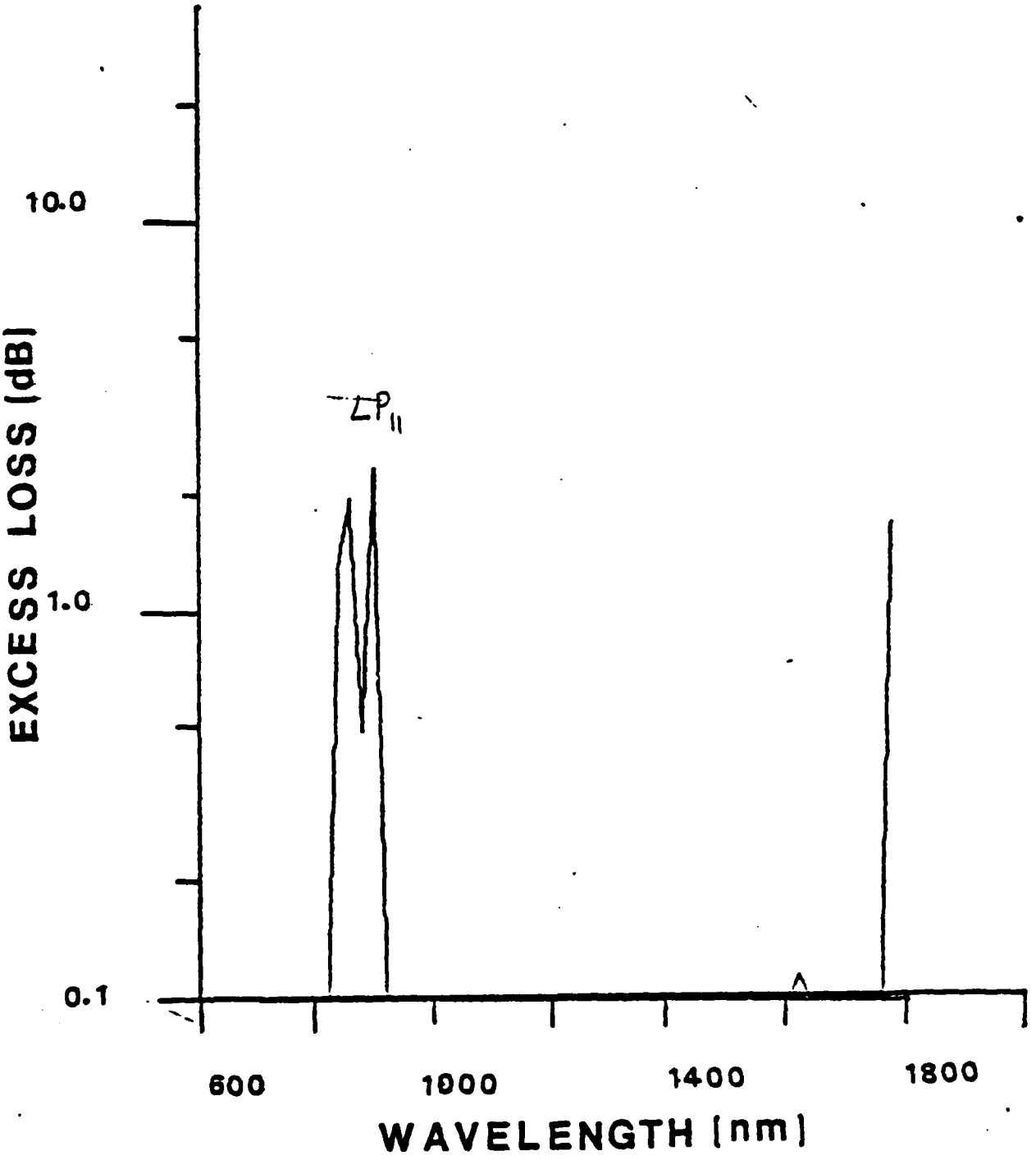

MICROBEND TEST

FIBER NO.: 506803

PIN ARRAY = 3 MM

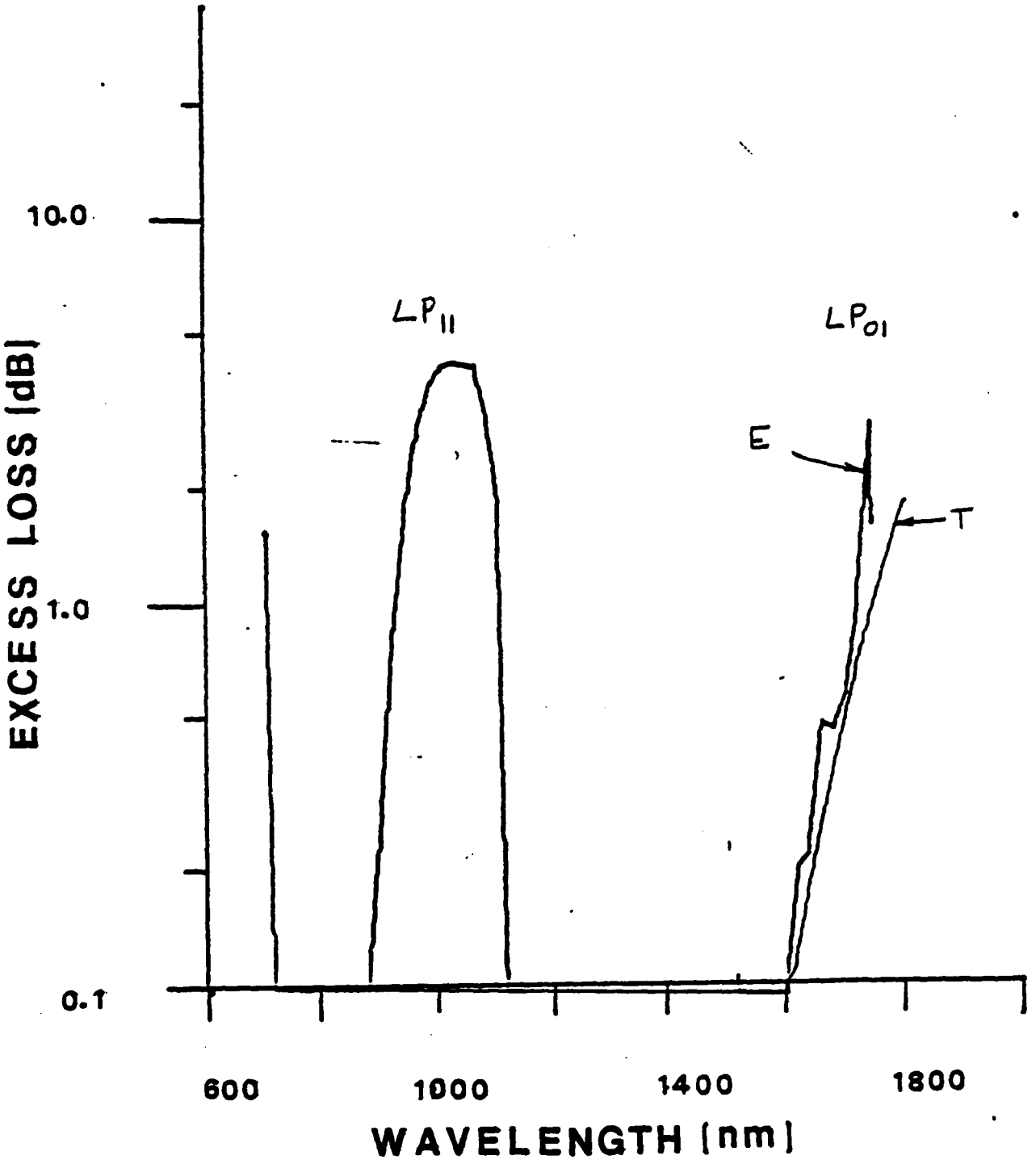

APPENDIX B

Lateral Offset Test Data

Excess loss as a function of lateral offset: comparison of experimental data (E) to Model (T).

LATERAL OFFSET

FIBER NO.: 507205

λ = 1300 nm

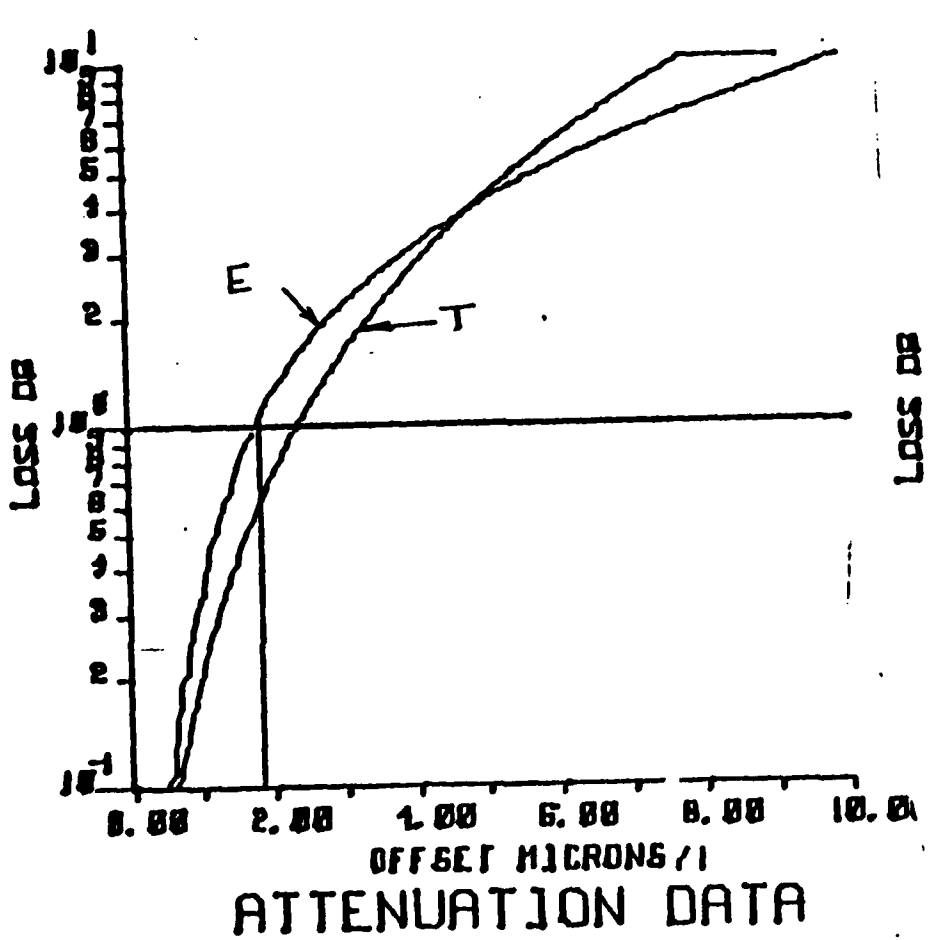

ATTENUATION DATA

λ = 1400 nm

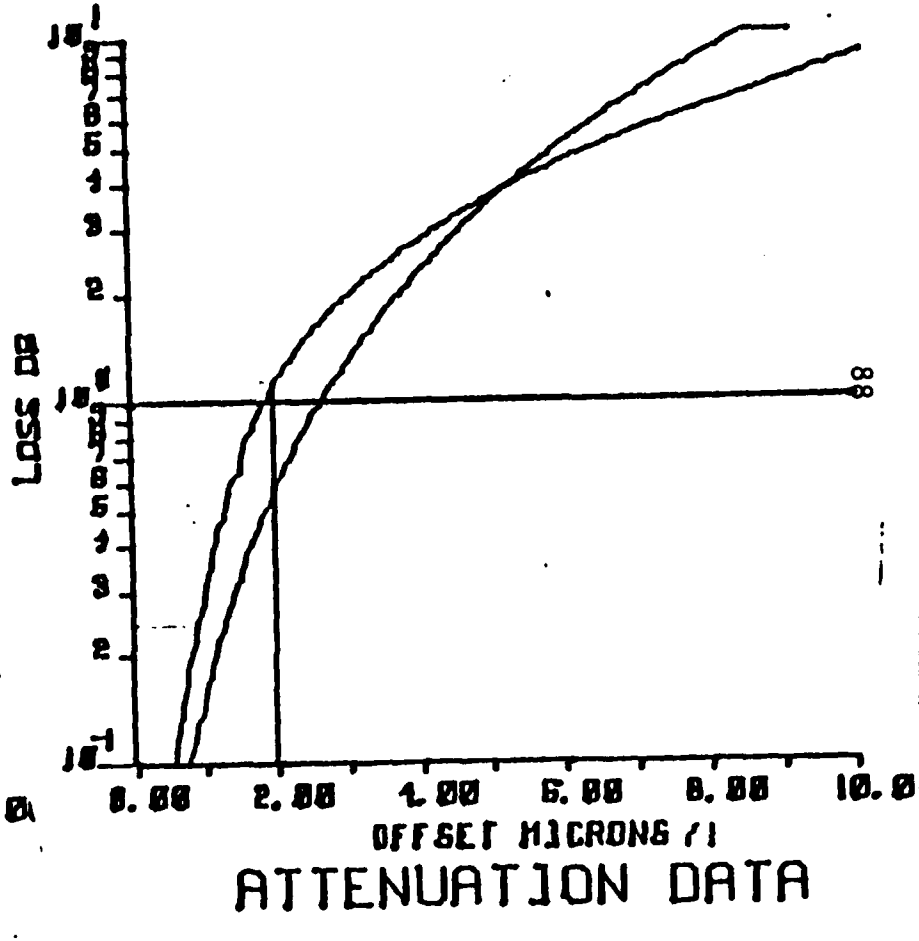

ATTENUATION DATA

LATERAL OFFSET

FIBER NO.: 507205

λ = 1100 nm

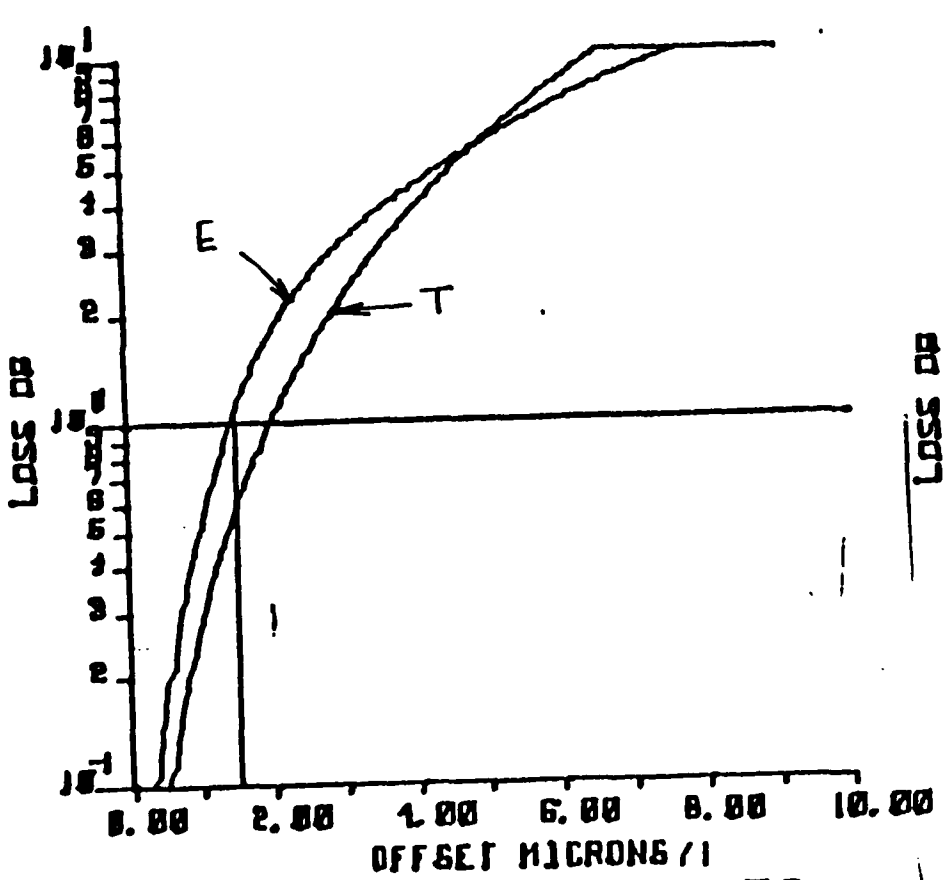

ATTENUATION DATA

λ = 1240 nm

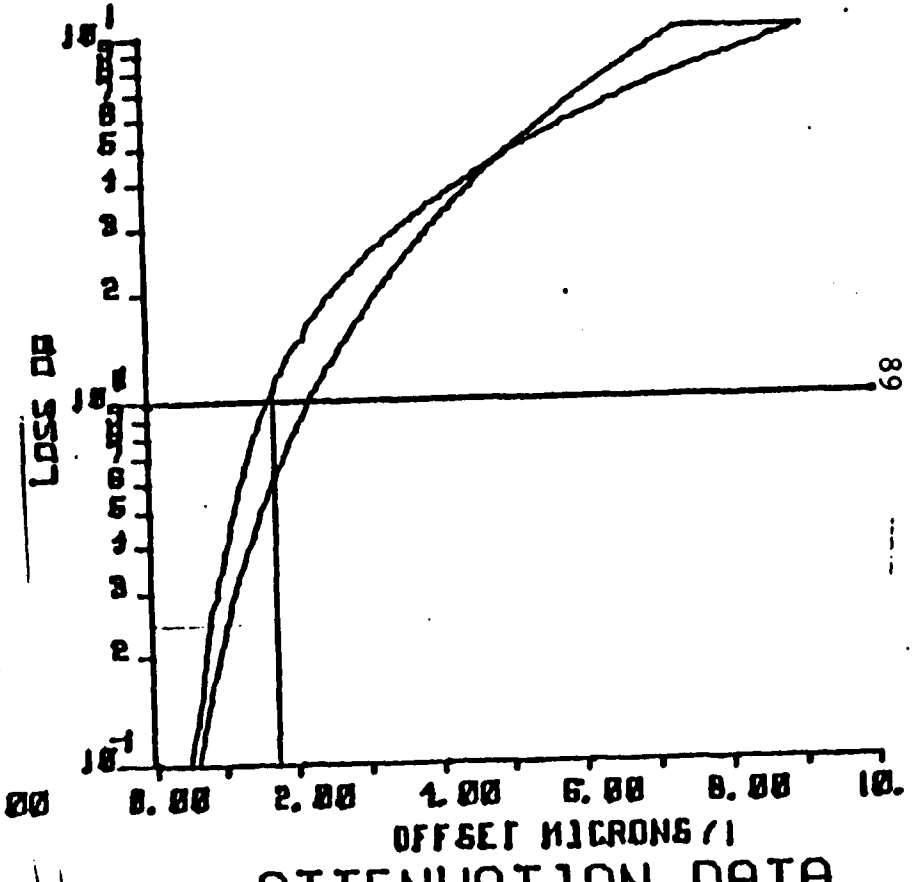

ATTENUATION DATA

LATERAL OFFSET

FIBER NO.: 510802

λ = 1300 nm

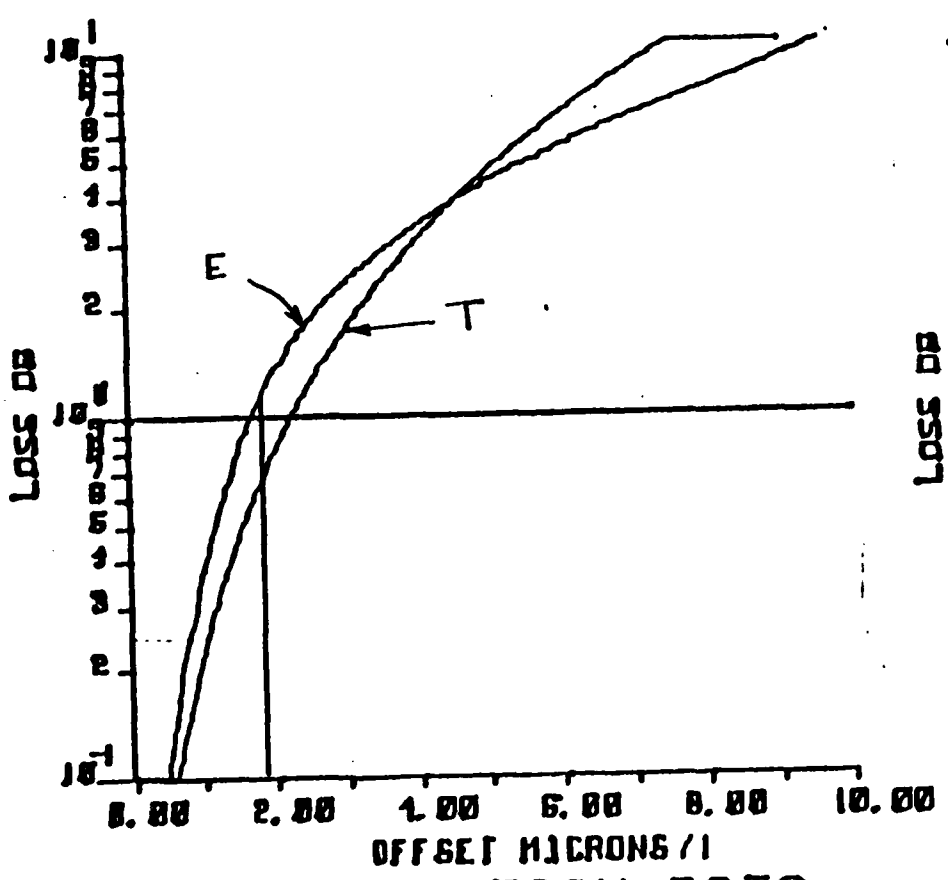

ATTENUATION DATA

λ = 1400 nm

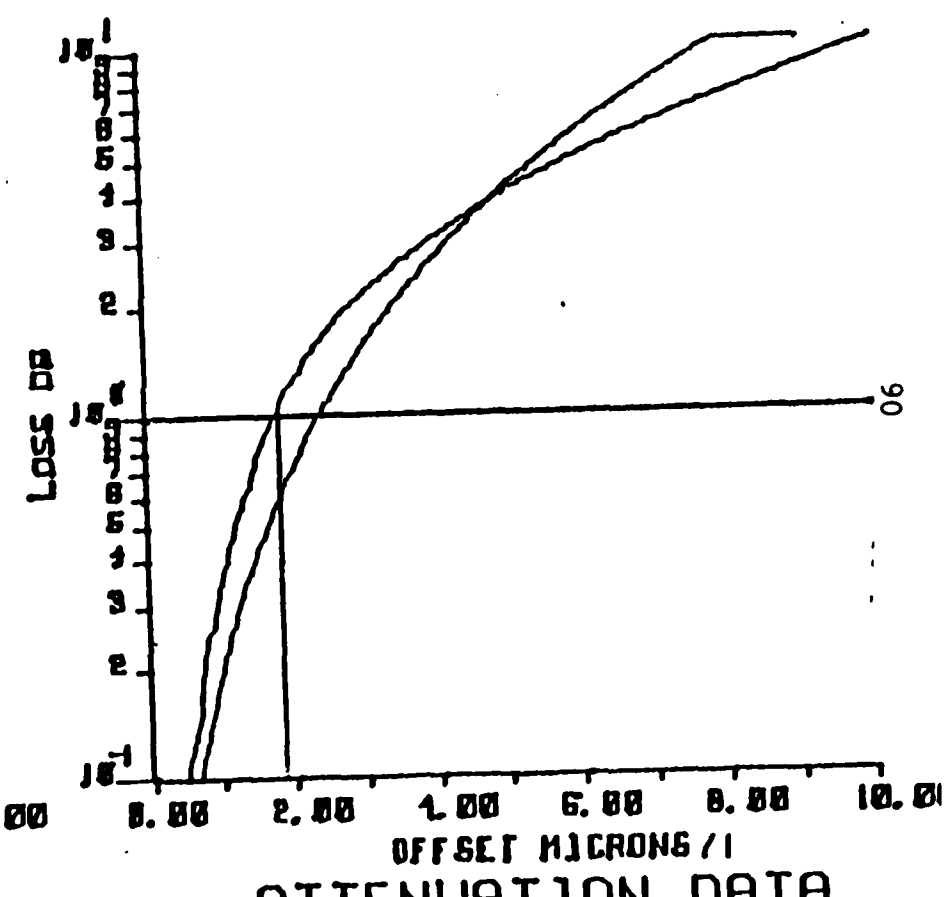

ATTENUATION DATA

31

LATERAL OFFSET

FIBER NO.: 510802

λ = 1100 nm

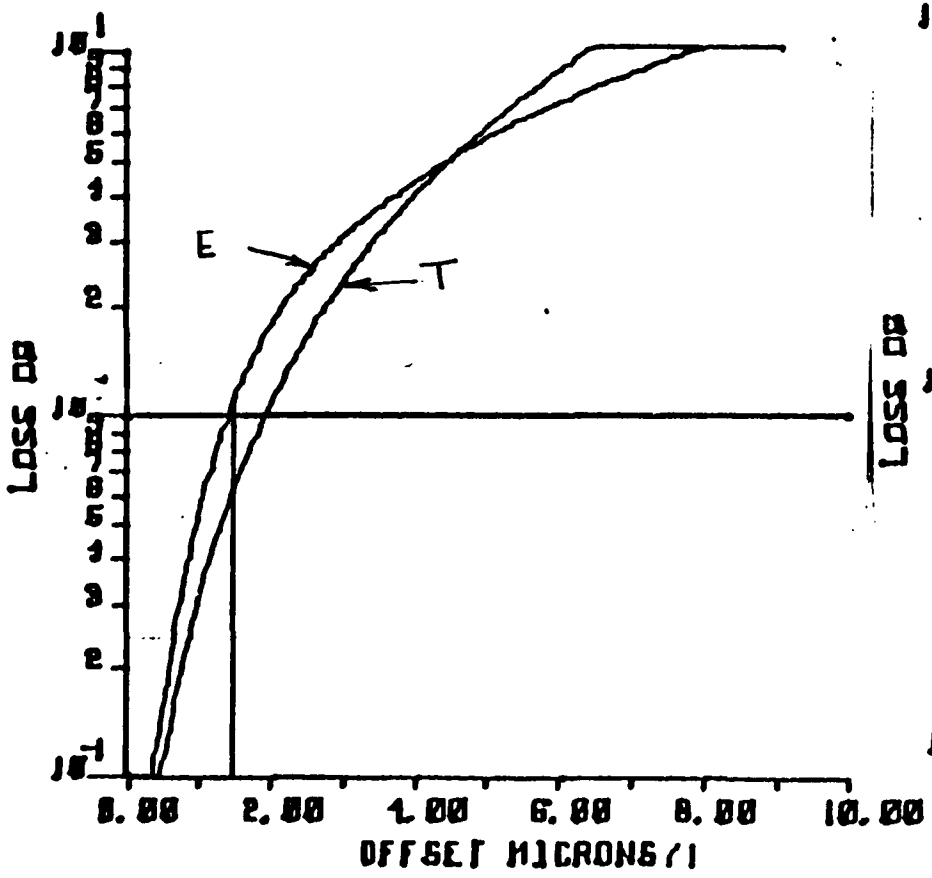

ATTENUATION DATA

λ = 1240 nm

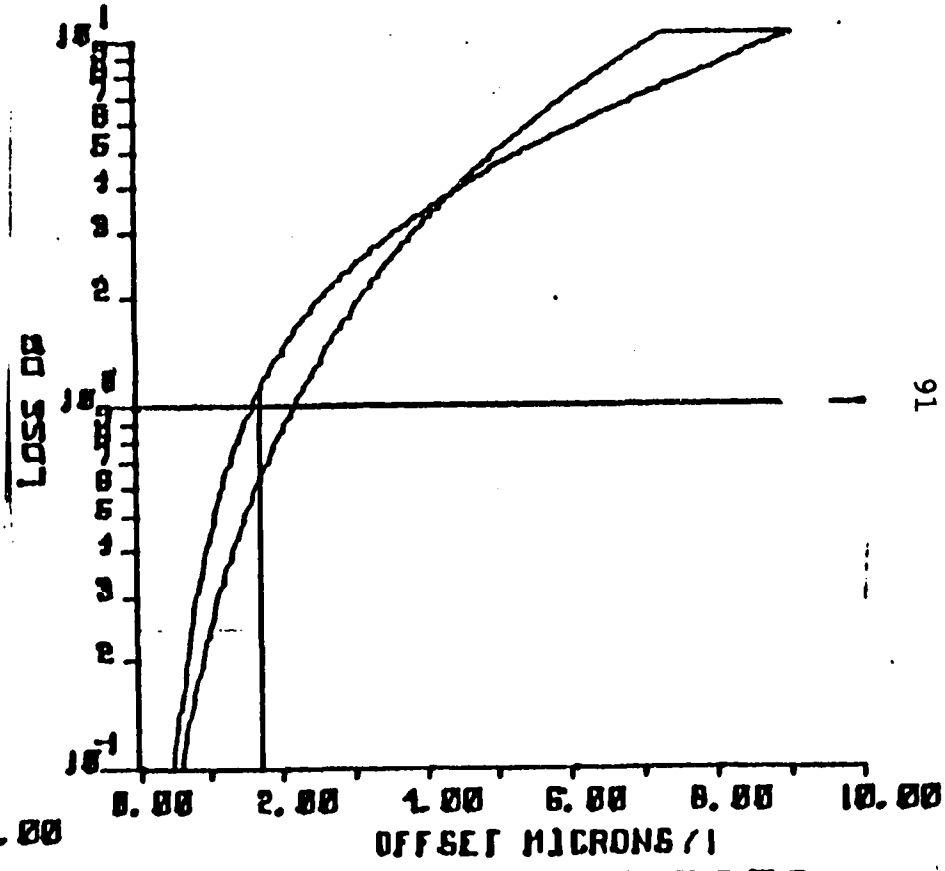

ATTENUATION DATA

LATERAL OFFSET

FIBER NO.: 509503

λ = 1500 nm

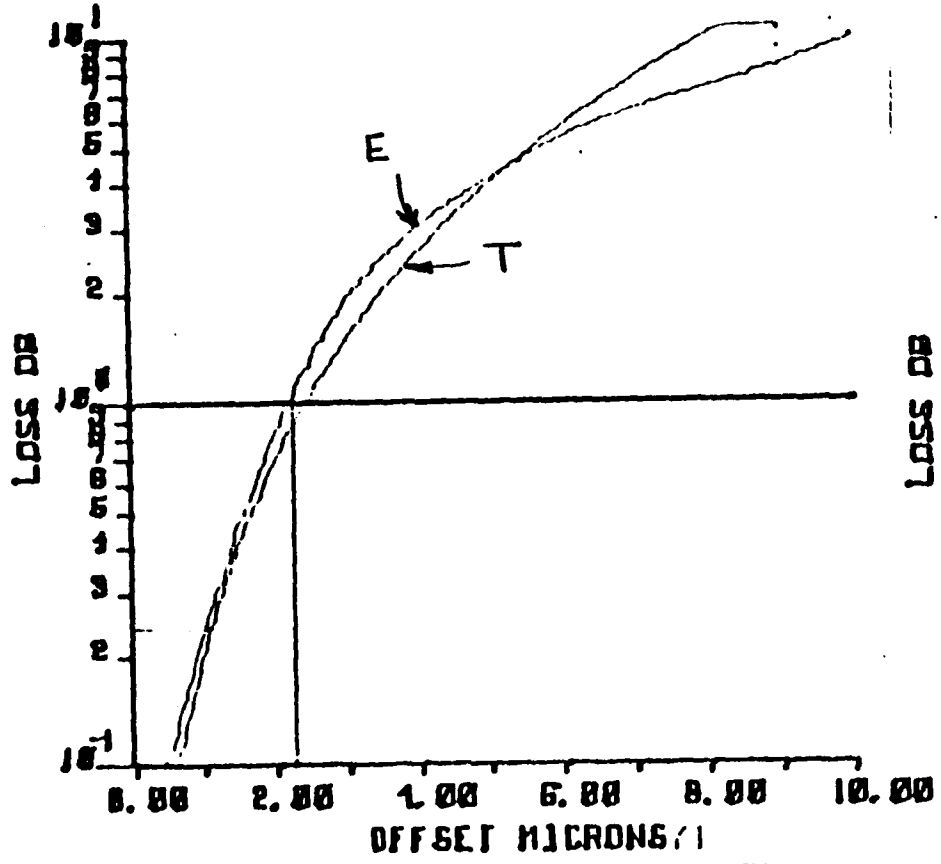

ATTENUATION DATA

λ = 1600 nm

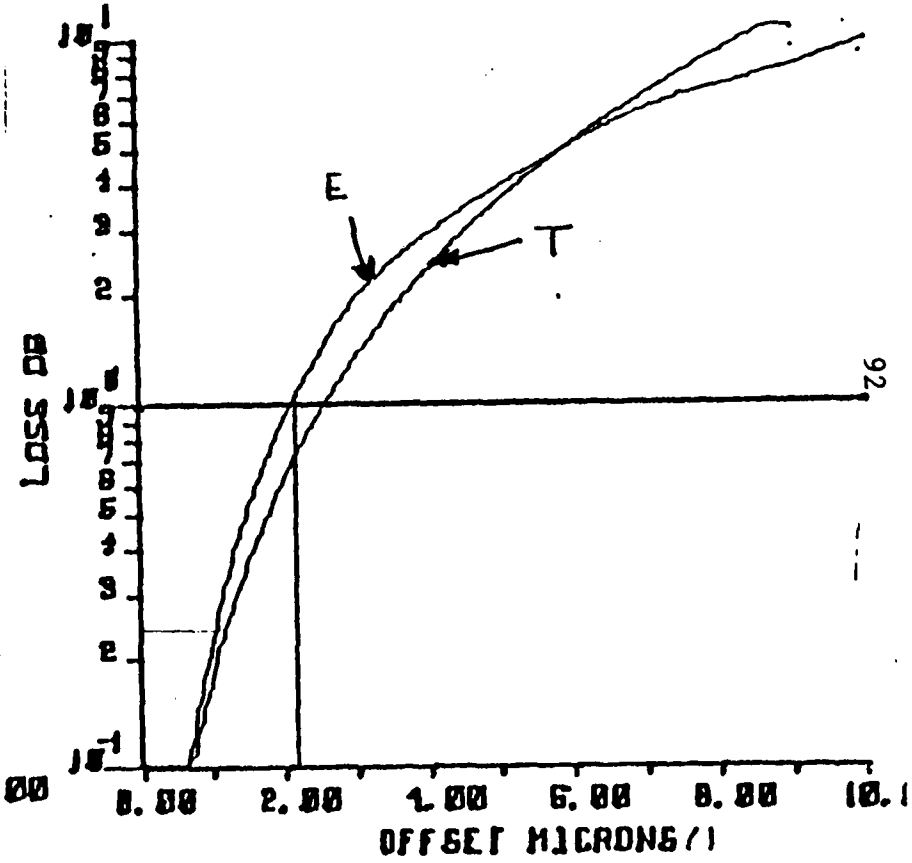

ATTENUATION DATA

AD-A109 621 CORNING GLASS WORKS NY F/G 20/6
SINGLE MODE OPTICAL WAVEGUIDE DESIGN STUDY.(U)
NOV 81 V A BHAGAVATULA, D B KECK, R A WESTWIG N00173-80-C-0563
UNCLASSIFIED NL

2 OF 2
AD A
109621

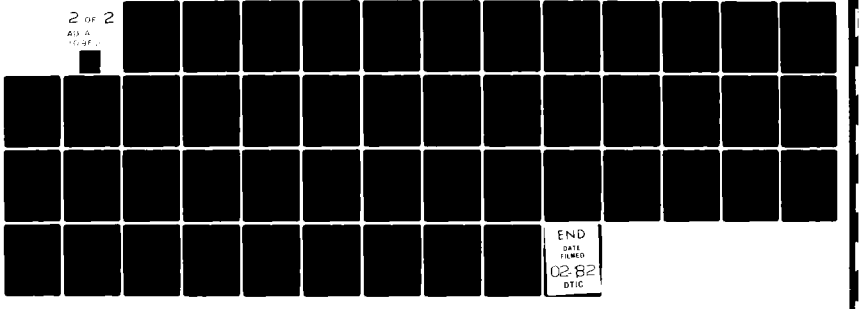

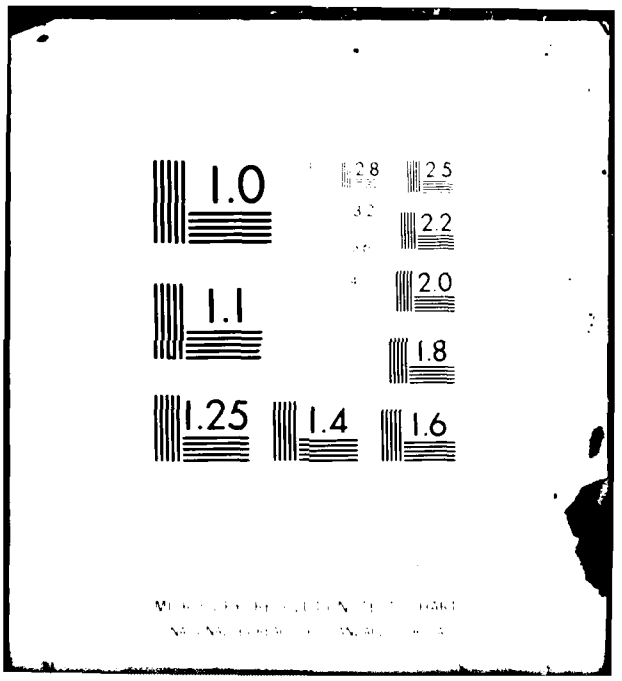
1.0
2.8
2.5
2.2
1.1
2.0
1.8
1.25
1.4
1.6

LATERAL OFFSET

FIBER NO.: 509503

λ = 1300 nm

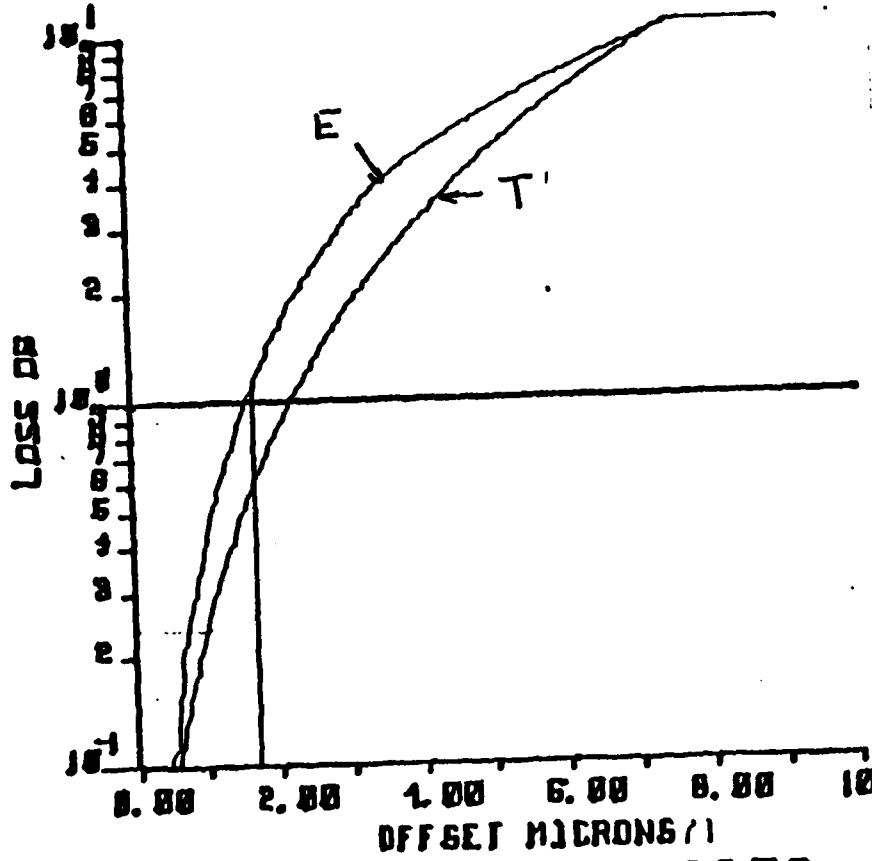

ATTENUATION DATA

λ = 1400 nm

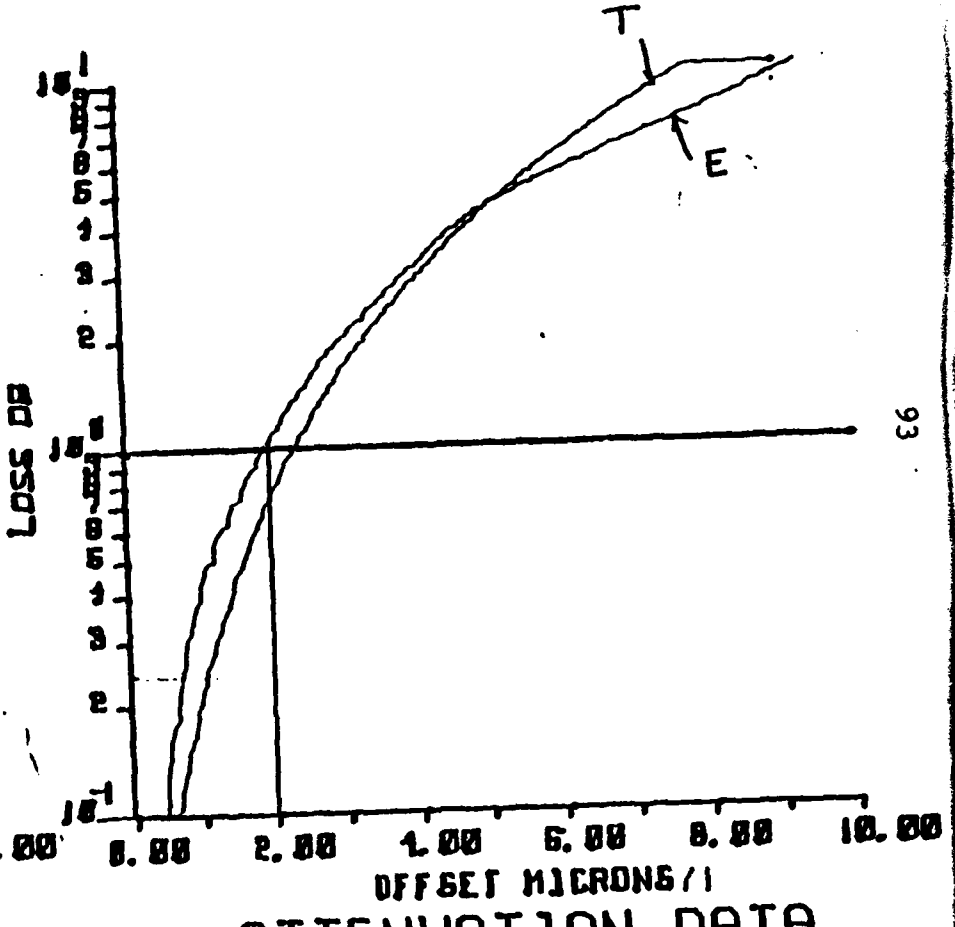

ATTENUATION DATA

93

86

LATERAL OFFSET

FIBER NO.: 509503

$\lambda =$ 1100 nm

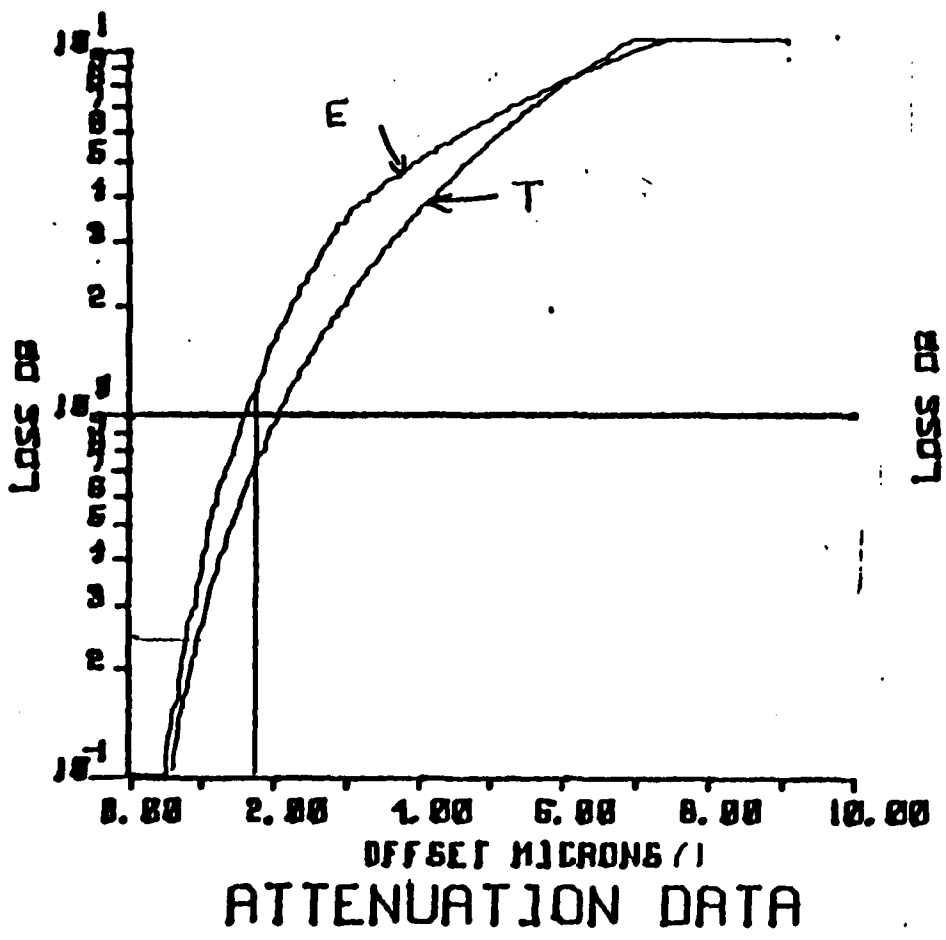

ATTENUATION DATA

$\lambda =$ 1240 nm

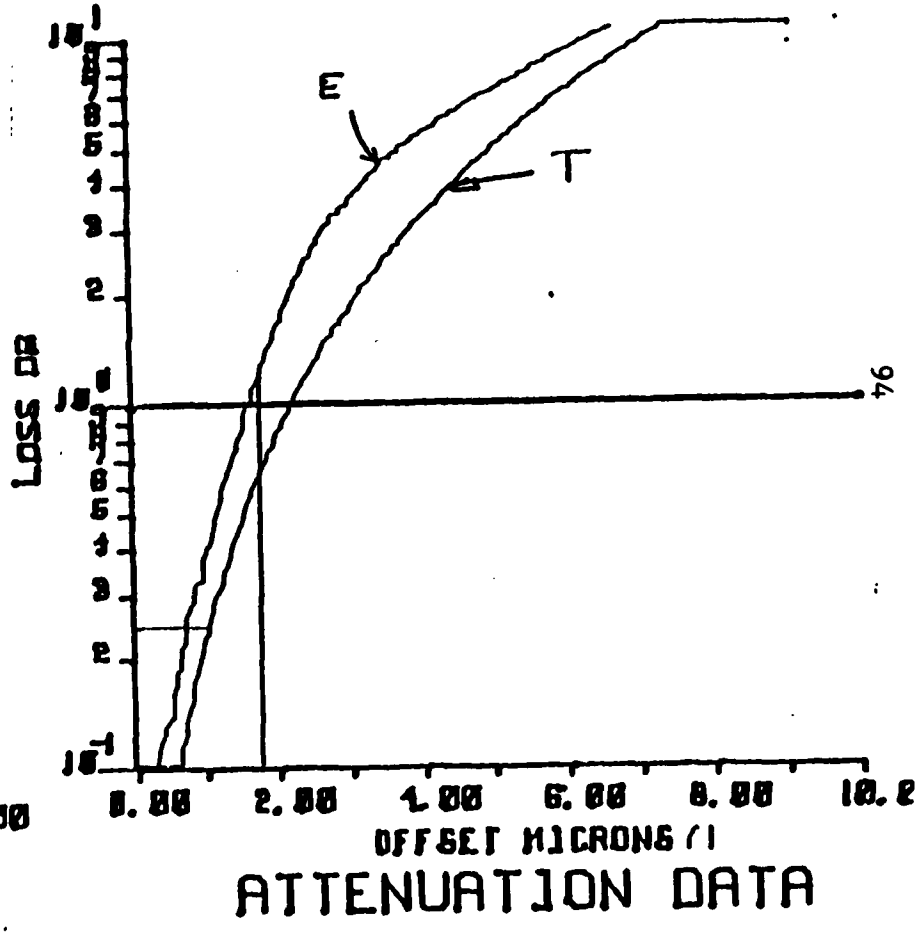

ATTENUATION DATA

05

LATERAL OFFSET

FIBER NO.: 343104

λ = 1500 nm

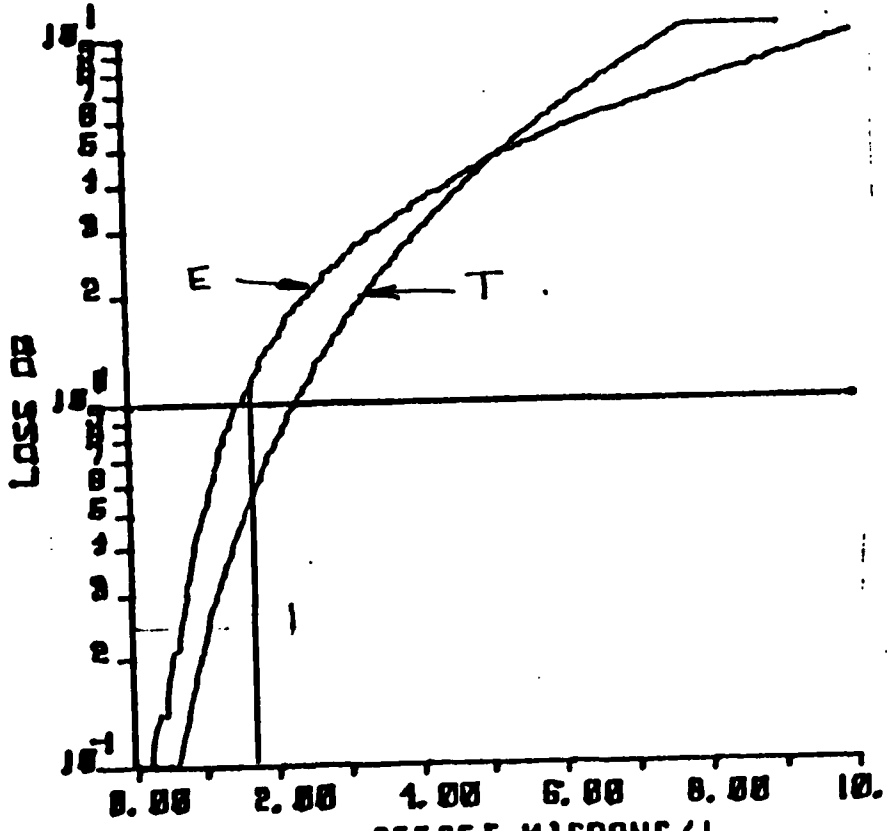

ATTENUATION DATA

λ = 1600 nm

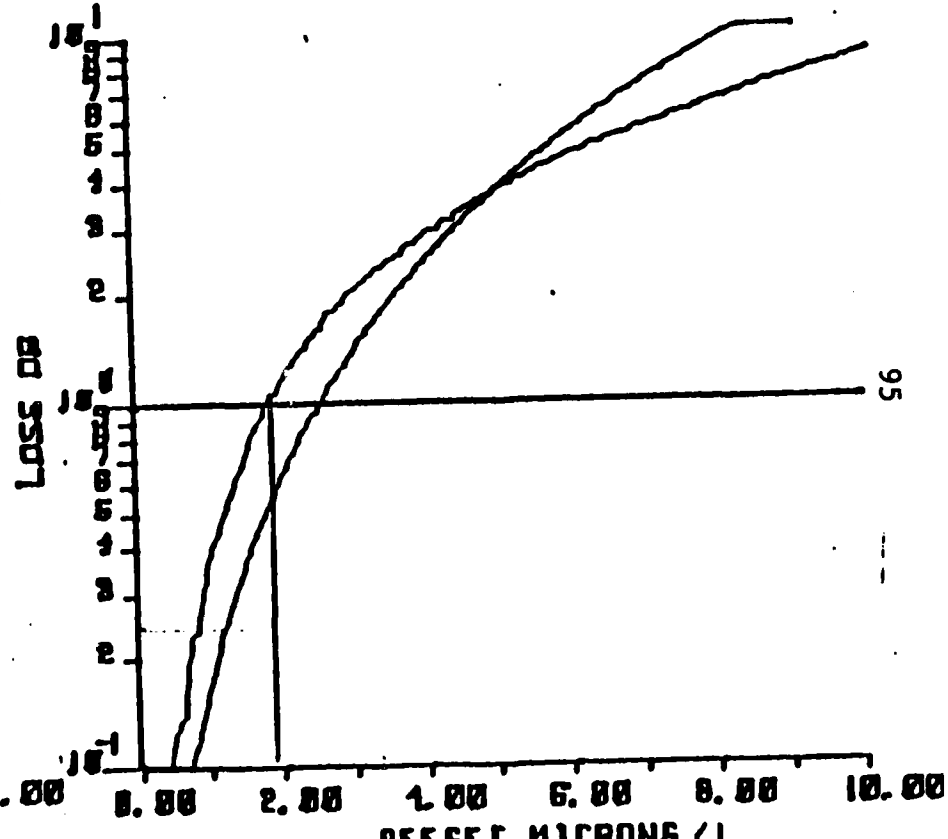

ATTENUATION DATA

LATERAL OFFSET

FIBER NO.: 343104

λ = 1240 nm

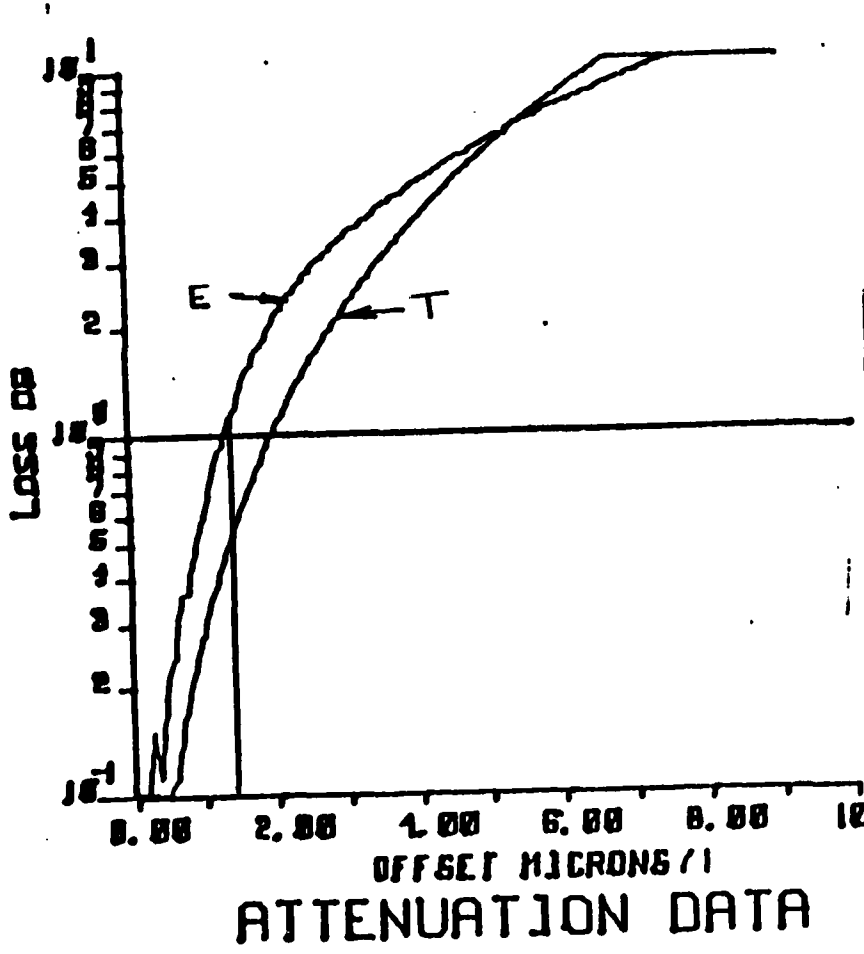

ATTENUATION DATA

λ = 1400 nm

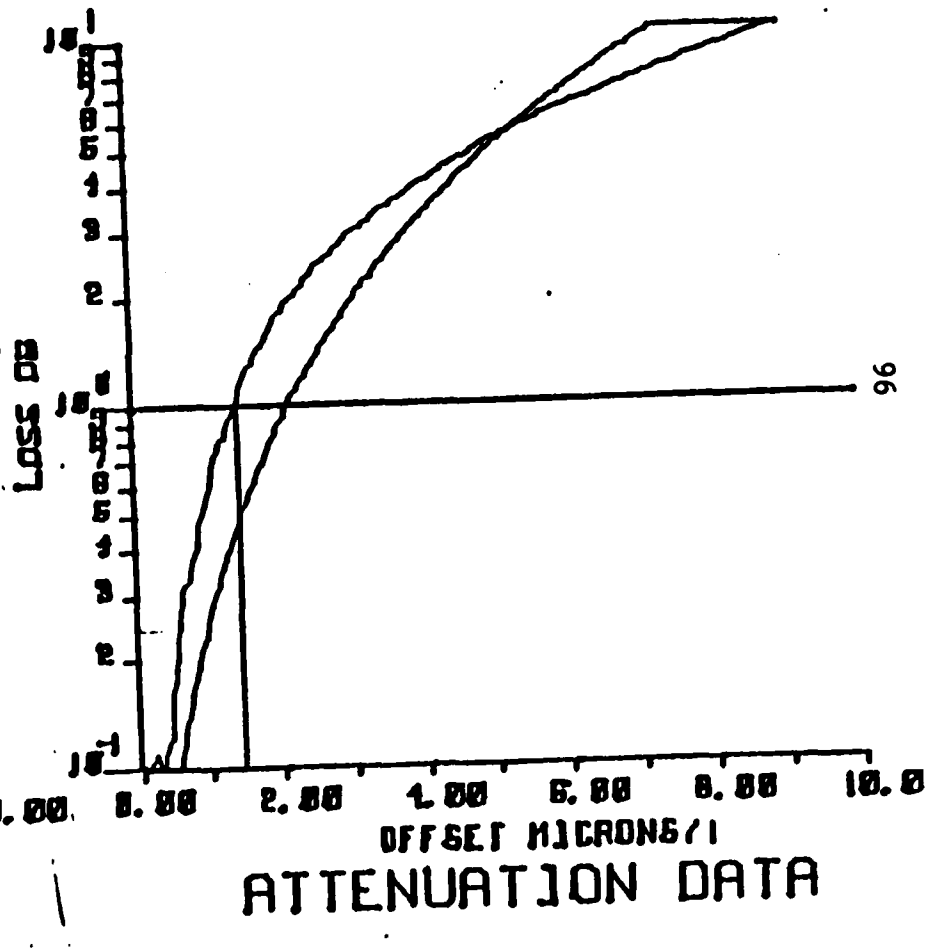

ATTENUATION DATA

LATERAL OFFSET

FIBER NO.: 343104

λ = 900 nm

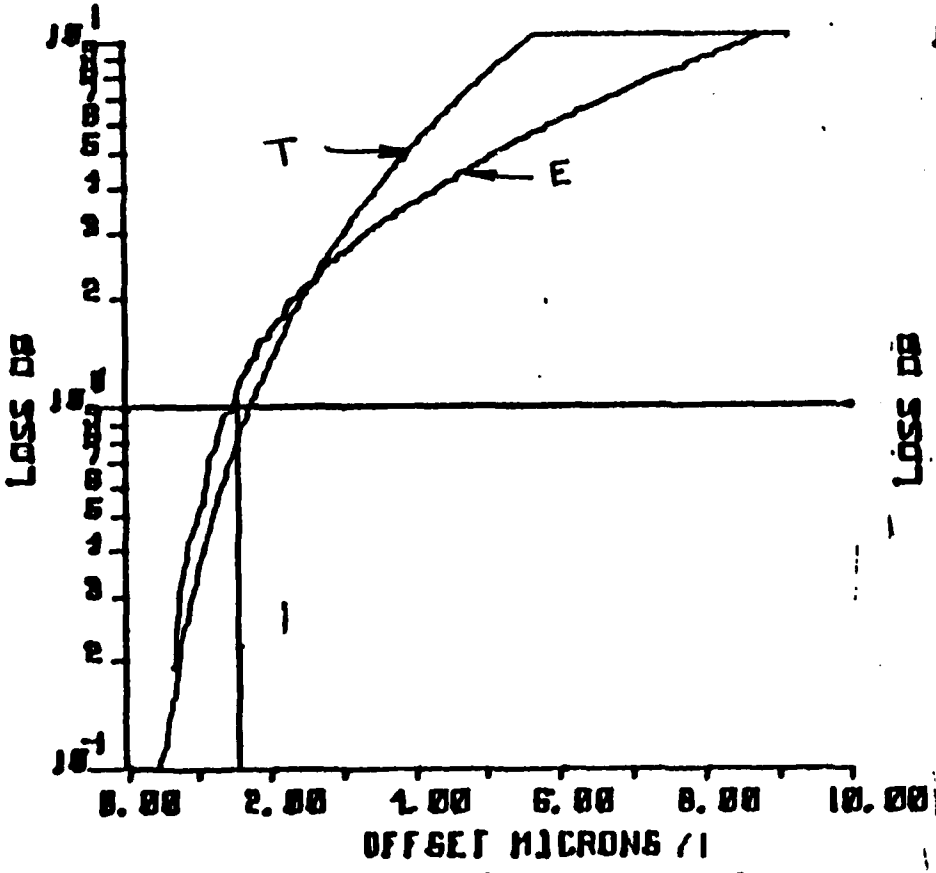

ATTENUATION DATA

λ = 1100 nm

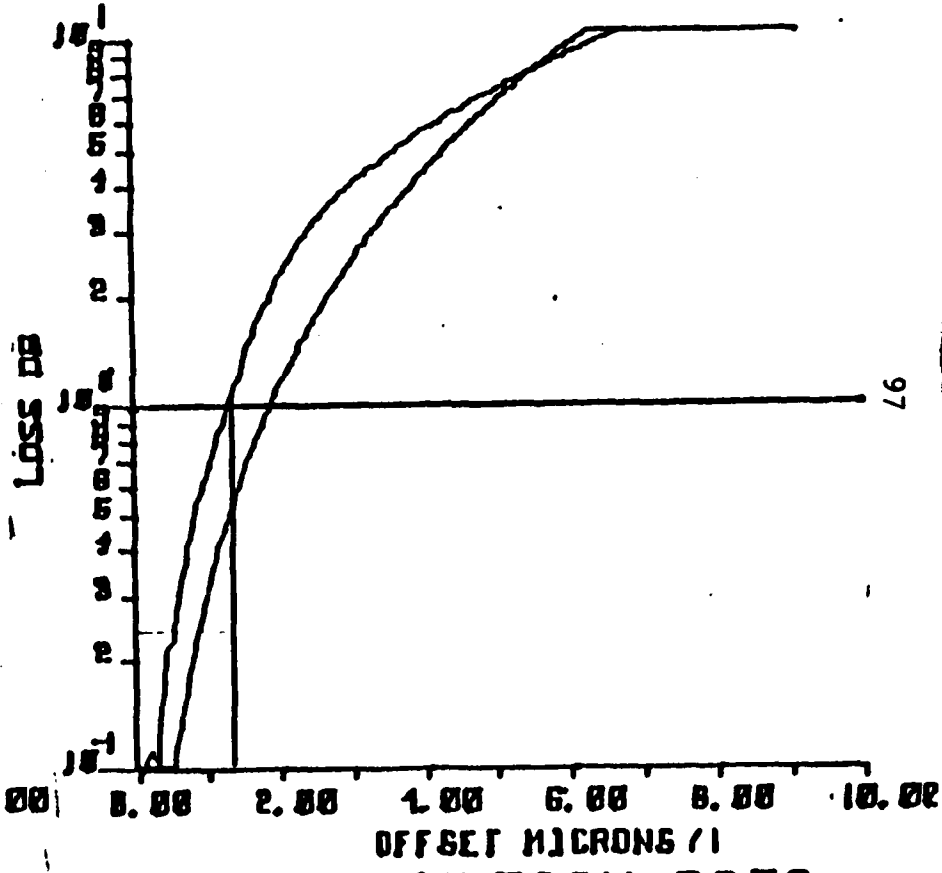

ATTENUATION DATA

97

81

LATERAL OFFSET

FIBER NO.: 506902

λ = 1400 nm

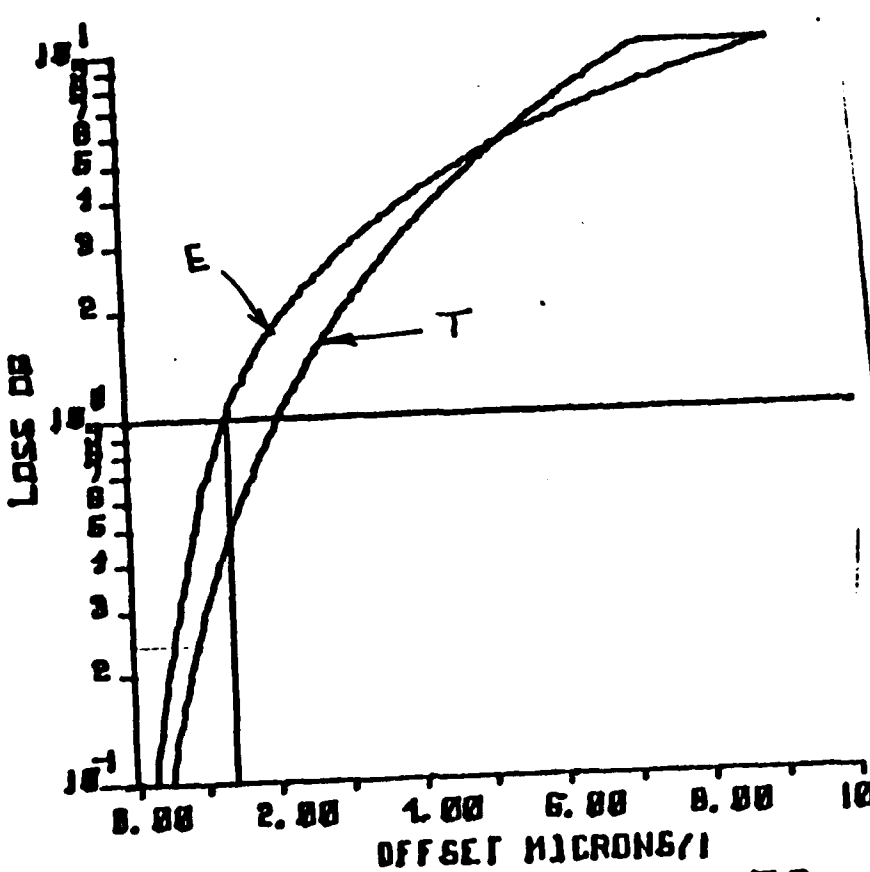

ATTENUATION DATA

λ = 1500 nm

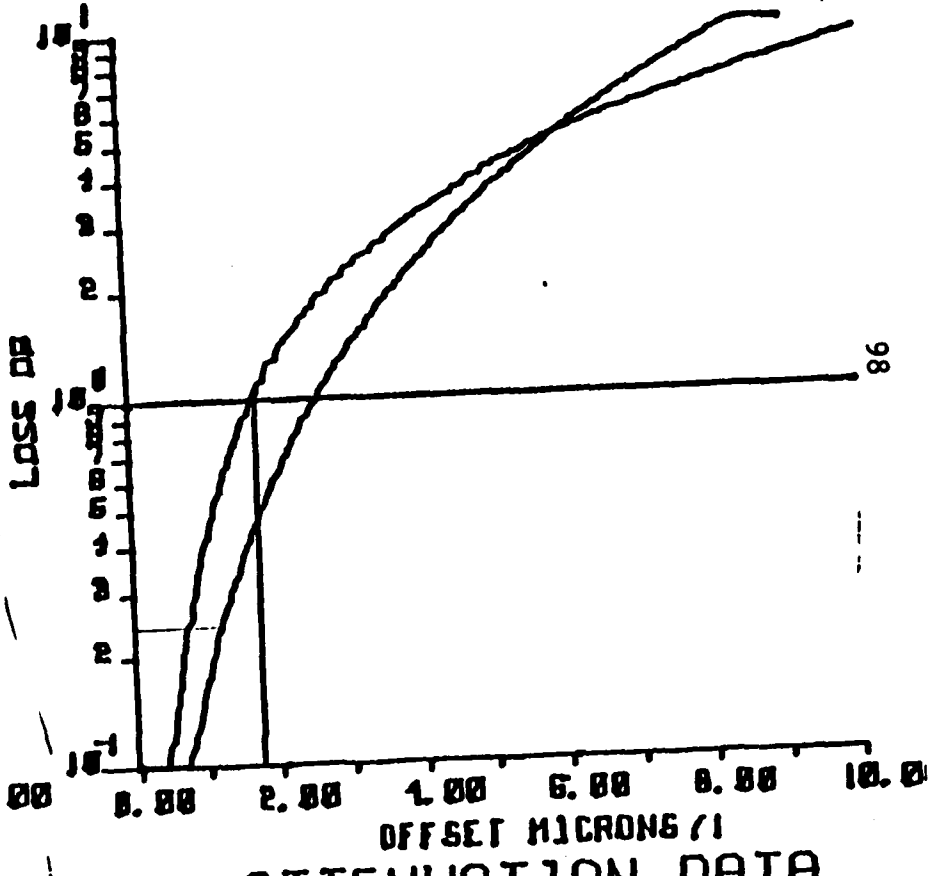

ATTENUATION DATA

LATERAL OFFSET

FIBER NO.: 506902

λ = 1240 nm

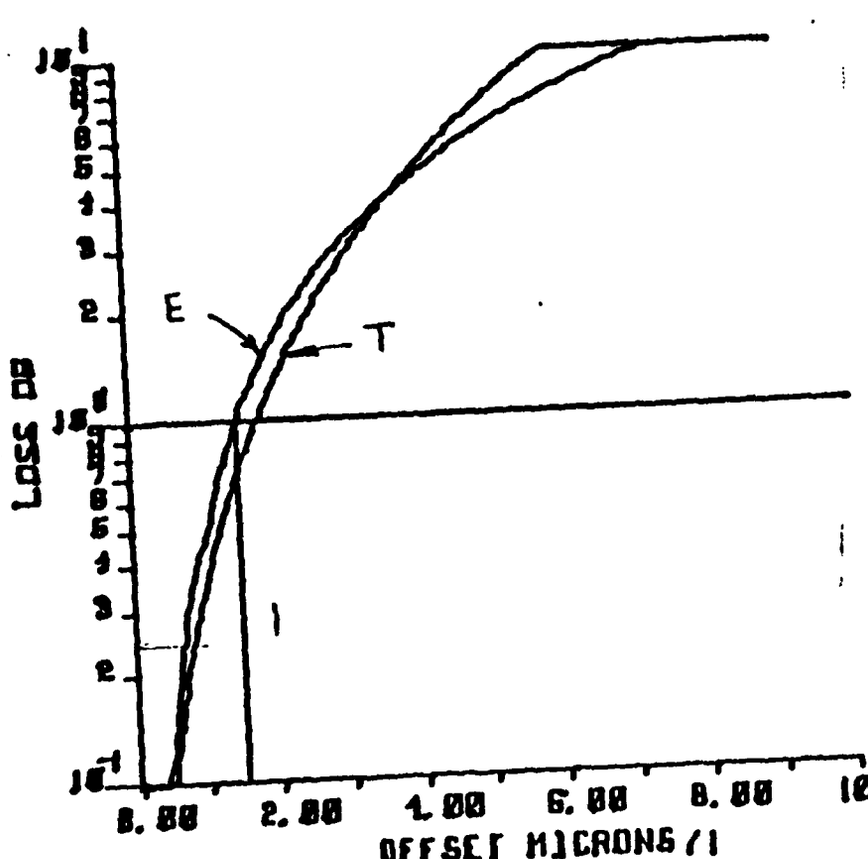

ATTENUATION DATA

λ = 1300 nm

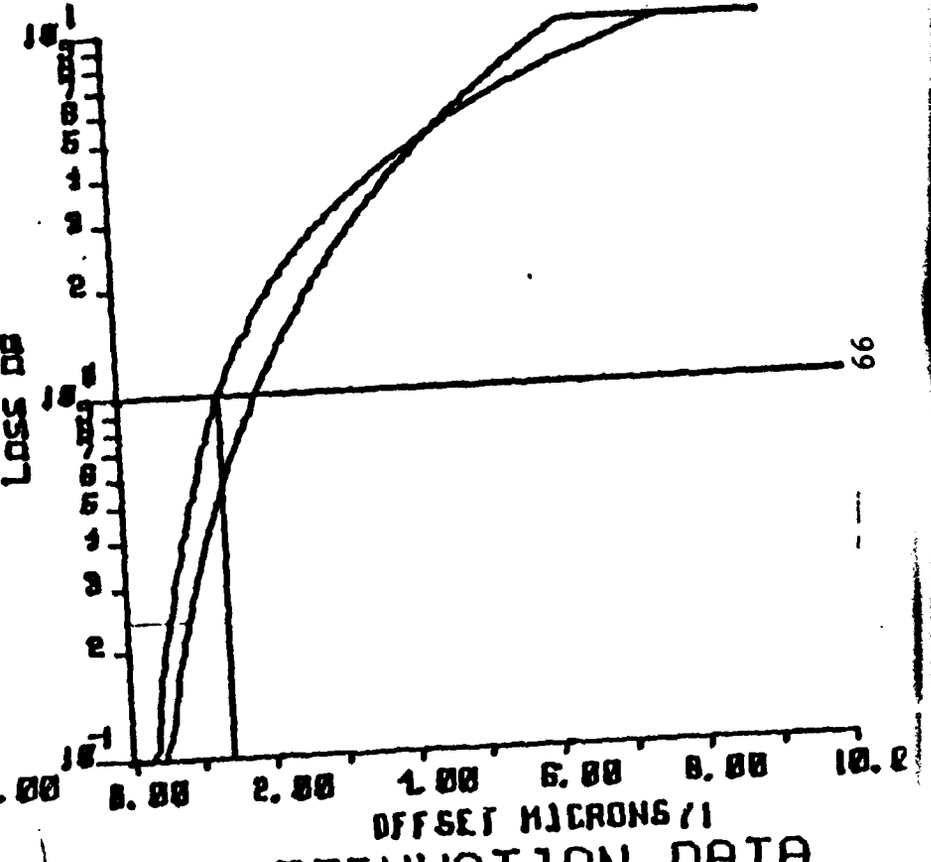

ATTENUATION DATA

81

LATERAL OFFSET

FIBER NO.: 506902

λ = 900 nm

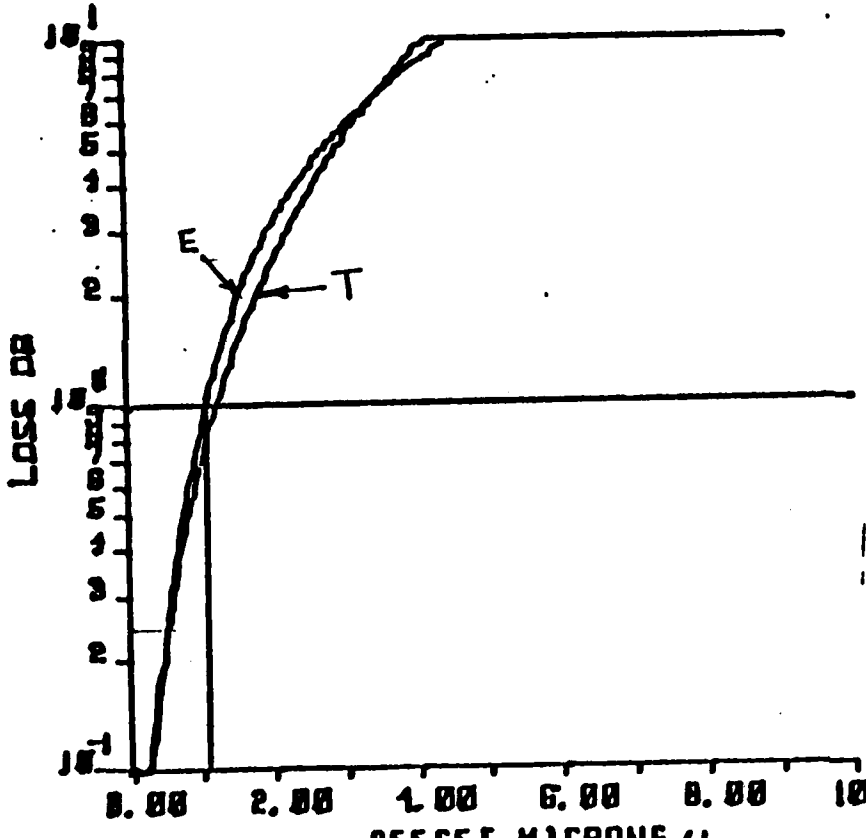

ATTENUATION DATA

λ = 1100 nm

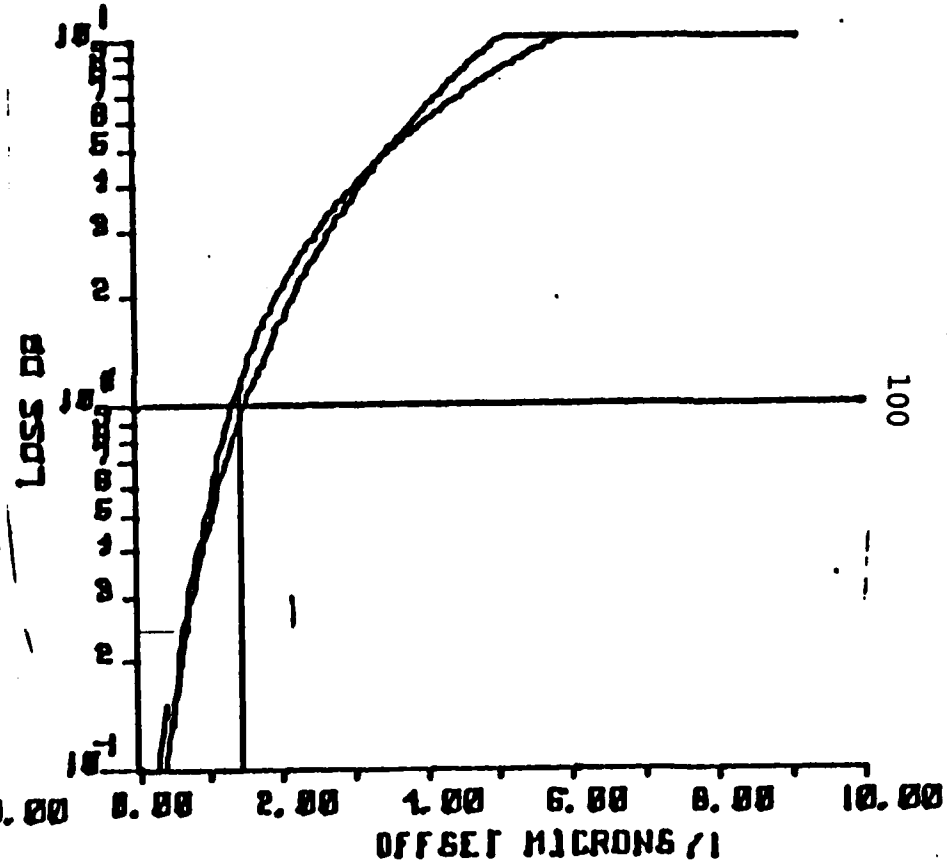

ATTENUATION DATA

LATERAL OFFSET

FIBER NO.: 434004

λ = 1300 nm

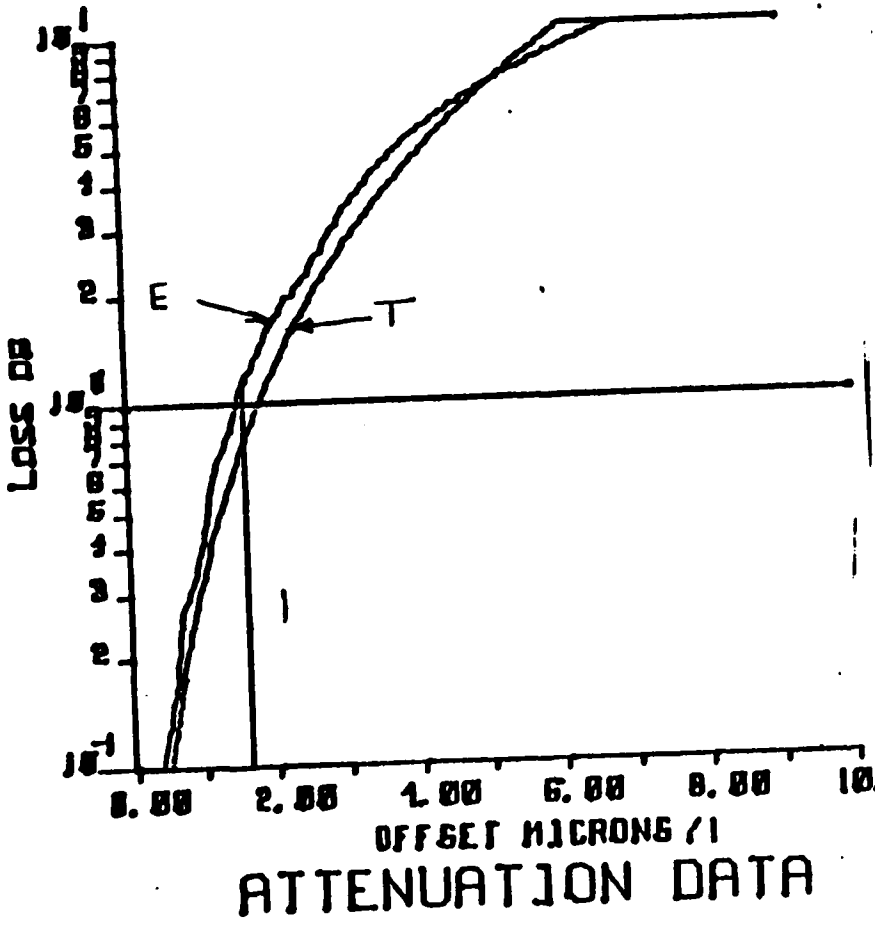

ATTENUATION DATA

λ = 1400 nm

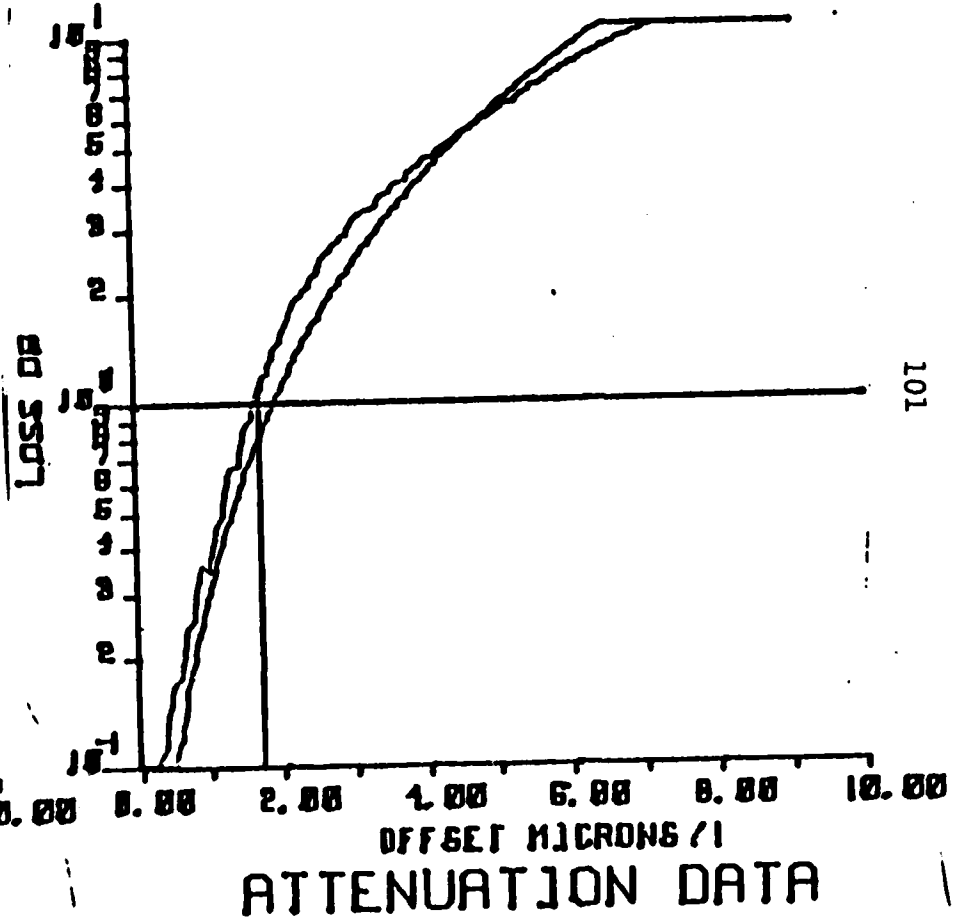

ATTENUATION DATA

LATERAL OFFSET

FIBER NO.: 434004

λ = 1500 nm

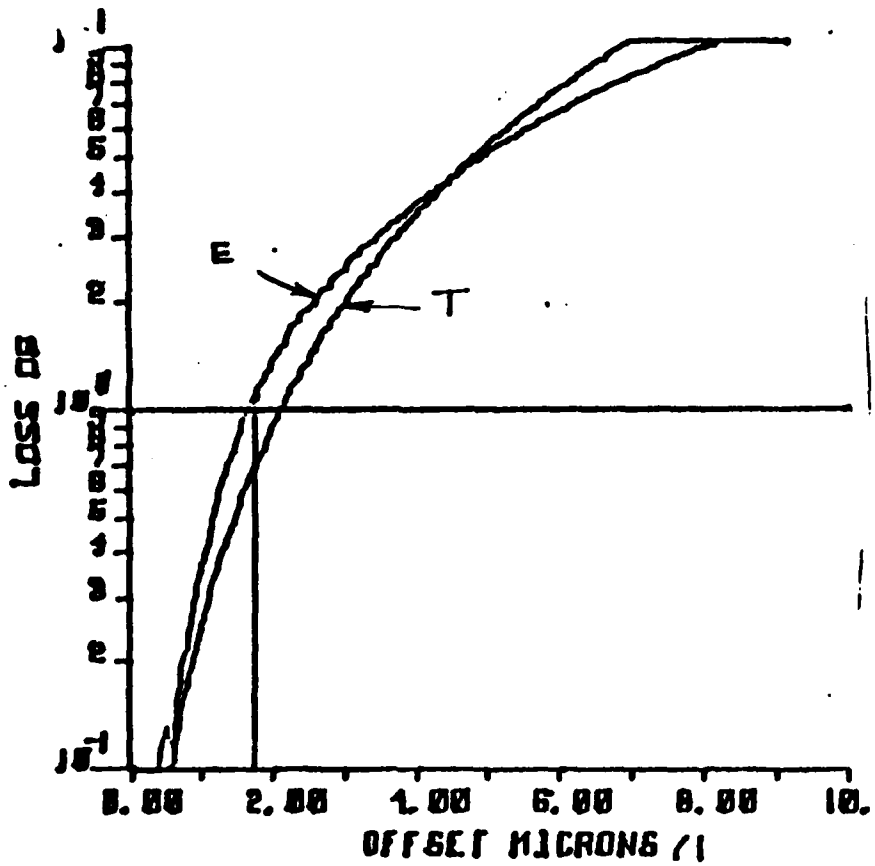

ATTENUATION DATA

λ = 1600 nm

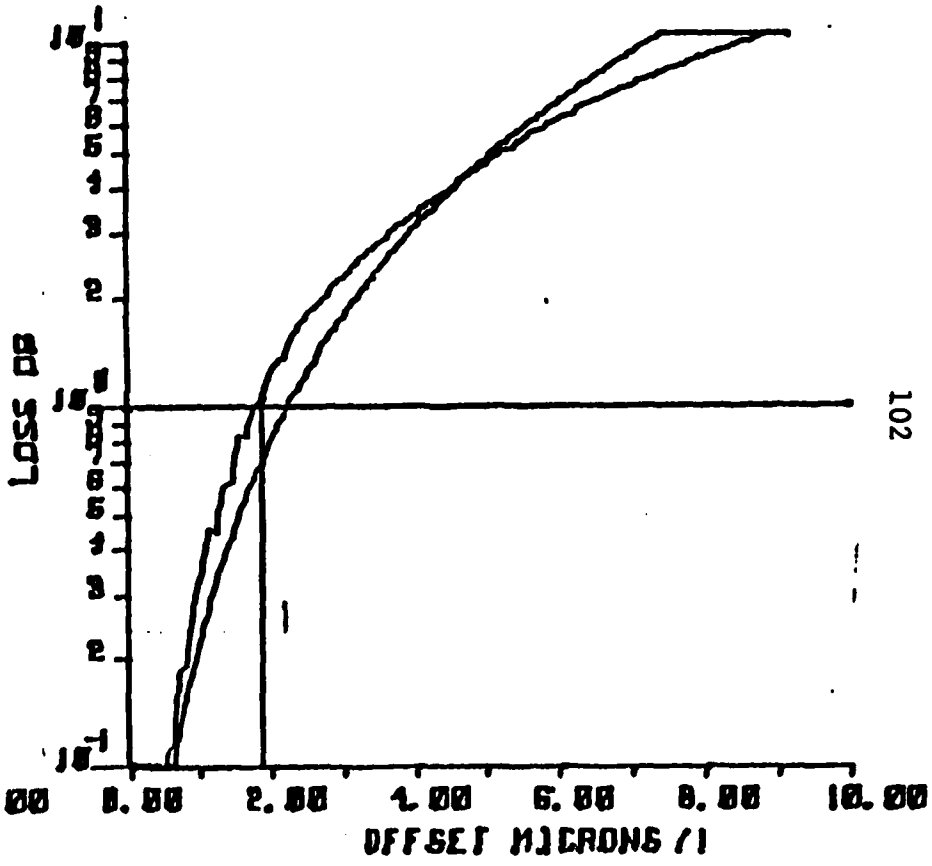

ATTENUATION DATA

LATERAL OFFSET

FIBER NO.: 502905

λ = 1300 nm

λ = nm

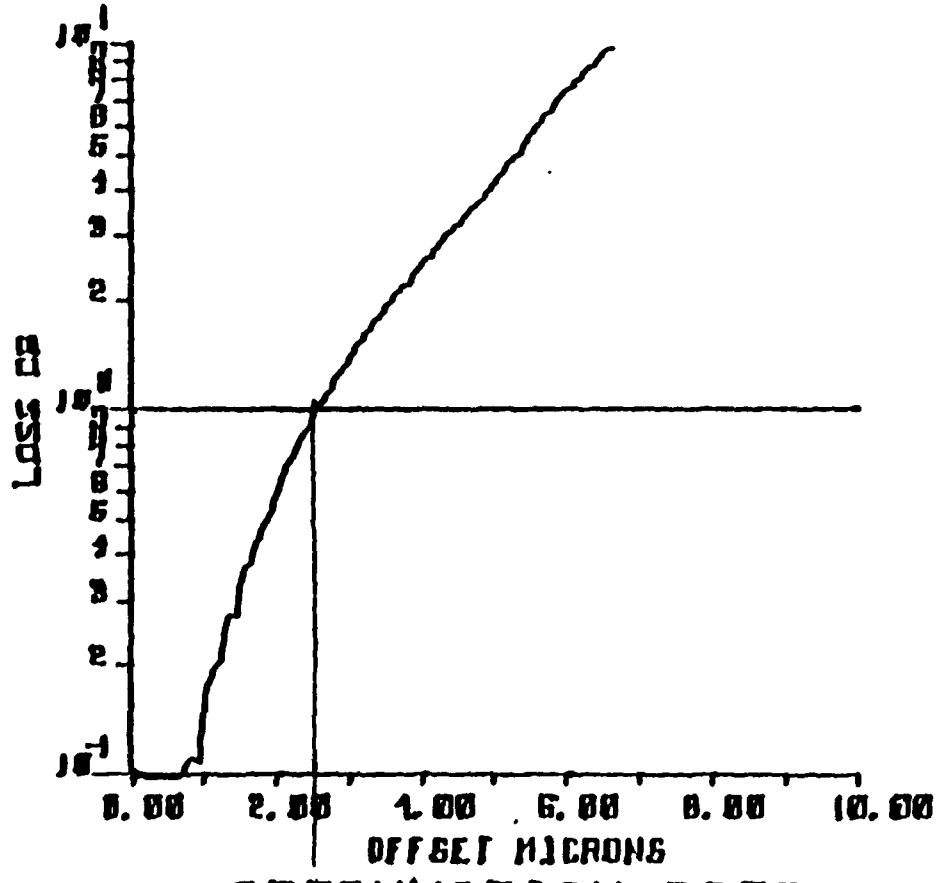

ATTENUATION DATA

11

LATERAL OFFSET

FIBER NO.: 503103

λ = 1300 nm

λ = nm

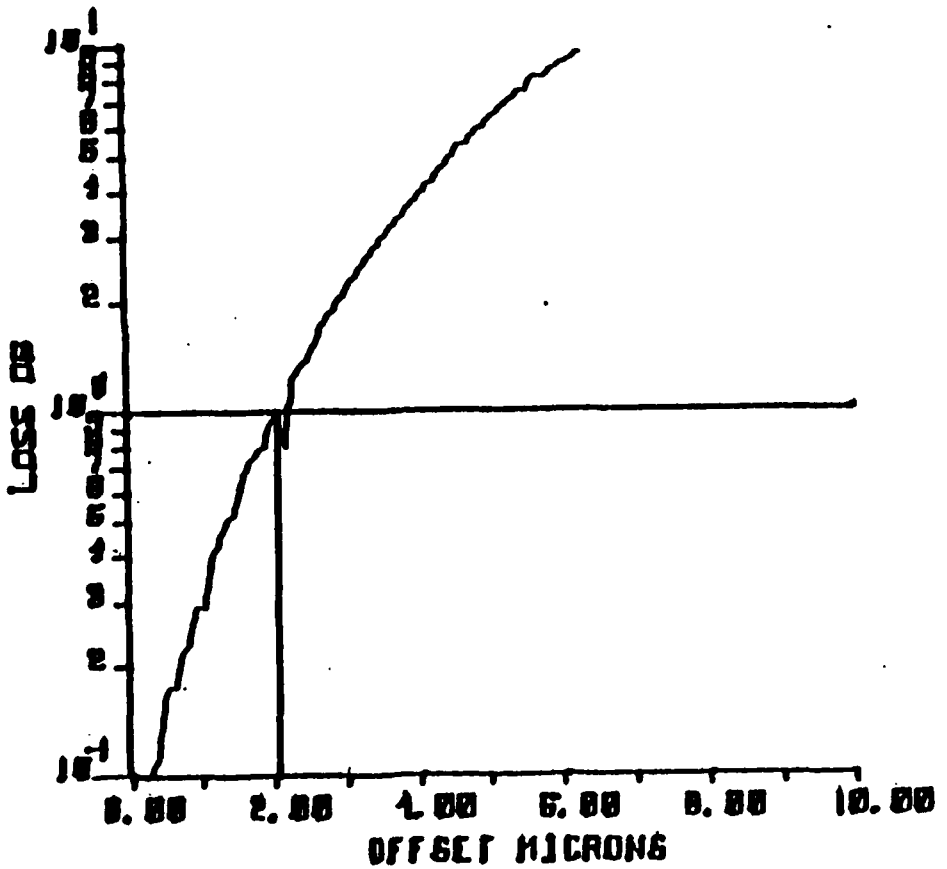

ATTENUATION DATA

LATERAL OFFSET

FIBER NO.: 503403

λ = 1600 nm

λ = nm

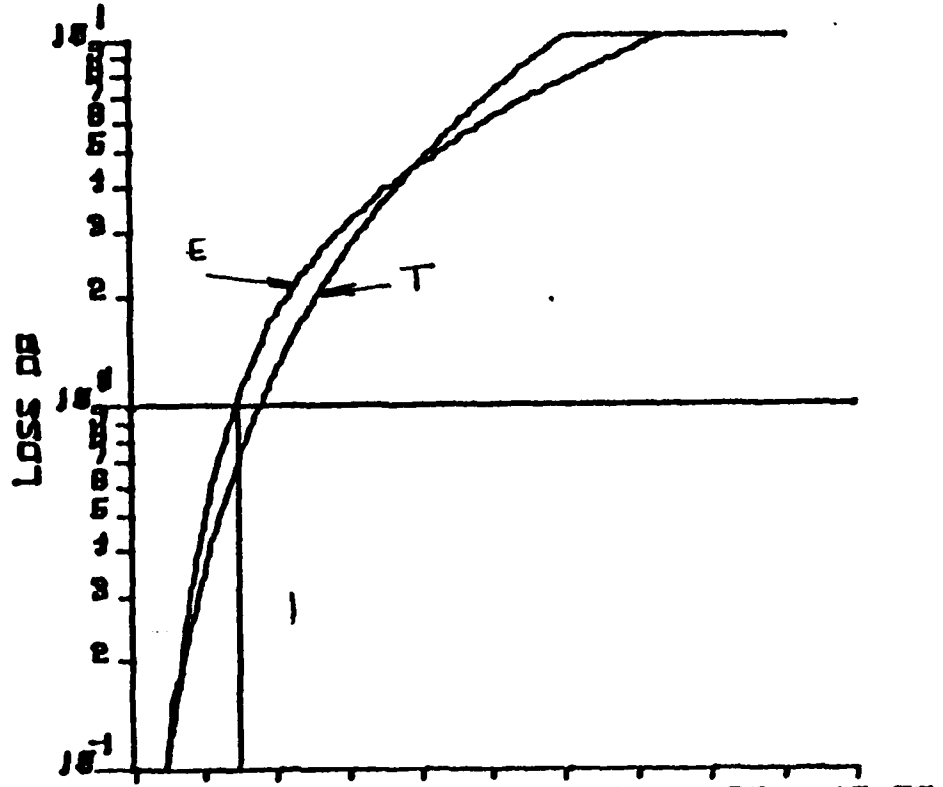

ATTENUATION DATA

DS

LATERAL OFFSET

FIBER NO.: 503403

λ = 1300 nm

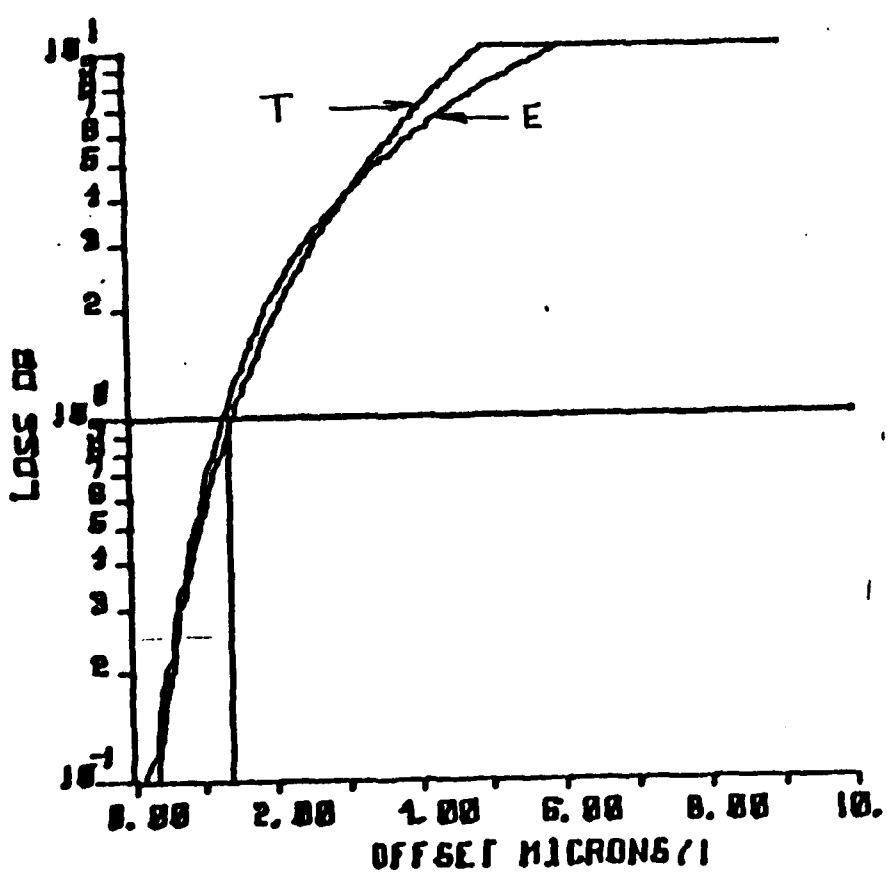

ATTENUATION DATA

λ = 1400 nm

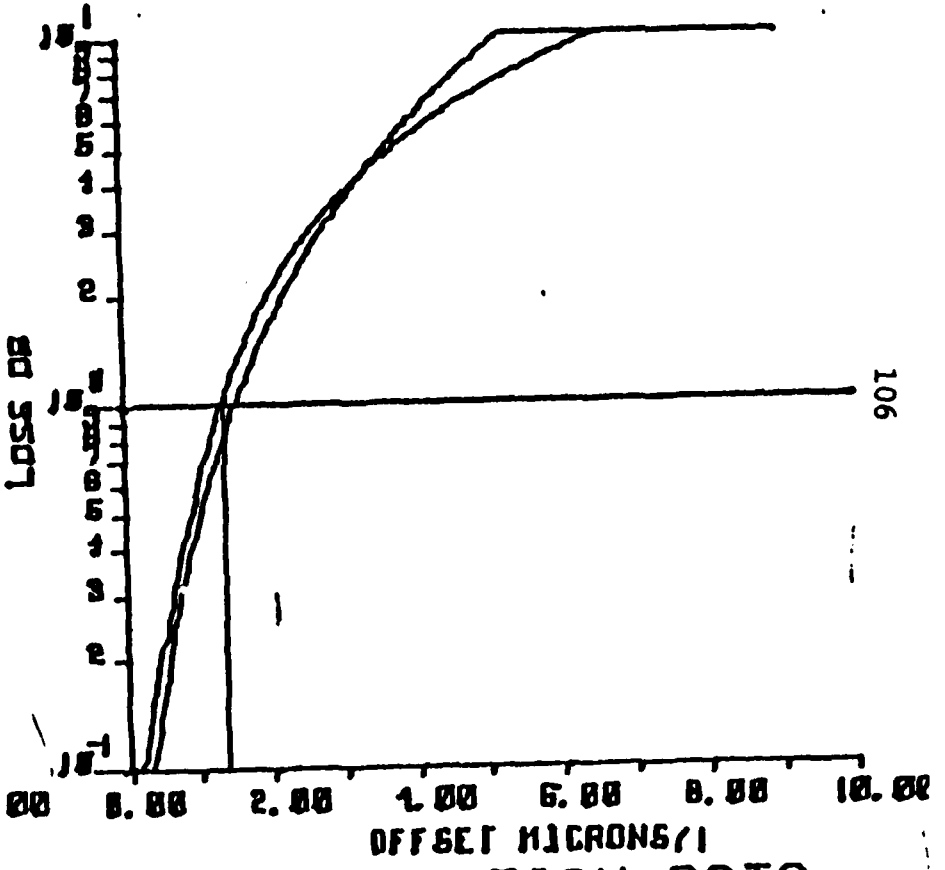

ATTENUATION DATA

106

11

LATERAL OFFSET

FIBER NO.: 503403

λ = 1100 nm

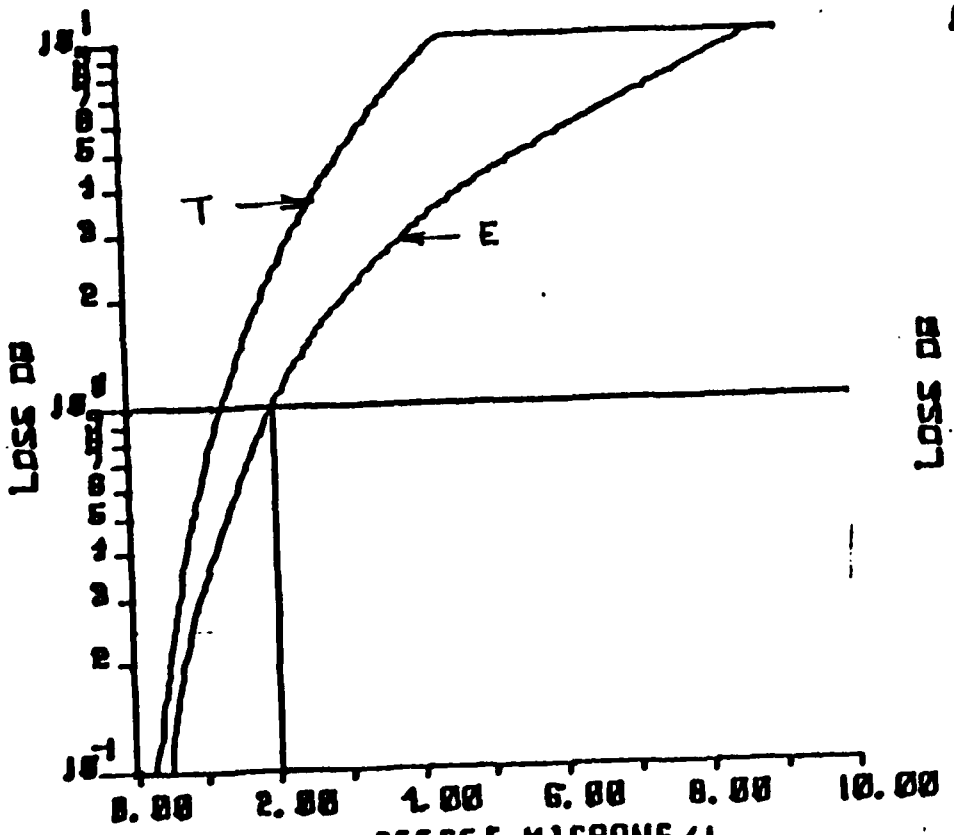

ATTENUATION DATA

λ = 1240 nm

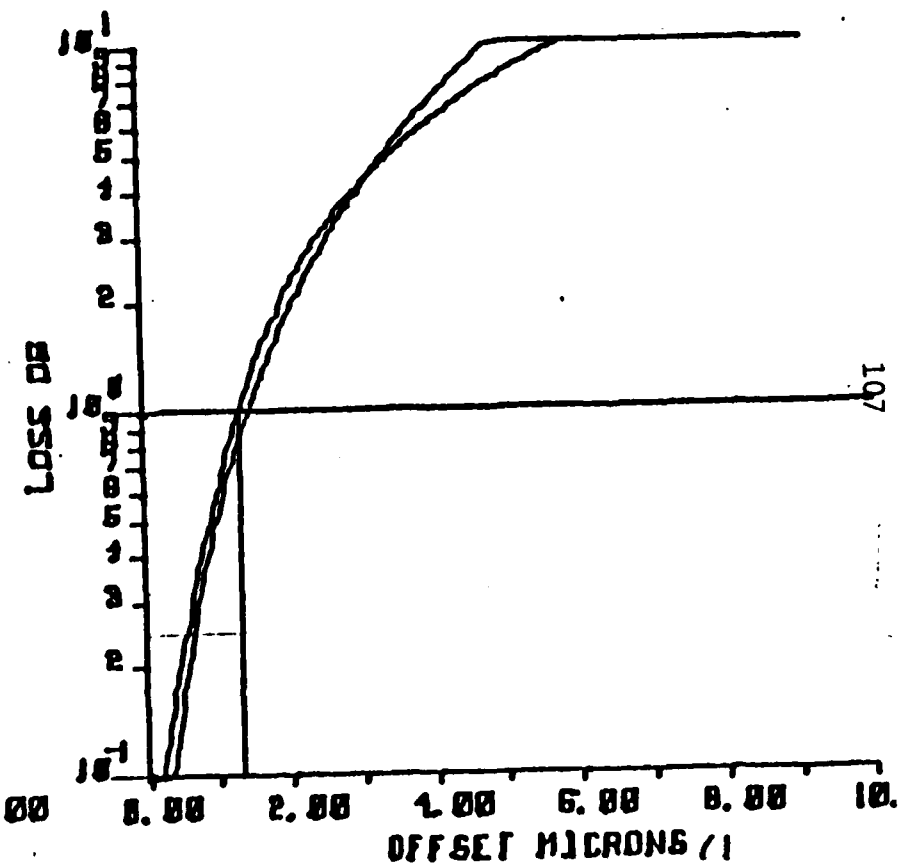

ATTENUATION DATA

LATERAL OFFSET

FIBER NO.: 509906

λ = 1600 nm

λ = nm

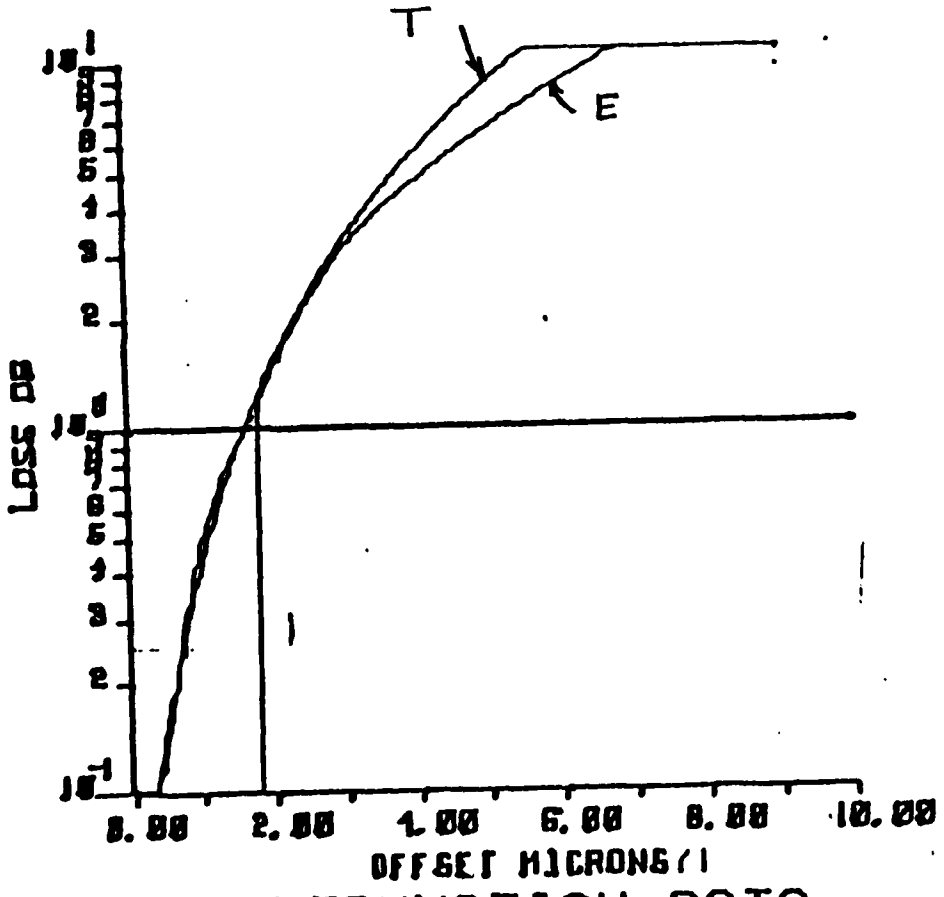

ATTENUATION DATA

LATERAL OFFSET

FIBER NO.: 509906

λ = 1300 nm

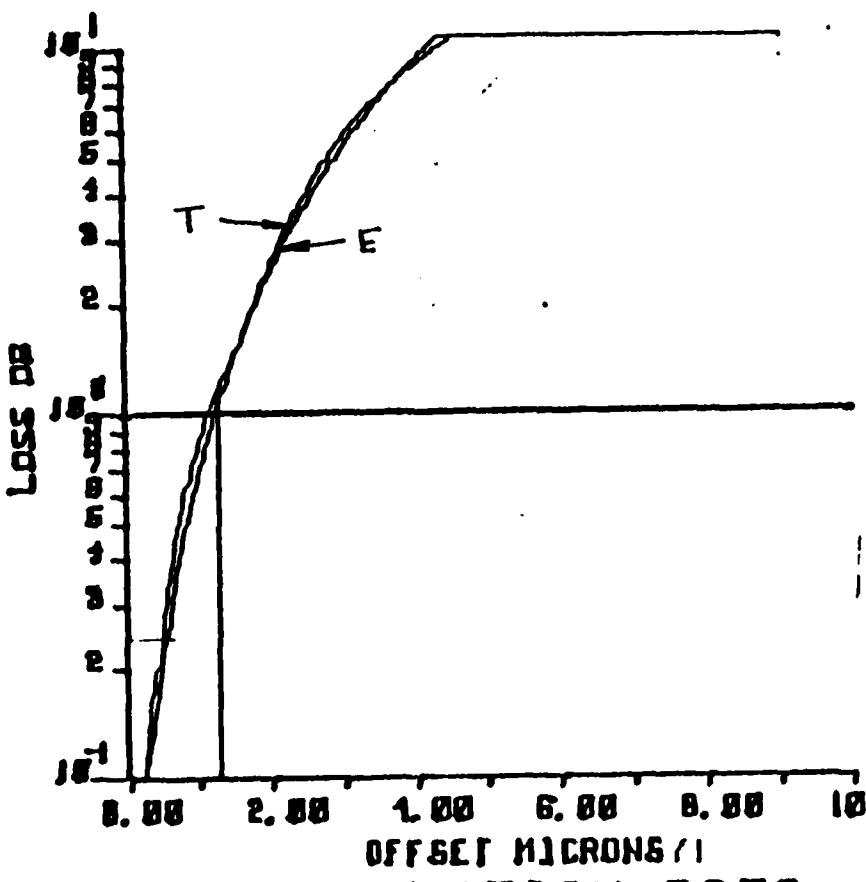

ATTENUATION DATA

λ = 1500 nm

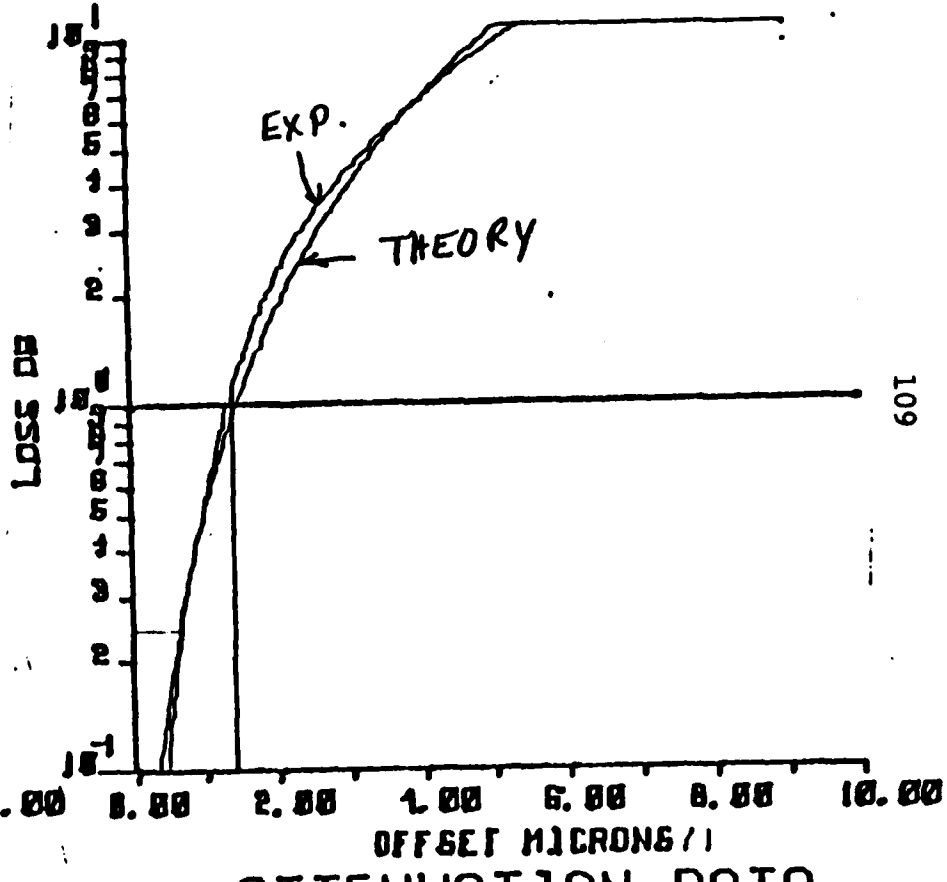

ATTENUATION DATA

109

LATERAL OFFSET

FIBER NO.: 509906

λ = 1100 nm

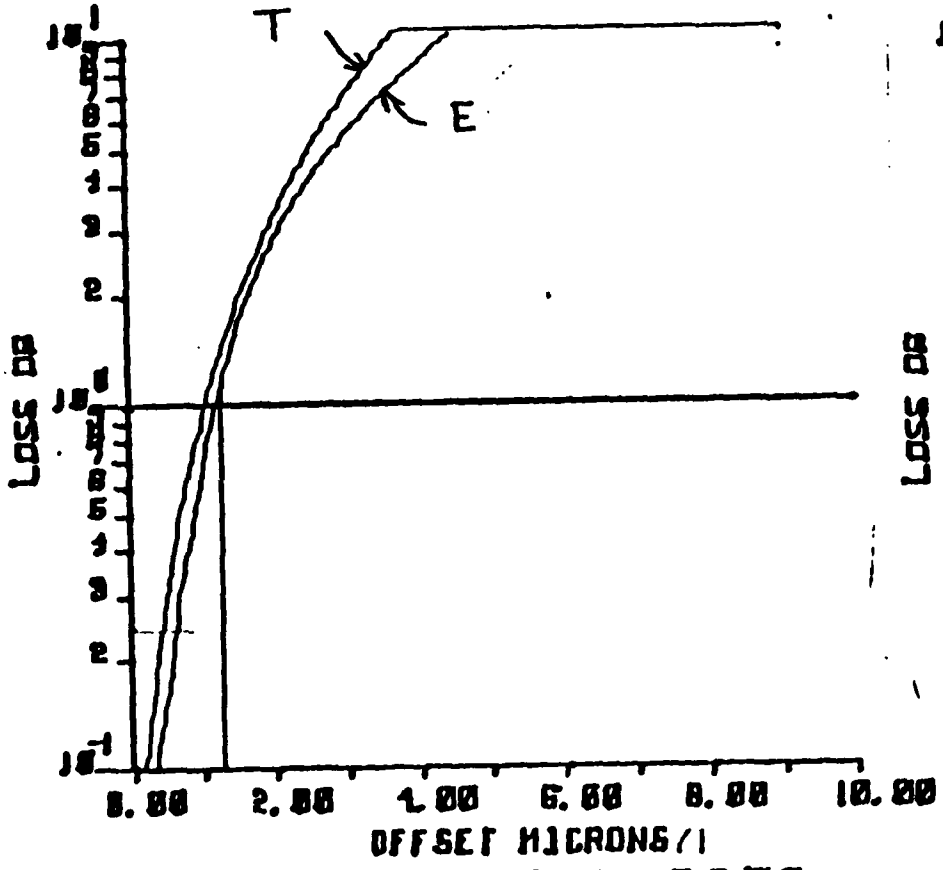

ATTENUATION DATA

λ = 1240 nm

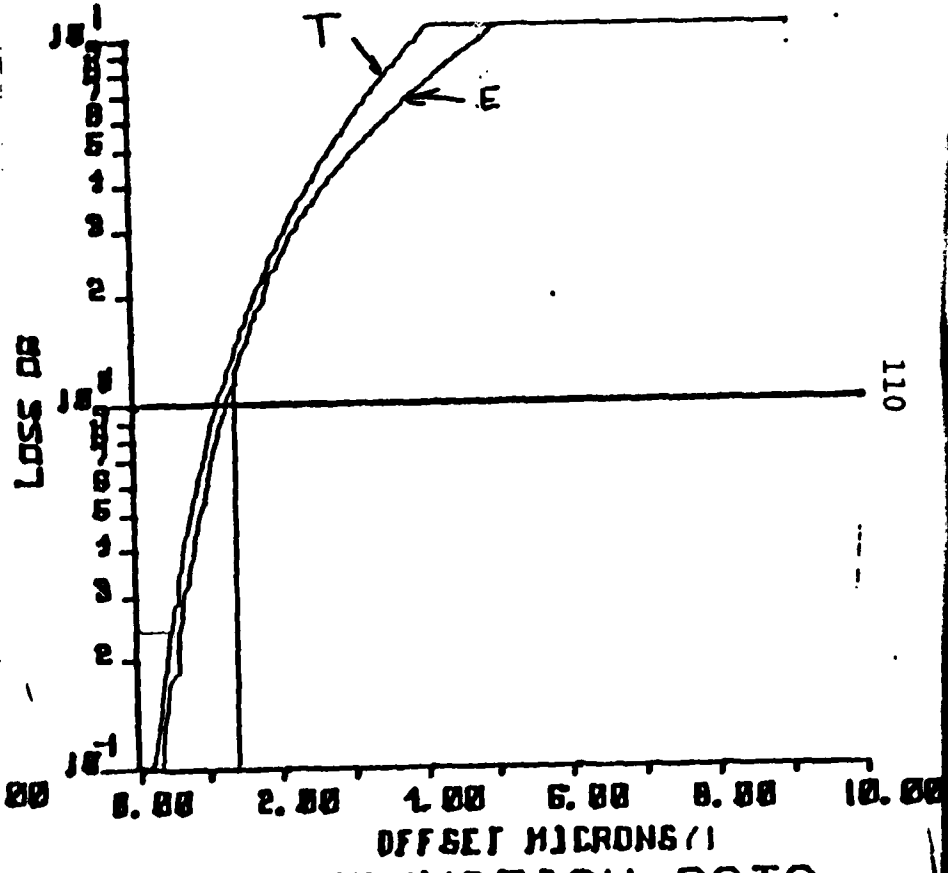

ATTENUATION DATA

LATERAL OFFSET

FIBER NO.: 506803

λ = 1600 nm

λ = nm

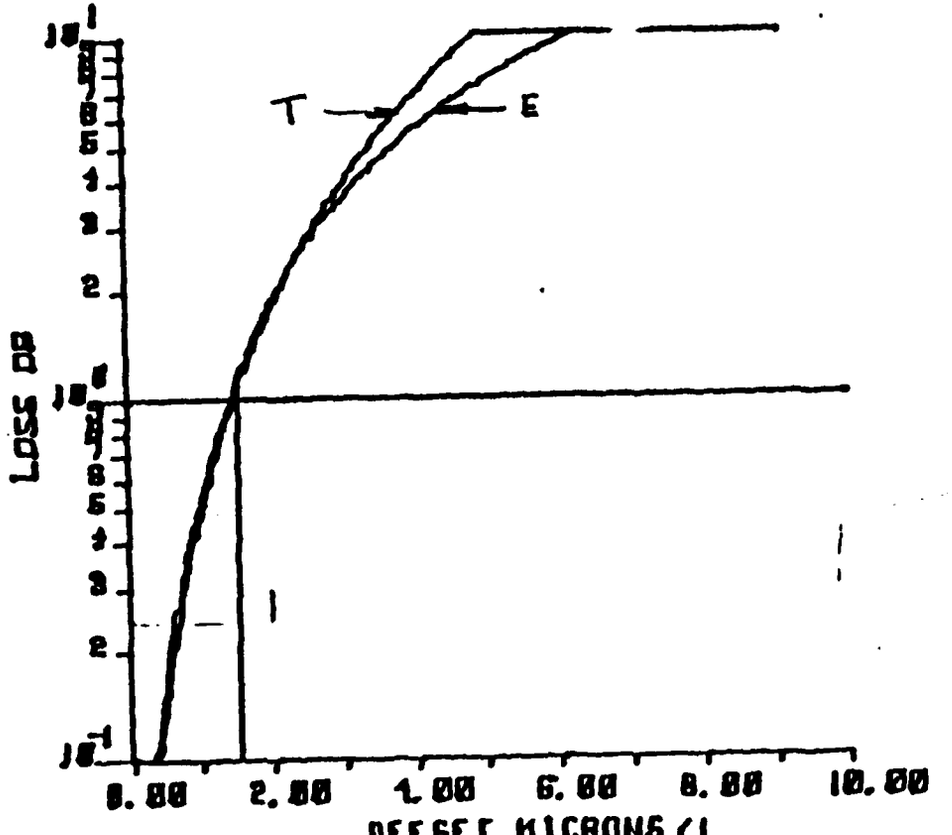

ATTENUATION DATA

LATERAL OFFSET

FIBER NO.: 506803

λ = 1400 nm

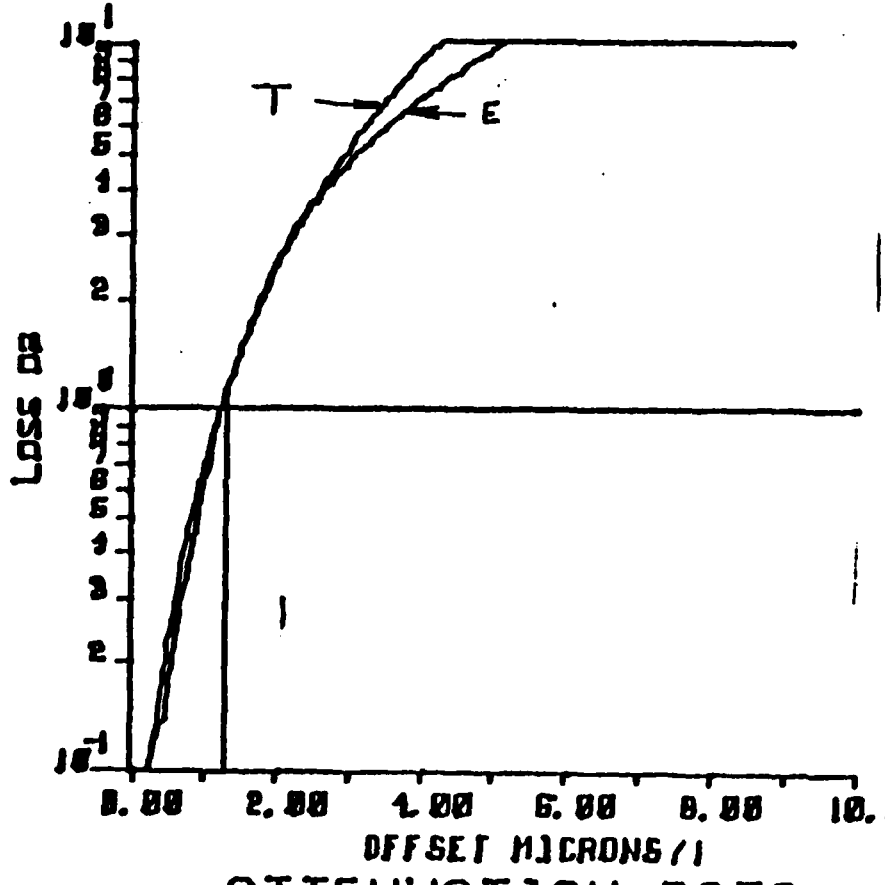

ATTENUATION DATA

λ = 1500 nm

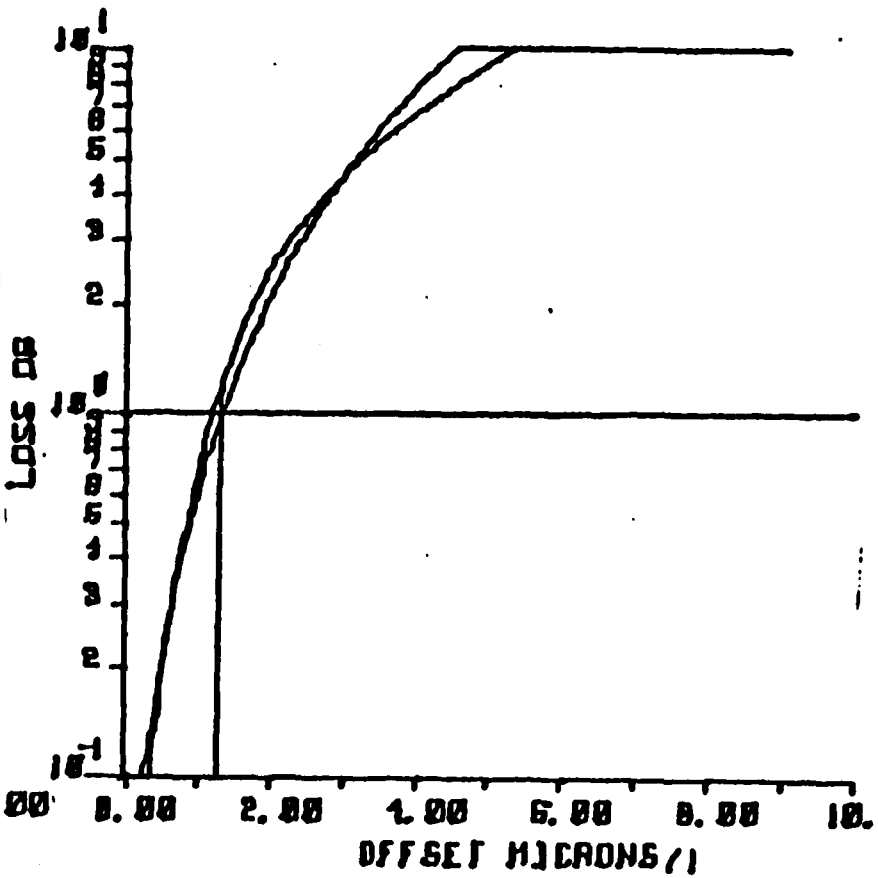

ATTENUATION DATA

112

50

LATERAL OFFSET

FIBER NO.: 506803

λ = 1240 nm

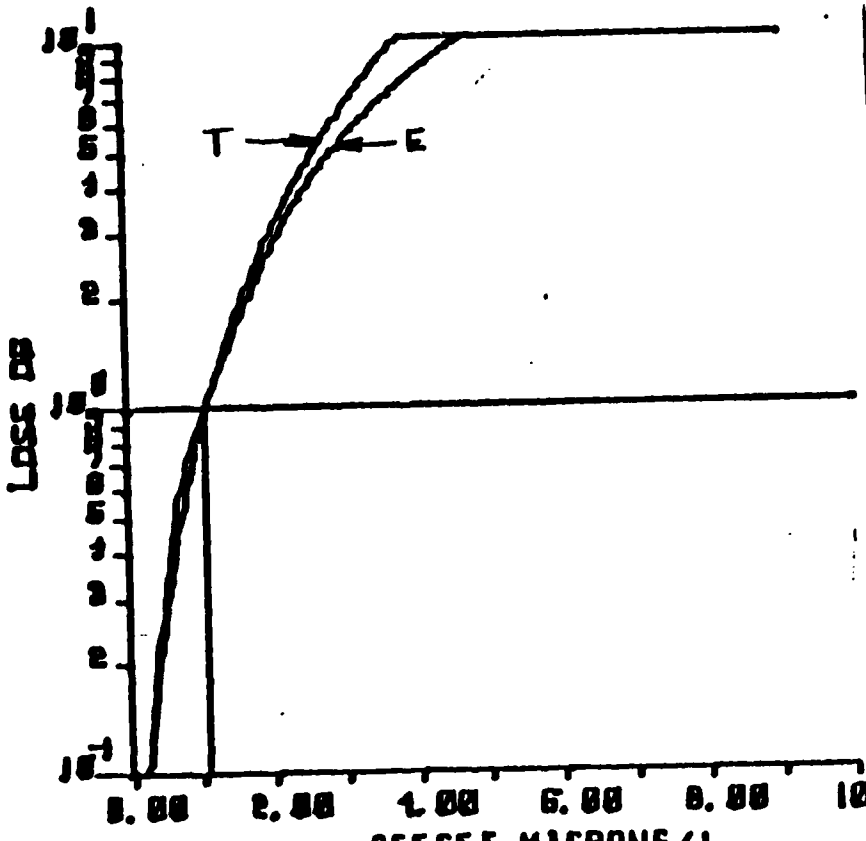

ATTENUATION DATA

λ = 1300 nm

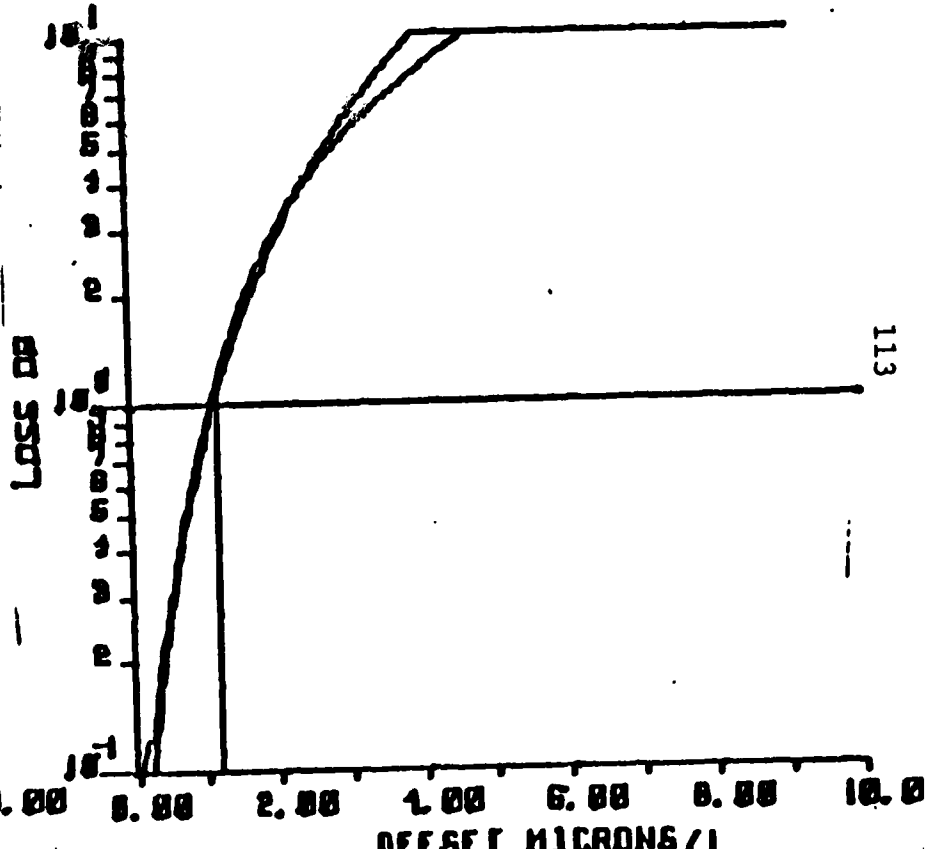

ATTENUATION DATA

15

LATERAL OFFSET

FIBER NO.: 508404

λ = 1300 nm

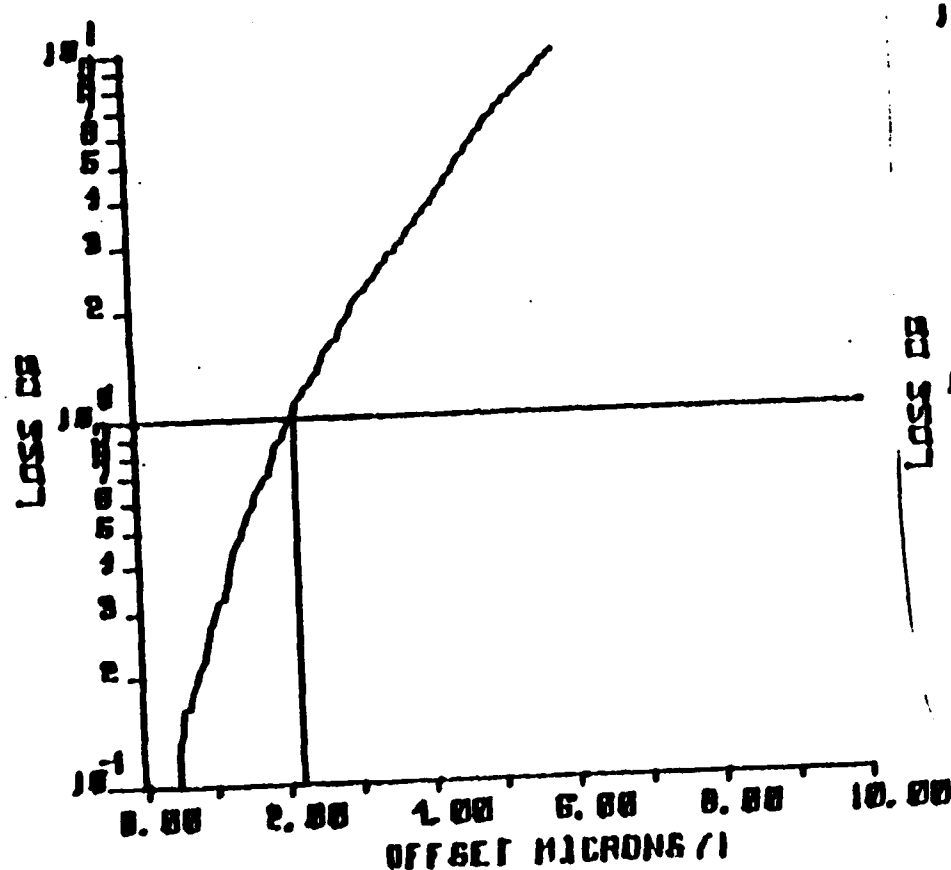

ATTENUATION DATA

λ = 1240 nm

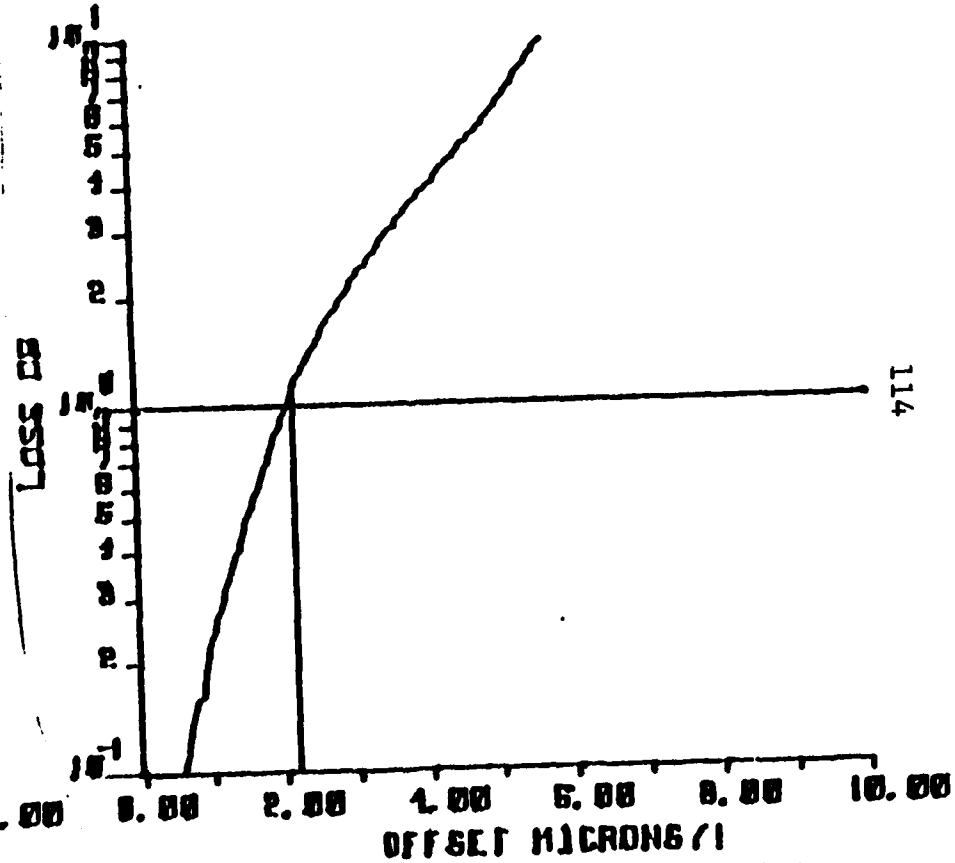

ATTENUATION DATA

87

114

APPENDIX C

Angular Offset Test Data

Excess loss as a function of angular offset: comparison of experimental data (E) with Model (T).

ANGULAR OFFSET

FIBER NO.: 507205

λ = 900 nm

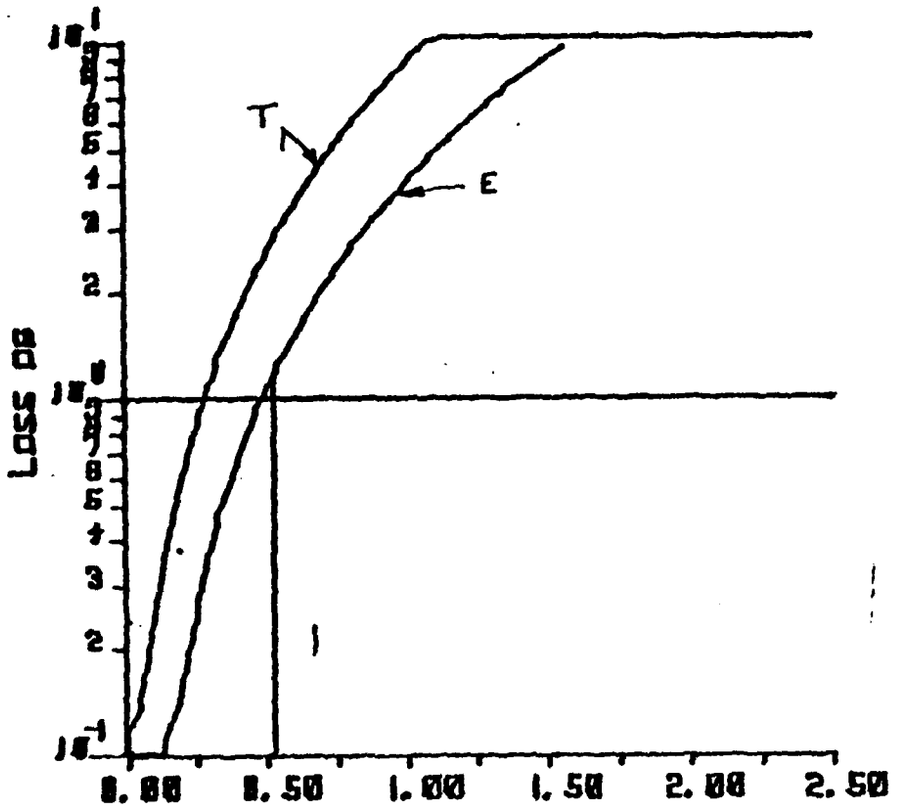

ATTENUATION DATA

λ = 1100 nm

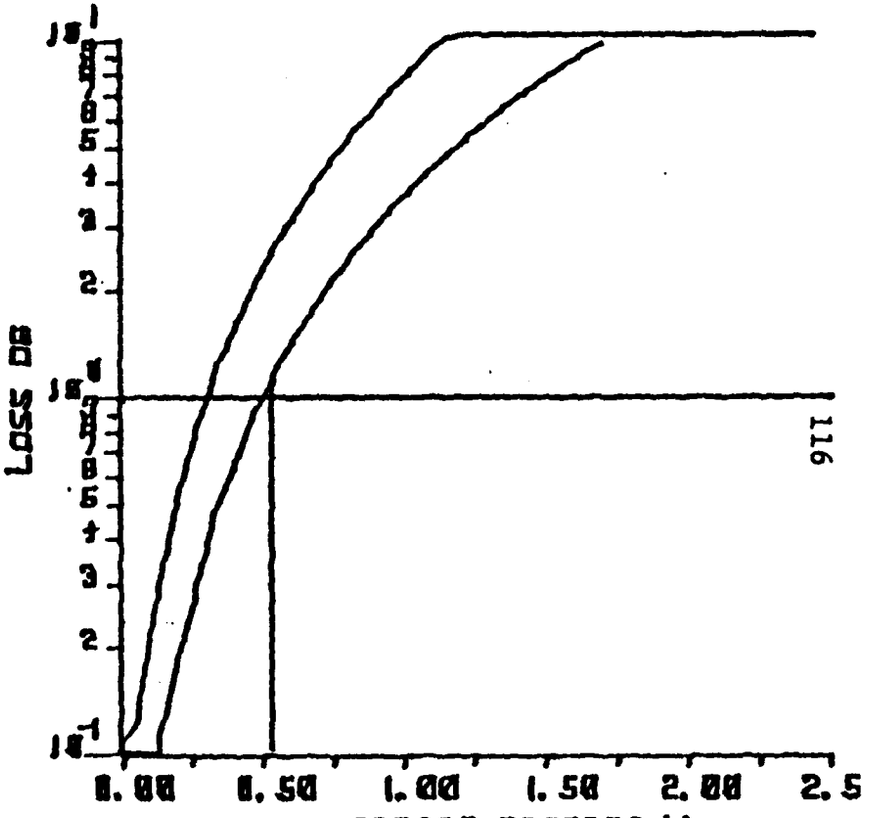

ATTENUATION DATA

ANGULAR OFFSET

FIBER NO.: 507205

λ = 1400 nm

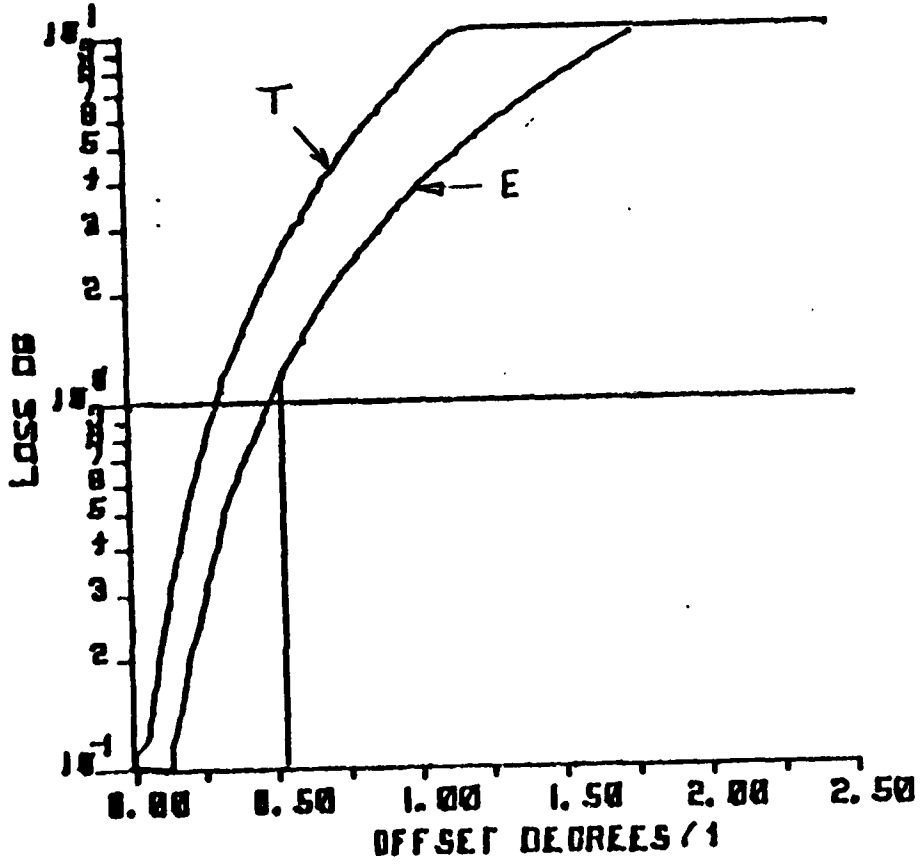

ATTENUATION DATA

λ = 1500 nm

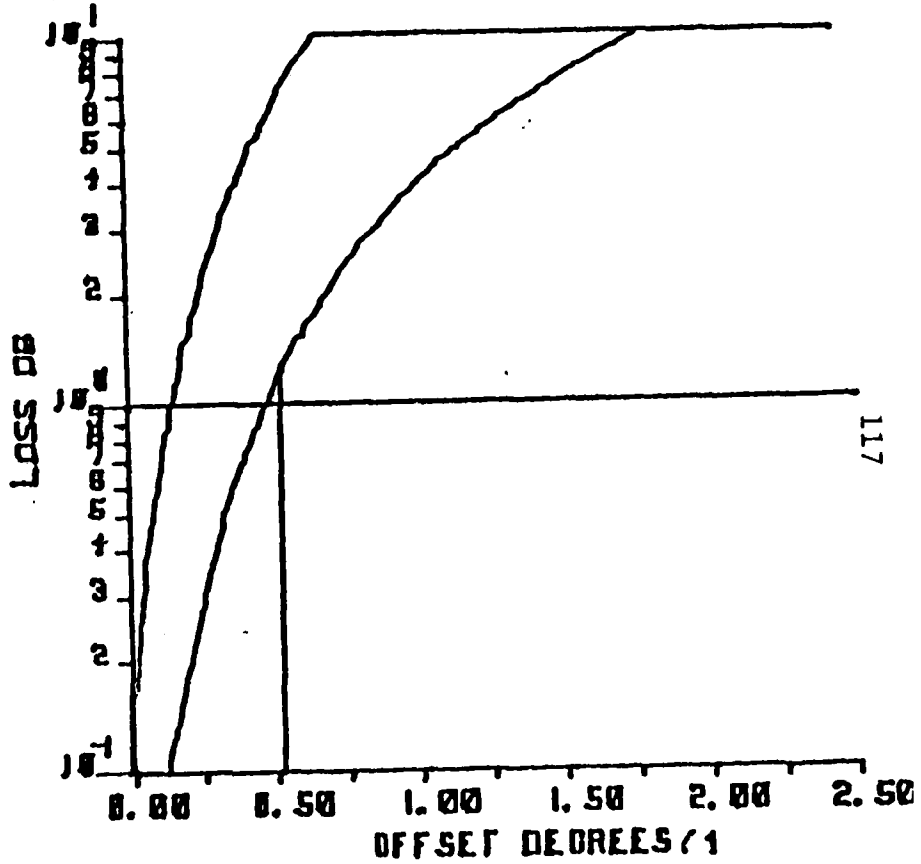

ATTENUATION DATA

ANGULAR OFFSET

FIBER NO.: 507205

λ = 1240 nm

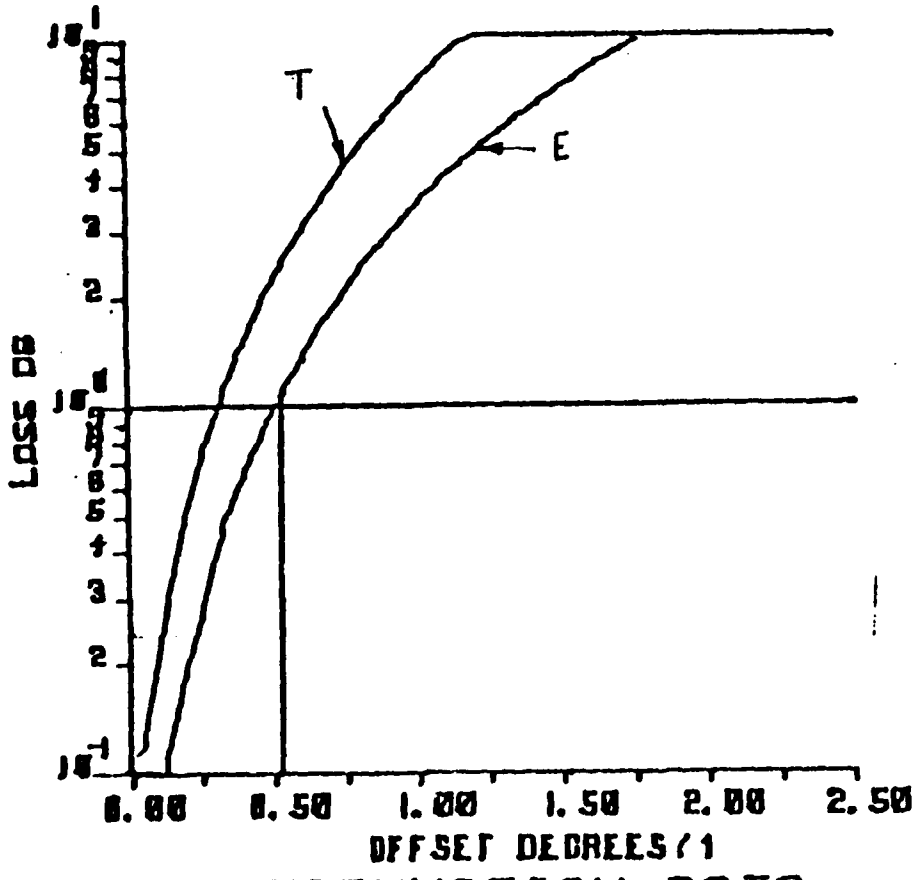

ATTENUATION DATA

λ = 1300 nm

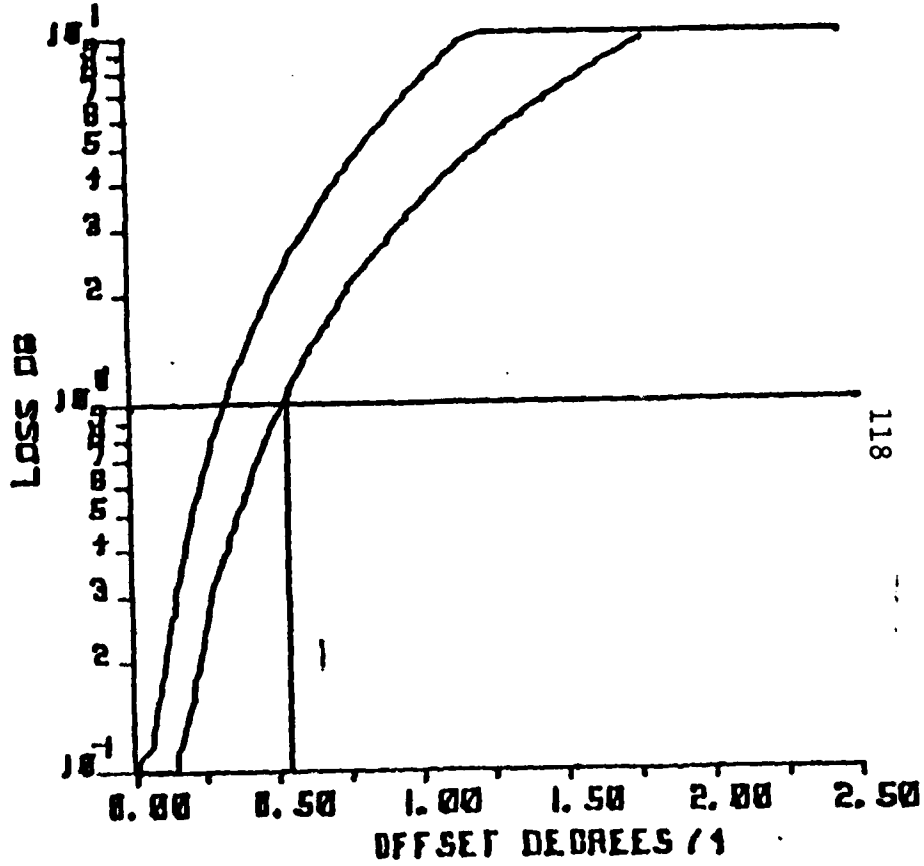

ATTENUATION DATA

ANGULAR OFFSET

FIBER NO.: 510802

λ = 1400 nm

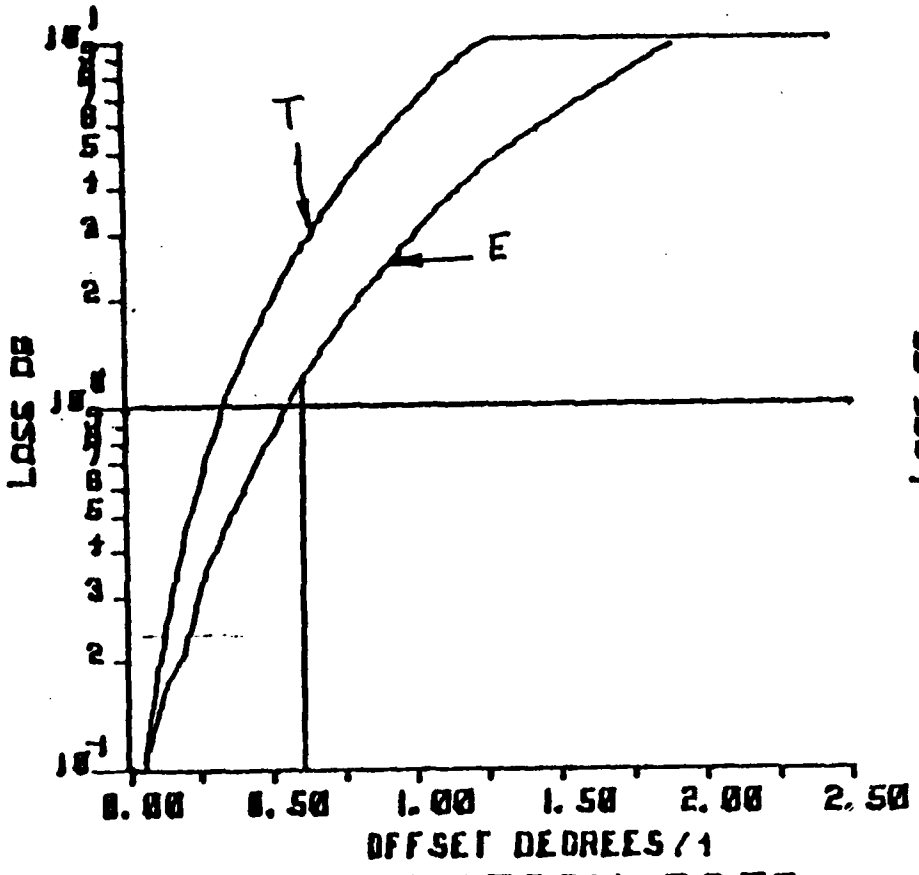

ATTENUATION DATA

λ = 1300 nm

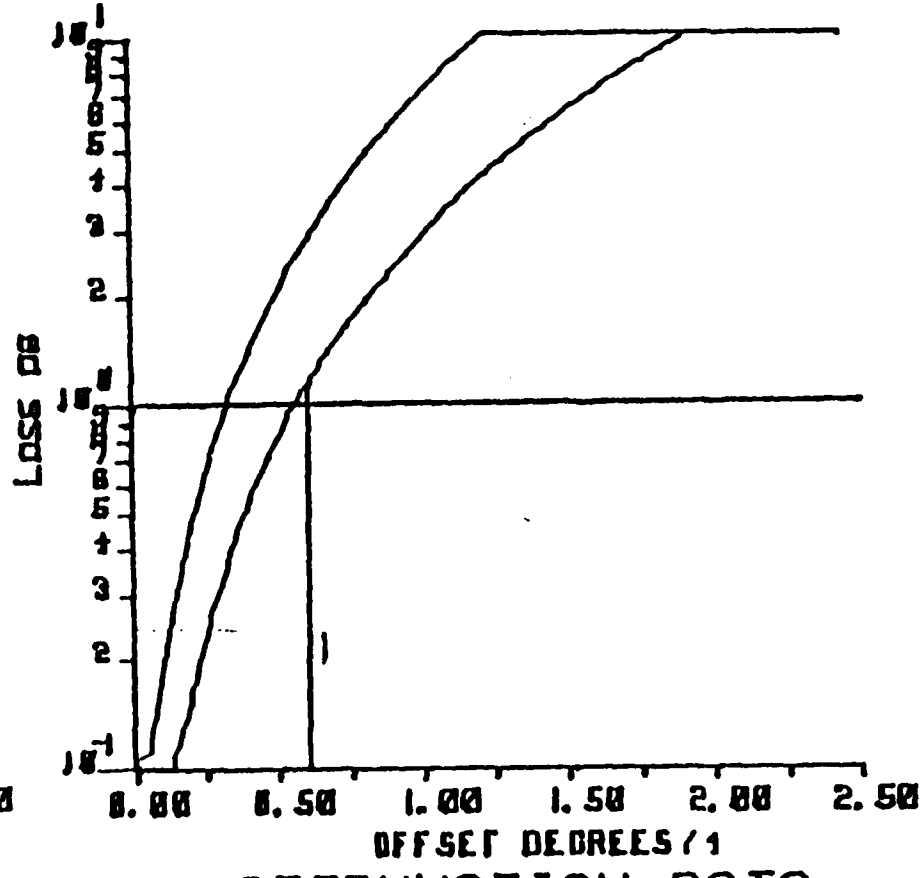

ATTENUATION DATA

83

ANGULAR OFFSET

FIBER NO.: 510802

λ = 1600 nm

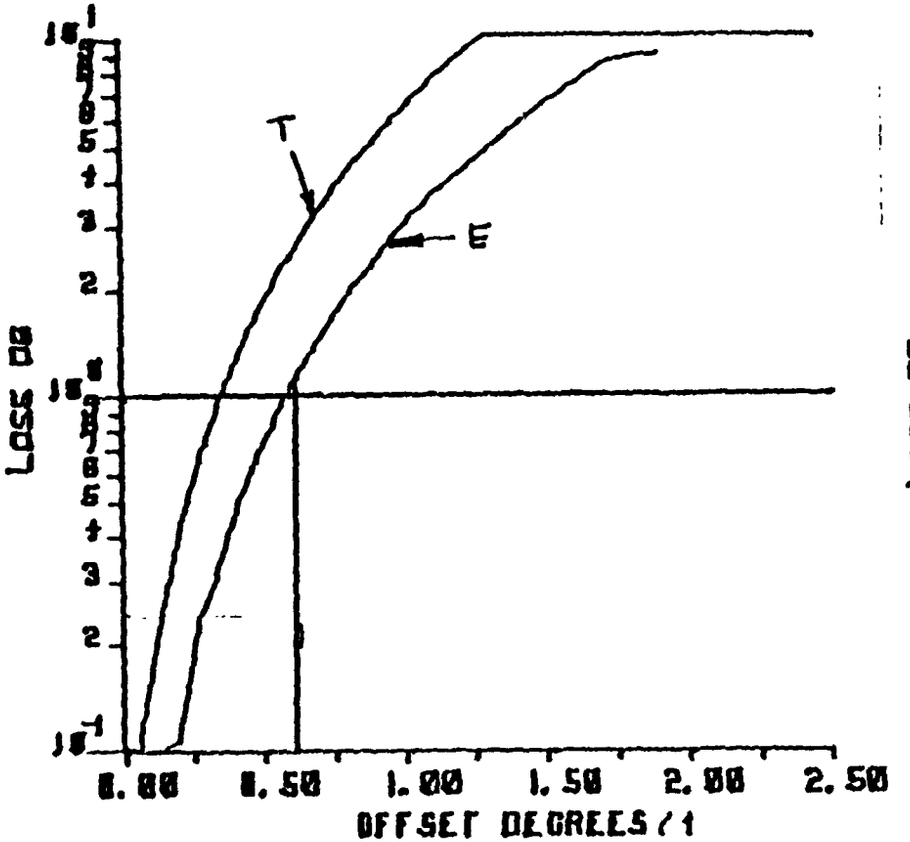

ATTENUATION DATA

λ = 1500 nm

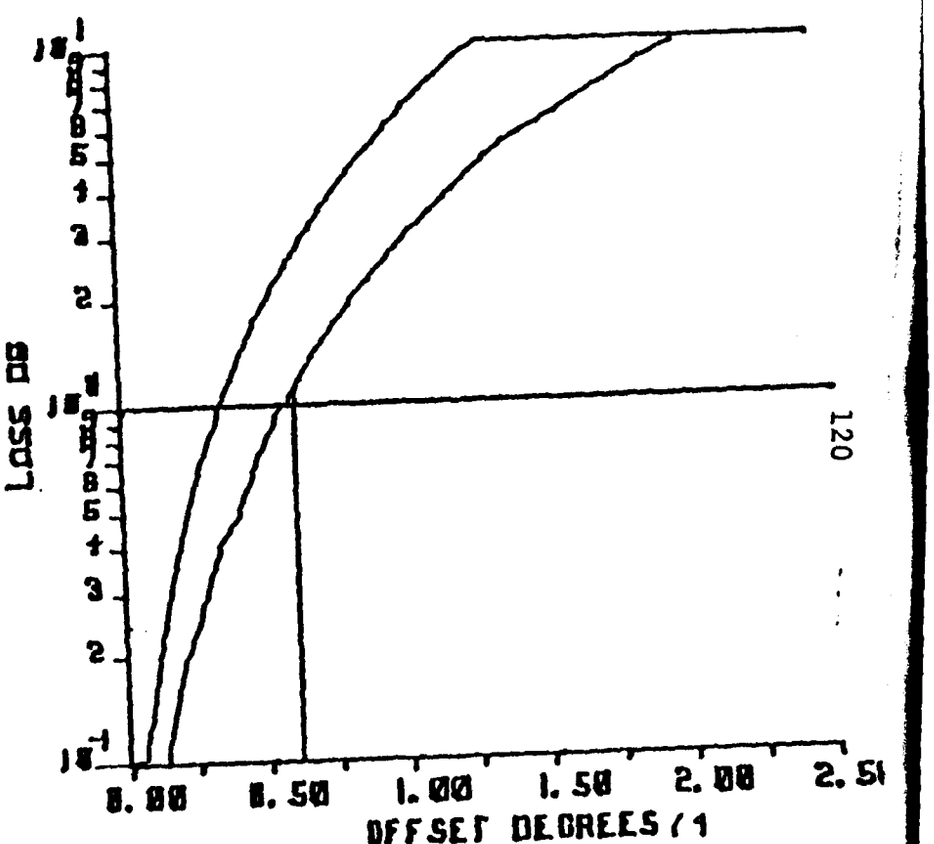

ATTENUATION DATA

120

02

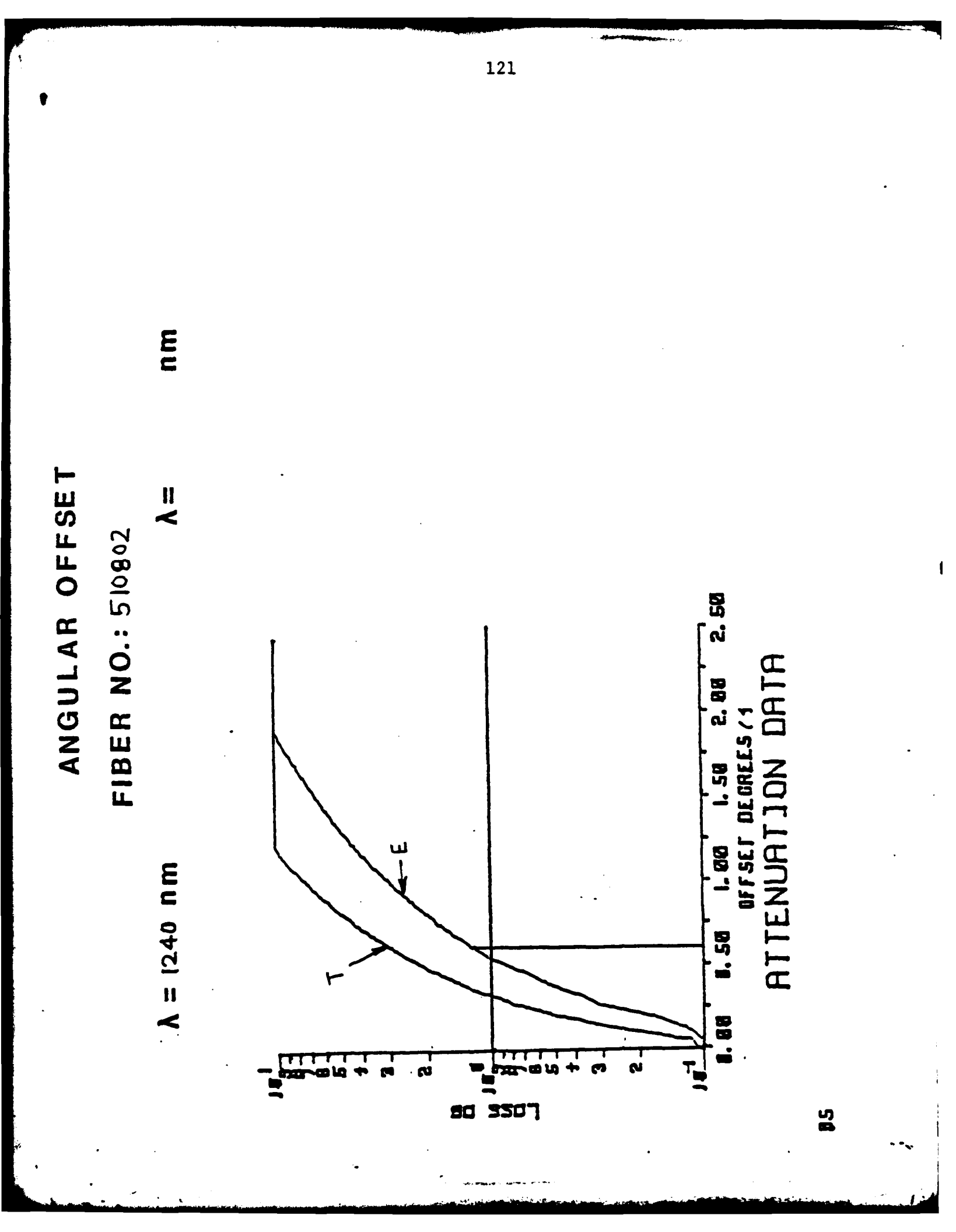
ANGULAR OFFSET
FIBER NO.: 510802
λ = 1240 nm
λ= nm
T
E
LOSS dB
OFFSET DEGREES (1
0.00
0.50
1.00
1.50
2.00
2.50
ATTENUATION DATA
85

ANGULAR OFFSET

FIBER NO.: 509503

λ = 1240 nm

λ = nm

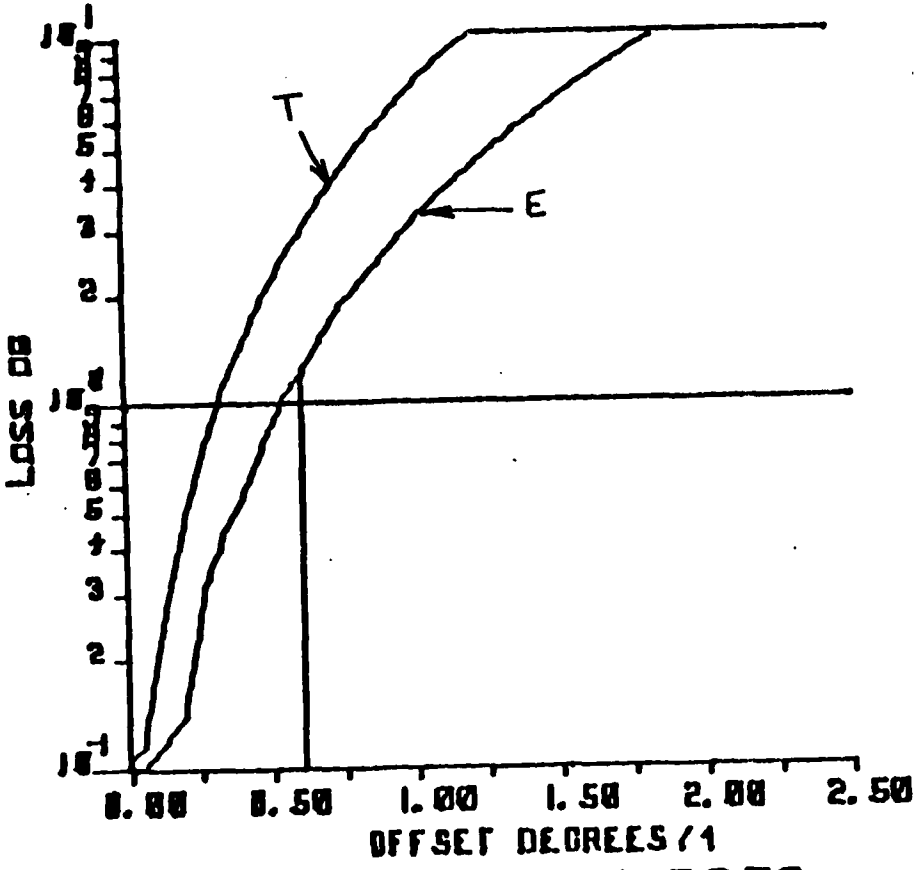

ATTENUATION DATA

01

ANGULAR OFFSET

FIBER NO.: 509503

λ = 1400 nm

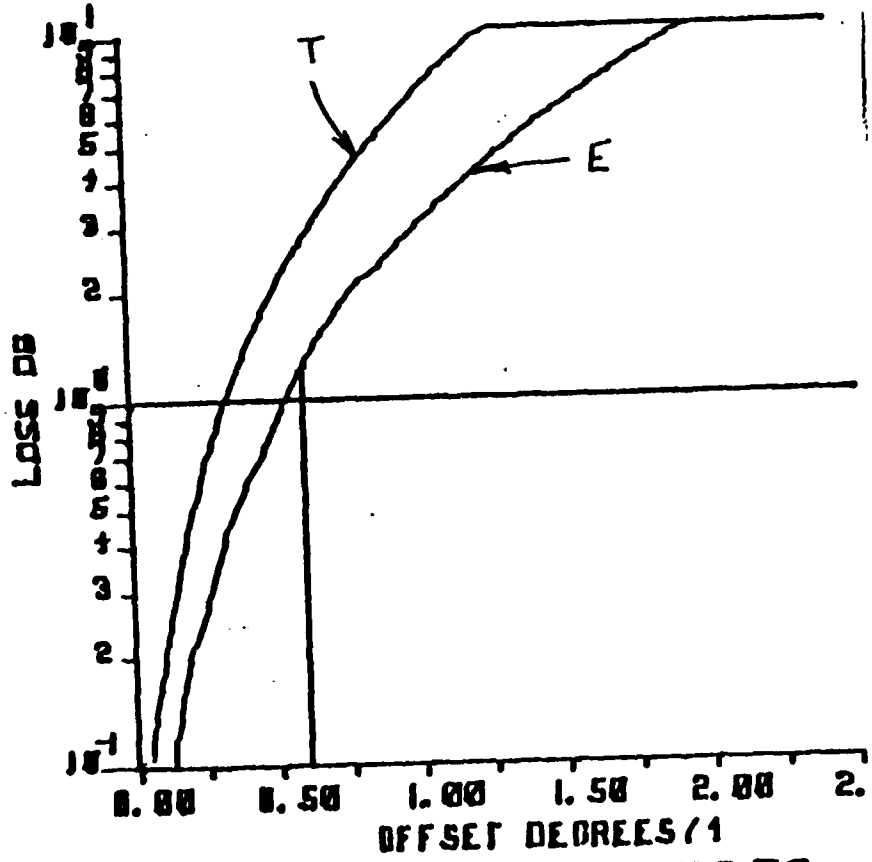

ATTENUATION DATA

λ = 1300 nm

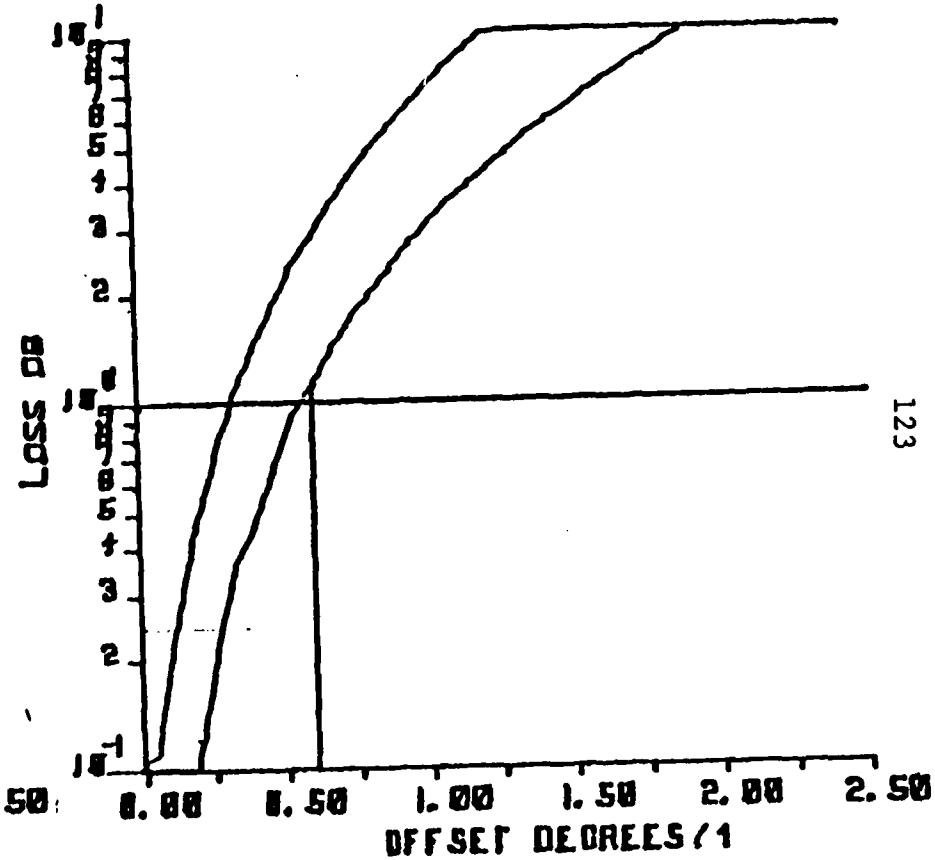

ATTENUATION DATA

07

ANGULAR OFFSET

FIBER NO.: 509503

λ = 1600 nm

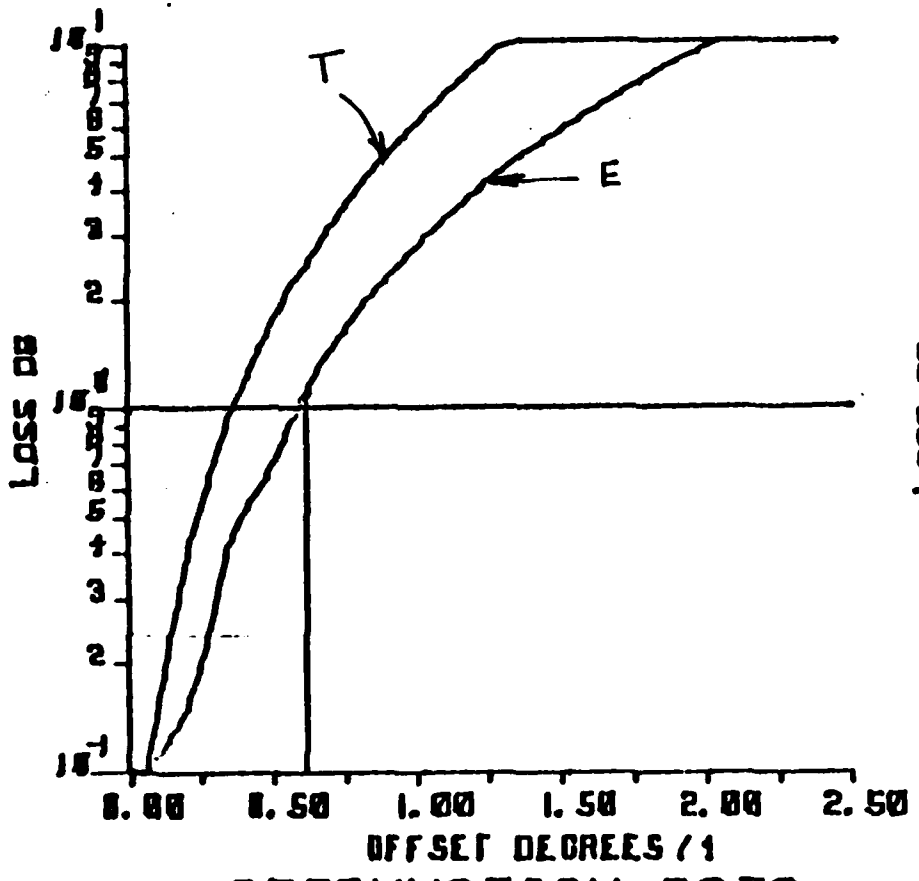

ATTENUATION DATA

λ = 1500 nm

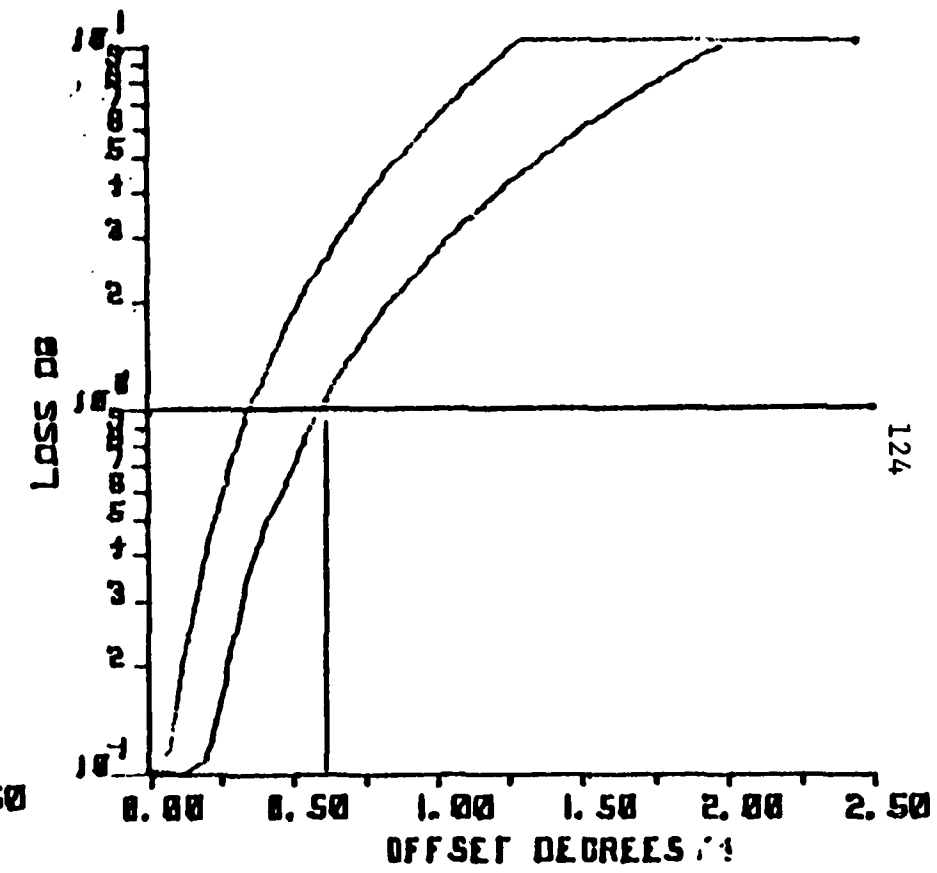

ATTENUATION DATA

11

ANGULAR OFFSET

FIBER NO.: 343104

λ = 1240 nm

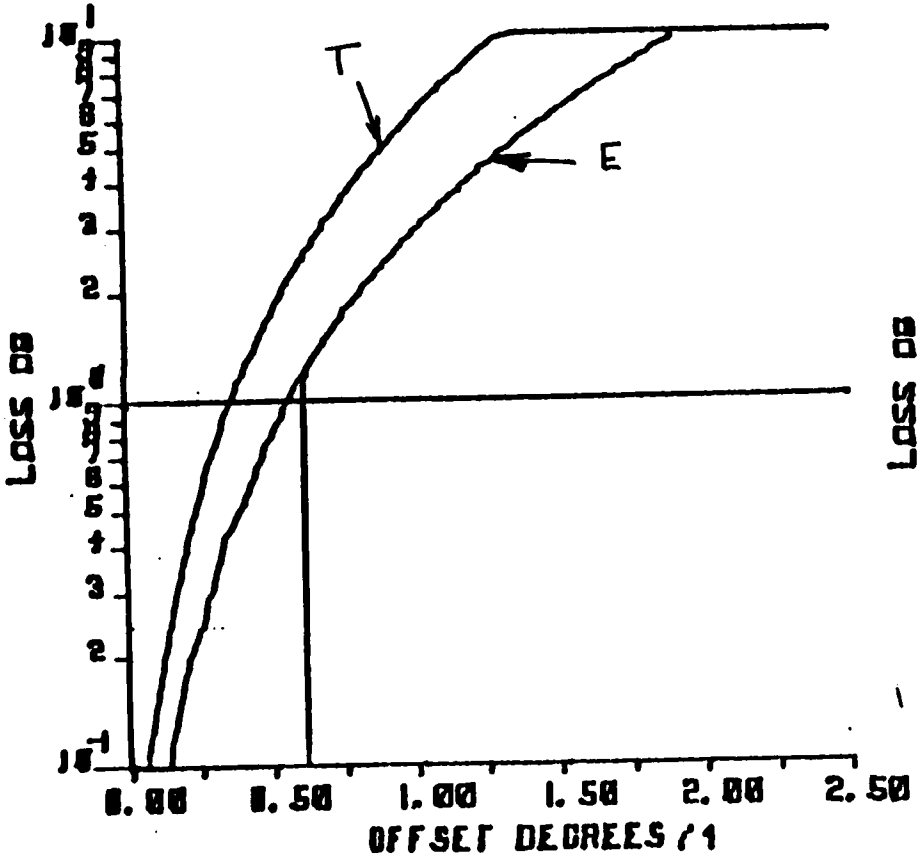

ATTENUATION DATA

λ = 1100 nm

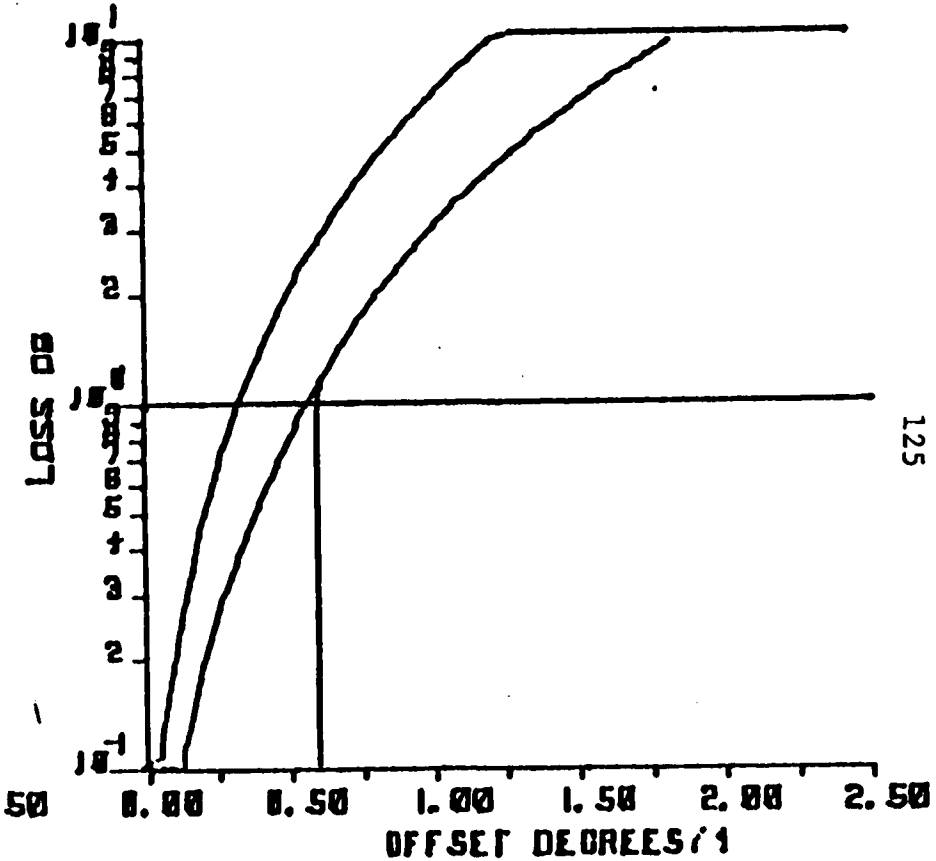

ATTENUATION DATA

125

85

ANGULAR OFFSET

FIBER NO.: 343104

λ = 1400 nm

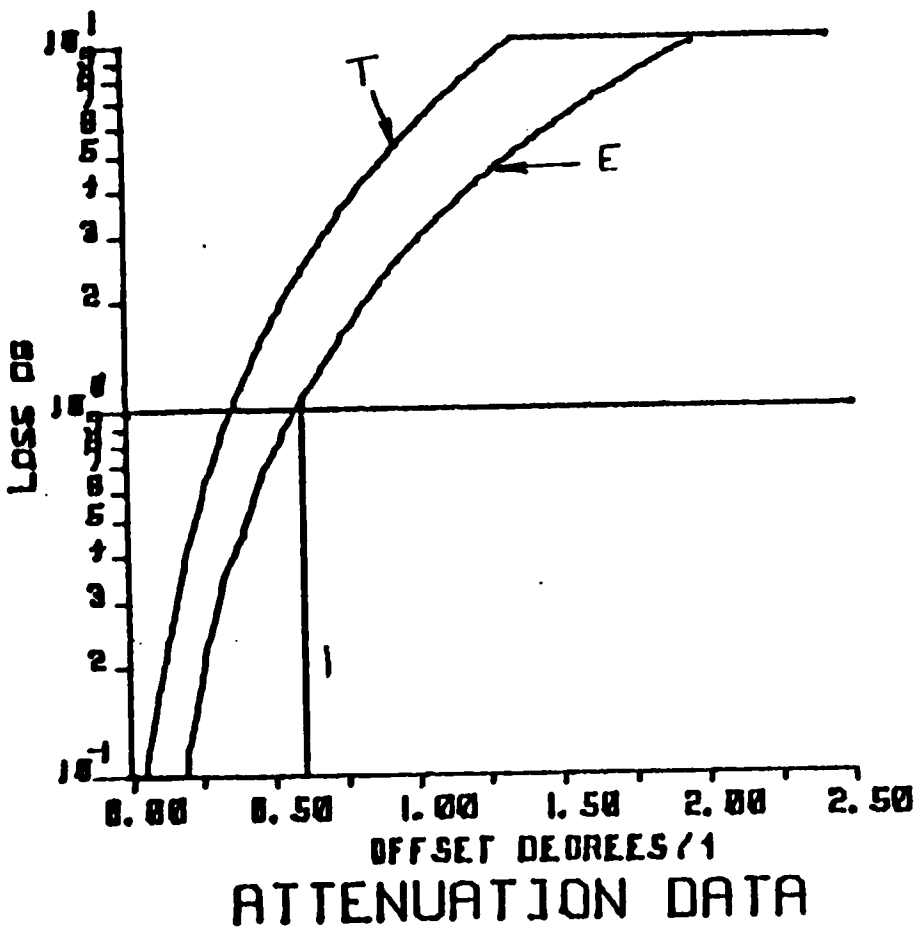

ATTENUATION DATA

λ = 1300 nm

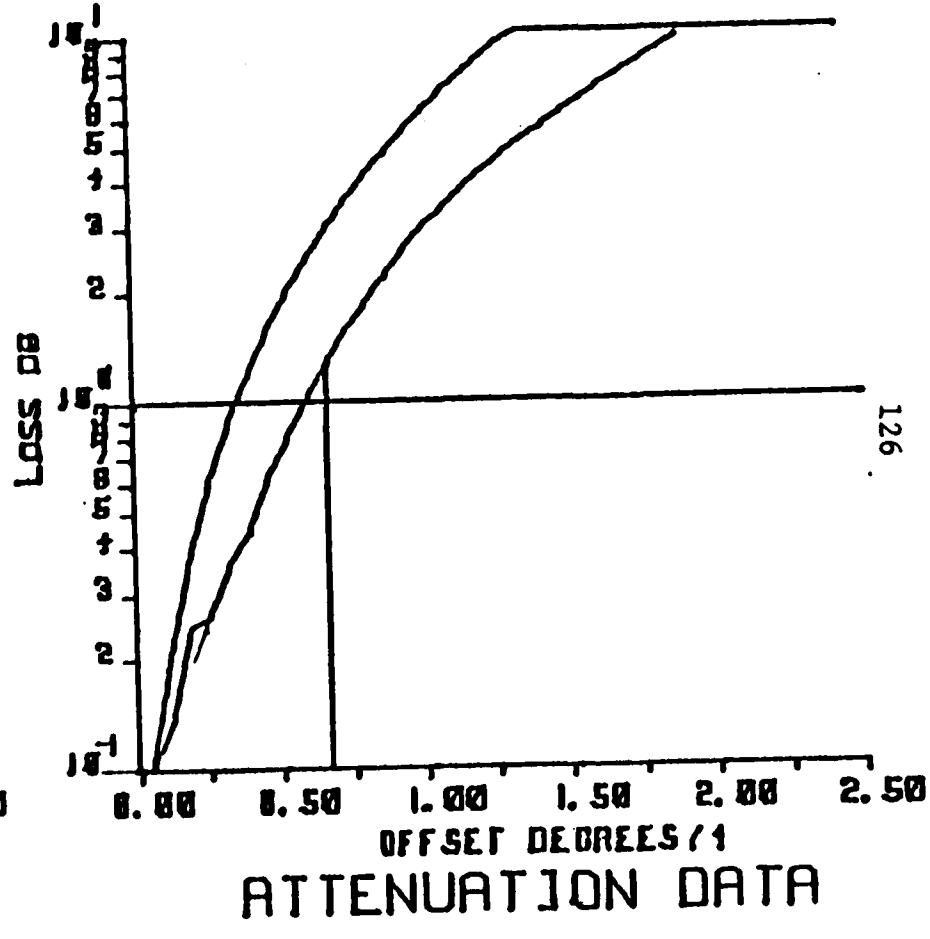

ATTENUATION DATA

126

03

ANGULAR OFFSET

FIBER NO.: 343104

λ = 1600 nm

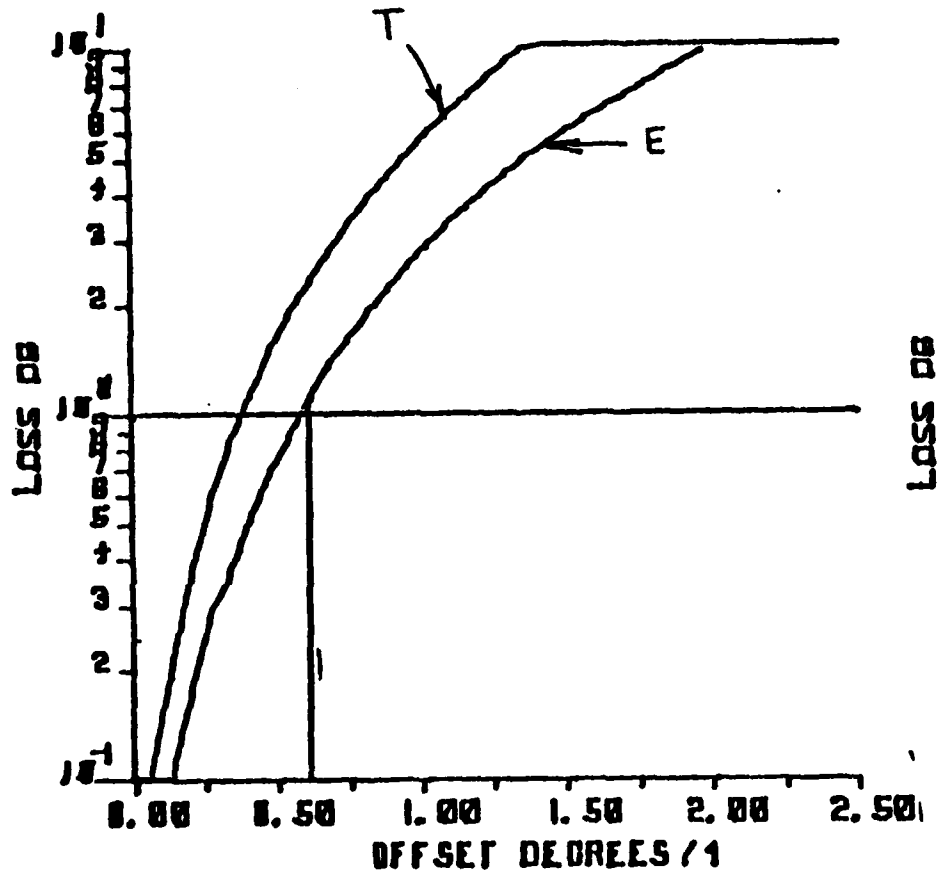

ATTENUATION DATA

λ = 1500 nm

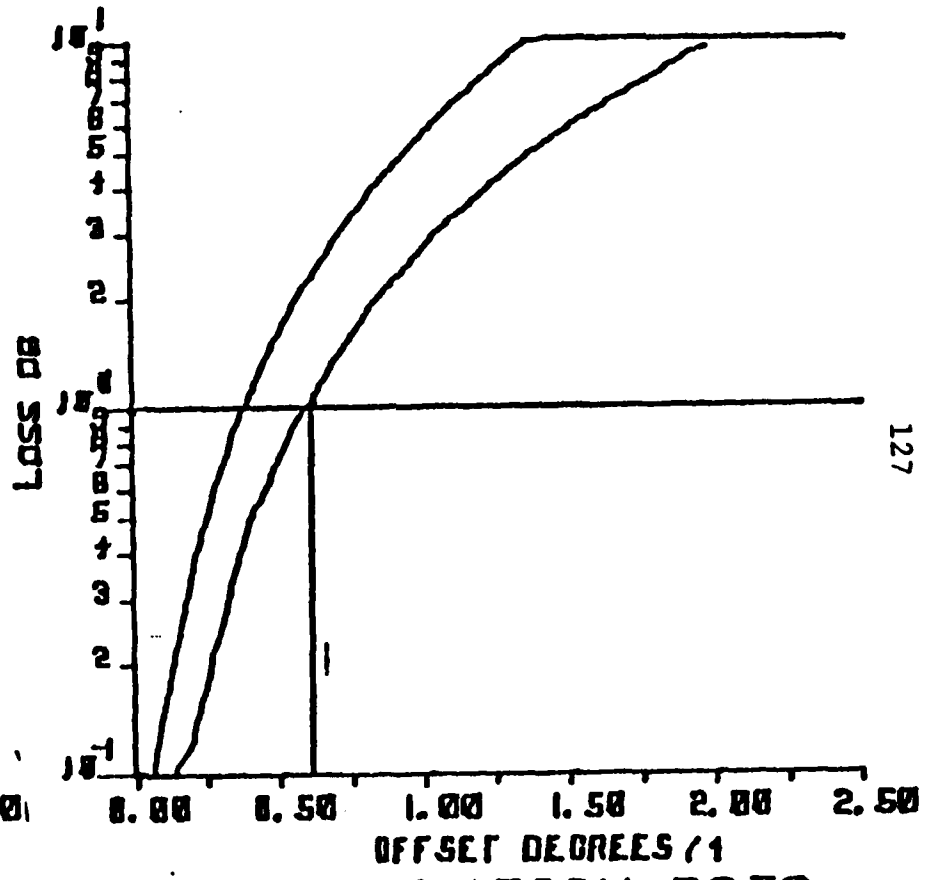

ATTENUATION DATA

ANGULAR OFFSET

FIBER NO.: 506902

λ = 1100 nm

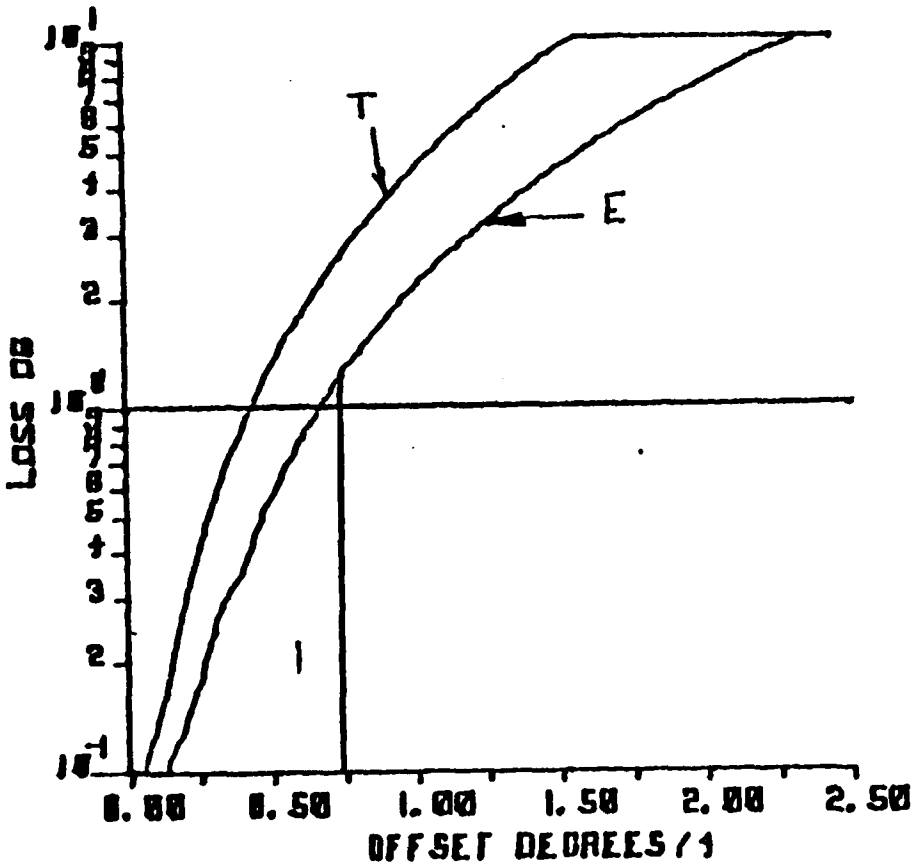

ATTENUATION DATA

λ = 900 nm

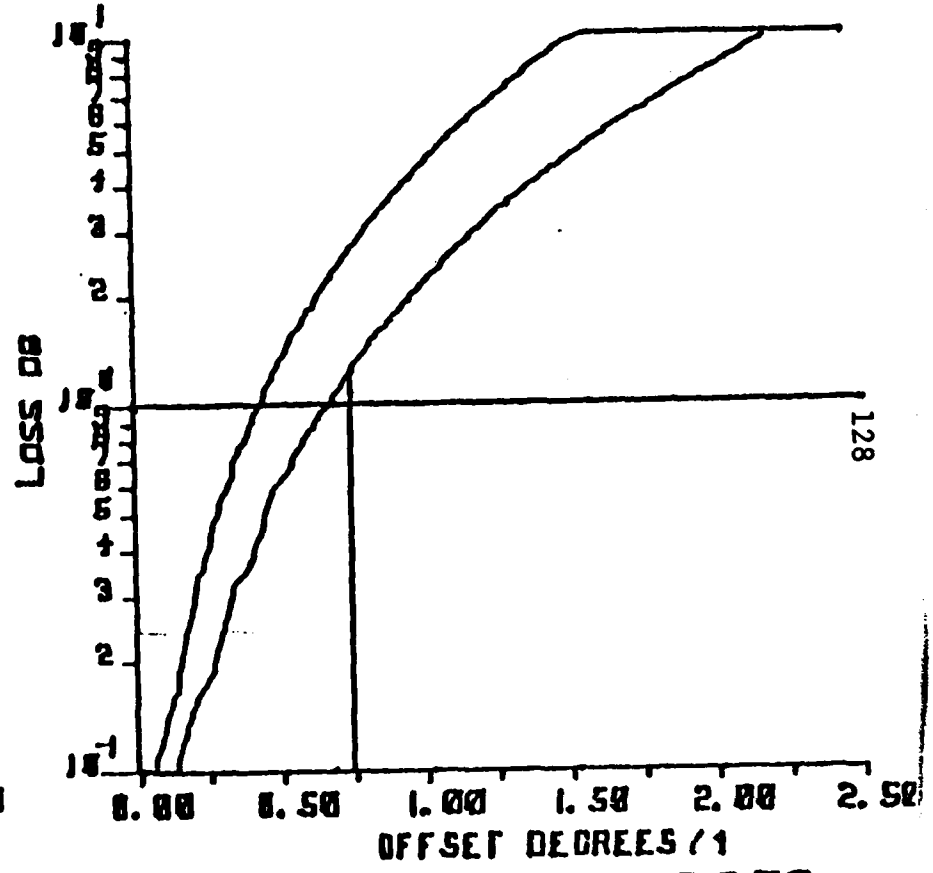

ATTENUATION DATA

02

ANGULAR OFFSET

FIBER NO.: 506902

λ = 1300 nm

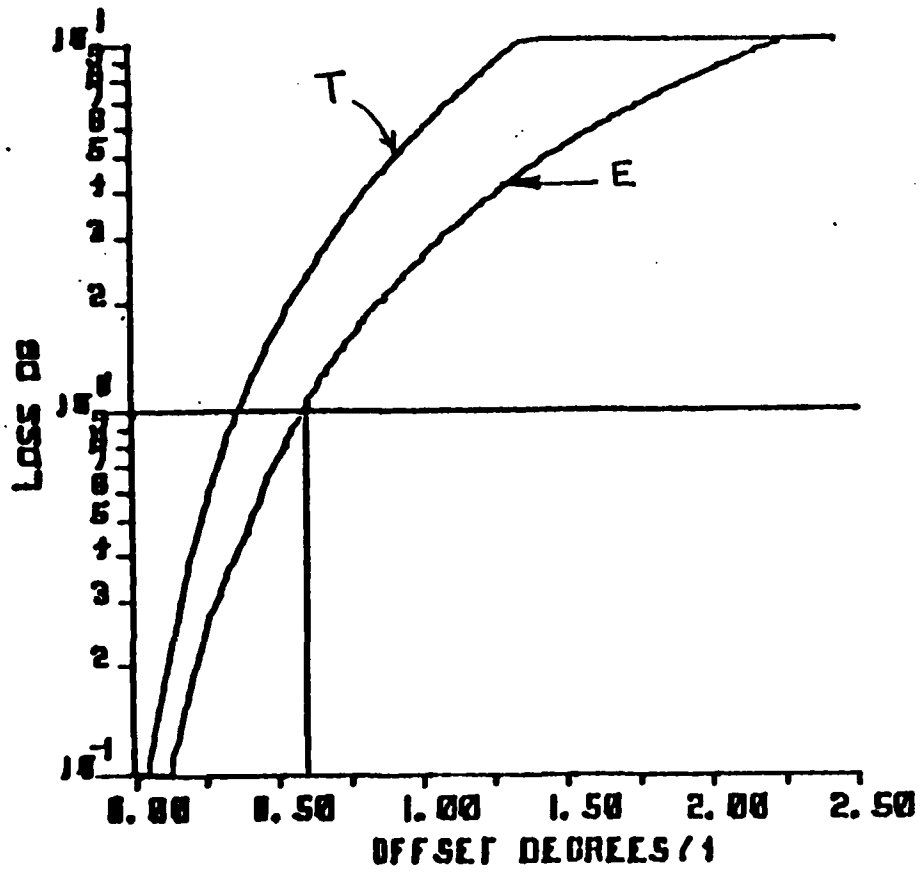

ATTENUATION DATA

λ = 1240 nm

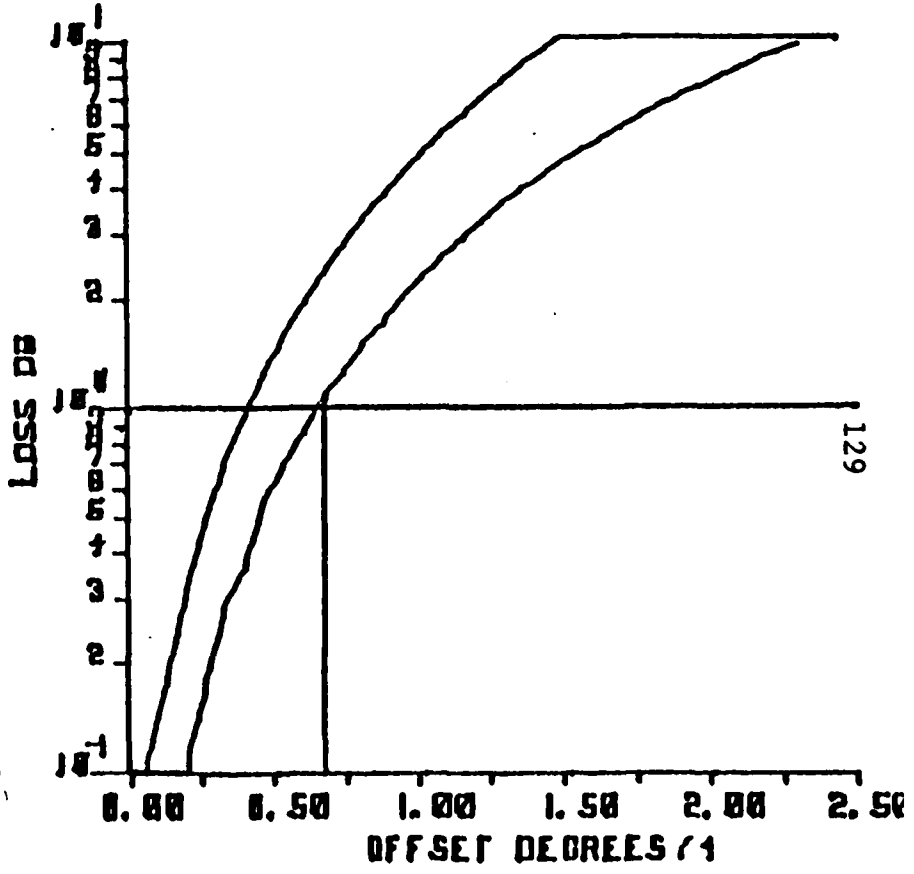

ATTENUATION DATA

05

ANGULAR OFFSET

FIBER NO.: 506902

λ = 1600 nm

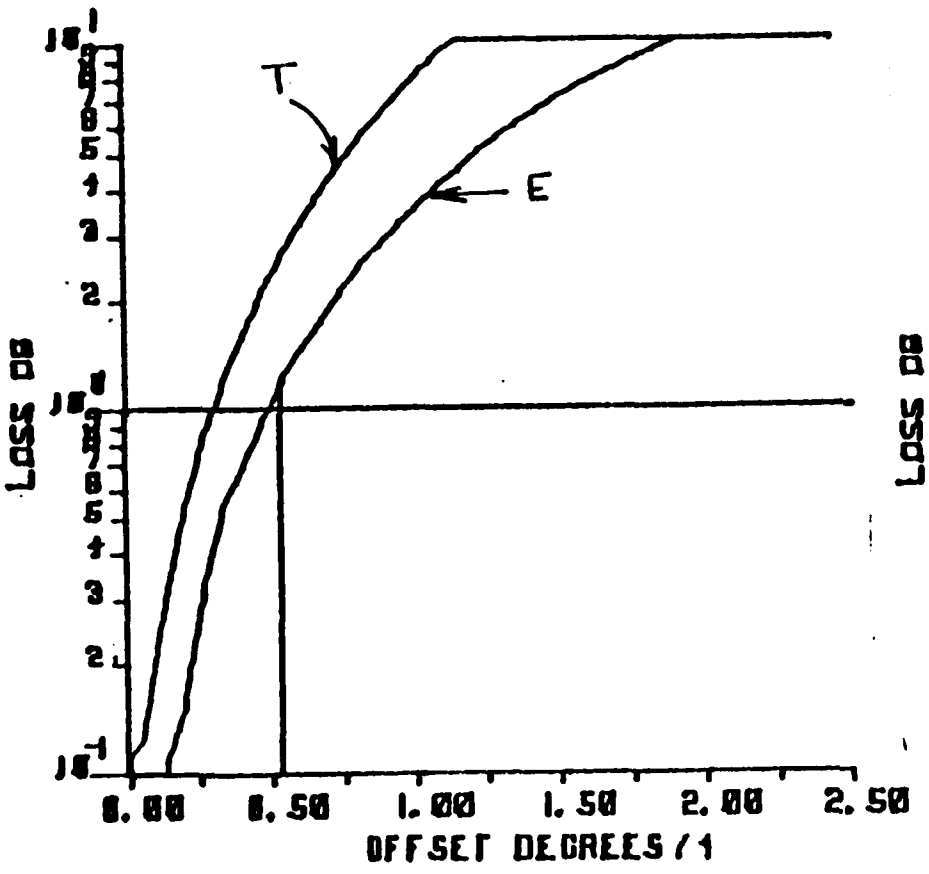

ATTENUATION DATA

λ = 1500 nm

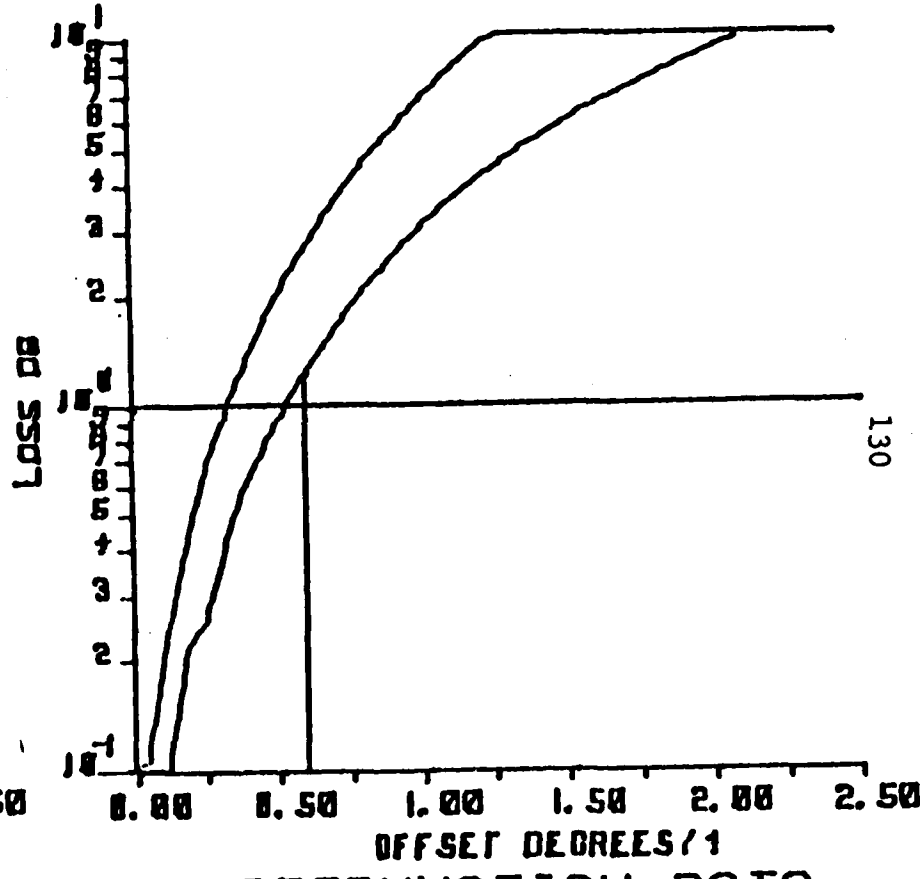

ATTENUATION DATA

87

130

ANGULAR OFFSET

FIBER NO.: 434004

λ = 1300 nm

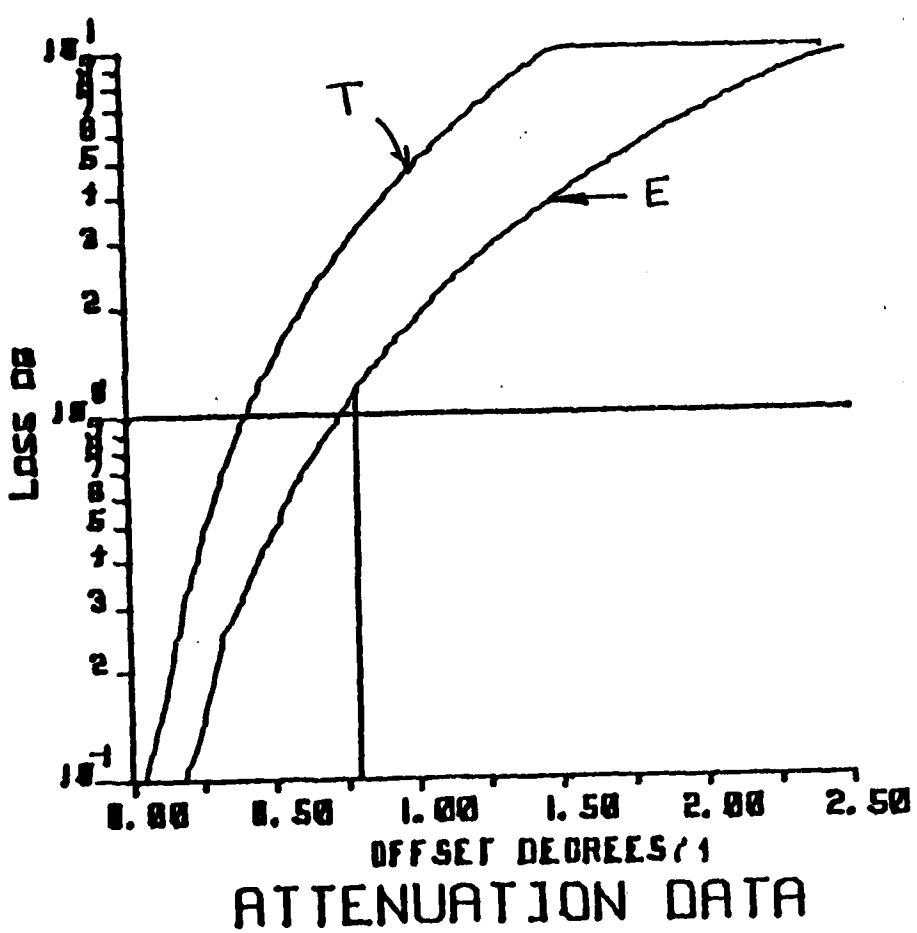

ATTENUATION DATA

λ = 1400 nm

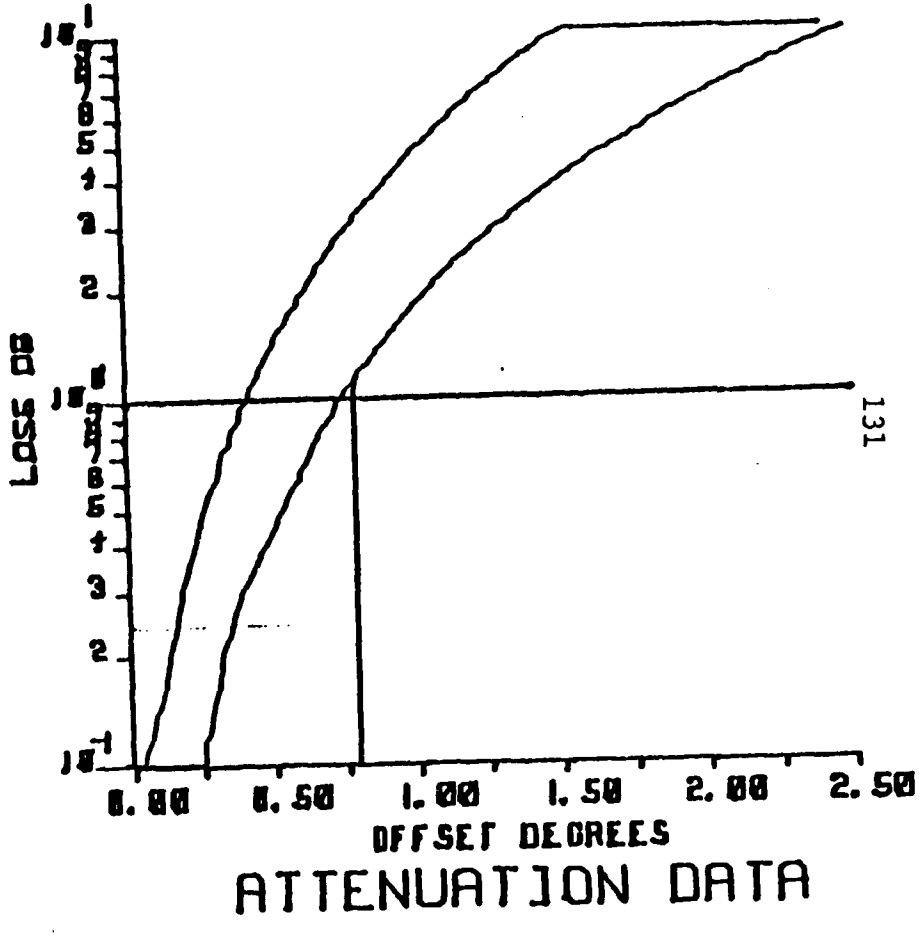

ATTENUATION DATA

02

ANGULAR OFFSET

FIBER NO.: 434004

λ = 1500 nm

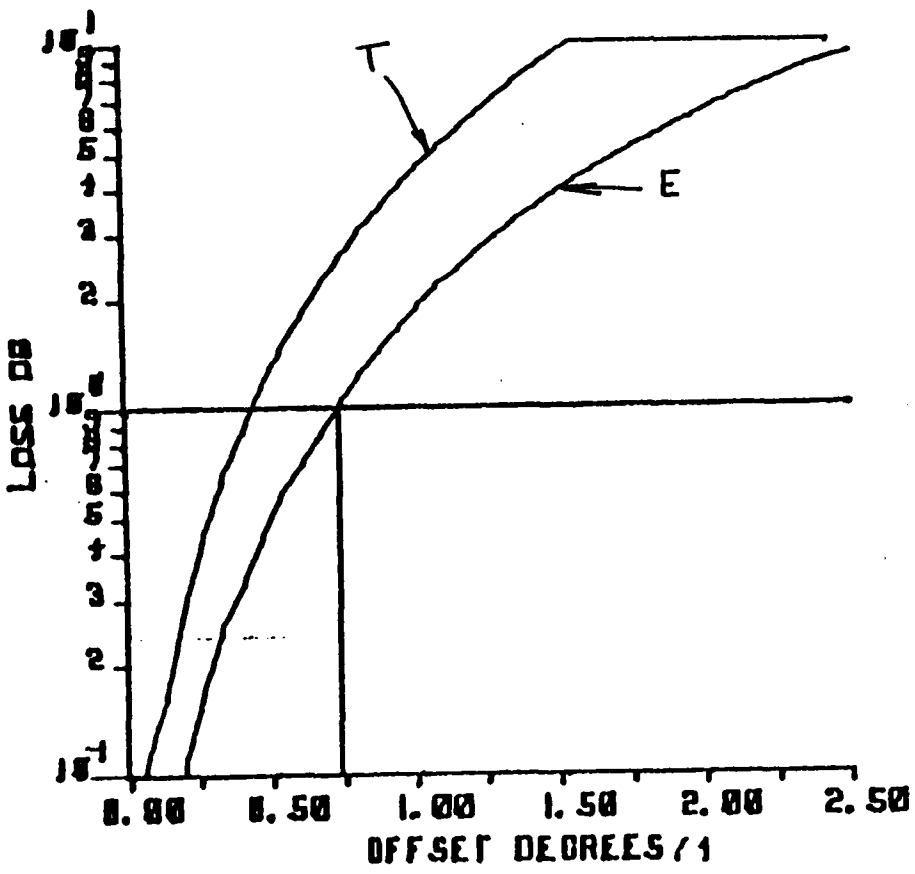

ATTENUATION DATA

λ = 1600 nm

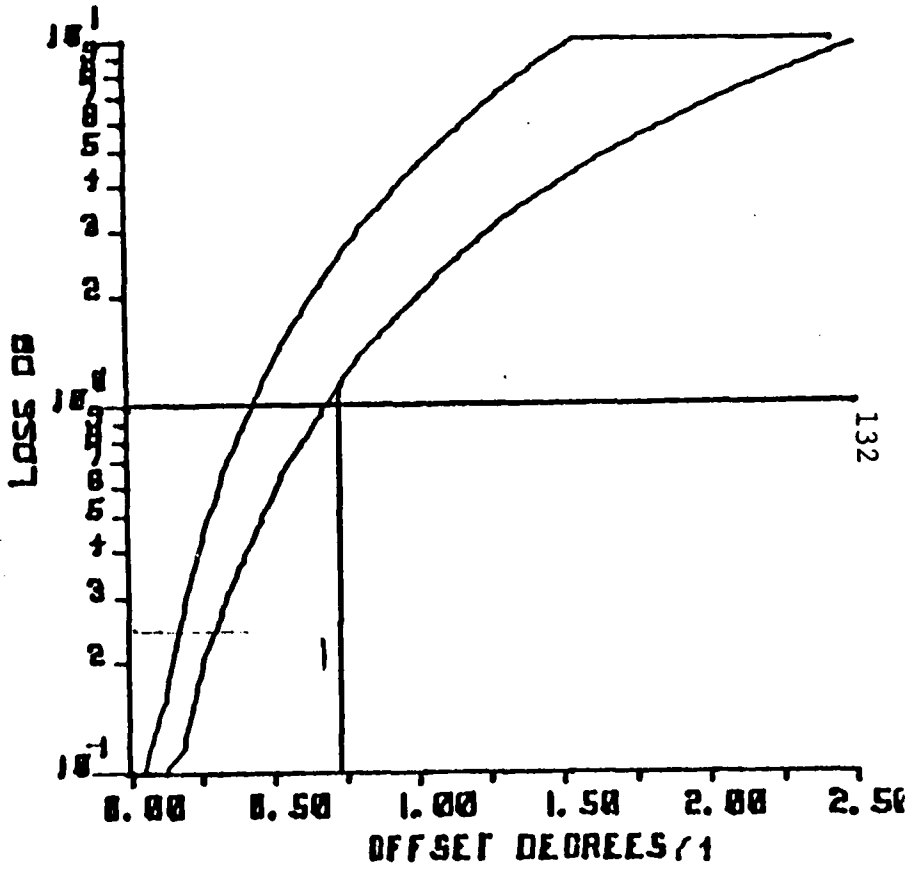

ATTENUATION DATA

ANGULAR OFFSET

FIBER NO.: 503403

λ = 1240 nm

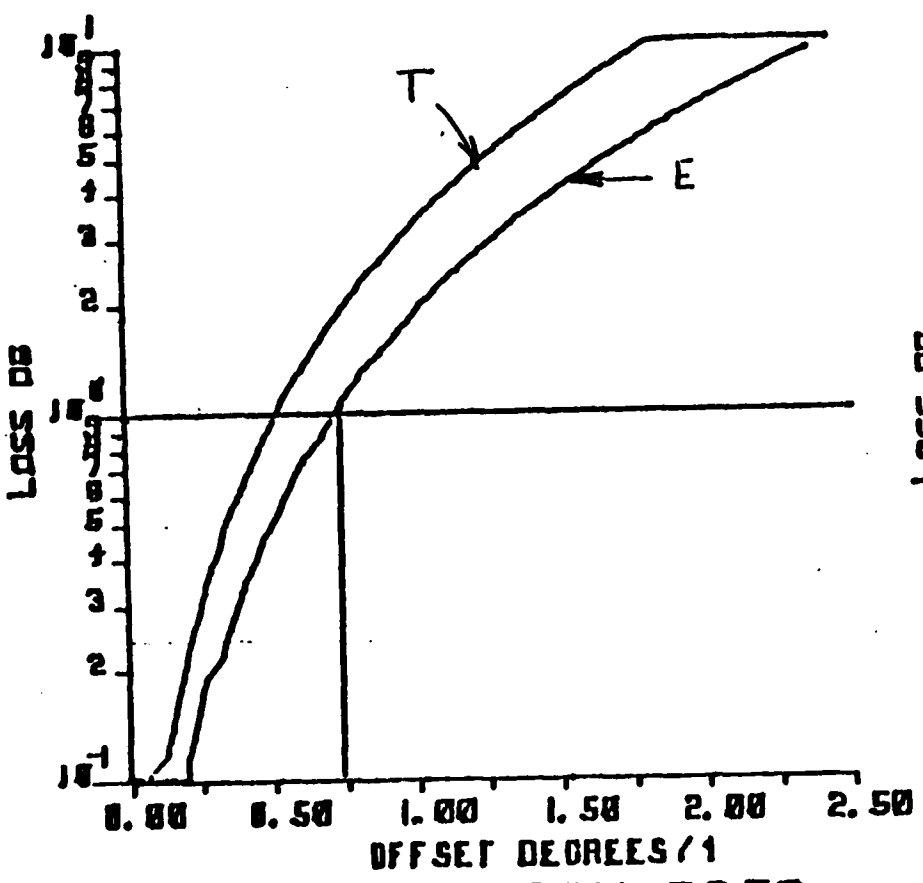

ATTENUATION DATA

λ = 1100 nm

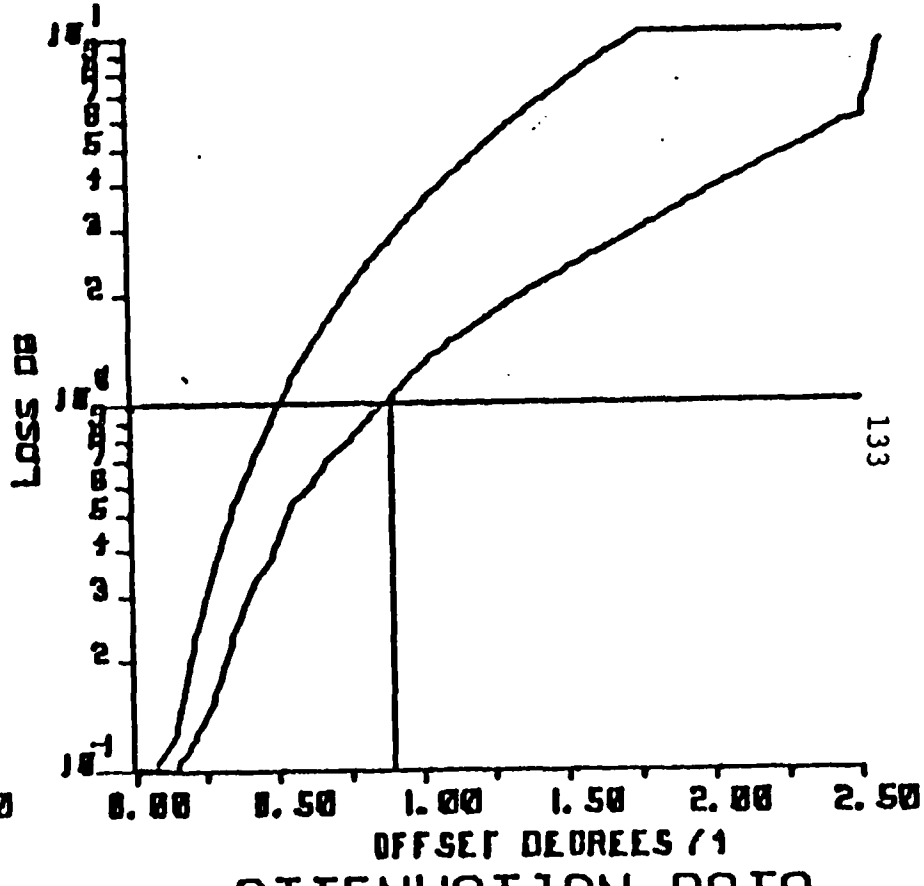

ATTENUATION DATA

88

ANGULAR OFFSET

FIBER NO.: 503403

λ = 1400 nm

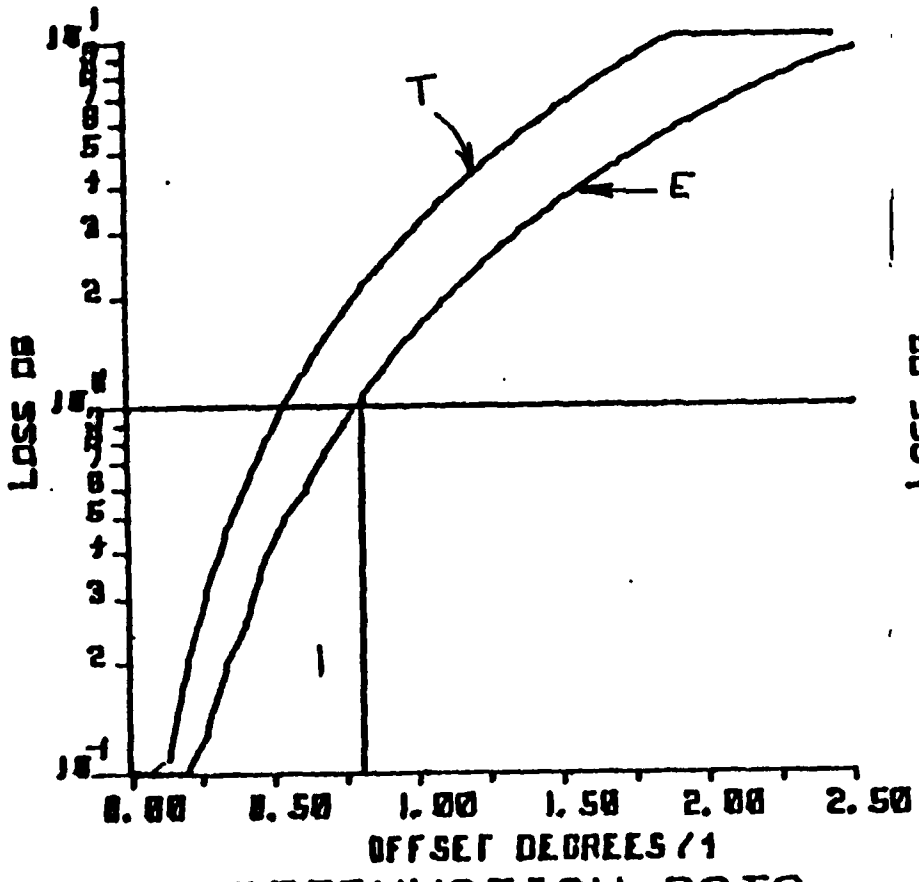

ATTENUATION DATA

λ = 1300 nm

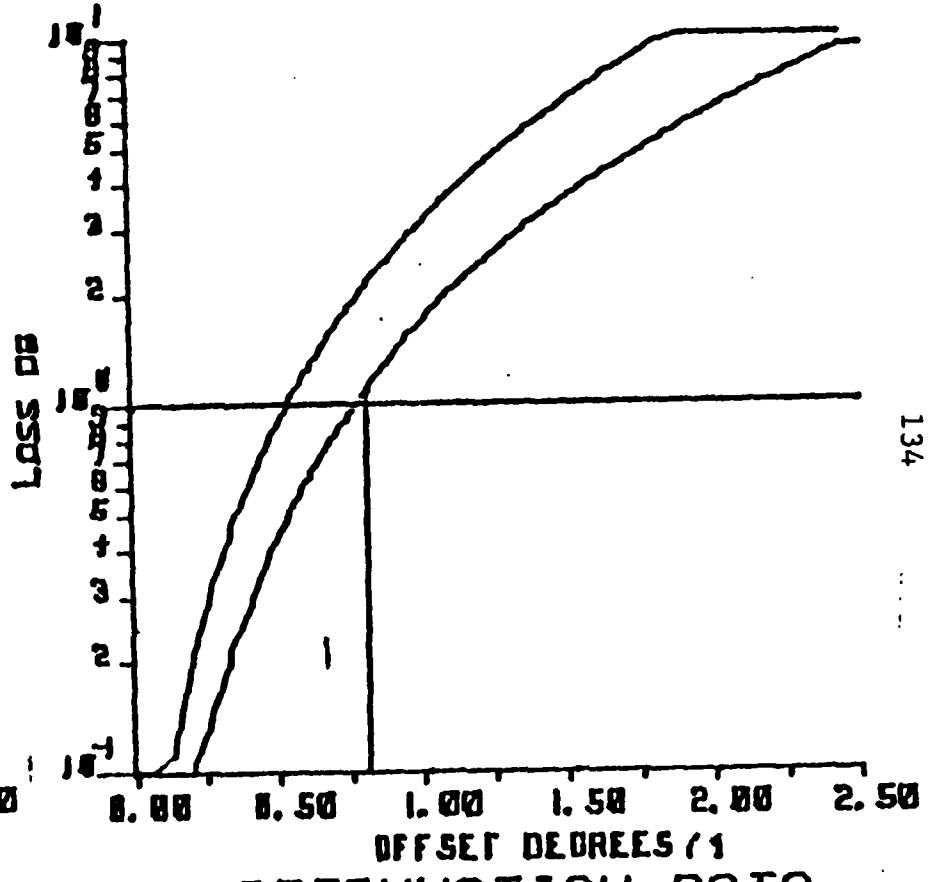

ATTENUATION DATA

ANGULAR OFFSET

FIBER NO.: 503403

λ = 1600 nm

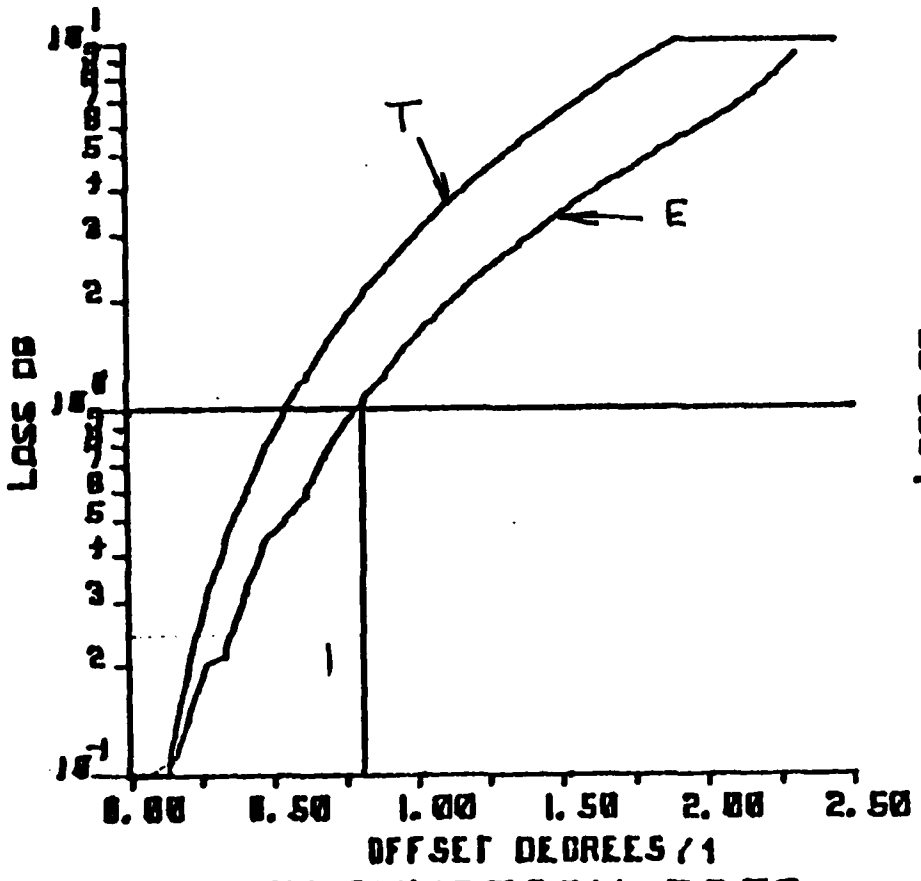

ATTENUATION DATA

λ = 1500 nm

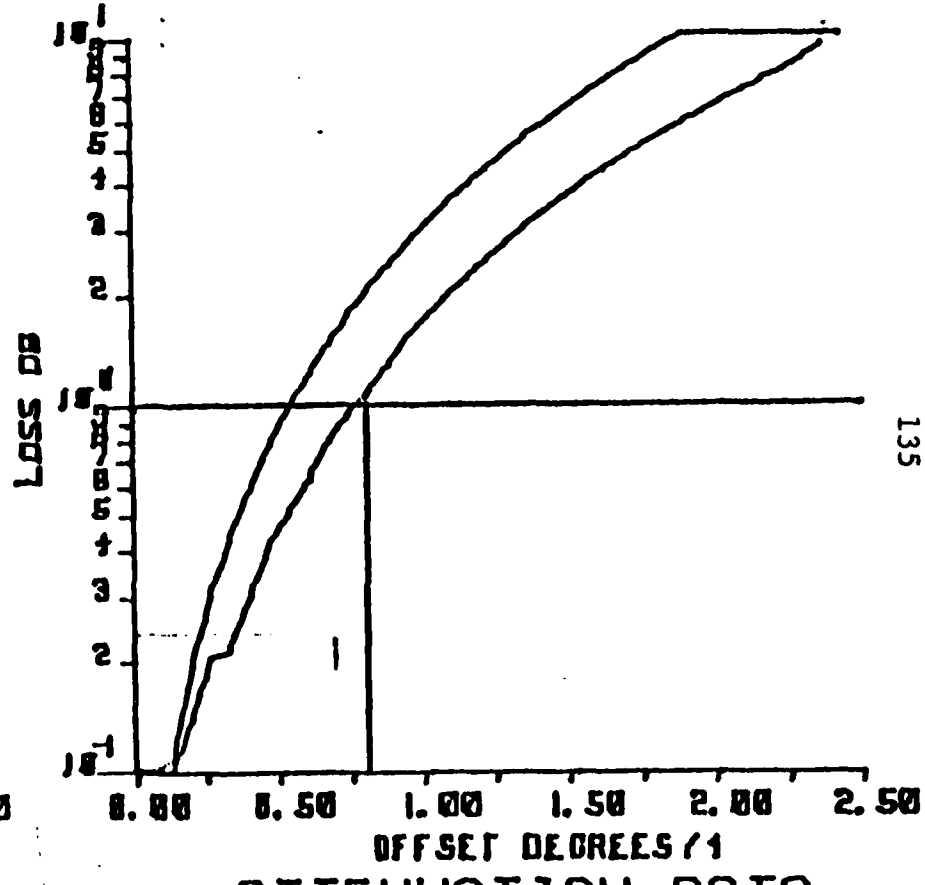

ATTENUATION DATA

81

ANGULAR OFFSET

FIBER NO.: 509906

λ = 1400 nm

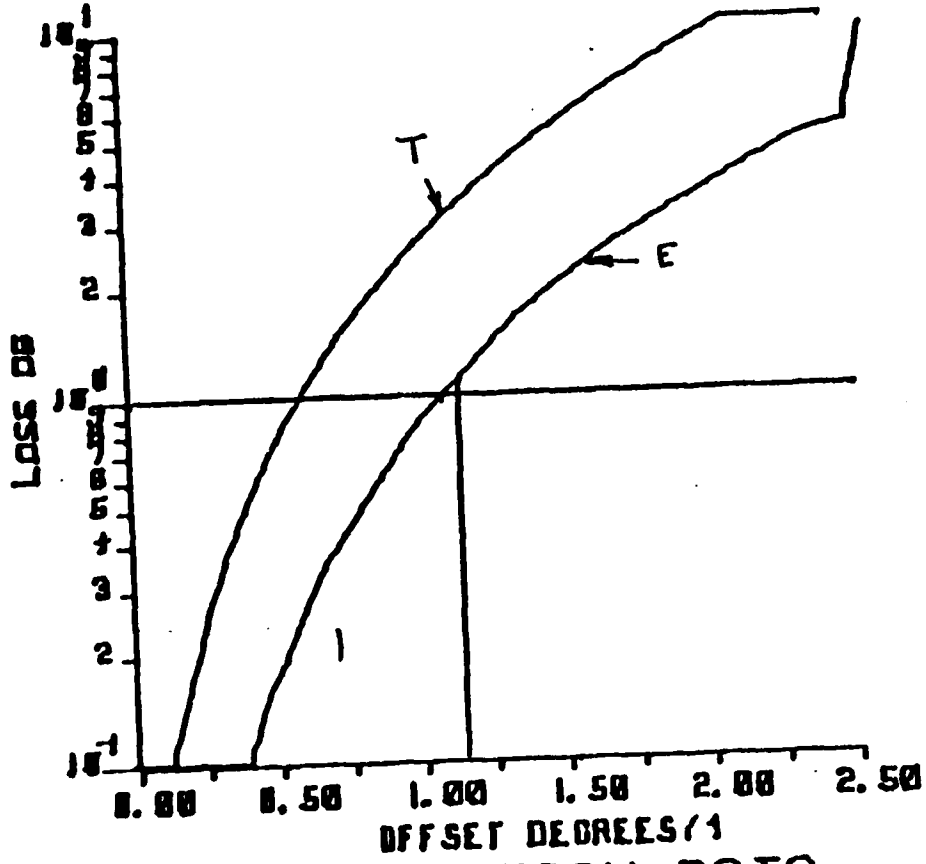

ATTENUATION DATA

λ = 1500 nm

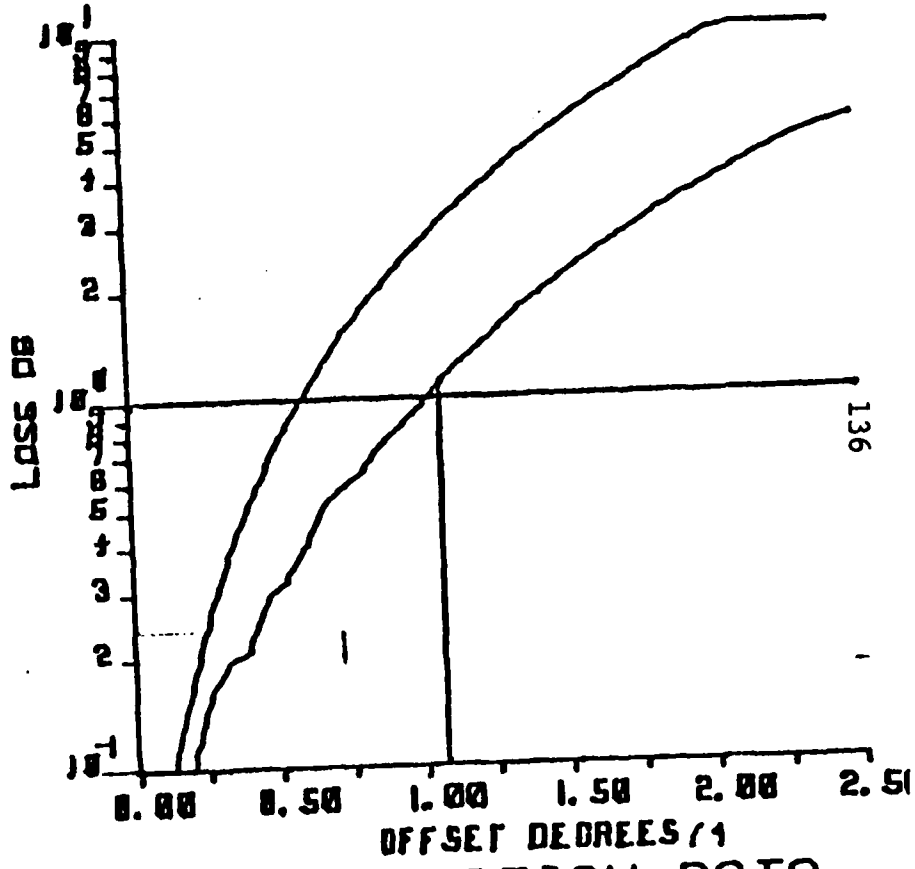

ATTENUATION DATA

136

.86

ANGULAR OFFSET

FIBER NO.: 506803

λ = 1240 nm

λ = nm

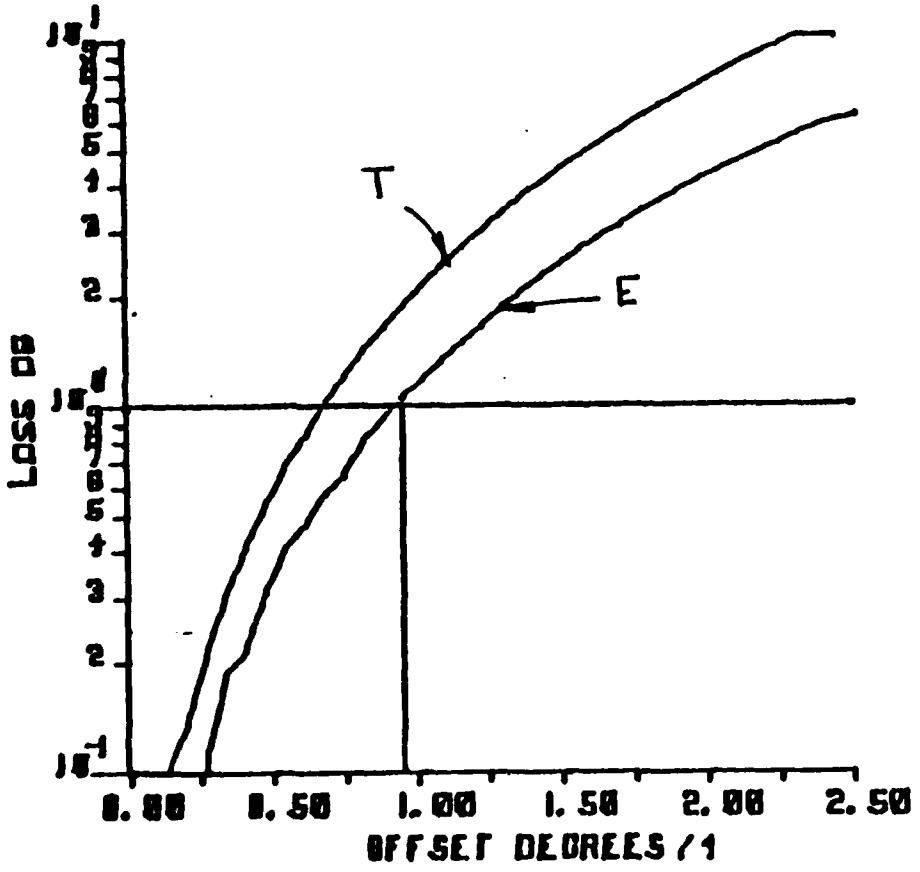

ATTENUATION DATA

85

ANGULAR OFFSET

FIBER NO.: 506803

λ = 1300 nm

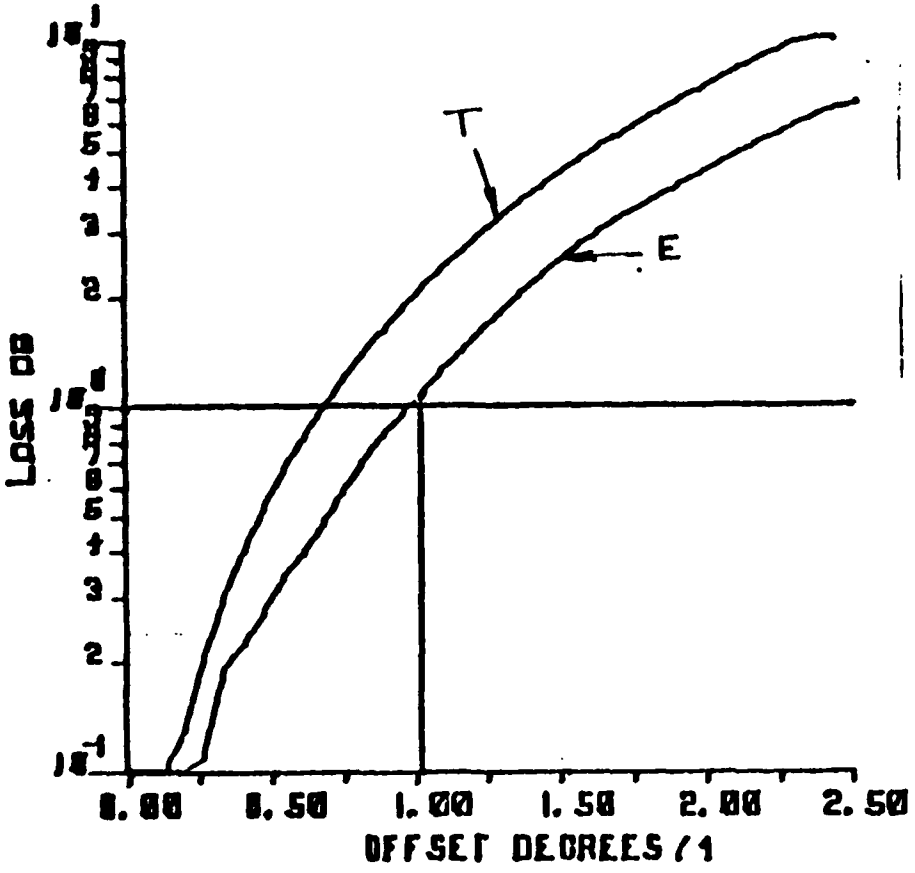

ATTENUATION DATA

λ = 1400 nm

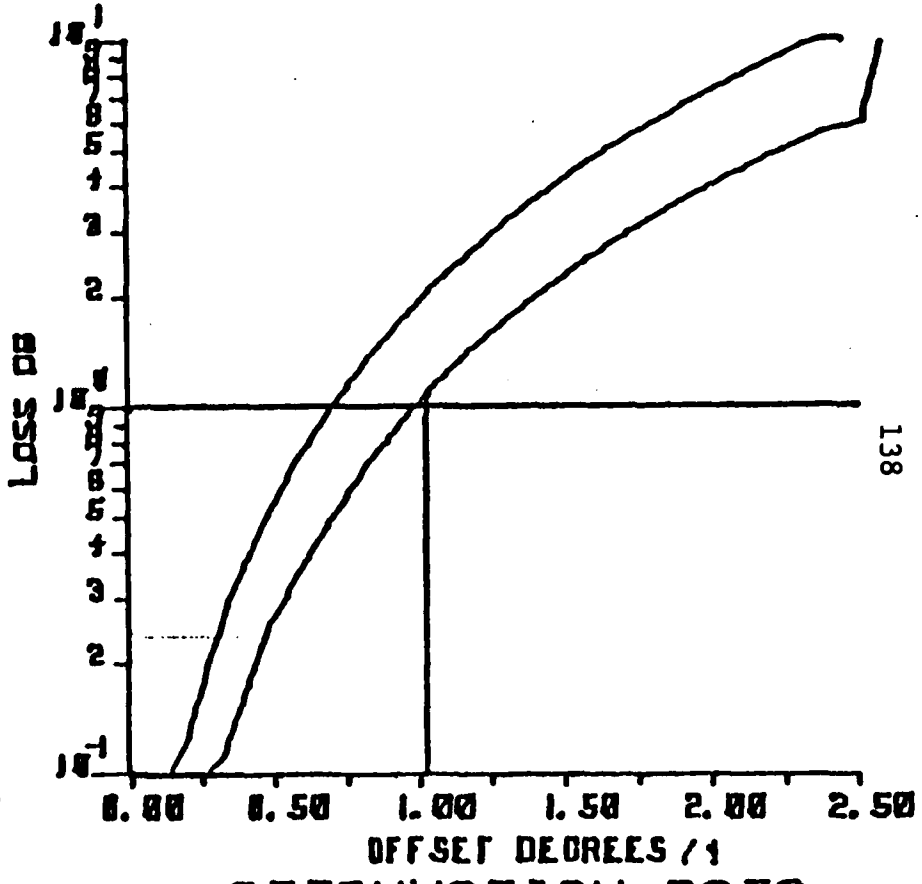

ATTENUATION DATA

06

ANGULAR OFFSET

FIBER NO.: 506803

λ = 1600 nm

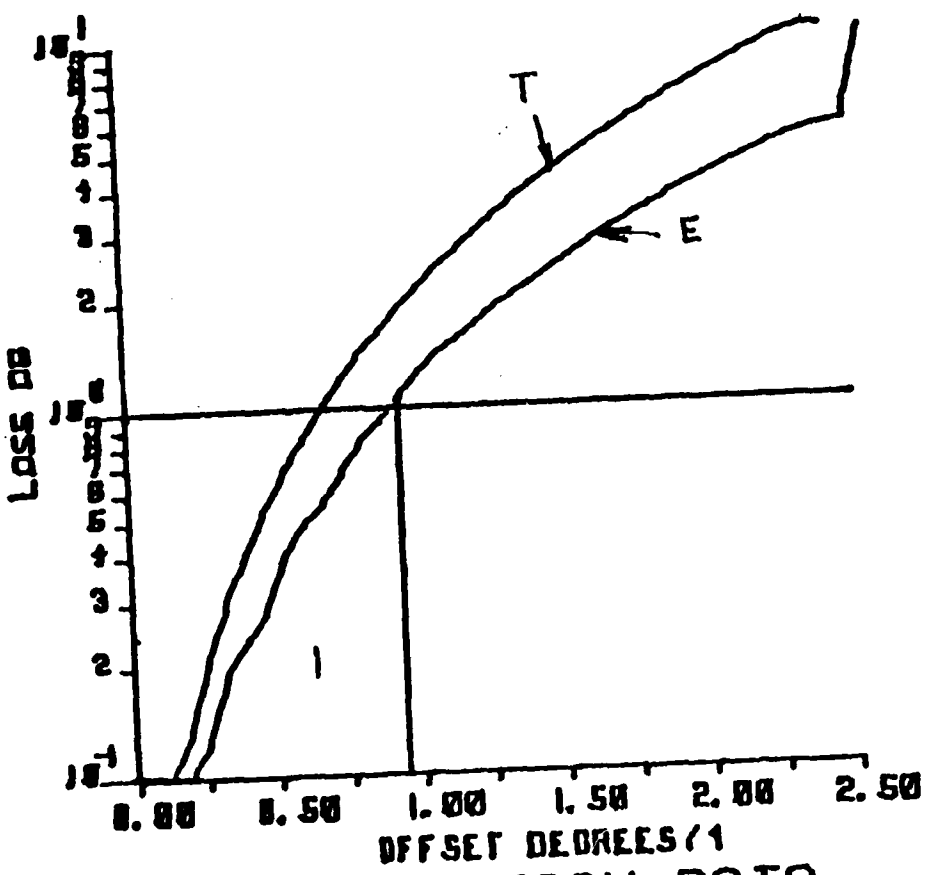

ATTENUATION DATA

λ = 1500 nm

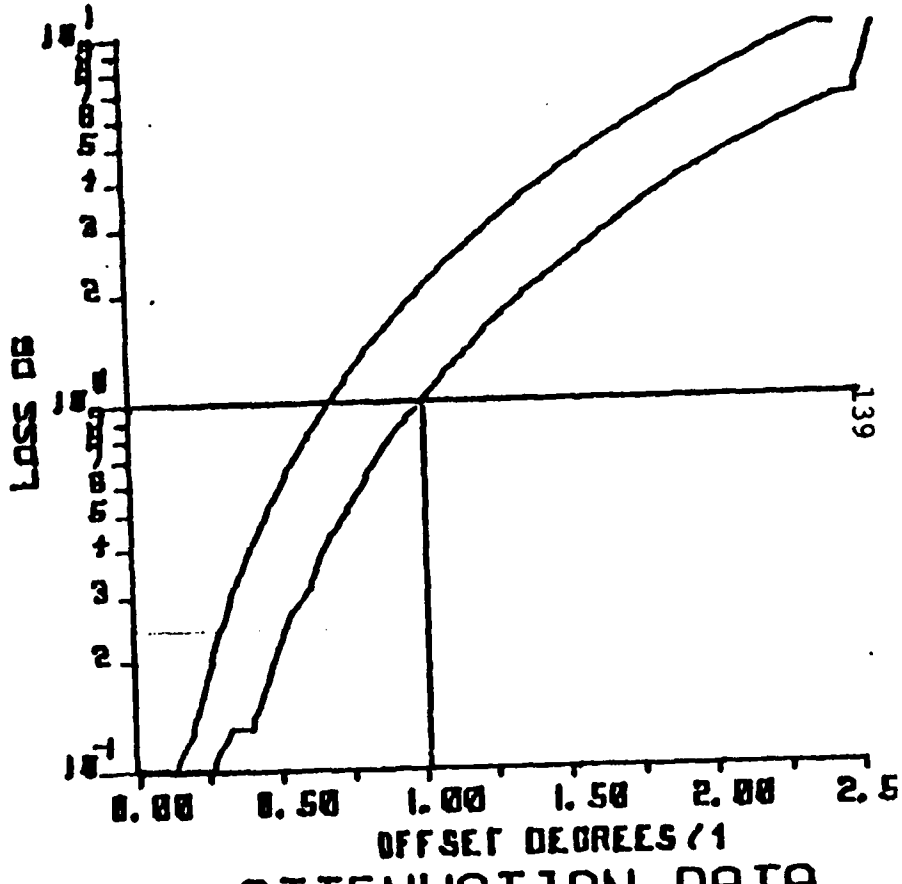

ATTENUATION DATA

ANGULAR OFFSET

FIBER NO.: 508404

λ = 1300 nm λ = nm

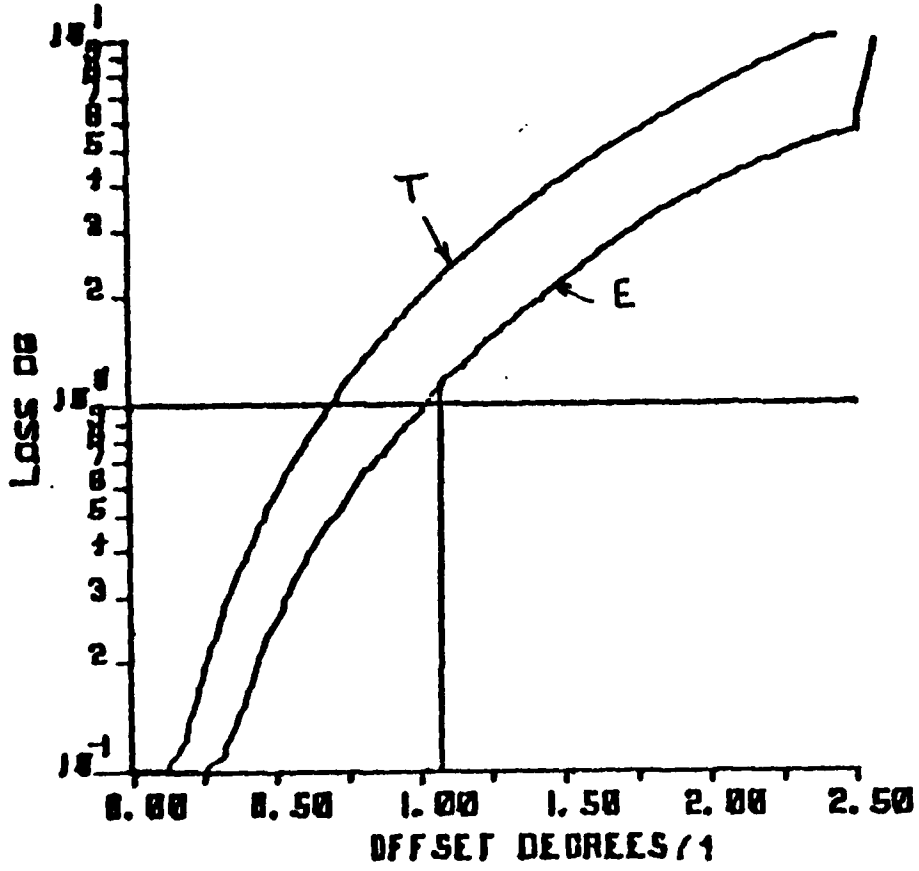

ATTENUATION DATA

03

ANGULAR OFFSET

FIBER NO.: 508404

λ = 1500 nm

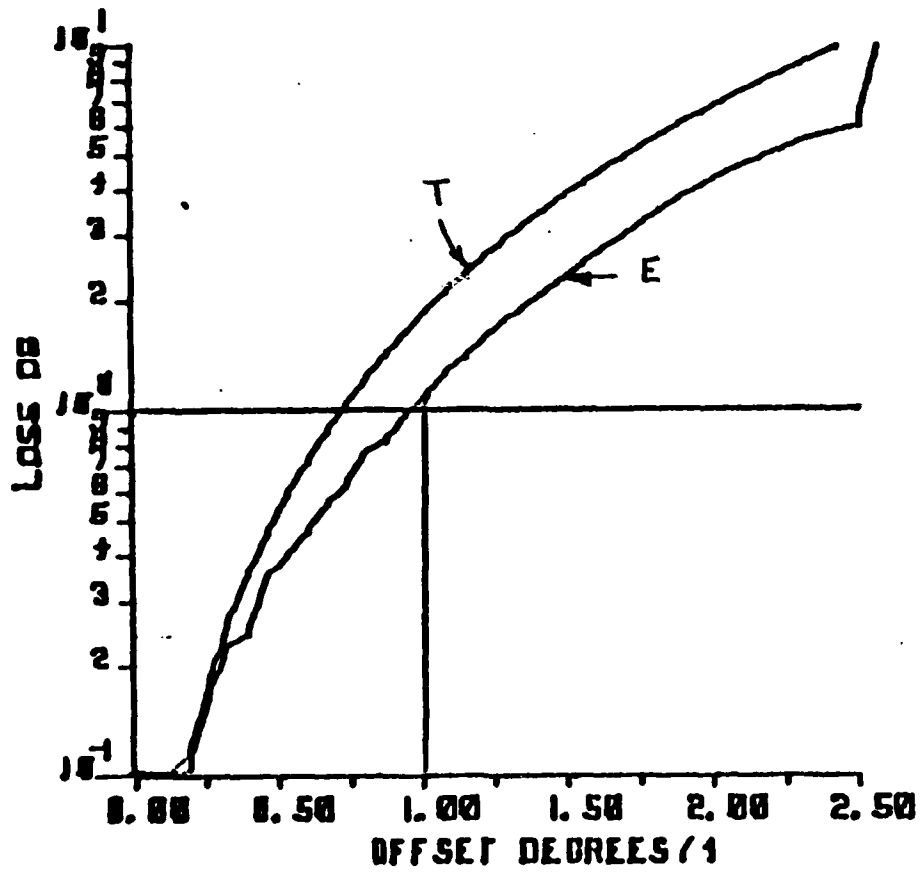

ATTENUATION DATA

λ = 1400 nm

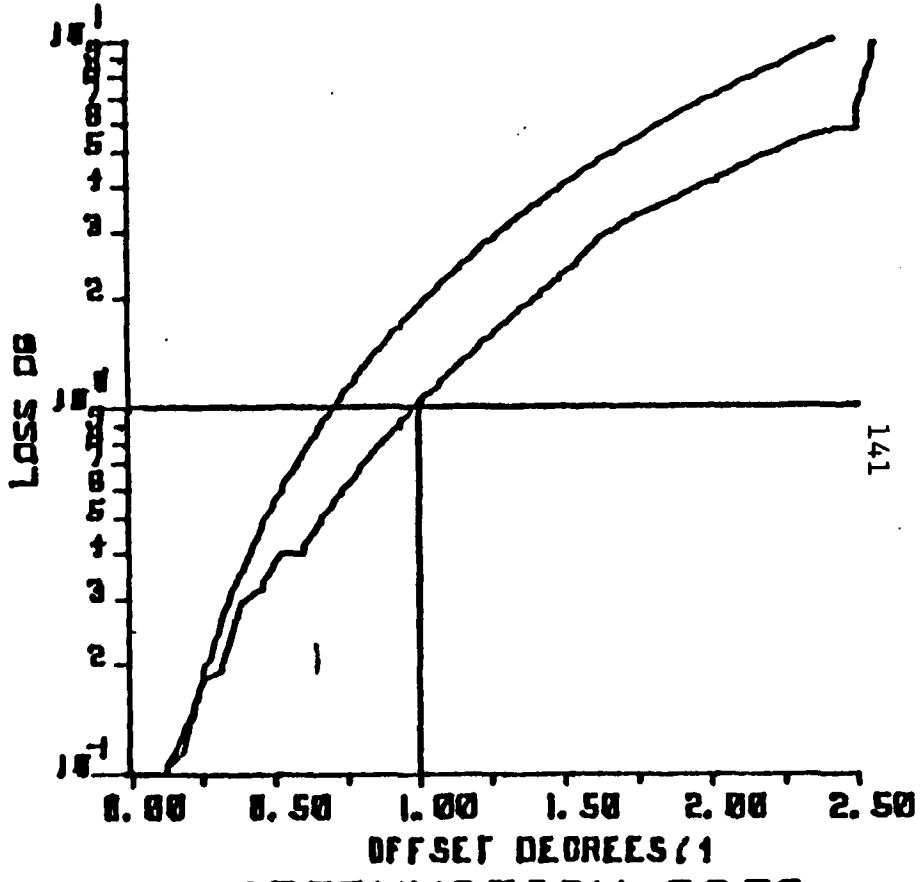

ATTENUATION DATA

141

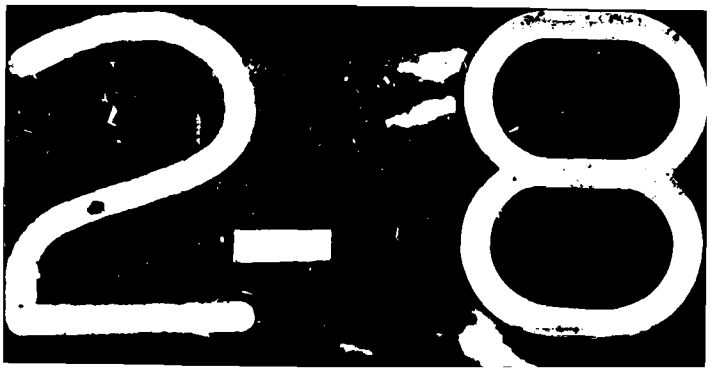
2-8